

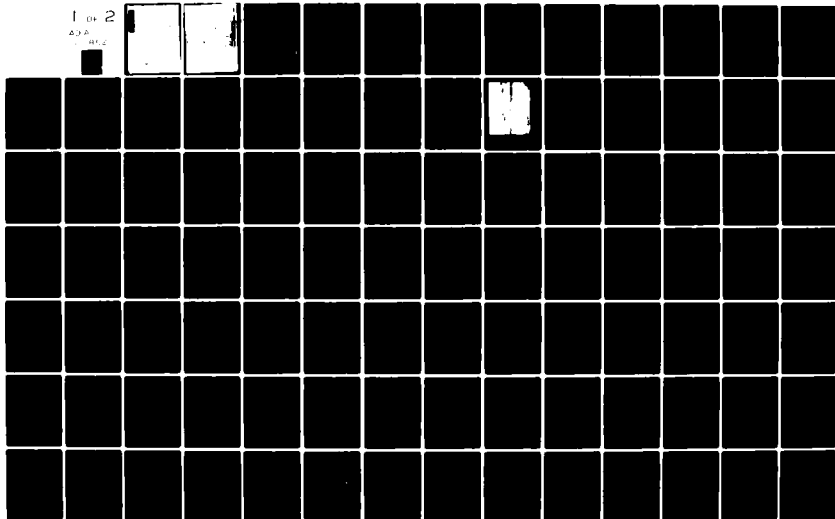
AD-A111 852 ROME AIR DEVELOPMENT CENTER GRIFFISS AFB NY
RADAR FREQUENCY RADIATION.(U)
UNCLASSIFIED NOV 81 E MALOWICKI
RADC-TR-81-347

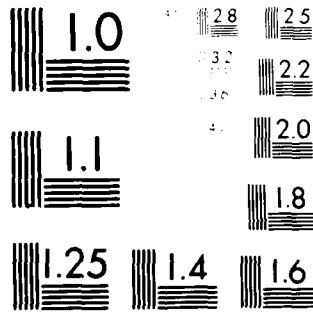
F/G 17/9

NL

1 of 2

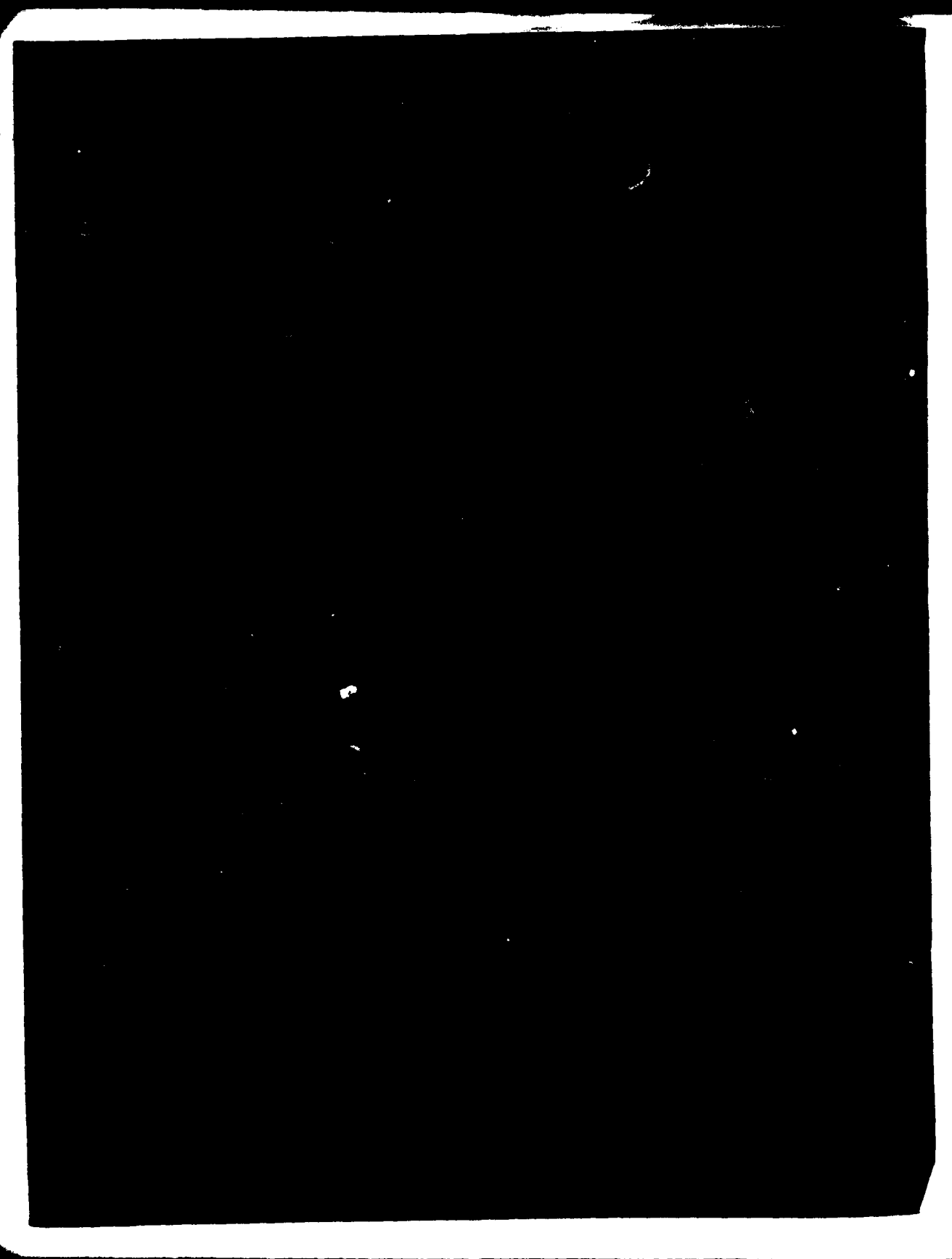
ADA
1862





MICROCOPY RESOLUTION TEST CHART
No. 1010-A

ADA 111852



UNCLASSIFIED

SECURITY CLASSIFICATION OF THIS PAGE (When Data Entered)

REPORT DOCUMENTATION PAGE		READ INSTRUCTIONS BEFORE COMPLETING FORM	
1. REPORT NUMBER RADC-TR-81-347	2. GOVT ACCESSION NO. AD-411832	3. RECIPIENT'S CATALOG NUMBER	
4. TITLE (and Subtitle) RADAR FREQUENCY RADIATION		5. TYPE OF REPORT & PERIOD COVERED In-House Report February 78 - September 81	
7. AUTHOR(s) Edward Malowicki		6. PERFORMING ORG. REPORT NUMBER N/A	
9. PERFORMING ORGANIZATION NAME AND ADDRESS Rome Air Development Center (OCSP) Griffiss AFB NY 13441		8. CONTRACT OR GRANT NUMBER(s) N/A	
11. CONTROLLING OFFICE NAME AND ADDRESS Rome Air Development Center (OCSP) Griffiss AFB NY 13441		10. PROGRAM ELEMENT, PROJECT, TASK AREA & WORK UNIT NUMBERS 12432F 20590101	
14. MONITORING AGENCY NAME & ADDRESS (if different from Controlling Office) Same		12. REPORT DATE November 1981	
		13. NUMBER OF PAGES	
		13. SECURITY CLASS. (of this report) UNCLASSIFIED	
		13a. DECLASSIFICATION/DOWNGRADING SCHEDULE N/A	
15. DISTRIBUTION STATEMENT (of this Report) Approved for public release; distribution unlimited			
17. DISTRIBUTION STATEMENT (of the abstract entered in Block 20, if different from Report) Same			
18. SUPPLEMENTARY NOTES None			
19. KEY WORDS (Continue on reverse side if necessary and identify by block number) Phased Array Radar Field Strength Radiation Antenna Pattern			
20. ABSTRACT (Continue on reverse side if necessary and identify by block number) A method is presented for the determination of radar frequency radiation power densities that the PAVE PAWS radar system could produce in its air and ground environment. The effort was prompted by the concern of the people in the vicinity of OTIS AFB MA and BEALE AFB CA about the possible radar frequency radiation hazard of the PAVE PAWS radar. The method is based on the following main assumptions that: a) the total field can be computed as the vector summation of the individual fields due to each (over)			

DD FORM 1 JAN 73 1473 EDITION OF NOV 68 IS OBSOLETE

UNCLASSIFIED

SECURITY CLASSIFICATION OF THIS PAGE (When Data Entered)

SELECTED
MAR 10 1982
A

UNCLASSIFIED

SECURITY CLASSIFICATION OF THIS PAGE(When Data Entered)

antenna element, b) the individual field can be calculated using distances for which the field point is in the far field of the antenna element. An RFR computer program was coded for the RADC HE 6180 digital computer and exercised to calculate the radiation levels in the air and ground space for the present baseline and the possible SIX DB and 10 DB growth systems of the PAVE PAWS radar system at OTIS AFB MA. The average radiation levels due to the surveillance fence were computed for three regions: in the air space in front of the radar, at the radar hazard fence at OTIS AFB MA and at representative ground points in the OTIS AFB vicinity. For the air space, the cases considered were: along the main beam axis with the beam radiating on-boresight and off-boresight, along the edge of the beam and elevation pattern densities at various azimuths and elevations. Numerous power density plots are presented. For example, the baseline system power density boresight beam axis power density plots show near field (from a 10 foot distance from the antenna to 500 feet), the transition region (from 500 feet to 4646 feet) and the far field region without discontinuities between regions. An air hazard zone where the power density levels, on a conservative boresight spotlight beam basis, could be 10 milliwatts/centimeter squared or higher is defined as a zone extending over an azimuth sector of 120 degrees per face with a radius of approximately 3035 feet for the baseline system, 6140 feet for the SIX DB system and 8710 feet for the 10 DB system. The calculated average power densities for the hazard fence periphery are well below the OSHA hazard level. Power density levels calculated for seven off-base ground points are in the safe low microwatts/centimeter squared region. The RFR computer program calculated values of power density for four ground points, when the radar is operating according to its beam position, frequency, and timing schedule, were within 3.5 dB of measured field data.

It is concluded that the radar frequency radiation of PAVE PAWS does not present a hazard to personnel provided there is no entry to the air hazard zone or to the area within the hazard fence. The method developed offers a cost effective way to determine radiation levels from a phased array radar especially in the near field and transition regions.

UNCLASSIFIED

SECURITY CLASSIFICATION OF THIS PAGE(When Data Entered)

Preface

Research described in this report was accomplished in-house at RADC under Job Order Number 20590101.

Appreciation is expressed to Mr. George Vogel, IRAE for the impetus he gave to this effort by his original work on the Time Scanned Array Radar and by the many productive discussions, to Capt Jimmie Boyd, OCSP for his coding of the RFR computer program, and to Mr. Donald Stebbins, OCSP for his debugging of the computer program, running the program and helping in the analysis of the results.



Accession No.
NTIS
DTIC TAB
Unannounced
Justification

A

Table Of Contents

	Page
1.0 Introduction	1
2.0 Method	3
2.1 Assumptions	3
2.2 Element Pattern	3
2.3 Total Field	4
3.0 Air Space Density	14
3.1 Beam Axial Densities	14
3.2 Edge of Beam Densities	16
3.3 Elevation Antenna Pattern Densities	17
3.4 Air Hazard	18
4.0 Ground Base Density	57
4.1 Hazard Fence	57
4.2 OTIS AFB Vicinity	59
4.3 Verification	62
4.4 Ground Hazard	64
5.0 Subarray Failures	111
5.1 Method	111
5.2 Results	111
5.3 Analysis	112
5.4 Failure Effects	114
6.0 Conclusions	136
References	137
Appendix A Mutual Coupling	139
Appendix B PAVE PAWS Element Check	150

Illustrations

Figures	Title	Page
1.1	PAVE PAWS -- BEALE AFB	8
1.2	Baseline System Active Element Layout	9
1.3	SIX DB System Active Element Layout	10
2.1	Raytheon Element Pattern	11
2.2	Midband Element Pattern	12
2.3	PAVE PAWS Geometry	13
3.1	Boresight Beam Density vs Beam Axis Distance -- Baseline System	19
3.2	Beam Axis Range Exponent	20
3.3	Beam Axis Range Exponent	21
3.4	Boresight Beam Density vs Beam Axis Distance -- SIX DB System	22
3.5	Beam Axis Power Density -- Baseline System Beam At 3 Degrees Elevation, 0 Degrees Azimuth	23
3.6	Beam Axis Power Density -- SIX DB System Beam At 3 Degrees Elevation, 0 Degrees Azimuth	24
3.7	Beam Axis Power Density -- 10 DB System Beam At 3 Degrees Elevation, 0 Degrees Azimuth	25
3.8	Beam Axis Power Density -- Baseline System Beam at 20 Degrees Elevation, 60 Degrees Azimuth	26
3.9	Beam Axis Power Density -- Baseline System Beam at 3 Degrees Elevation, 60 Degrees Azimuth	27
3.10	Edge Beam Density vs Distance -- Baseline System	28
3.11	Edge Beam Density vs Distance -- SIX DB System	29
3.12	Edge Beam Density vs Distance -- 10 DB System	30
3.13	Baseline Elevation Pattern -- Distance 145 Feet	31
3.14	Baseline Elevation Pattern -- Distance 290 Feet	32

3.15	Baseline Elevation Pattern -- Distance 580 Feet	33
3.16	Baseline Elevation Pattern -- Distance 1161 Feet	34
3.17	Baseline Elevation Pattern -- Distance 1600 Feet	35
3.18	Baseline Elevation Pattern -- Distance 1800 Feet	36
3.19	Baseline Elevation Pattern -- Distance 2323 Feet	37
3.20	Baseline Elevation Pattern -- Distance 3100 Feet	38
3.21	Baseline Elevation Pattern -- Distance 3900 Feet	39
3.22	Baseline Elevation Pattern -- Distance 4646 Feet	40
3.23	Elevation Pattern -- SIX DB System, Distance 145 Feet	41
3.24	Elevation Pattern -- SIX DB System, Distance 245 Feet	42
3.25	Elevation Pattern -- SIX DB System, Distance 290 Feet	43
3.26	Elevation Pattern -- SIX DB System, Distance 580 Feet	44
3.27	Elevation Pattern -- SIX DB System, Distance 1161 Feet	45
3.28	Elevation Pattern -- SIX DB System, Distance 1600 Feet	46
3.29	Elevation Pattern -- SIX DB System, Distance 1800 Feet	47
3.30	Elevation Pattern -- 10 DB System, Distance 143 Feet	48
3.31	Elevation Pattern -- 10 DB System, Distance 287 Feet	49
3.32	Elevation Pattern -- 10 DB System, Distance 574 Feet	50
3.33	Elevation Pattern -- 10 DB System, Distance 2299 Feet	51
3.34	Elevation Pattern -- 10 DB System, Distance 4598 Feet	52
3.35	Elevation Pattern -- 10 DB System, Distance 9196 Feet	53
3.36	Baseline System 10 Dbm Elevation Limits	54
3.37	SIX DB System 10 Dbm Elevation Limits	55
3.38	10 DB System 10 Dbm Elevation Limits	56
4.1	Hazard Fence Geometry	66
4.2	Hazard Fence Point Density vs Beam Position, Baseline System	67
4.3	Hazard Fence Point Density vs Beam Position, SIX DB System	68
4.4	Fence Power Density -- Baseline System	69

4.5	Fence Power Density -- SIX DB System	70
4.6	Hazard Fence Density vs Fence Angle -- Baseline System Beam 0 Degrees Azimuth	71
4.7	Hazard Fence Density vs Fence Angle -- Baseline System Beam 20 Degrees Azimuth	72
4.8	Hazard Fence Density vs Fence Angle -- Baseline System Beam 40 Degrees Azimuth	73
4.9	Hazard Fence Density vs Fence Angle -- Baseline System Beam 60 Degrees Azimuth	74
4.10	Hazard Fence Density vs Fence Angle -- SIX DB System Beam 0 Degrees Azimuth	75
4.11	Hazard Fence Density vs Fence Angle -- SIX DB System Beam 20 Degrees Azimuth	76
4.12	Hazard Fence Density vs Fence Angle -- SIX DB System Beam 40 Degrees Azimuth	77
4.13	Hazard Fence Density vs Fence Angle -- SIX DB System Beam 60 Degrees Azimuth	78
4.14	Selected Points	79
4.15	OTIS Height Profile -- Sagamore Bridge Line	80
4.16	OTIS Height Profile -- Mid-Cape Highway C	81
4.17	OTIS Height Profile -- Mid-Cape Highway S	82
4.18	OTIS Height Profile -- Sagamore Line	83
4.19	OTIS Height Profile -- Smoke Stack Line	84
4.20	Highway 25 Point Density vs Beam Position -- Baseline System	85
4.21	Mid-Cape C Point Density vs Beam Position -- Baseline System	86
4.22	Mid-Cape S Point Density vs Beam Position -- Baseline System	87
4.23	Mid-Cape N Point Density vs Beam Position -- Baseline System	88
4.24	Sagamore Point Density vs Beam Position -- Baseline System	89

4.25	Sagamore Bridge Point Density vs Beam Position -- Baseline System	90
4.26	Smoke Stack Point Density vs Beam Position -- Baseline System	91
4.27	Highway 25 Point Density vs Beam Position -- SIX DB System	92
4.28	Mid-Cape C Point Density vs Beam Position -- SIX DB System	93
4.29	Mid-Cape S Point Density vs Beam Position -- SIX DB System	94
4.30	Mid-Cape N Point Density vs Beam Position -- SIX DB System	95
4.31	Sagamore Point Density vs Beam Position -- SIX DB System	96
4.32	Sagamore Bridge Point Density vs Beam Position -- SIX DB System	97
4.33	Smoke Stack Point Density vs Beam Position -- SIX DB System	98
4.34	Search Density -- Azimuth 158 Degrees	99
4.35	Search Density -- Azimuth 158 Degrees	100
4.36	Search Density -- Azimuth 158 Degrees	101
4.37	Search Density -- Azimuth 104 Degrees	102
4.38	Search Density -- Azimuth 104 Degrees	103
4.39	Search Density -- Azimuth 104 Degrees	104
4.40	Search Density -- Azimuth 155 Degrees	105
4.41	Search Density -- Azimuth 155 Degrees	106
4.42	Search Density -- Azimuth 155 Degrees	107
4.43	Search Density -- Azimuth 167 Degrees	108
4.44	Search Density -- Azimuth 167 Degrees	109
4.45	Search Density -- Azimuth 167 Degrees	110
5.1	Array With No Failed Subarrays	116
5.2	Baseline Elevation Pattern -- Inactive Subarrays - None	117
5.3	Array With 1 Failed Subarray	118
5.4	Baseline Elevation Pattern -- Inactive Subarrays - Nr 22	119
5.5	Array With 2 Failed Subarrays	120
5.6	Baseline Elevation Pattern -- Inactive Subarrays -	121

	Nr 22, Nr 23	
5.7	Array With 4 Failed Subarrays	122
5.8	Baseline Elevation Pattern -- Inactive Subarrays	123
	Nr 19, Nr 22, Nr 23, Nr 26	
5.9	Array With 6 Failed Subarrays	124
5.10	Baseline Elevation Pattern -- Inactive Subarrays	125
	Nr 17, Nr 19, Nr 22, Nr 23, Nr 26, Nr 28	
5.11	Array With 12 Failed Subarrays	126
5.12	Baseline Elevation Pattern -- 12 Inactive Subarrays	127
5.13	Array With 16 Failed Subarrays	128
5.14	Baseline Elevation Pattern -- 16 Inactive Subarrays	129
5.15	Array With 20 Failed Subarrays	130
5.16	Baseline Elevation Pattern -- 20 Inactive Subarrays	131
5.17	Array With 24 Failed Subarrays	132
5.18	Baseline Elevation Pattern -- 24 Inactive Subarrays	133
5.19	Array With 28 Failed Subarrays	134
5.20	Baseline Elevation Pattern -- 28 Inactive Subarrays	135
A1	Element Geometry	142
A2	Horizontal Polarization Port Coupling	143
A3	Vertical Polarization Port Coupling	144
B1	Face C/NFE Geometry	154
B2	Face C Element Failure vs Beam Position	155
B3	Face C Element Failure - 7 Degree Azimuth Beam	156
B4	Face C Element Failure - 17 Degree Azimuth Beam	157
B5	Face C Element Failure - 37 Degree Azimuth Beam	158
B6	Face C Element Failure - 57 Degree Azimuth Beam	159
B7	Face C Steering Bit Failures - 7 Degrees Beam Azimuth	160
B8	Face C Steering Bit Failures - 17 Degrees Beam Azimuth	161

89	Face C Steering Bit Failures - 37 Degrees Beam Azimuth	162
810	Face C Steering Bit Failures - 57 Degrees Beam Azimuth	163
811	Face C Azimuth Pattern - 60 Degrees Azimuth, 71 Feet No Element Failed	164
812	Face C Azimuth Pattern - 60 Degrees Azimuth, 71 Feet Nr 1 Element Failed	165
813	Face C Azimuth Pattern - 0 Degrees Azimuth, 2000 Feet No Element Failed	166
814	Face C Azimuth Pattern - 0 Degrees Azimuth, 2000 Feet Nr 1 Element Failed	167
815	Face C Azimuth Pattern - 57 Degrees Azimuth, 2000 Feet No Element Failed	168
816	Face C Azimuth Pattern - 57 Degrees Azimuth, 2000 Feet Nr 1 Element Failed	169

Tables

Table	Title	Page
3.1	Beam Axial Density	16
4.1.1	Hazard Fence Maxima Densities (Arc Segment)	59
4.2.1	Point Locations	60
4.2.2	Average Point Densities For 435 MHz	61
4.3.1	Field Intensities	62
4.3.2	Beamwidth Comparison	64
5.1	Subarray Failure Effects	115
A1	First Ring Coupling	145
A2	Effect Of Frequency On The First Ring Coupling	146
A3	Second Ring Coupling At 420 MHz	147
A4	Second Ring Coupling At 435 MHz	148
A5	Total Coupling	149
B1	Face C Amplitude Taper	150

1.0 Introduction: In the late 1970's period there was a great deal of concern expressed by the people living in the area of OTIS Air Force Base Massachusetts and of BEALE Air Force Base California about the possible radar frequency radiation hazard that might be caused by the large phased array radar of PAVE PAWS system. In order to determine whether or not PAVE PAWS could present a radiation hazard to personnel, RADC developed and exercised an RFR (Radar Frequency Radiation) computer program.

The prime mission of the PAVE PAWS radar system is to detect and track sea launched ballistic missiles and to provide the National Military Command Center, the North American Air Defense Command Center and the Strategic Air Command with warning and attack characterization data. The secondary mission is to support satellite surveillance and tracking. The PAVE PAWS radar system consists of two radars -- one located on the east coast at OTIS AFB Massachusetts and one located on the west coast at BEALE AFB California. Figure 1.1 shows the PAVE PAWS radar located at BEALE AFB . The radar is housed in a five story building 105 feet high. The building is shaped approximately like a truncated pyramid with a triangular base 105 feet on a side. The PAVE PAWS radar is a dual-faced radar system with two radiating radar antennas -- Faces A and B which are visible in Figure 1.1 and with one passive antenna -- Face C which is located at the rear of the building. At present, in the baseline system, each radar face is a spatially thinned array with an active area diameter of 72.5 feet. Each radar face can radiate independently in the 420 to 450 MHz frequency band with a peak power of approximately 580 kilowatts at a duty cycle of 0.25. Faces A and B operate in a surveillance and tracking mode. The surveillance fence is maintained at a nominal 3 degrees elevation over an azimuth sector of 120 degrees per face. Each radar face has 1792 active elements which can transmit and receive and 885 "dummy" elements which neither transmit nor receive. Each active element has a solid

state transmit/receive module. In addition to the two radiating faces, the PAVE PAWS radar has a receive only Face C linear array which has 21 elements and is used for interference monitoring purposes. In the future, either of two growth systems -- a SIX DB system or a 10 DB system could be implemented. The SIX DB system would have an active array diameter of 102.5 feet with 3584 active elements and 1770 "dummy" elements and with a peak transmitted power double that of the baseline system at the same duty cycle for each face A and B. Figures 1.2 and 1.3 show the active element layout for the baseline and the SIX DB systems, respectively. The 10 DB system would have an active array diameter of 102.5 feet with uniform illumination, a total of 5354 active elements and no "dummy" elements with a peak transmitted power approximately three times that of the baseline system at the same duty cycle for each face A and B.

All three systems were considered in the RADC field intensity calculations with the emphasis placed on the baseline and the SIX DB systems. The calculations were performed using the RADC RFR computer program. This computer program was developed by RADC and coded for the RADC Honeywell HE 6180 digital computer. The RFR computer program has the capability of calculating the field intensity levels that a phased array would produce anywhere in its environment. This method applies to any phased array, facilitates the antenna design stage and reduces the need for expensive field measurements. The radiation levels due to the operation of the PAVE PAWS surveillance fence were computed for three regions using the slightly higher design value of 344 transmit peak watts/module. The particular radar treated in this report is the PAVE PAWS radar at OTIS AFB. First, in order to determine the exposure levels to airborne personnel, the radiation levels were computed in the air space in front of the radar. Second, in order to evaluate the effectiveness of the radar hazard fence, the radiation levels were computed at and near the radar hazard fence. Third, in order to determine the exposure levels to personnel outside the base itself, the radiation levels were computed at

representative points of interest in the OTIS AFB vicinity.

2.0 Method:

2.1 Assumptions: The field intensity algorithm development is based on the following assumptions and constraints:

a. Two isotropic radiators with suitable phasing and separation can represent an antenna array element mounted in front of the array plane.

b. The total field can be computed as the vector summation of the individual fields due to each array antenna element.

c. The individual field due to an array antenna element is calculated using distances for which the field point is in the far field of the antenna array element.

d. The mutual coupling effects between antenna array elements can be ignored. A negligible error (less than 6 percent -- Appendix A) results in the calculation of the field intensity. But there results a significant lessening of the computational complexity.

e. Refraction effects are neglected.

f. The beam steering phases are not quantized and consequently no random/parabolic corrections for phase step errors are applied. Rather correct steering phases are usually assumed. The effect of errors in the steering phase can be considered and is treated in Appendix B.

2.2 Element Pattern: The PAVE PAWS element was represented in the RFR computer program by a pattern due to two isotropic radiators spaced one half of the wavelength at the midband frequency of 435 MHz along the array normal with each radiator spaced 0.25λ (wavelength) from the plane which would contain the array face. The phasing between the radiators was taken as 180 degrees at the band center. Equation (2.1) represents this pattern.

$$\vec{E} = \frac{e^{-j(kr_1)}}{r_1} + \frac{e^{-j(kr_2 + 180)}}{r_2} \quad (2.1)$$

where \vec{E} is the electric field intensity at a field point normalized to a unity excitation

k is the wavenumber

180 is the phasing between the radiators at the midband frequency in degrees

r_1 is the distance from the field point to the radiator in front of the array plane

r_2 is the distance from the field point to the radiator in back of the array plane

Figure 2.1 shows the midband (435 MHz) element patterns measured by Raytheon in four different planes. The "rapid" variations are measurement effects due to the rotation of the linear sampling antenna of the circularly polarized actual antenna element. The "slow" variations are due to the edge effects of the partial array (320 elements) used as a test array. The beamwidth is on the order of 60 degrees. There are some undulations in the pattern (less than 1 dB); the measured gain is 5.77 dB. Figure 2.2 shows the midband (435 MHz) element patterns computed by the RADC RFR computer program for the vertical plane. Figure 2.2A is a rectangular power plot, and Figure 2.2B is a polar voltage plot. The beamwidth is 60 degrees. Figure 2.2 is without the undulations evident in the Raytheon plot. The gain is 6 dB. It is considered that this pattern is a good representation of the actual PAVE PAWS element pattern.

2.3 Total Field: Since the array antenna element is small and has short dimensions (in the order of 16 inches) it has a far field distance of approximately 1.6 feet. Thus it can be considered that the field density

calculations for the element can be performed for points at distances greater than 10 feet from the element on the basis of far field conditions where the energy propagates according to the inverse distance squared law. Equation (2.2) applies:

$$P = \frac{W}{4\pi r^2} \quad (2.2)$$

where P = power density at the field point
 W = power radiated by the radiator in watts
 r = distance from the radiator to the field point

The power density can also be expressed by equation (2.3).

$$P = \frac{|\vec{E}|^2}{2Z} \quad (2.3)$$

where \vec{E} = electric field intensity vector
 Z = free space resistance of 120π

Combining equations (2.2) and (2.3), one obtains

$$|\vec{E}| = \frac{\sqrt{60 W}}{r} \quad (2.4)$$

which leads to

$$\vec{E}_1 = \frac{\sqrt{60 W}}{r_1} e^{-jkr_1} \quad (2.5)$$

and to

$$\vec{E}_2 = \frac{\sqrt{60 W}}{r_2} e^{-j(kr_2 + 180)} \quad (2.6)$$

where the subscripts 1 and 2 refer to the front and rear radiators, respectively, and where the exponential terms account for the phases accumulated due to the

distances and the phase of the radiator position in front or rear of the plane containing the array face. From equation (2.3), it is evident that the total power density P for i isotropic radiators is given by

$$P = \frac{1}{2Z} \sum |E_i|^2 \quad (2.7)$$

where the summation is summed for 1792 front radiators and for 1792 rear radiators for the case of the baseline system which has 1792 radiating antenna elements. These numbers double for the case of the SIX DB system and increase to 5354 for the 10 DB system. Equation (2.7) leads to

$$P = \frac{30 W}{Z} \left| \sum \frac{e^{-j(kr_i + \phi_i)}}{r_i} \right|^2 \quad (2.8)$$

where ϕ_i is the phase at the i -th radiator. This phase term includes the 180 degree phase at the midband frequency for the rear element and the beam steering phases.

Based on equations (2.5), (2.6), and (2.8) and based on the PAVE PAWS geometry of Figure 2.3, an RFR computer program was coded for the RADC HE 6180 computer. The pair of points F and R of Figure 2.3 depicting the location of the front and rear isotropic radiators, respectively, for one antenna array element are located in the x', y', z' radar face cartesian coordinate (RFCC) system. The field sample point Q is located in the radar topocentric system. The orientation of the x, y, z coordinate system was chosen to simplify the calculations of r the distance from a radiator (R or F) to the field point Q. This distance r was calculated from

$$r = (\Delta x^2 + \Delta y^2 + \Delta z^2)^{\frac{1}{2}} \quad (2.9)$$

where

$$\Delta x = x + x'$$

$$\Delta y = y + y' \cos T \pm d \sin T$$

$$\Delta z = z - y' \sin T \pm d \cos T - h$$

and where

x, y, z are the topocentric coordinates of the point Q

x', y', z' are the RFCC coordinates of the isotropic radiators

T is the array face tilt angle from the horizontal xy plane

h is the array face center height above the xy plane

the $+d$ term applies to front radiator

the $-d$ term applies to the rear radiator

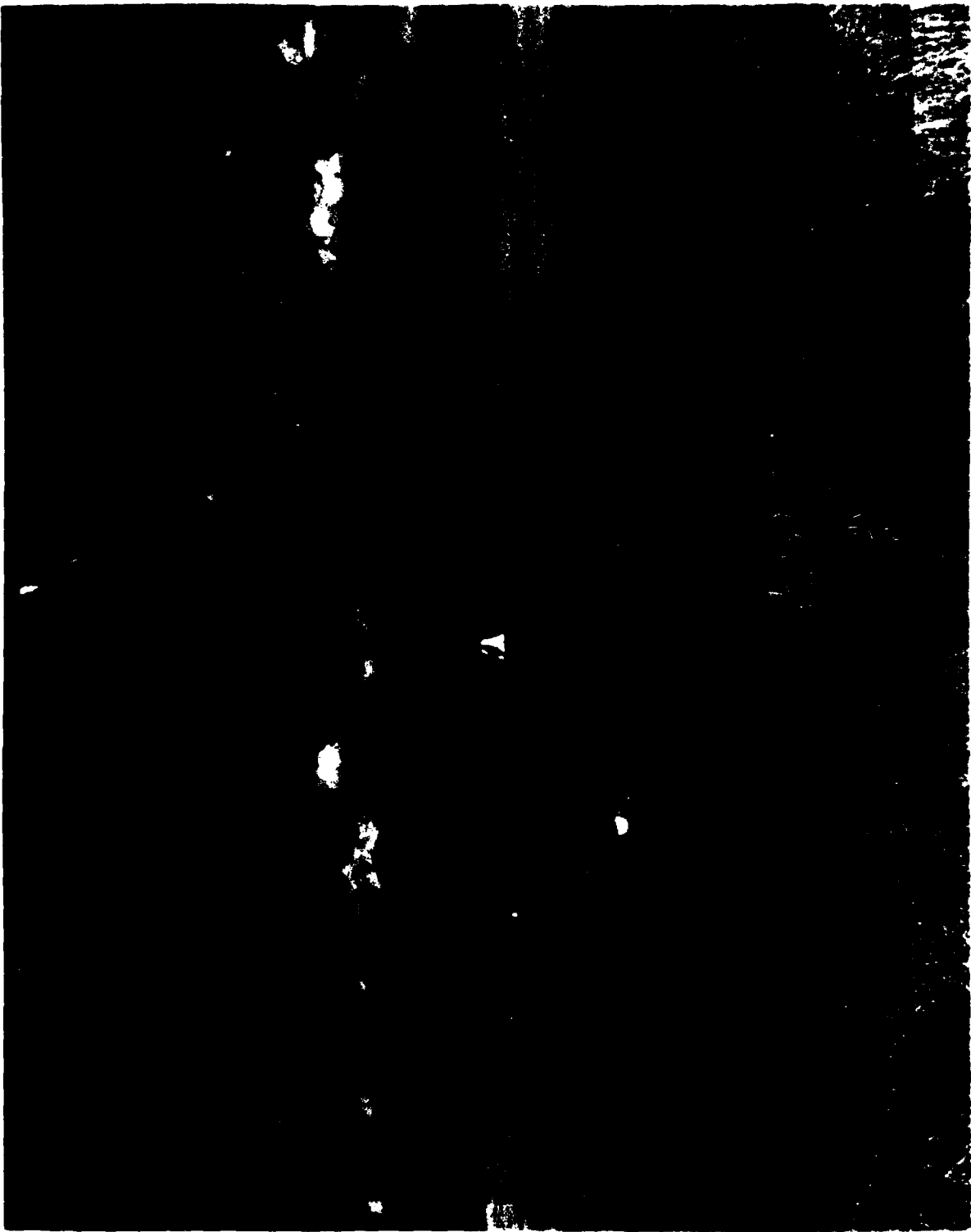
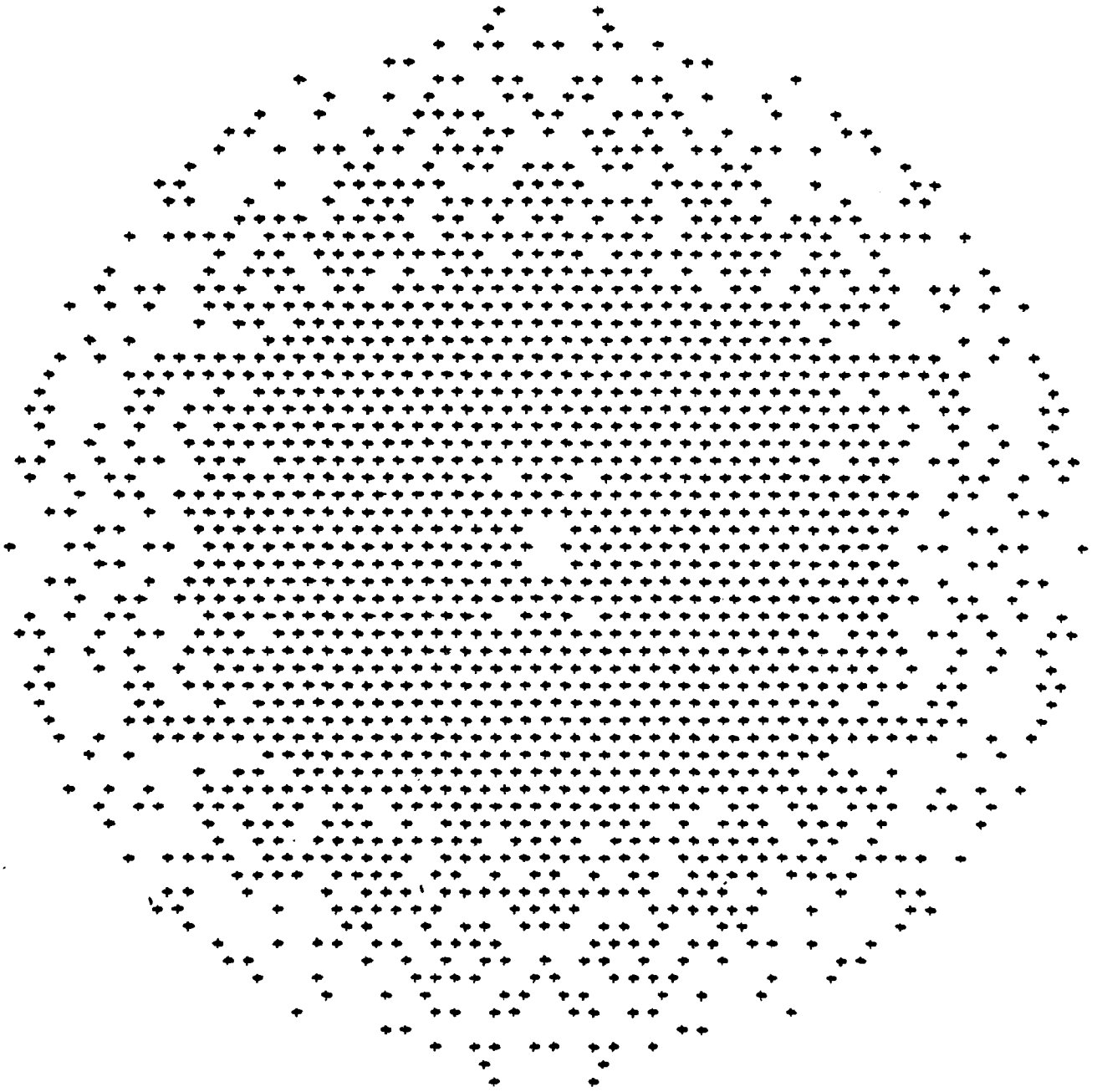


FIG. 1.1 PAVE PAMS - Beale AFB CA



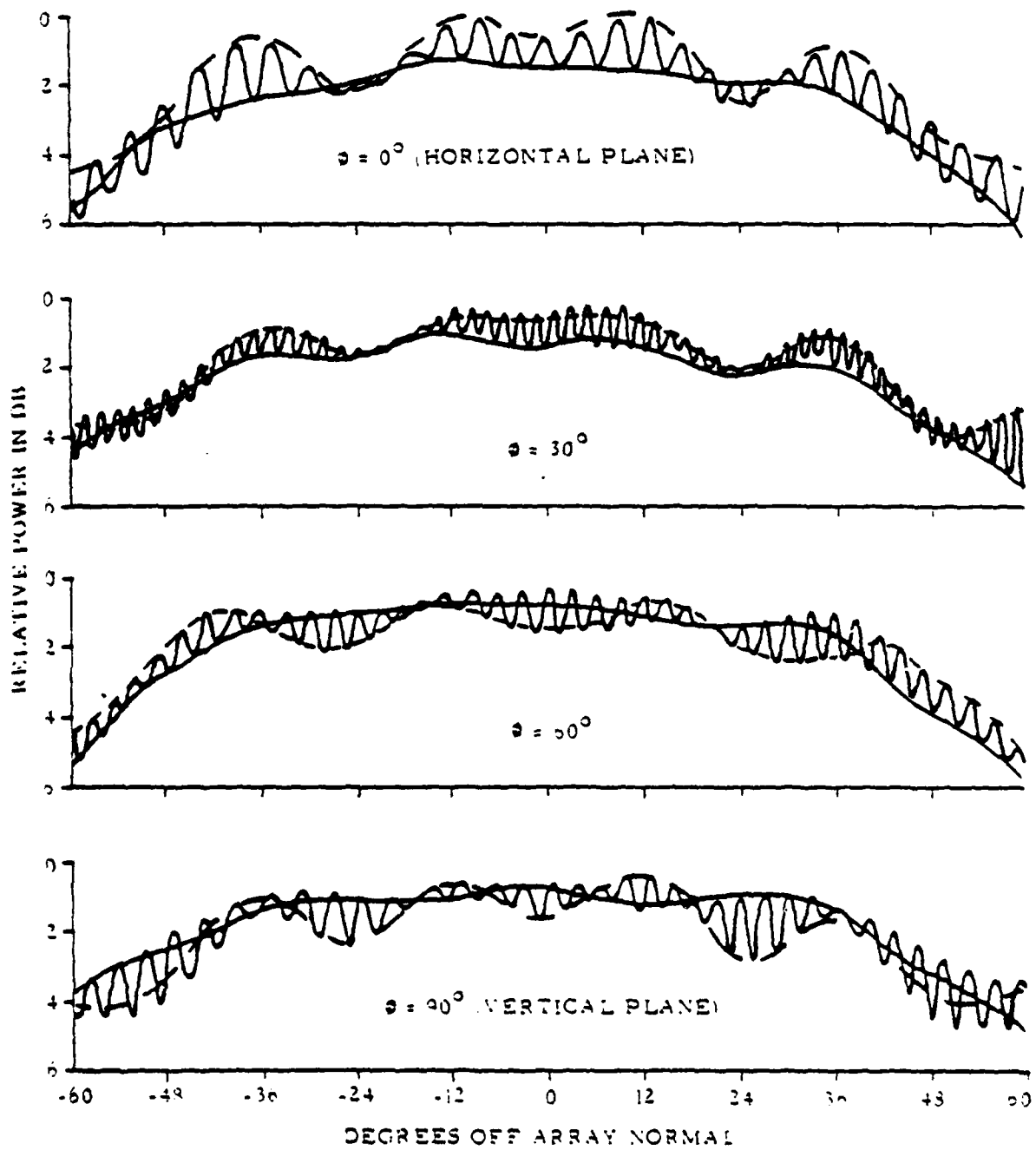
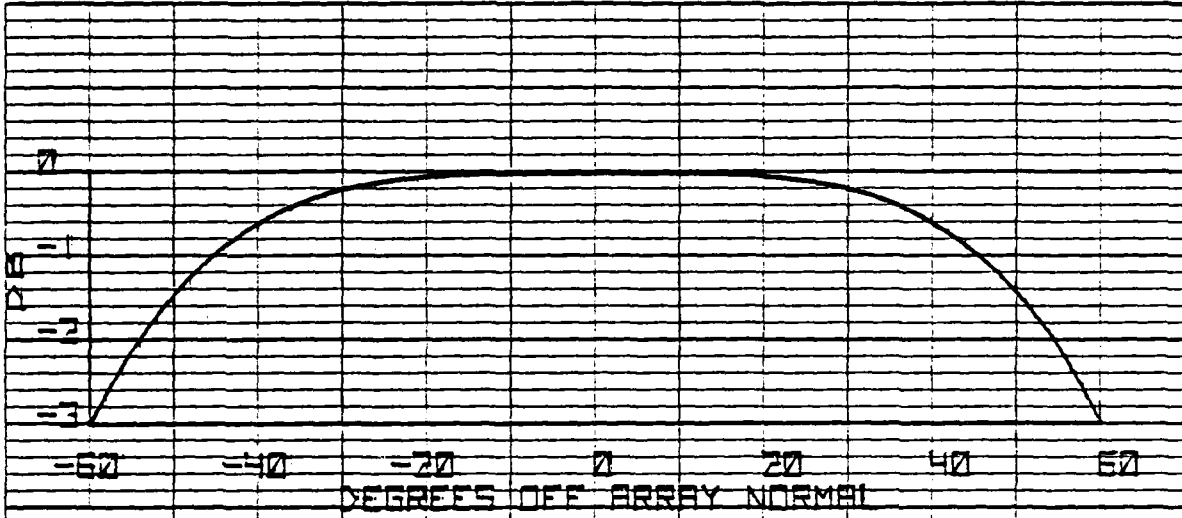
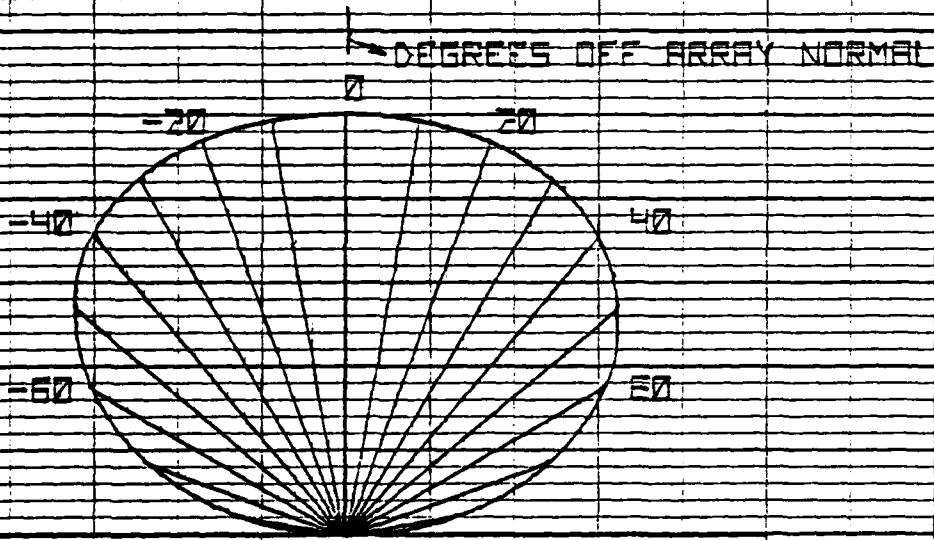


Fig. 2.1 RAYTHEON ELEMENT PATTERN



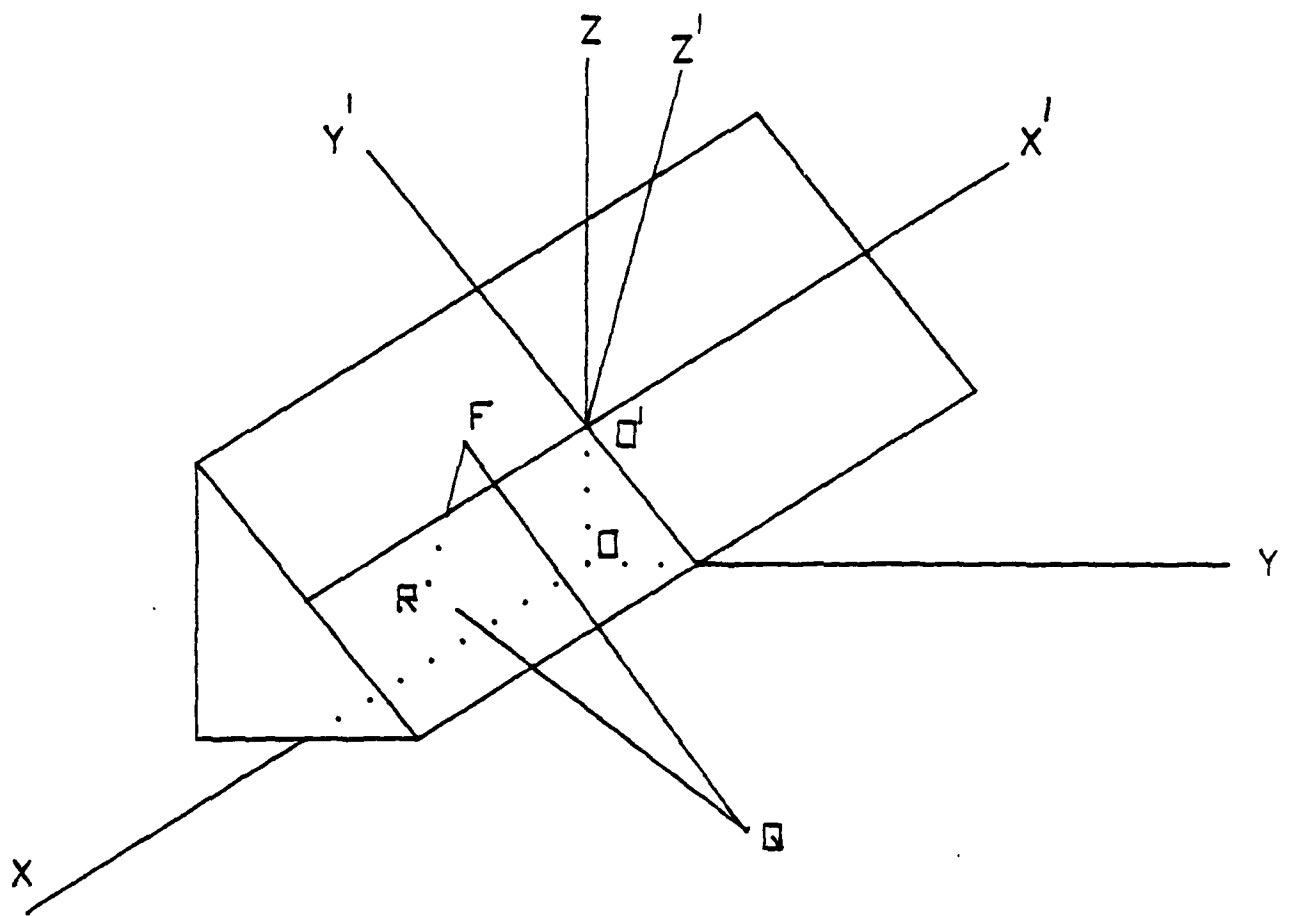
A. RECTANGULAR PLOT



B. POLAR PLOT

FIG 2.2 MIDBAND ELEMENT PATTERN

FIG. 2.3 PAVE PAWS GEOMETRY



NOT TO SCALE

3.0 Air Space Densities: To determine the radiation hazard to personnel, average power density levels were calculated for various samples of space in front of the array. Cases considered were: a) along the main beam axis with the beam radiating on-boresight and off-boresight, b) along the edge of the main beam and c) elevation antenna pattern densities at various azimuths and distances. Spotlight beams i.e. the worst case of a beam fixed in space were considered. It is to be noted that in actual operation the spotlight beam densities would be decreased by the beam motion factor.

3.1 Beam Axial Densities: Figure 3.1 shows the baseline system power density levels along the main beam axis when the radar transmit beam is fixed on array boresight i.e. at 20 degrees elevation and zero degrees azimuth, where azimuth is taken with respect to array boresight. There are three regions apparent: a near field or Fresnel region, a transition region, and a far field or Fraunhofer region. The power density undergoes rapid changes in the near field - the region between the antenna array and the last peak. The last peak with a power density level of 145 milliwatts/centimeter squared is located at a distance R_2 of 500 feet away from the antenna. There are many different power density peaks and nulls in the near field with some peaks higher than the last peak. The highest peak in the near field has a value of 197 milliwatts/centimeter squared and occurs at a distance of R_1 of 79 feet away from the antenna. In the transition region which exists for distances greater than R_2 and lesser than, say, the far field distance of $2D^2/\lambda$ (here - 4646 feet), the power density levels decrease monotonically with distance. A power density level of 10 milliwatts/centimeter squared exists at a distance of 3030 feet. In the far field region the power density levels decrease pretty much with the

distance squared. Figure 3.2 shows the variation of the range exponent n where the power density is taken to vary as the distance raised to the exponent n . The exponent n undergoes rapid changes in sign and magnitude in the near field and monotonically decreases in the transition region. Figure 3.3 is an expanded plot of the previous Figure 3.2. The range exponent approaches an asymptotic value of minus 2, the range exponent value normally used in far field calculations. Figure 3.4 shows the SIX DB system power density levels along the main beam axis for the beam on boresight. Figure 3.4 is similar to Figure 3.1 but the near field is larger and extends to R_2 equal to 976 feet where the last peak is 151 milliwatts/centimeter squared. The near field highest peak is higher, has a value of 248 milliwatts/centimeter squared and occurs at a distance R_1 of 50 feet. Figures 3.5, 3.6, and 3.7 show the power density levels along the main beam axis with the radar beam in the mid position of the surveillance fence i.e. at 3 degrees elevation and zero degrees azimuth with respect to boresight for the baseline system, the SIX DB system and the 10 DB system, respectively. It is to be noted that even in the 10 DB system case (where the antenna aperture is filled and with uniform excitation) the near field exhibits many different power density peaks and valleys. Figures 3.8 and 3.9 show the power density levels along the main beam axis when the radar transmit beam is off boresight at 60 degrees azimuth and 20 degrees elevation and 3 degrees elevation, respectively. As the beam axis moves away from the boresight position, the last power density peak, the start of the transition region, moves in closer to the array and increases in magnitude. As the antenna radiating aperture increases the extent of the near field increases. Table 3.1 shows the beam axis power density levels for the fixed beam at different azimuths and

elevations. The peaks in the near field which are higher than the last peak are designated P1. The P1 peaks occur at distances of R1. The peaks designated P2 occur at the distance R2, the start of the transition region. The distances at which the power density levels of 10 milliwatts/centimeter squared occur are indicated by R3. Dashes in Table 3.1 indicate no P1 peaks and indicate no data in the R3 column.

Table 3.1. Beam Axial Density

System	Beam		R1	P1	R2	P2	R3
	Azimuth	Elevation					
	Degrees	Degrees	Feet	Mw/cm	Feet	Mw/cm	Feet
Baseline	0	20	79	197	500	145	3038
Baseline	0	3	24	175	478	157	3035
Baseline	40	20	28	231	398	187	2994
Baseline	60	3	-	-	199	218	2333
Six DB	0	20	50	248	976	151	-
Six DB	0	3	67	174	936	164	-
Six DB	60	20	-	-	378	228	4673
10 DB	0	3	-	-	1124	270	8707

3.2 Edge of Beam Densities: Figures 3.10, 3.11, and 3.12 show the edge of beam power density variation with distance for the baseline, SIX DB, and 10 DB systems, respectively. The beam was defined here as in T.O 31Z-10-4 "Radiation Hazards" which defines the beam as a cylinder with about the same size as the projected area of the aperture. The edge of the beam considered here is the top edge of the beam. The power density does not remain constant in any of the regions but changes rapidly with

many peaks and valleys showing the effects of the constructive and destructive interference from the individual radiating antenna element sources. The edge of the beam densities for the baseline and SIX DB systems change most rapidly within the first 60 feet (approximately) distance from the antenna reaching a highest peak of 67.6 milliwatts/centimeter squared at a distance of 31.5 feet from the antenna for the baseline system and a highest peak of 72.2 milliwatts/centimeter squared at a distance of 25 feet from the antenna for the SIX DB system. The 10 DB system edge of beam densities vary less violently with distance with the highest peak of 28 milliwatts/centimeter squared occurring at a distance of 14.5 feet from the antenna. The density level of 10 milliwatts/centimeter squared occurs at a distance of 2540 feet from the antenna for the baseline system and 5050 feet for the SIX DB system.

3.3 Elevation Antenna Pattern Densities: Figures 3.13 through 3.22 show the baseline system elevation antenna pattern average power densities at the midband frequency for various distances from the antenna and for the transmit beam at zero degrees azimuth and 3 degrees elevation. Figures 3.23 through 3.29 and figures 3.30 through 3.35 are similar plots for the SIX DB and 10 DB systems, respectively. The beam formation is evident as one progresses through the near field, the transition region into the far field. In the near field region the beam is not yet formed, the beam is much wider than the far field beamwidth and the pattern has higher sidelobes. The upper limit of the elevation angular extent over which the power density is greater than or equal to 10 milliwatts/centimeter squared is plotted as a function of distance from the antenna in figures 3.36, 3.37 and 3.38 for the baseline, SIX DB and the 10 DB systems, respectively. This elevation angular extent varies

inversely with distance. Thus the baseline system upper elevation limit is 15 degrees for the 145 feet distance, 9 degrees for the 290 feet distance and 6 degrees for the 580 feet distance. A similar effect occurs for the case of the azimuth patterns where e.g. the azimuth angular extent over which the baseline power density is equal to greater than 10 milliwatts/centimeter squared occurs between plus and minus 6.5 degrees for the distance of 290 feet, 3.4 degrees for the distance of 580 feet and 1.8 degrees for the distance of 1161 feet when the beam is at zero degrees azimuth and 20 degrees elevation. For the same distances from the antenna the elevation angular extent widens as the aperture increases in size and in number of radiators.

3.4 Air Hazard: Based on a worst case assumption (spotlight boresight beam), the air hazard zone in front of the radar for airborne personnel is a zone extending over an azimuth sector of 240 degrees (120 degrees per Face) and with a radius equal to approximately 3035 feet for the present baseline PAVE PAWS radar system, 6140 feet for the SIX DB system, if implemented, and 8710 feet for the possible 10 DB system. This worst case assumes a stationary boresight radar beam and makes no allowance for off-boresight losses and no allowance for the possible shielding effect of the aircraft.

FIG. 3.1 BORESIGHT BEAM DENSITY
VS BEAM AXIS DISTANCE

BASELINE SYSTEM
435 MHZ
344 PEAK WATTS/MODULE
BEAM AT 20 DEG ELEVATION
0 DEG AZIMUTH

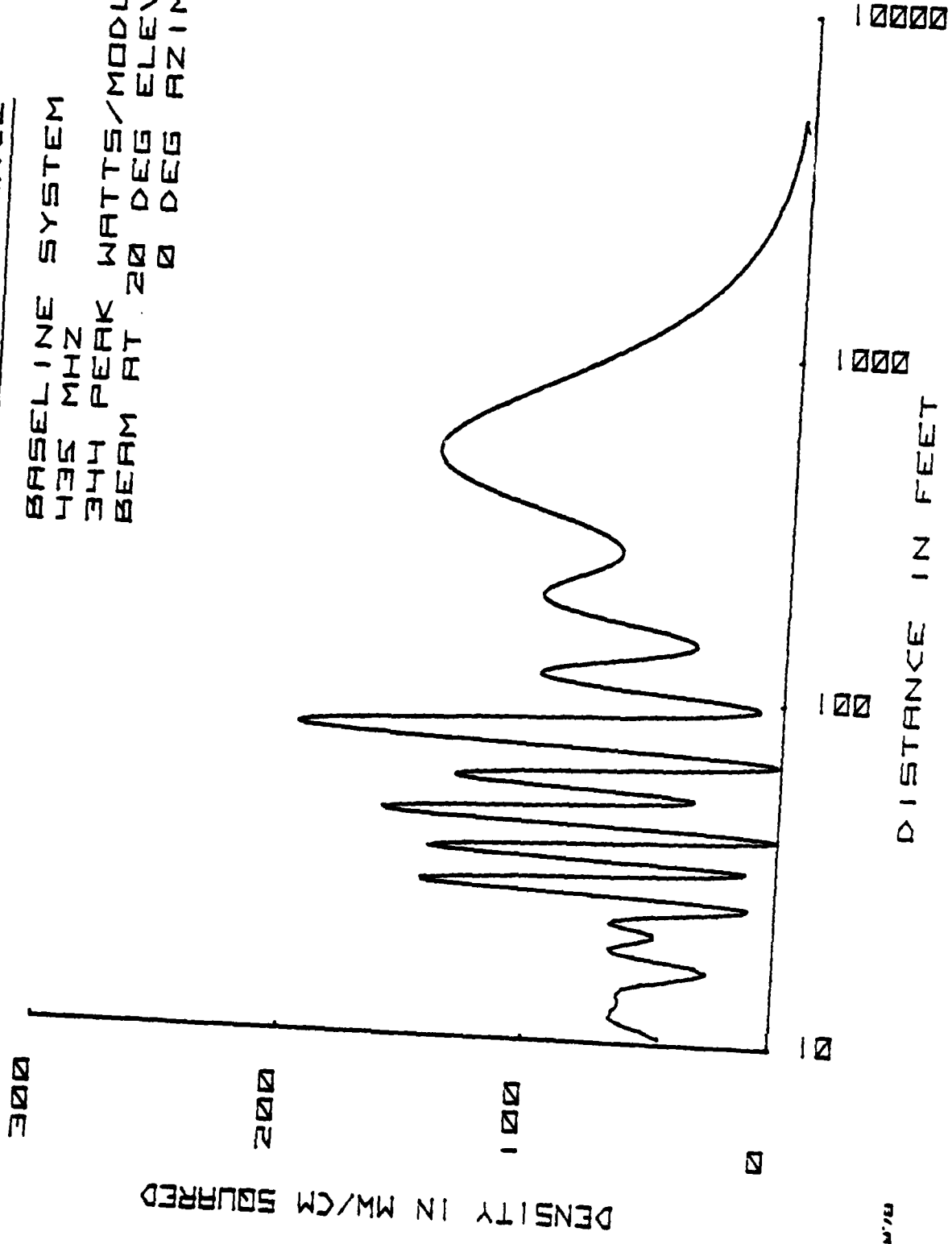
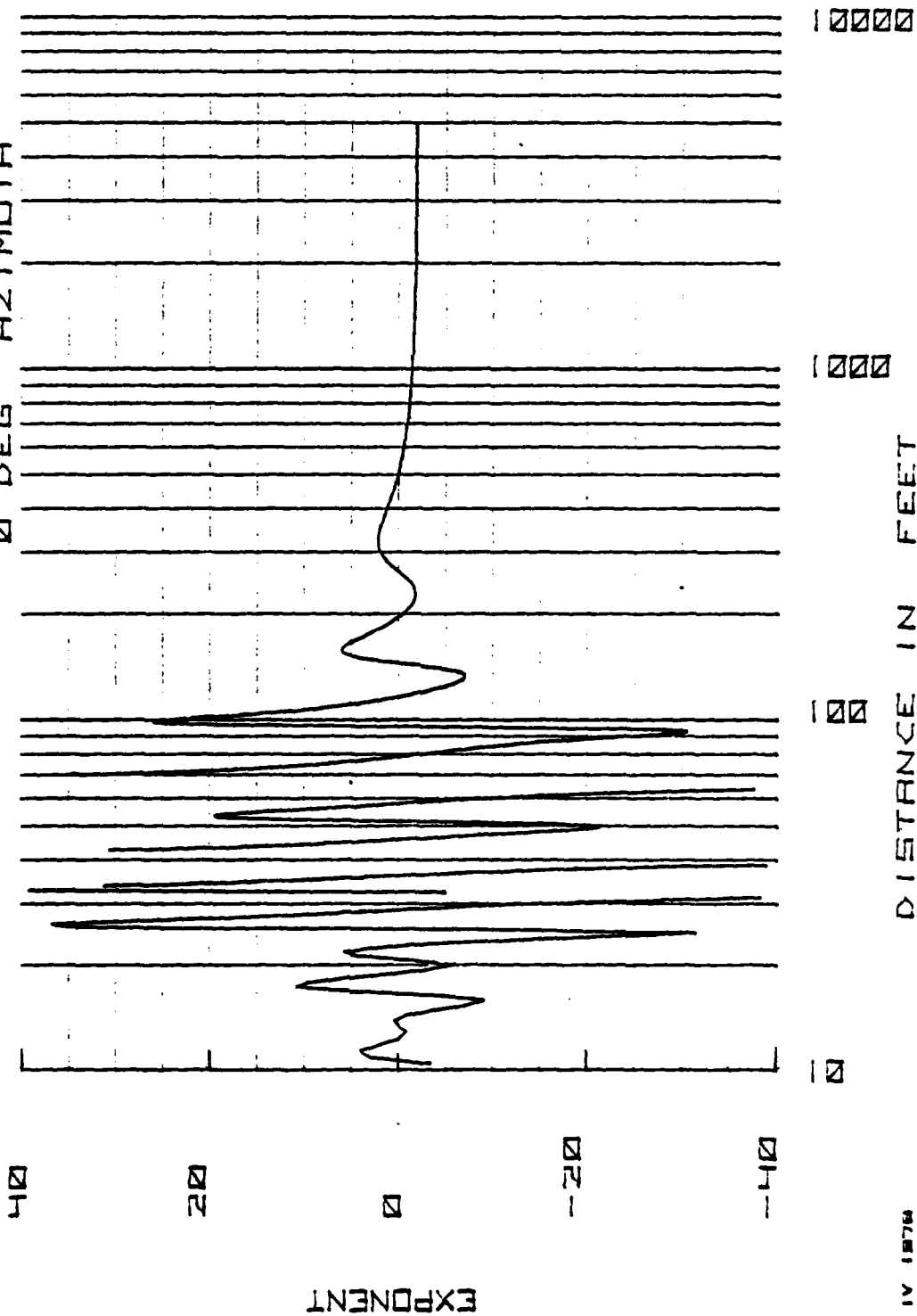


FIG 3.2 BEAM AXIS RANGE EXPONENT

BASELINE SYSTEM
435 MHZ
344 PPK WATTS/MODULE
BEAM AT 20 DEG ELEVATION
0 DEG AZIMUTH

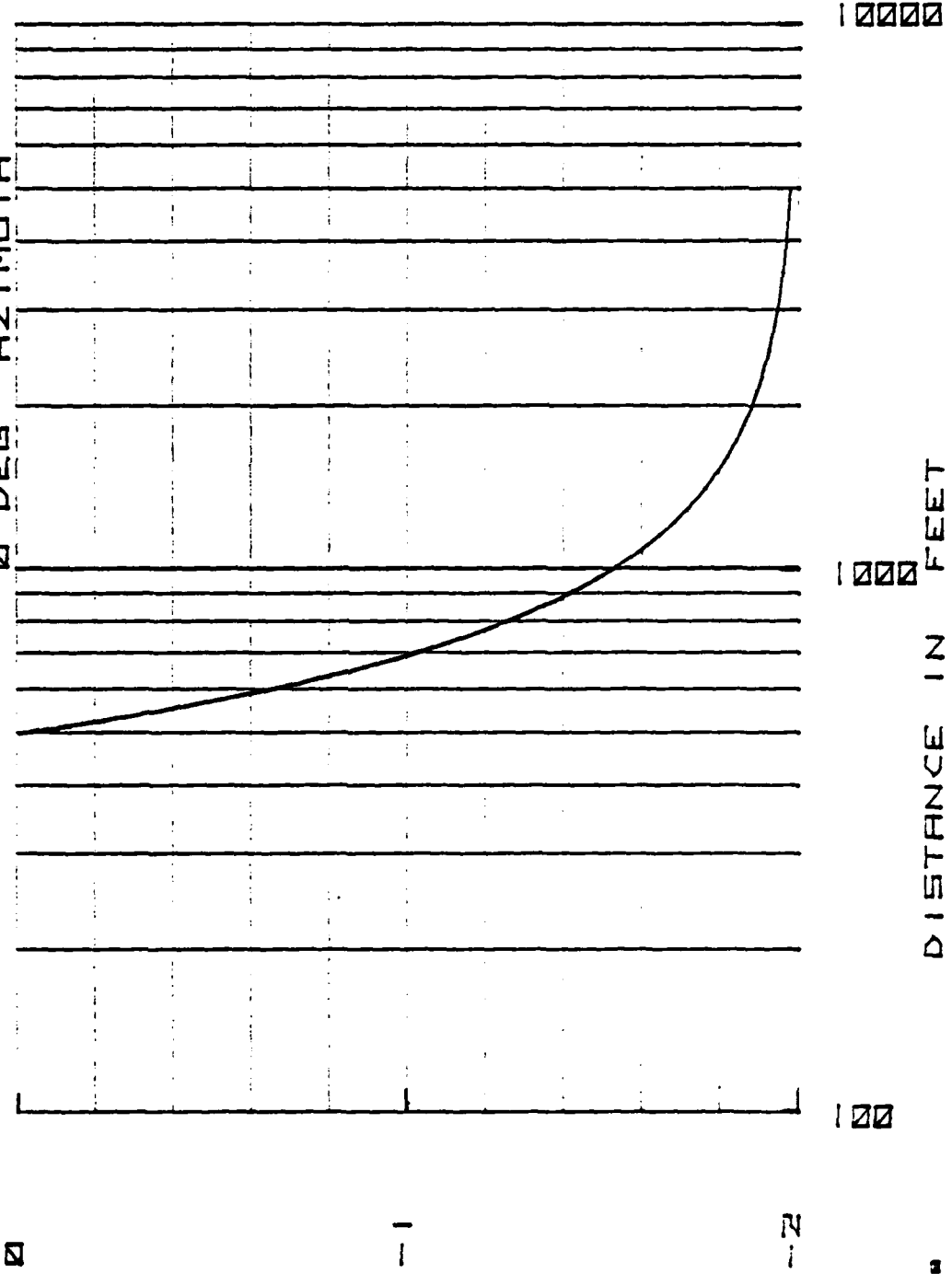


EXPONENT

16 IV 1976

FIG 3.3 BEAM AXIS RANGE EXPONENT

BASELINE SYSTEM
435 MHZ
344 PEAK WATTS/MODULE
BEAM AT 20 DEG ELEVATION
0 DEG AZIMUTH

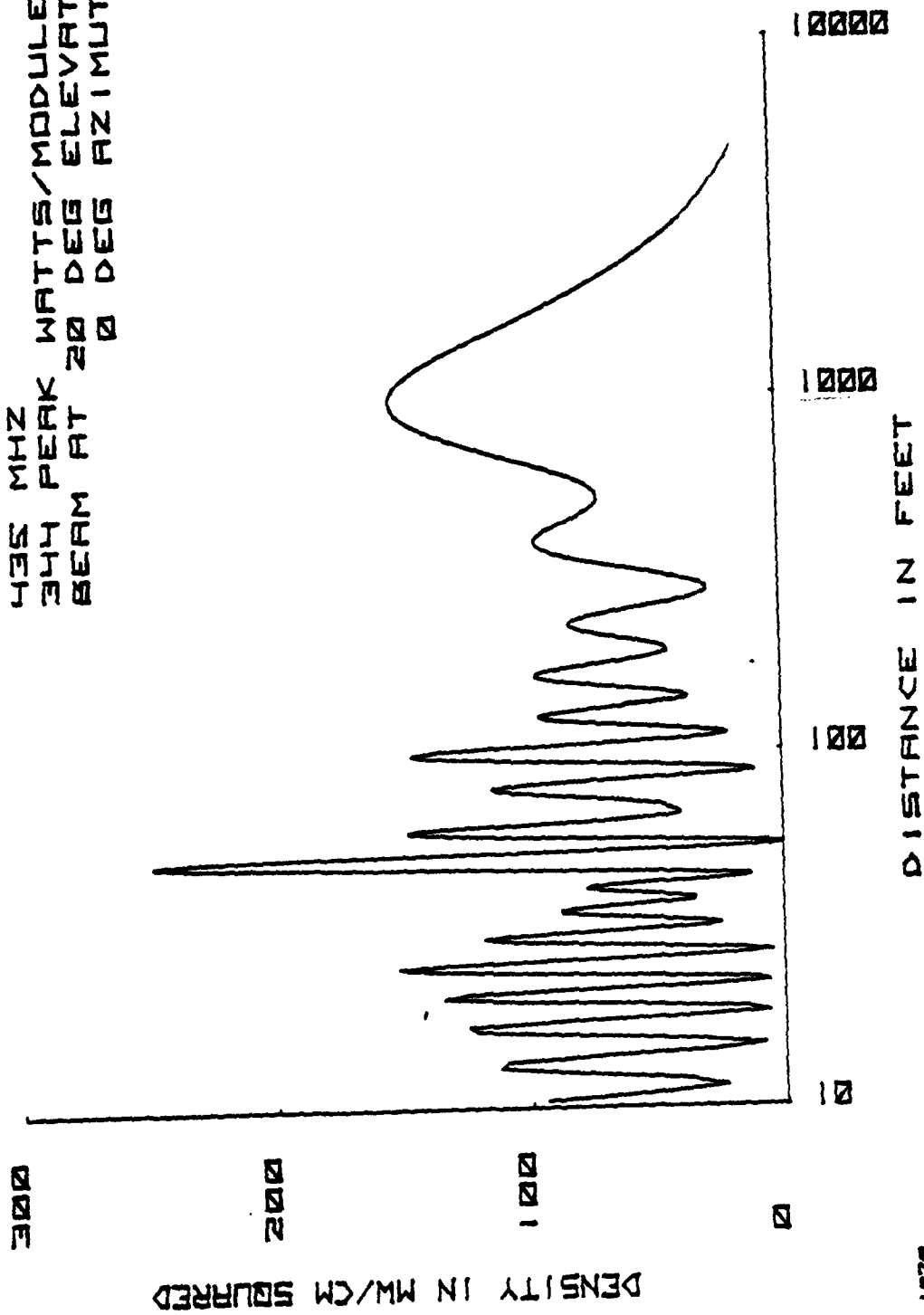


EXPONENT

10 IV 1978

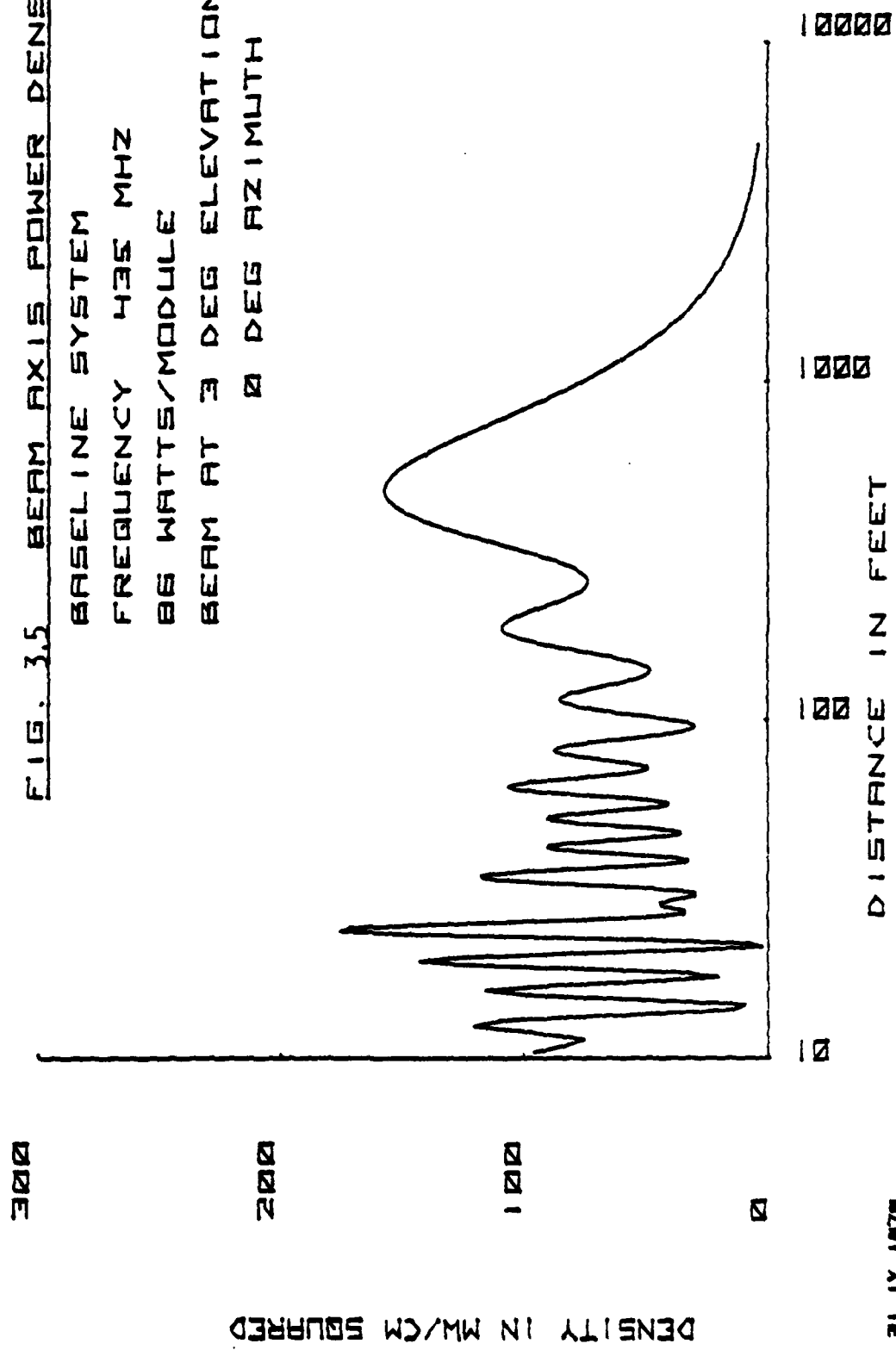
FIG. 3.4 BORISIGHT BEAM DENSITY
VS BEAM AXIS DISTANCE

SIX DB SYSTEM
435 MHZ
344 PEAK WATTS/MODULE
BEAM AT 20 DEG ELEVATION
0 DEG AZIMUTH



17 IV 1978

FIG. 3.5 BEAM AXIS POWER DENSITY
 BASELINE SYSTEM
 FREQUENCY 435 MHZ
 86 WATTS/MODULE
 BEAM AT 3 DEG ELEVATION
 0 DEG AZIMUTH



DENSITY IN MW/CM SQUARED

DISTANCE IN FEET

21 IV 1978

3000

2000

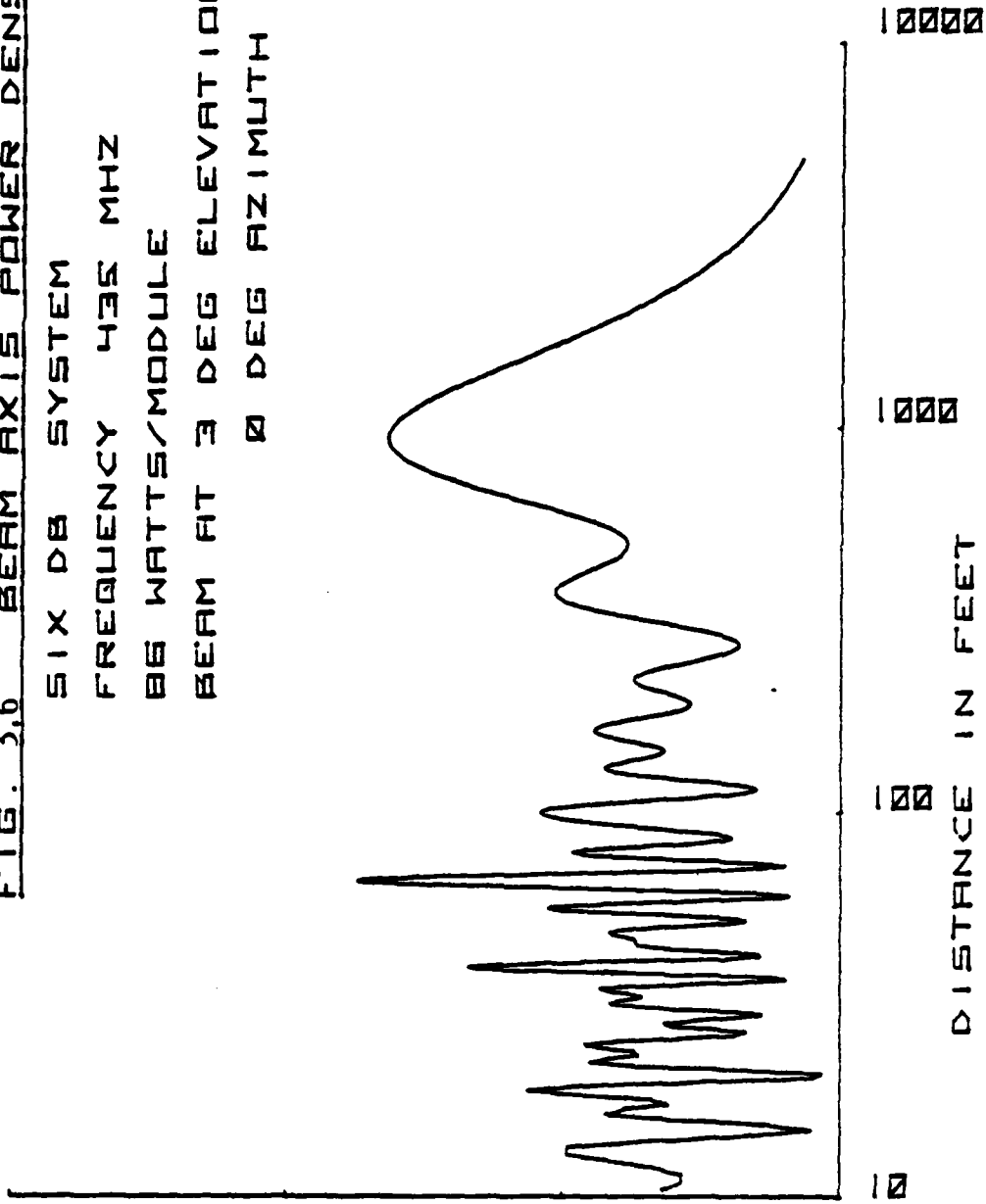
1000

0

DENSITY IN MW/CM SQUARED

FIG. 3.6 BEAM AXIS POWER DENSITY

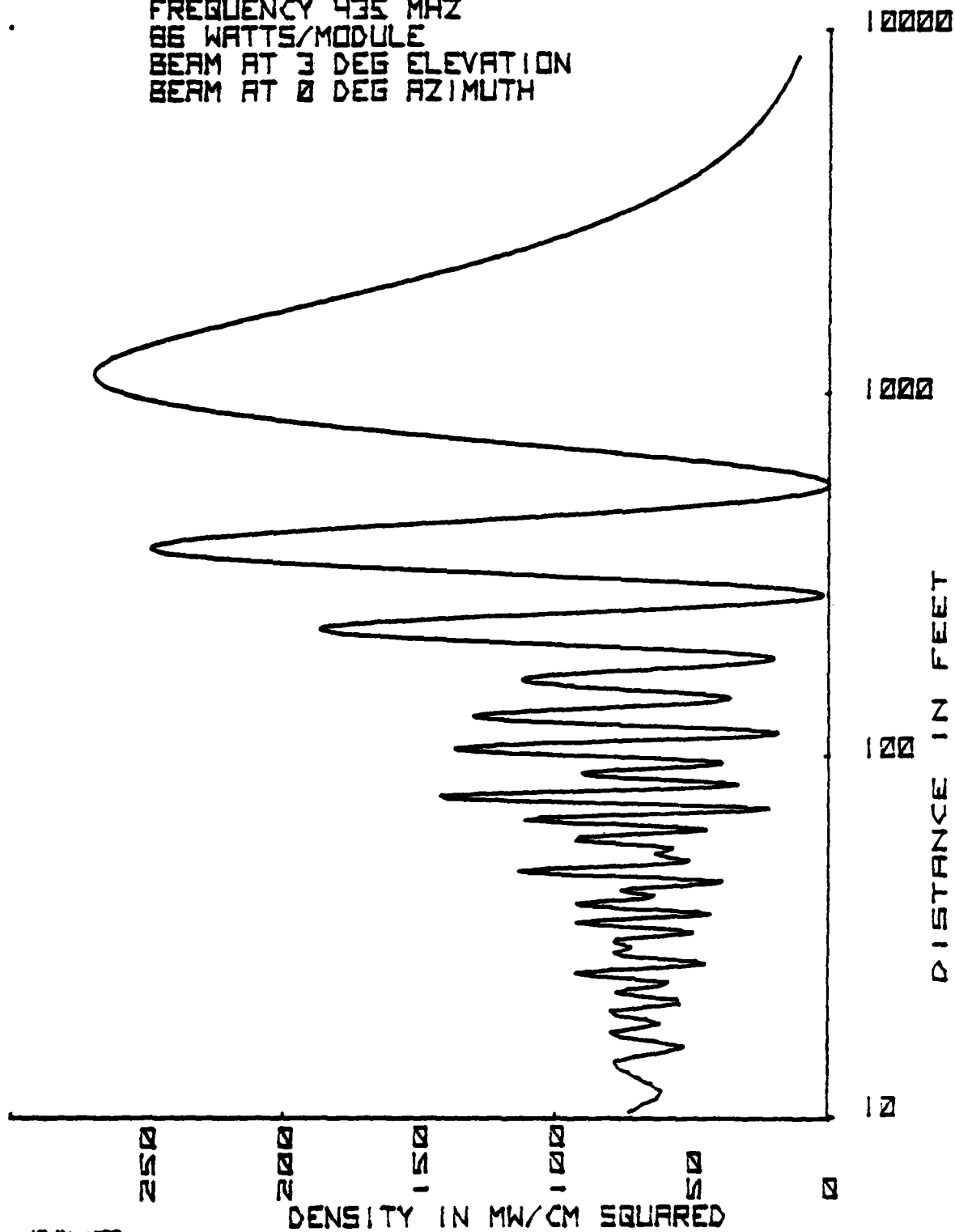
SIX DB SYSTEM
FREQUENCY 435 MHZ
86 WATTS/MODULE
BEAM AT 3 DEG ELEVATION
0 DEG AZIMUTH



1 VI 1878

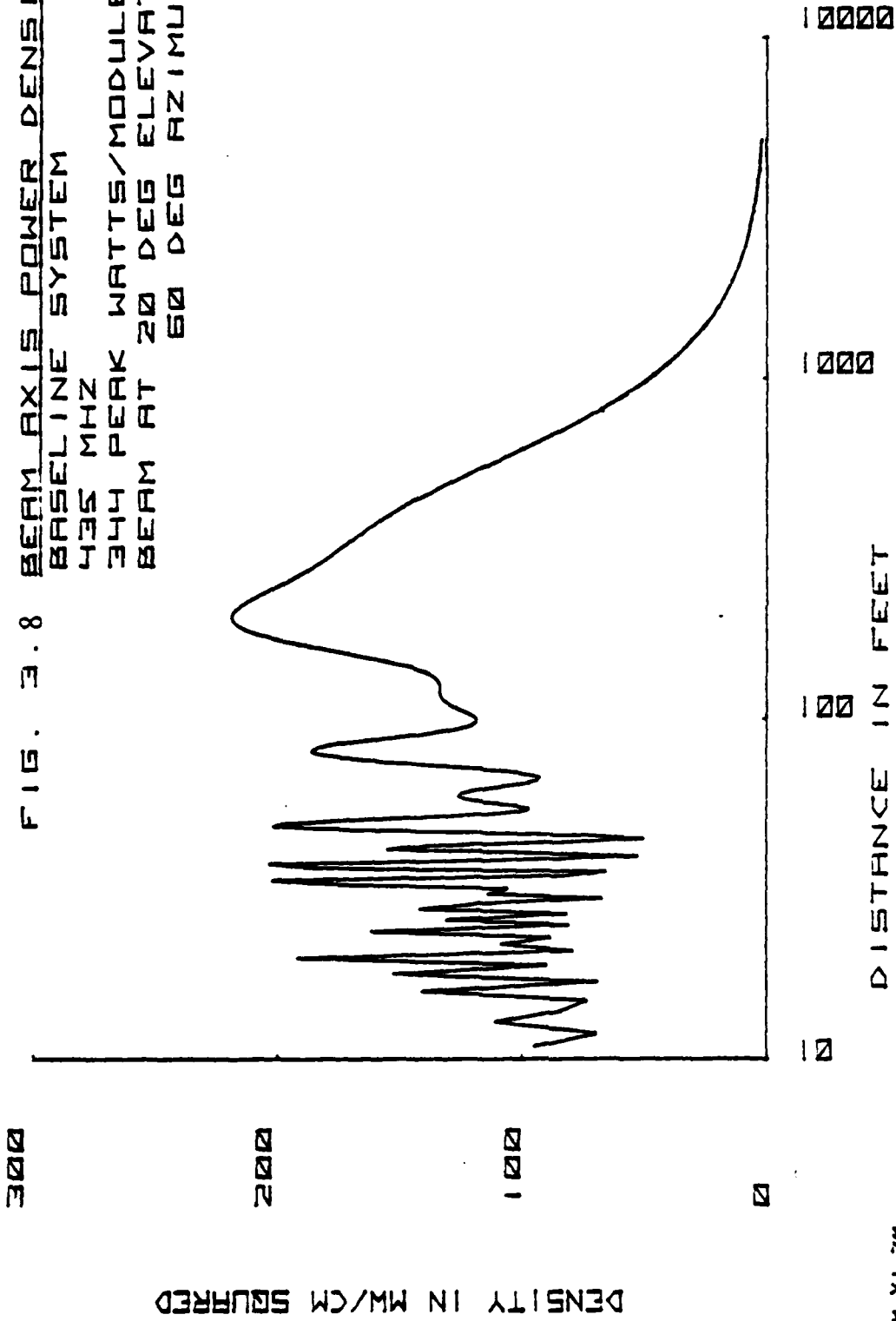
FIG. 3.7 BEAM AXIS POWER DENSITY

10 DB SYSTEM
FREQUENCY 435 MHZ
86 WATTS/MODULE
BEAM AT 3 DEG ELEVATION
BEAM AT 0 DEG AZIMUTH



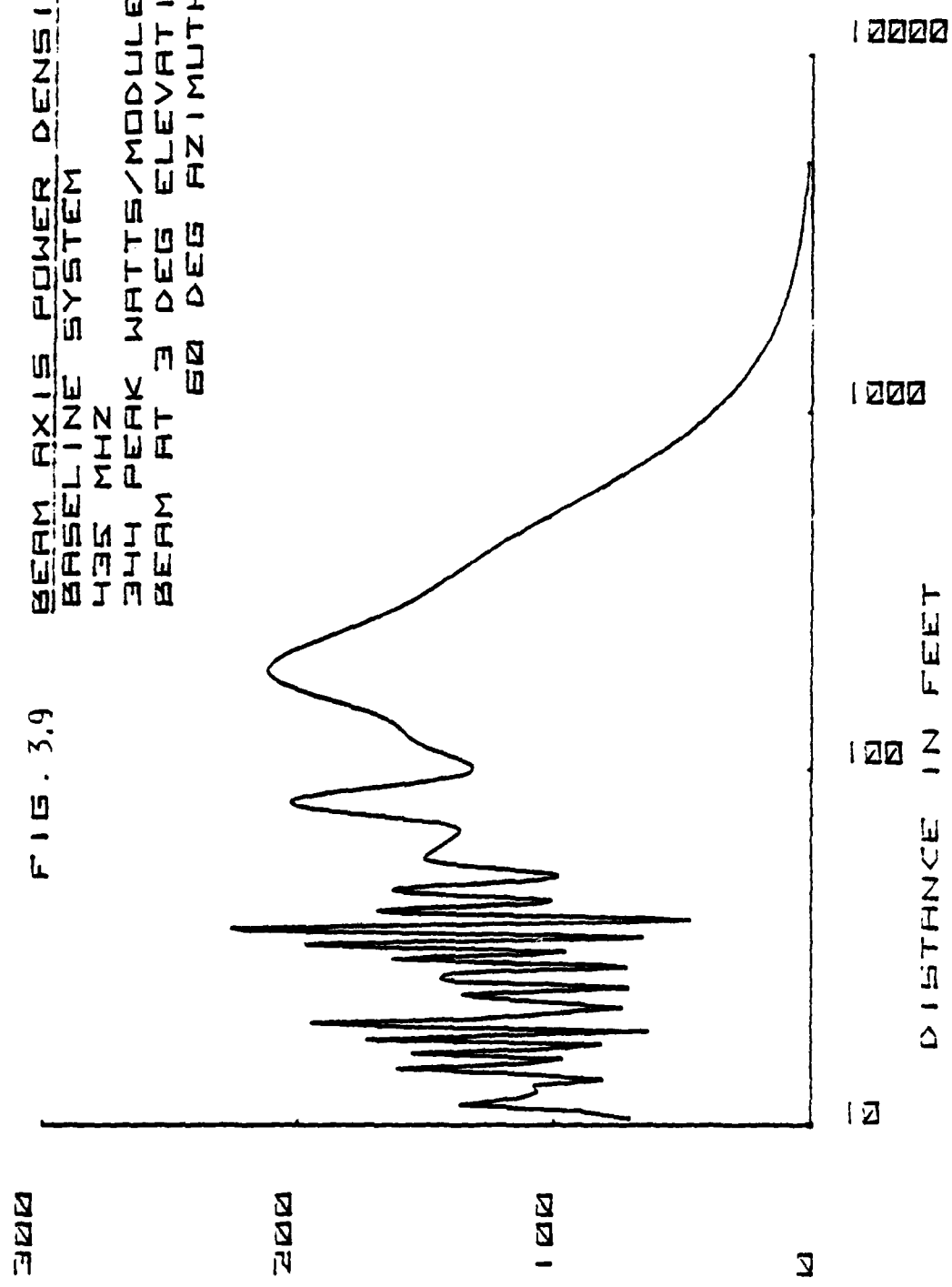
13 71 1070

FIG. 3.8 BEAM AXIS POWER DENSITY
 BASELINE SYSTEM
 435 MHZ
 344 PEAK WATTS/MODULE
 BEAM AT 20 DEG ELEVATION
 60 DEG AZIMUTH



BEAM AXIS POWER DENSITY
 BASELINE SYSTEM
 435 MHZ
 344 PEAK WATTS/MODULE
 BEAM AT 3 DEG ELEVATION
 60 DEG AZIMUTH

FIG. 3.9



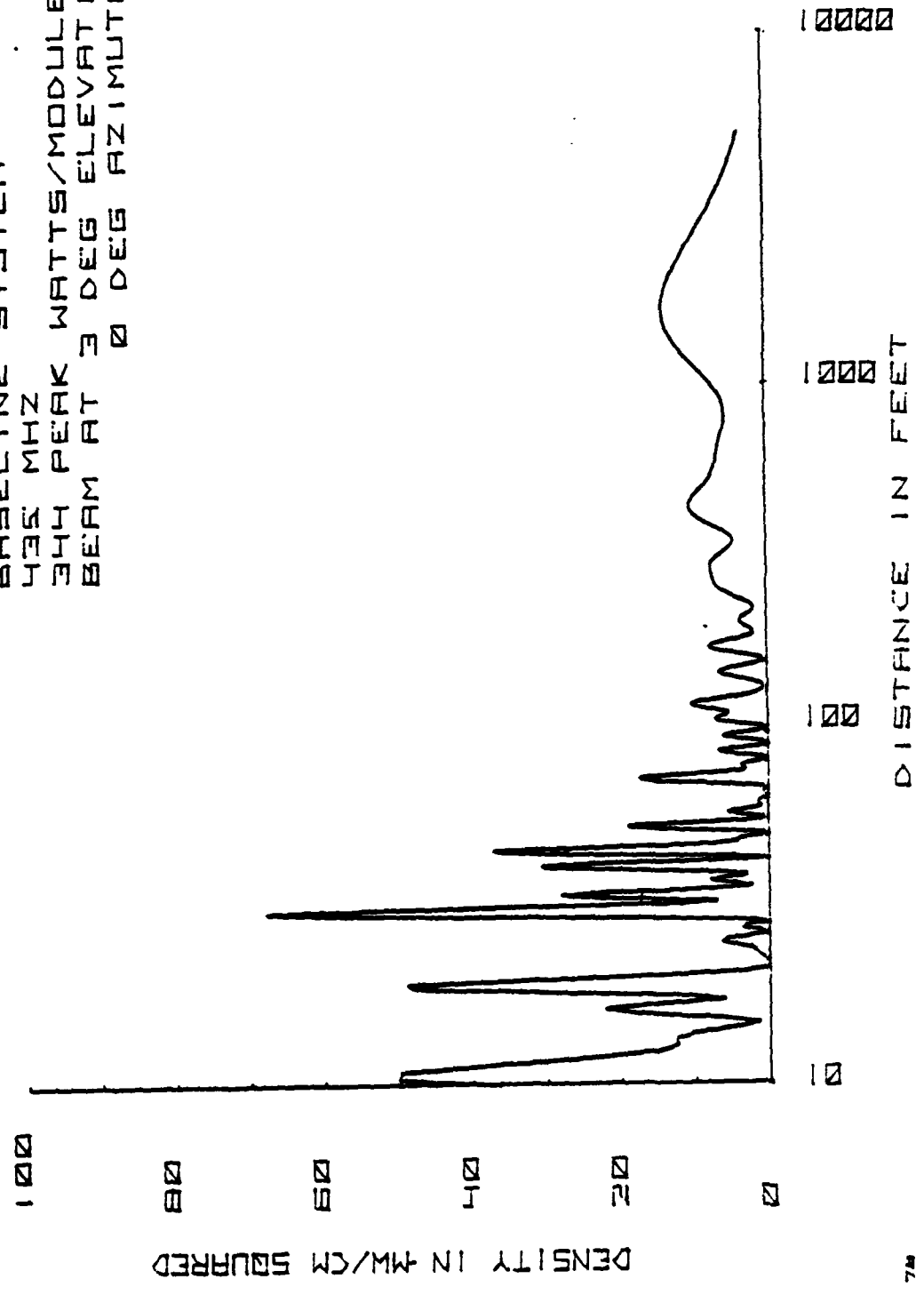
DENSITY IN MW/CM SQUARED

DISTANCE IN FEET

IN VI 72

FIG. 3.10 EDGE BEAM DENSITY VS DISTANCE

BASELINE SYSTEM
435 MHZ
344 WATTS/MODULE
BEAM AT 3 DEG ELEVATION
0 DEG AZIMUTH



345 IV 74

FIG. 3.11 EDGE BEAM DENSITY VS DISTANCE

SIX DB SYSTEM
435 MHZ
344 PEAK WATTS/MODULE
BEAM AT 3 DEG ELEVATION
0 DEG AZIMUTH

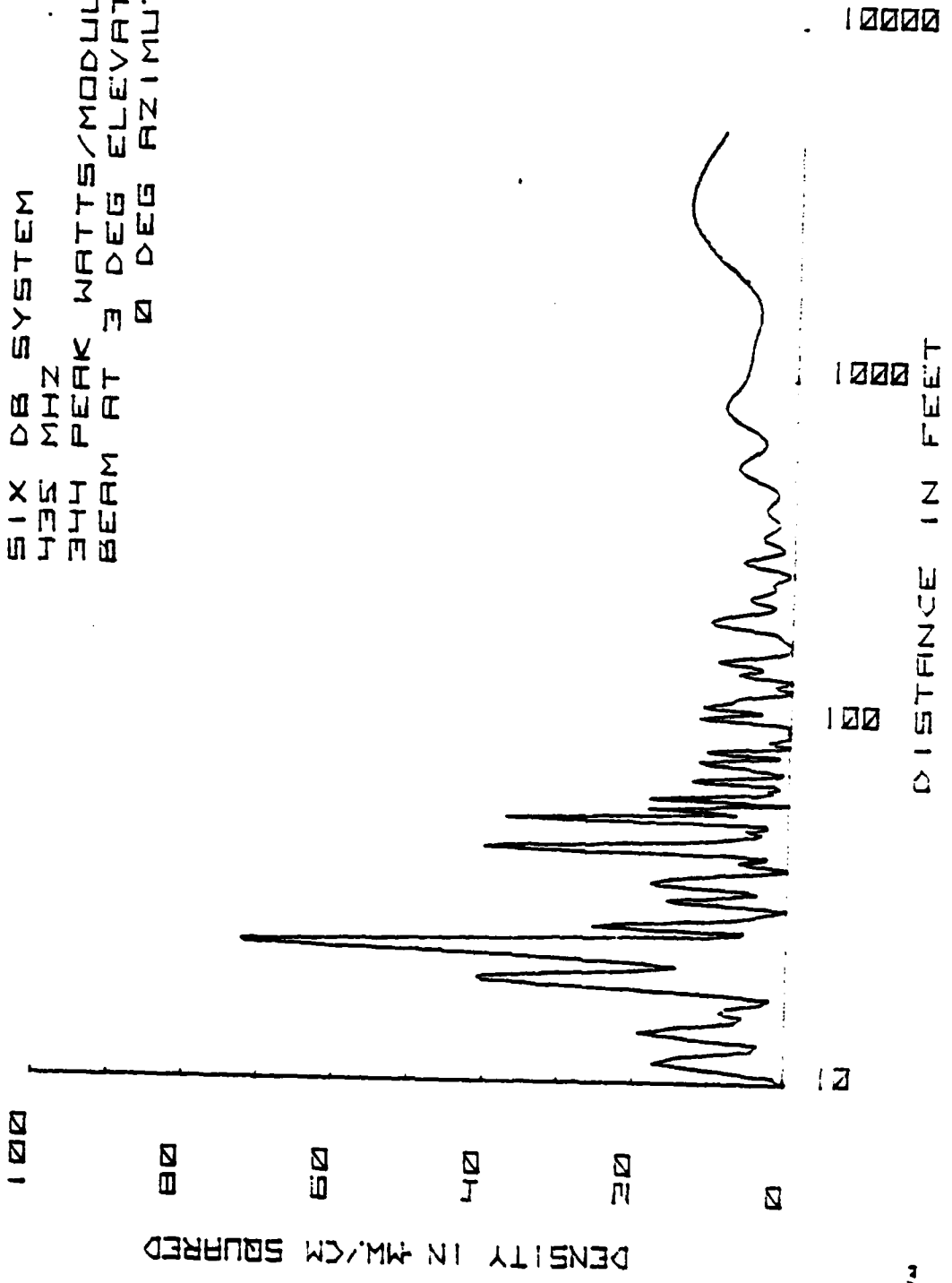
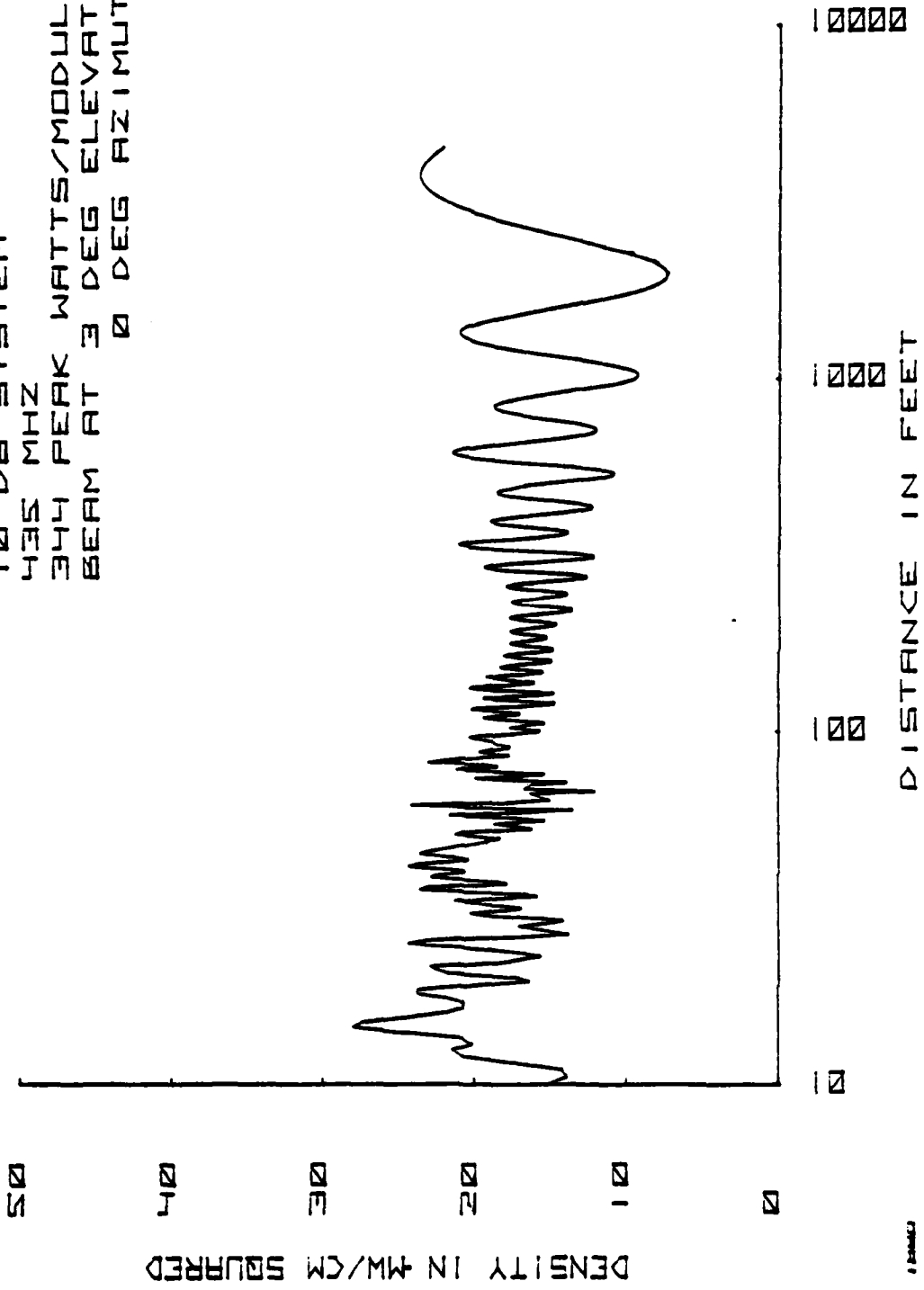
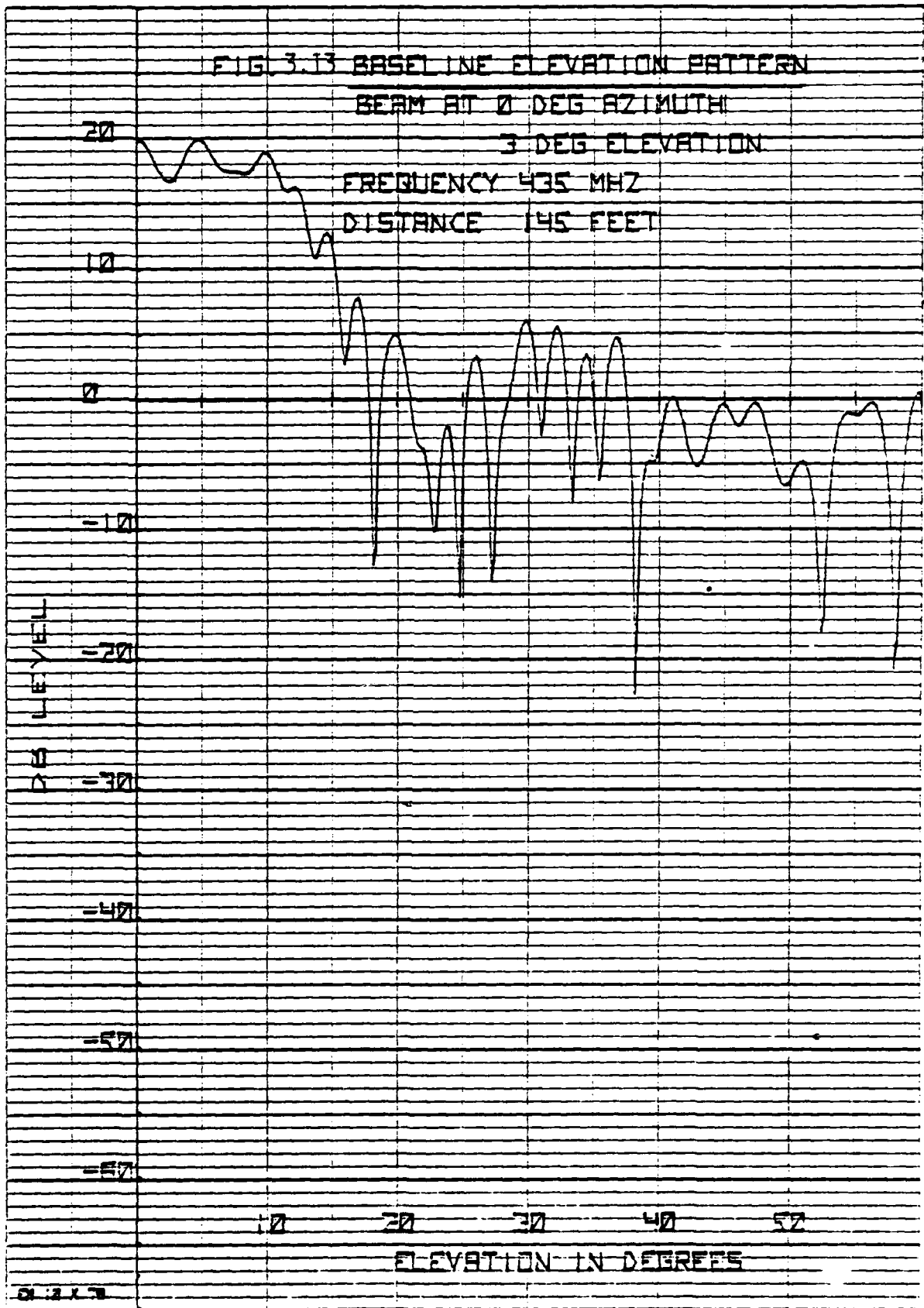


FIG. 3.12 EDGE BEAM DENSITY VS DISTANCE

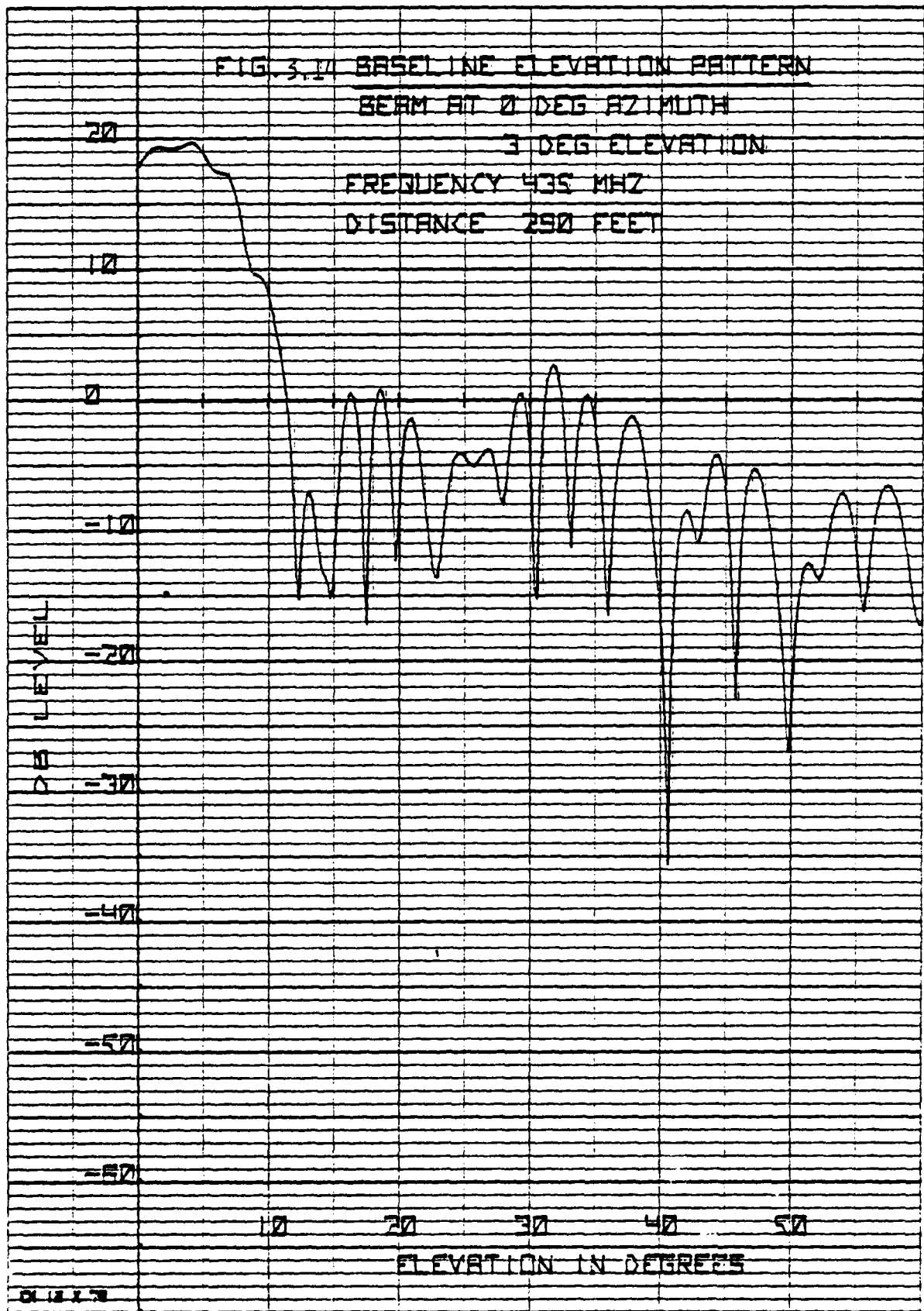
10 DB SYSTEM
435 MHZ
344 PEAK WATTS/MODULE
BEAM AT 3 DEG ELEVATION
0 DEG AZIMUTH



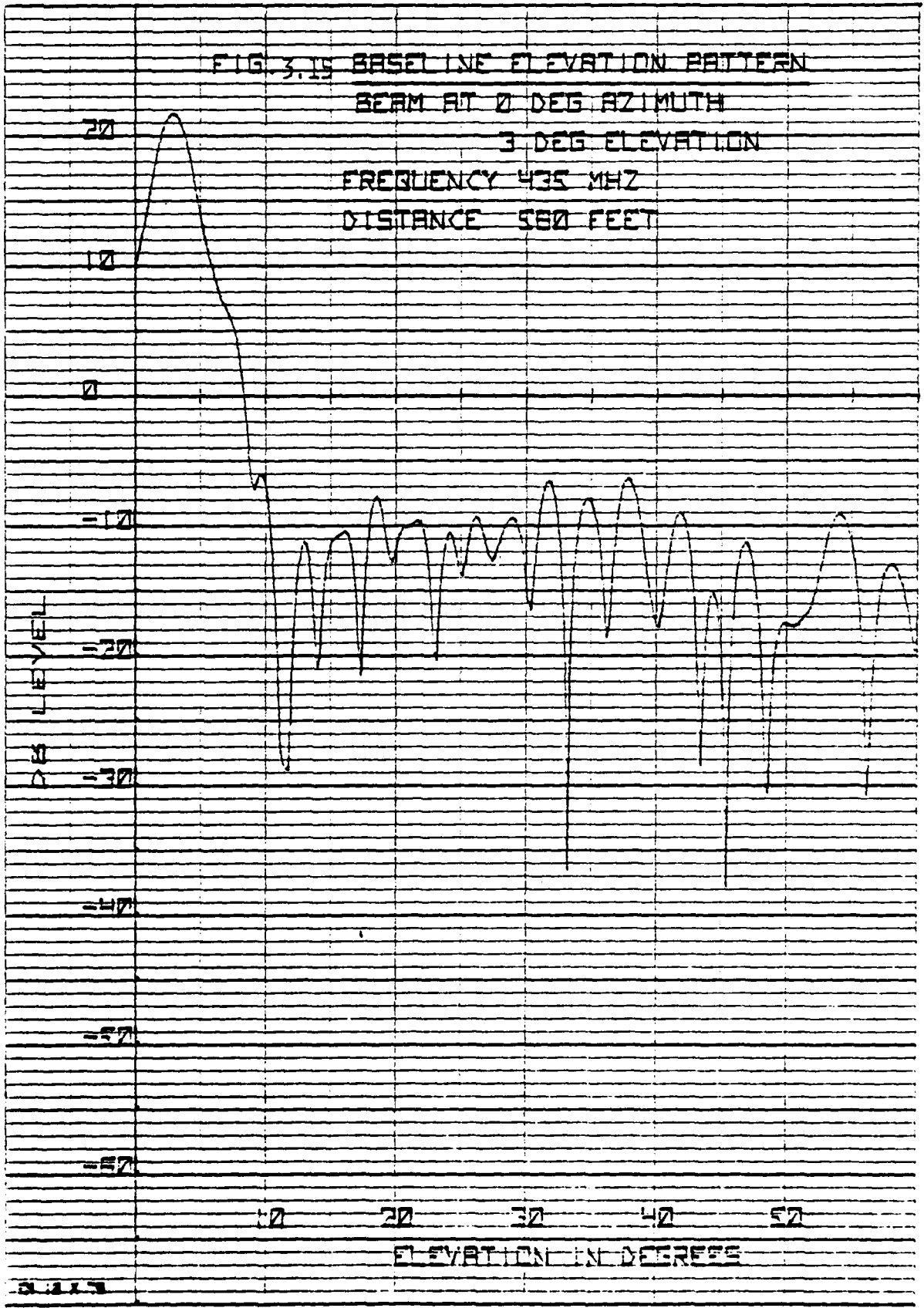
HEWLETT PACKARD 82701004

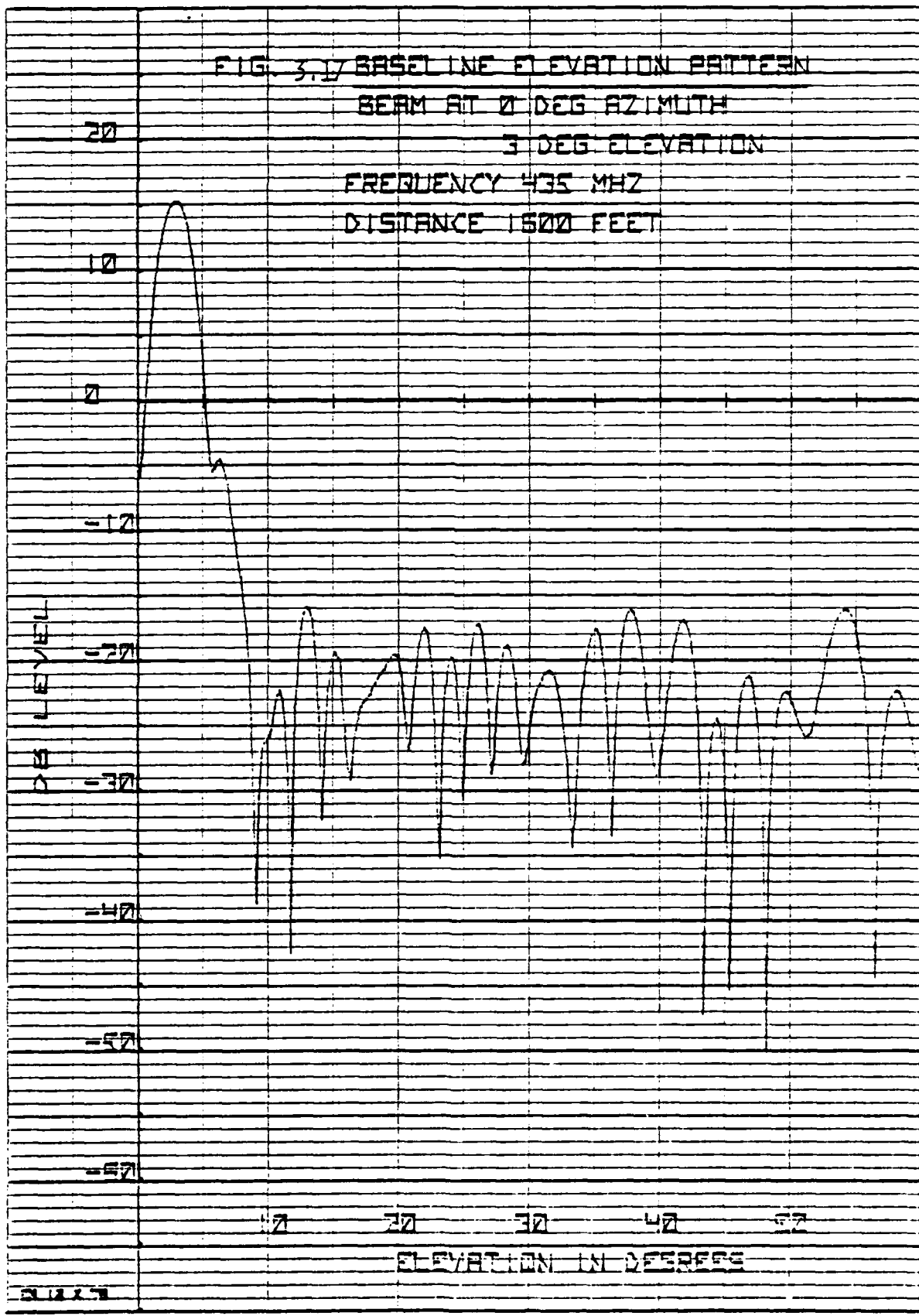


16W111 PAK-KARD 0270 NOV64

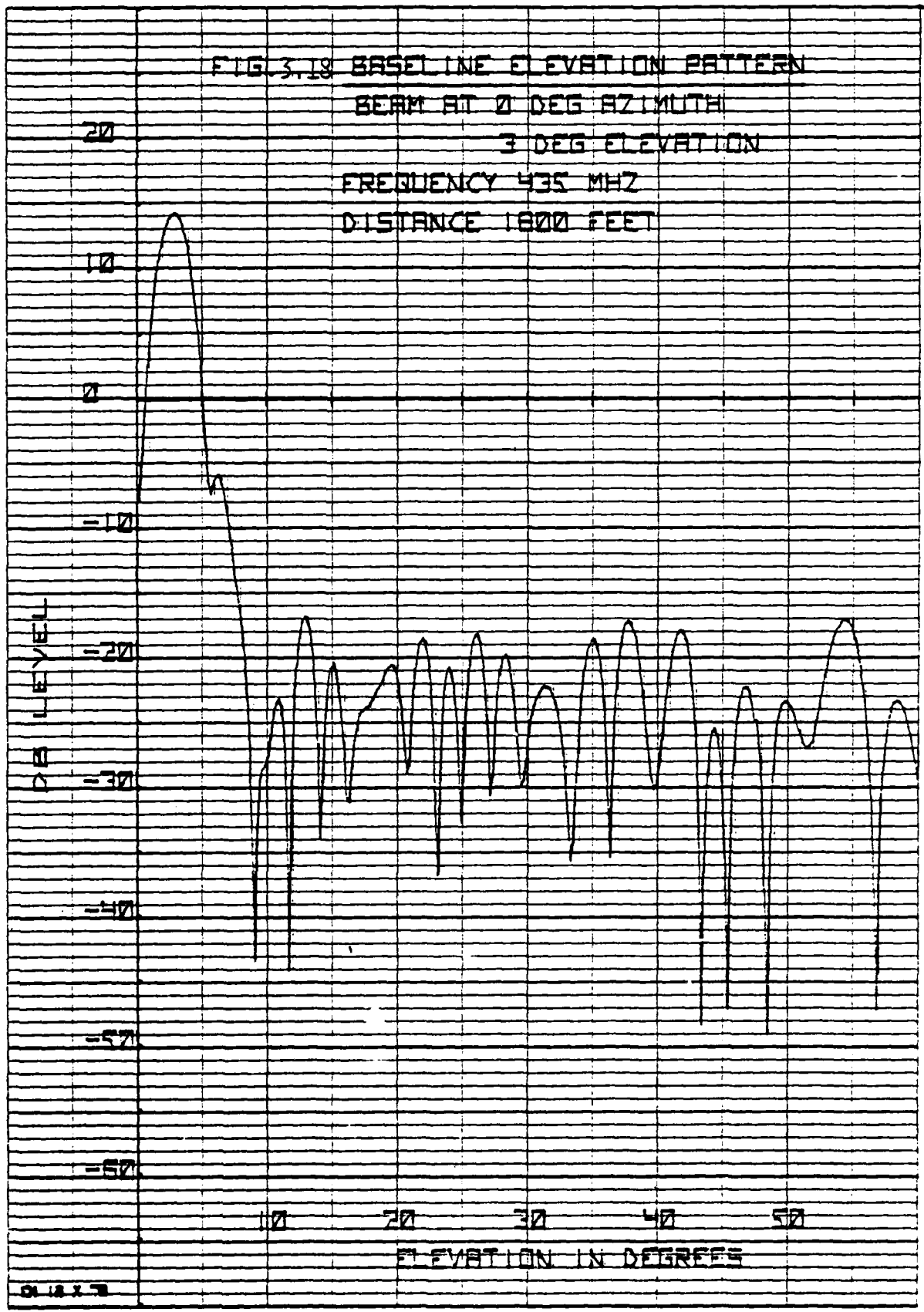


011W1111 PALMARD 92700000

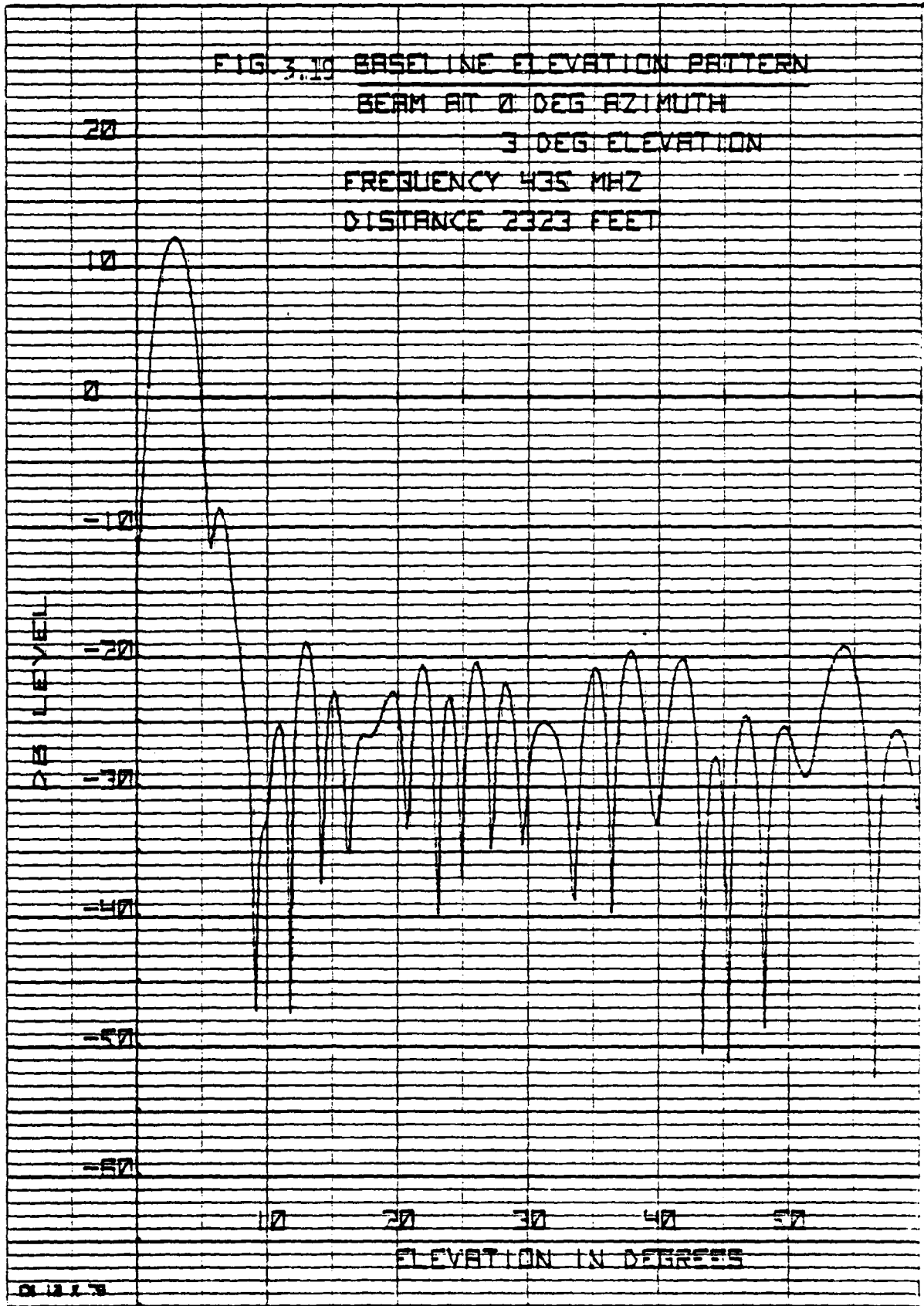


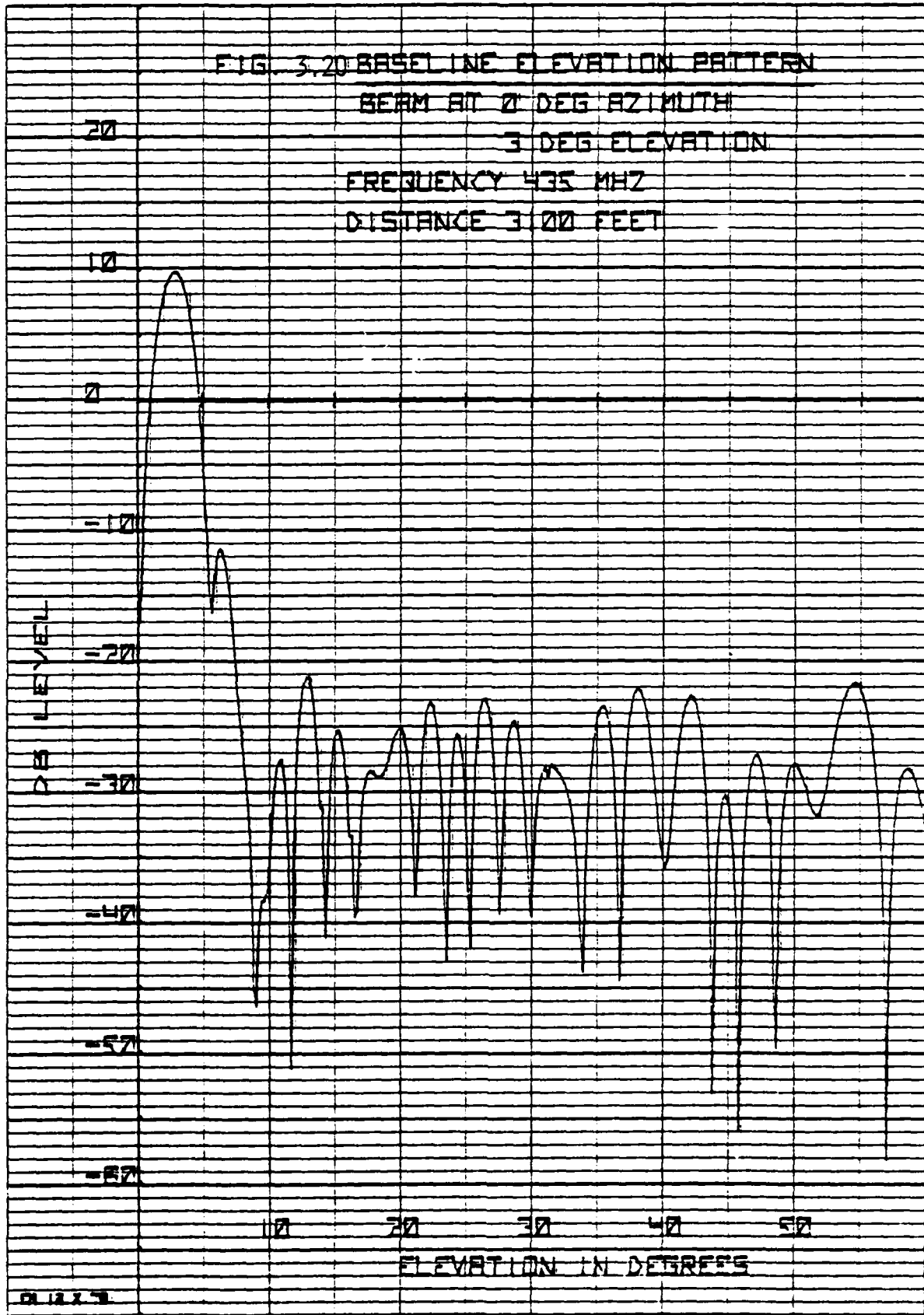


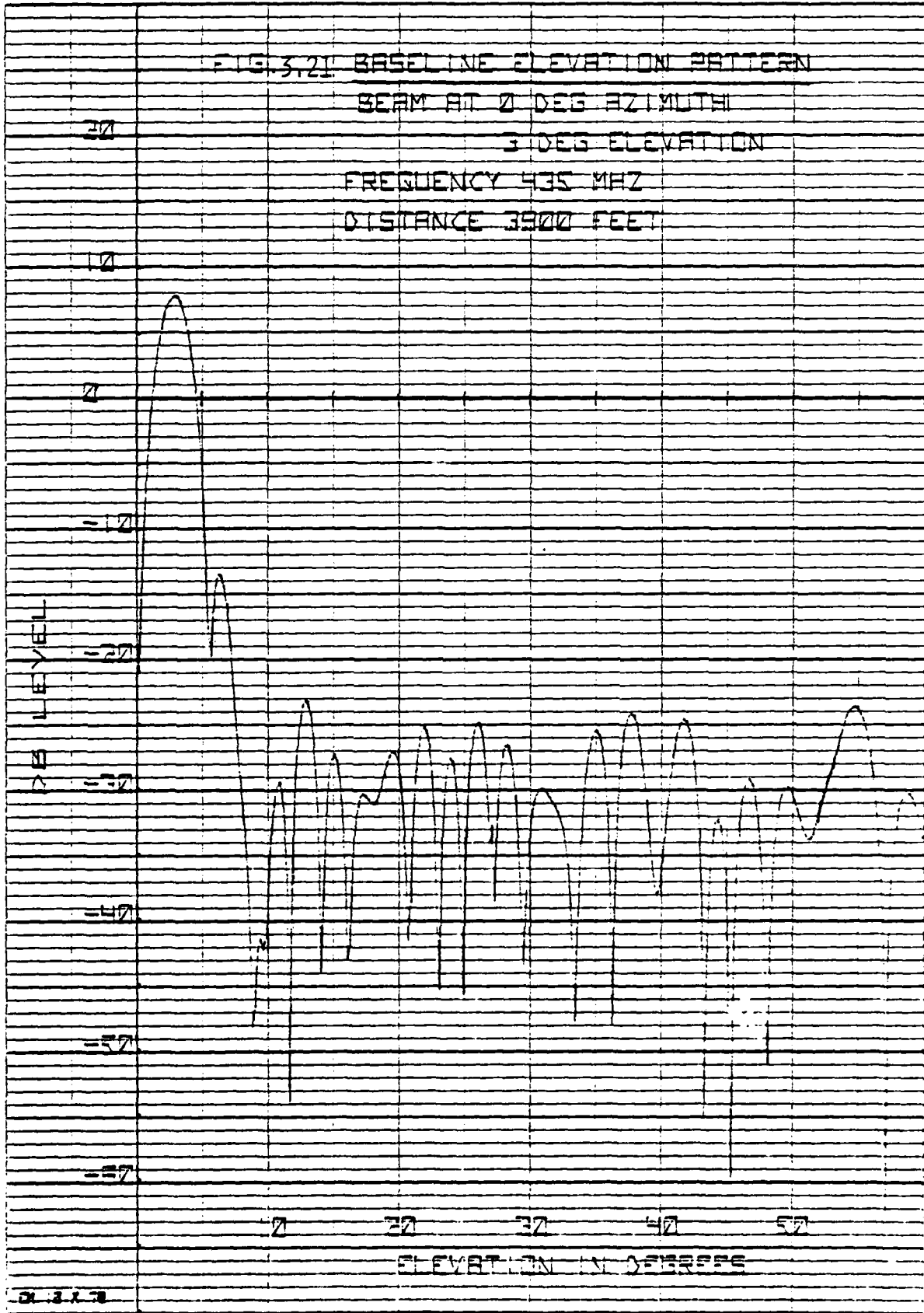
HEWLETT PACKARD 3270 10000

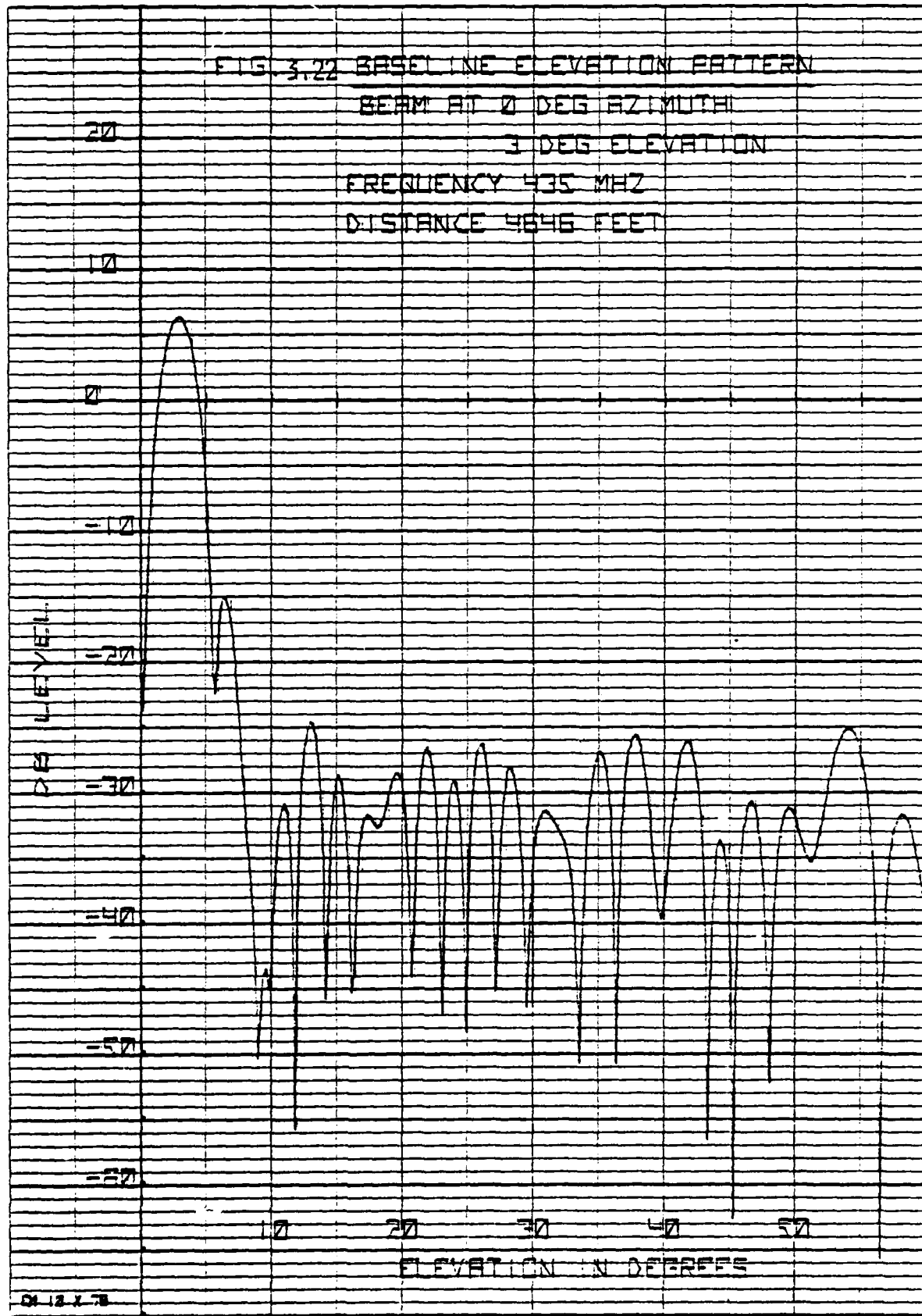


HEWLETT-PACKARD 92701000

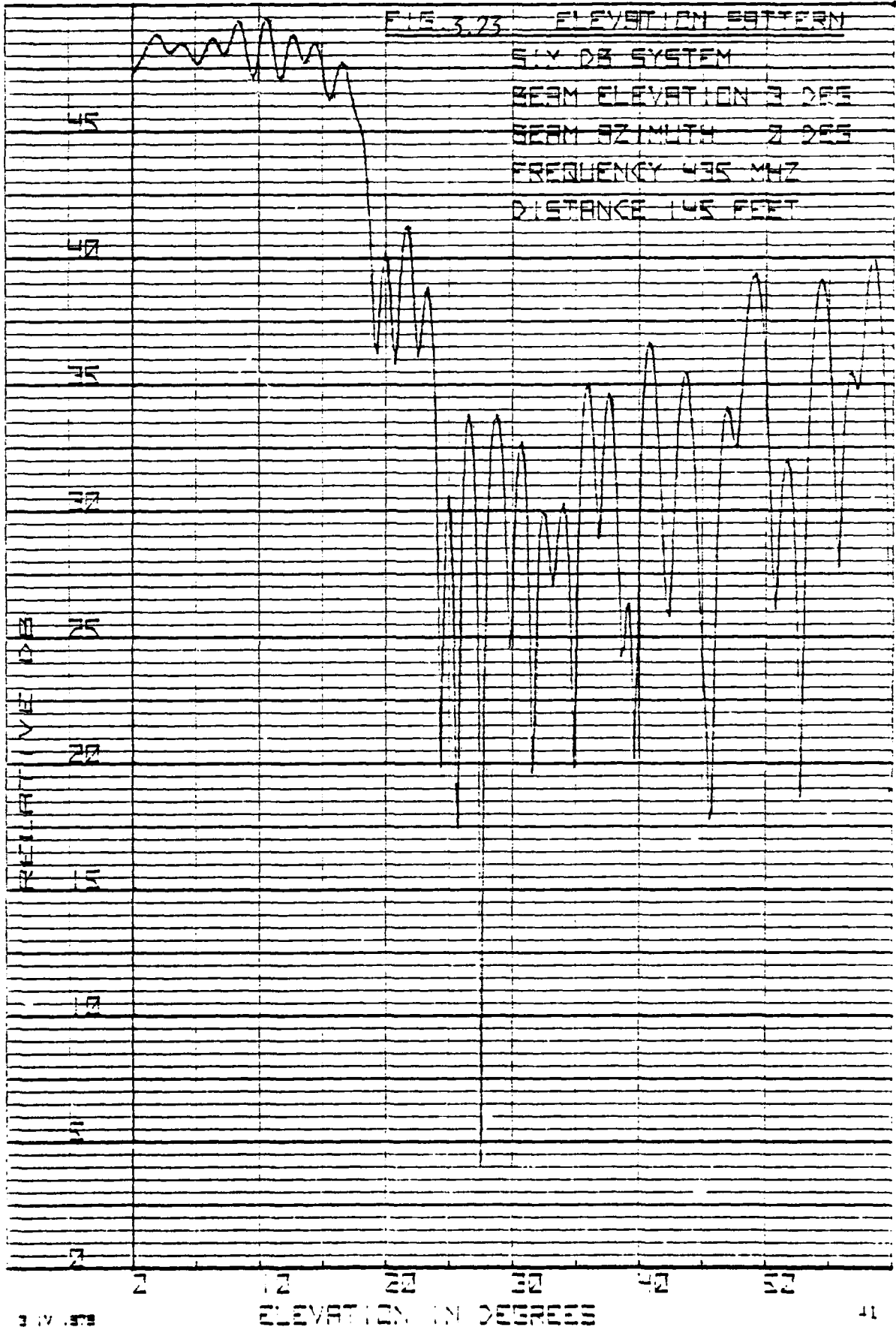




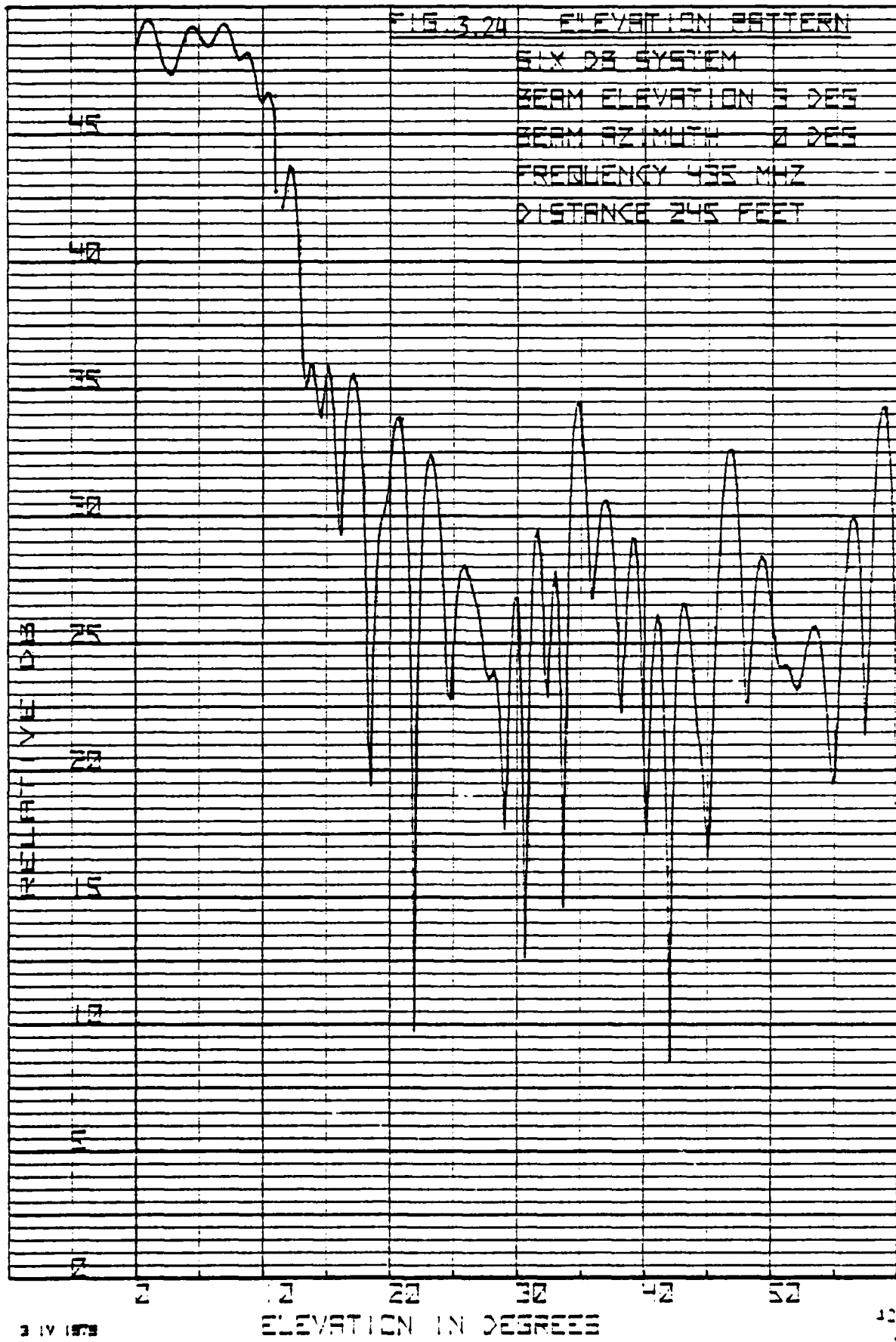




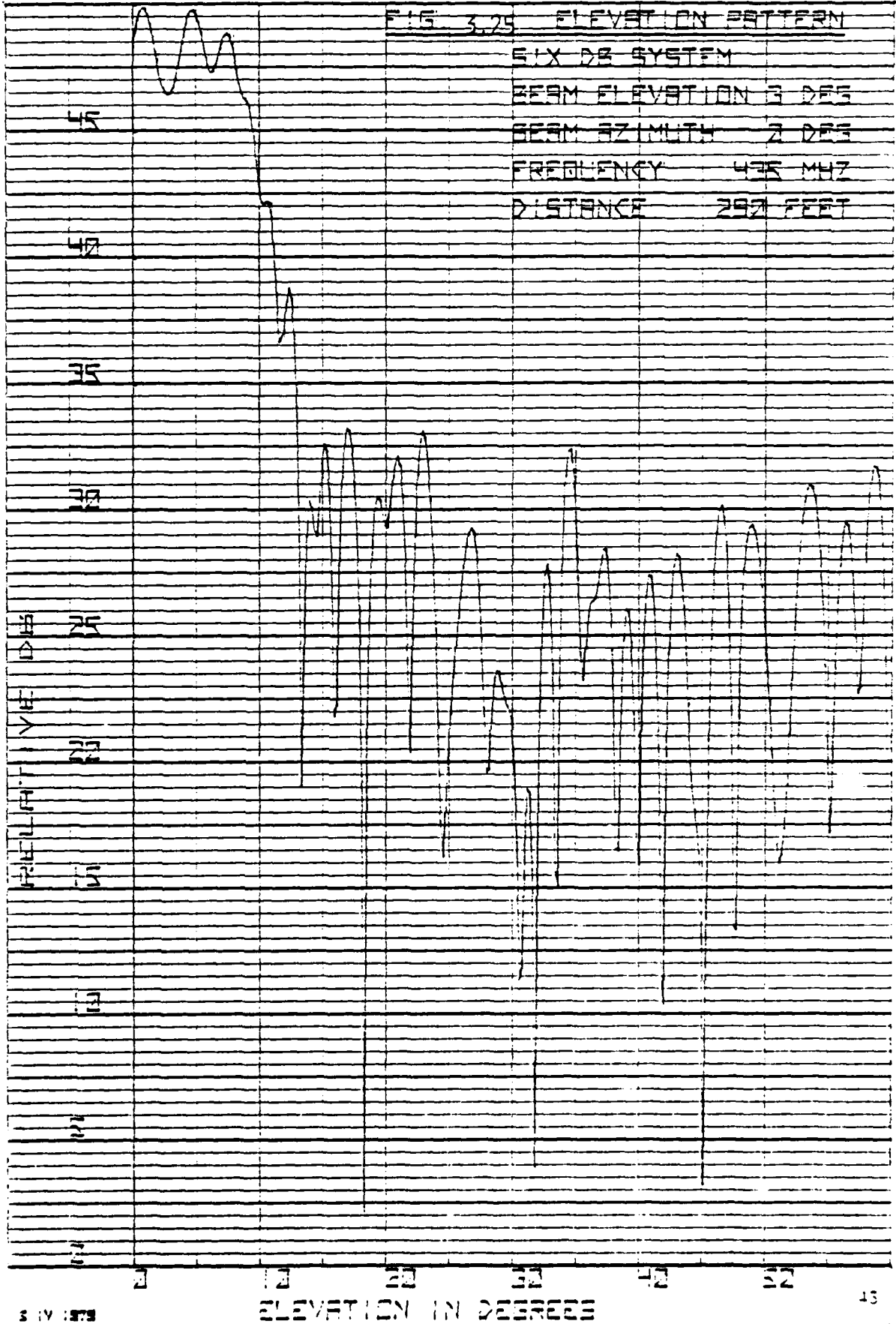
HEWLETT PACKARD 5770 1006



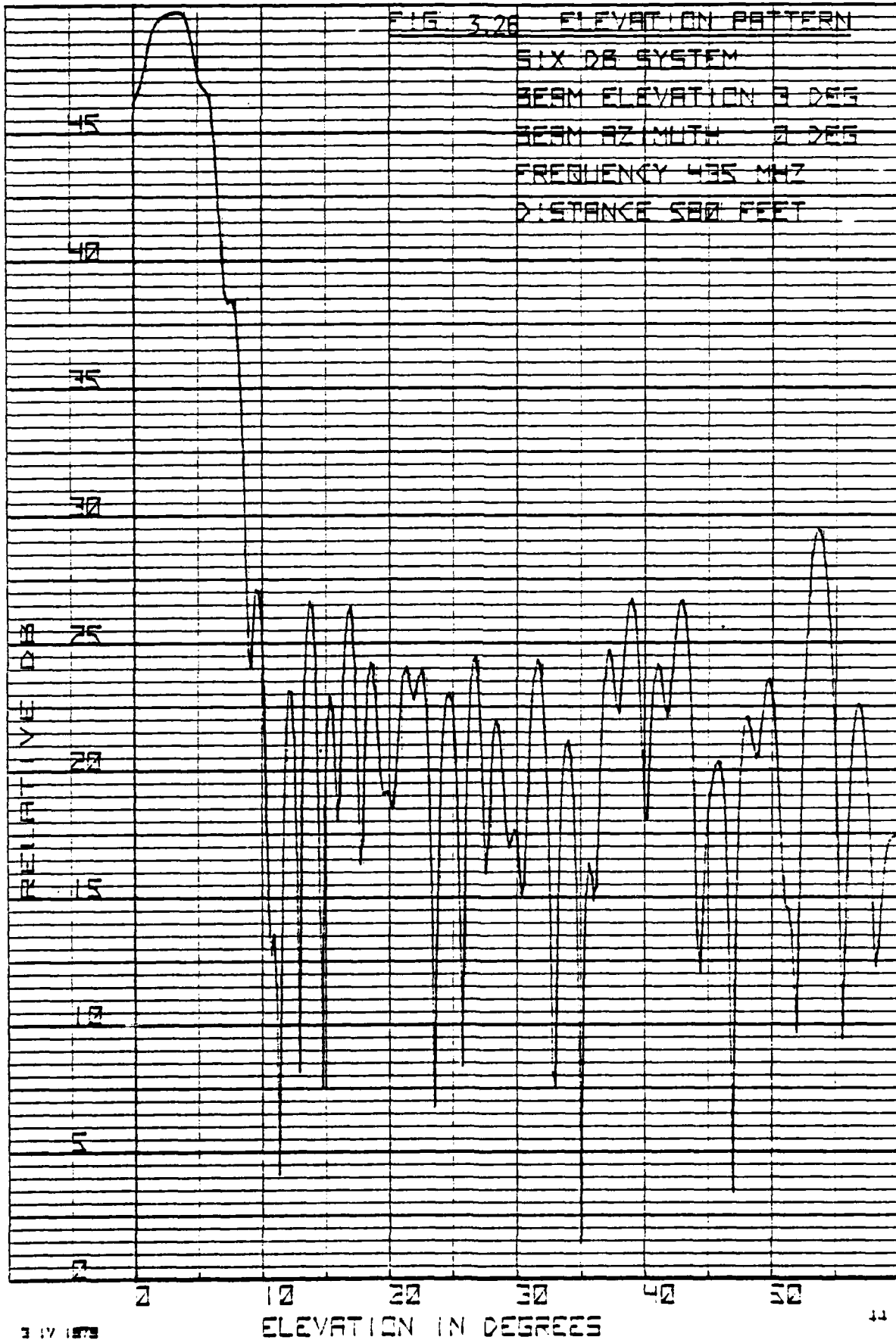
111 WELLS PAV. NABU 52701000



HILWELL PAT. NO. 5270 1000



REPRODUCED FROM 100-1000



HUWELI PASKAUD 32701000

FIG 3.27 ELEVATION PATTERN

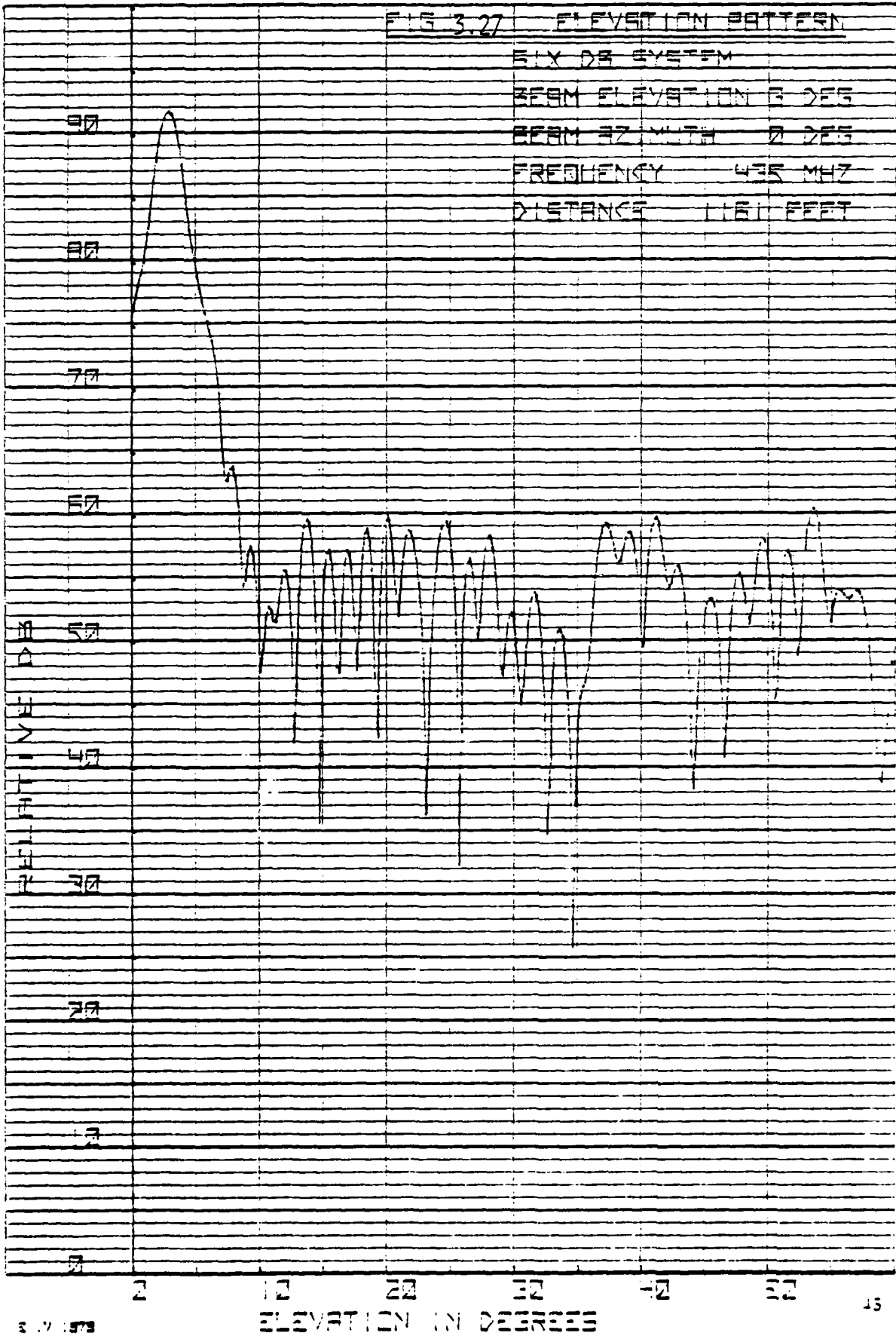
SIX DB SYSTEM

BEAM ELEVATION 3 DEG

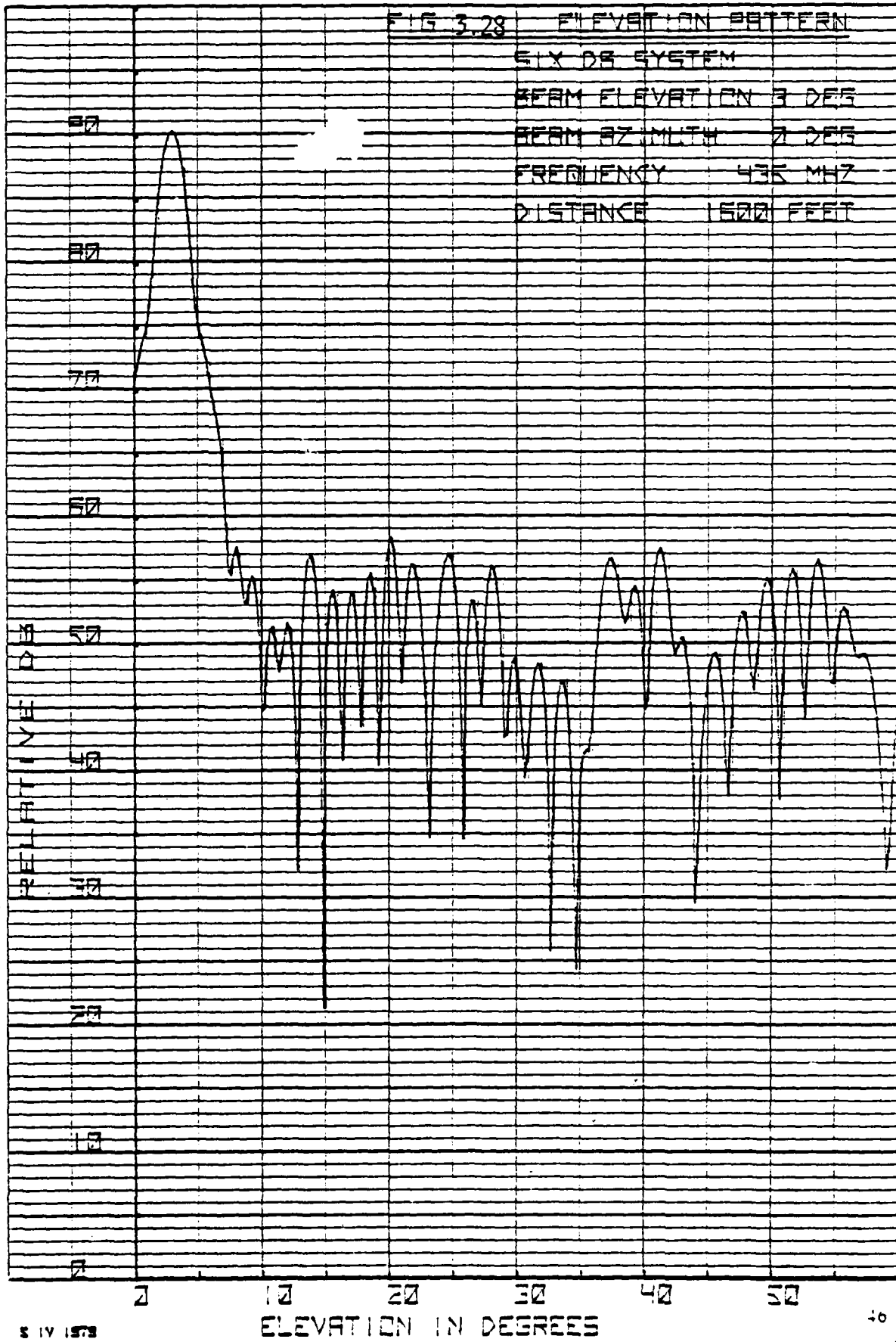
BEAM AZIMUTH 0 DEG

FREQUENCY 435 MHZ

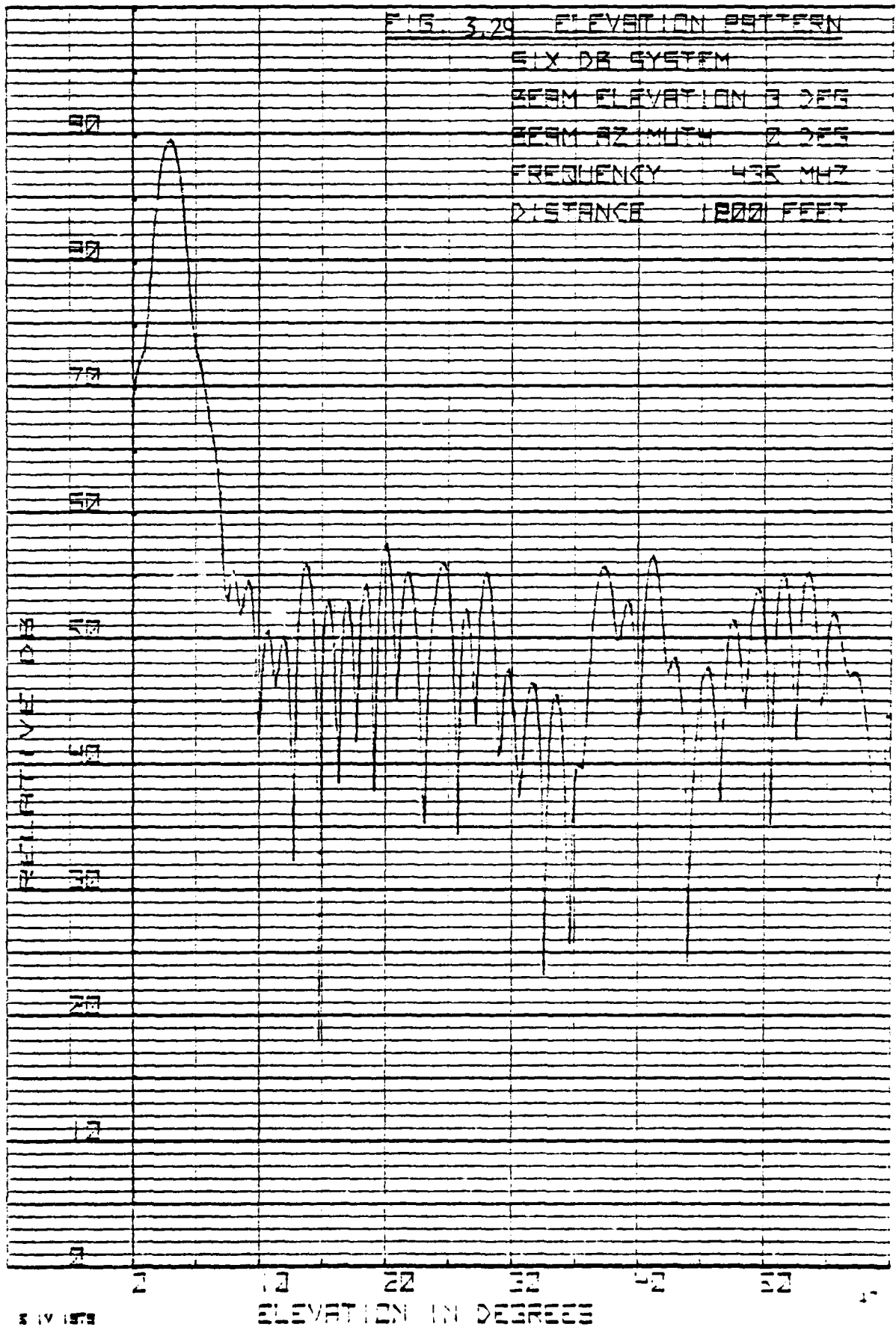
DISTANCE 1161 FEET



HW 111 PA 1.1410 9270 0000



HEWLETT PACKARD 8270 UNIV



3 14 1979

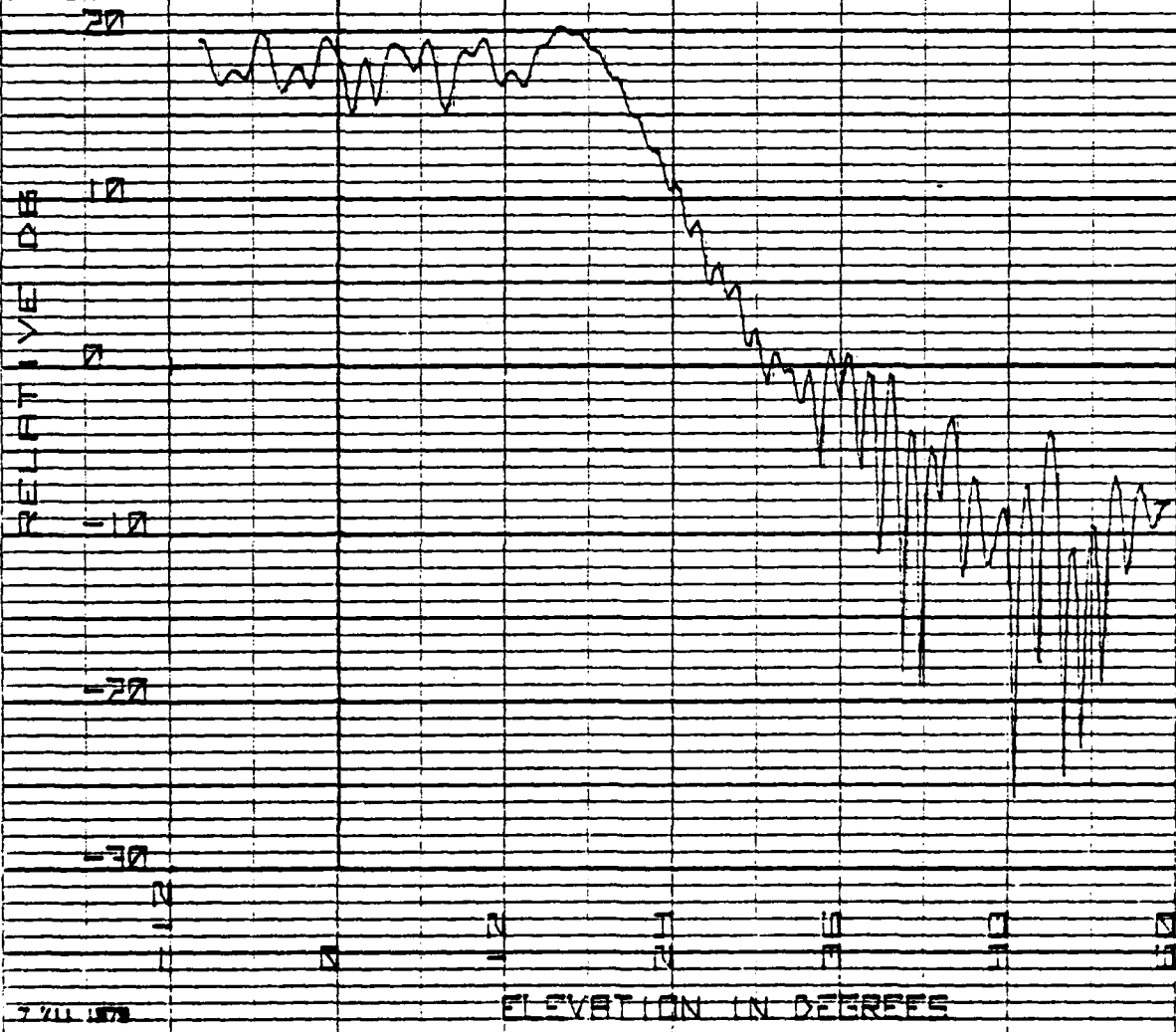
FIG. 3.30 10 DB SYSTEM ELEVATION PATTERN

BEAM AT 0 DEG AZIMUTH

3 DEG ELEVATION

FREQUENCY 435 MHZ

DISTANCE 143.55 FEET



7/11/59

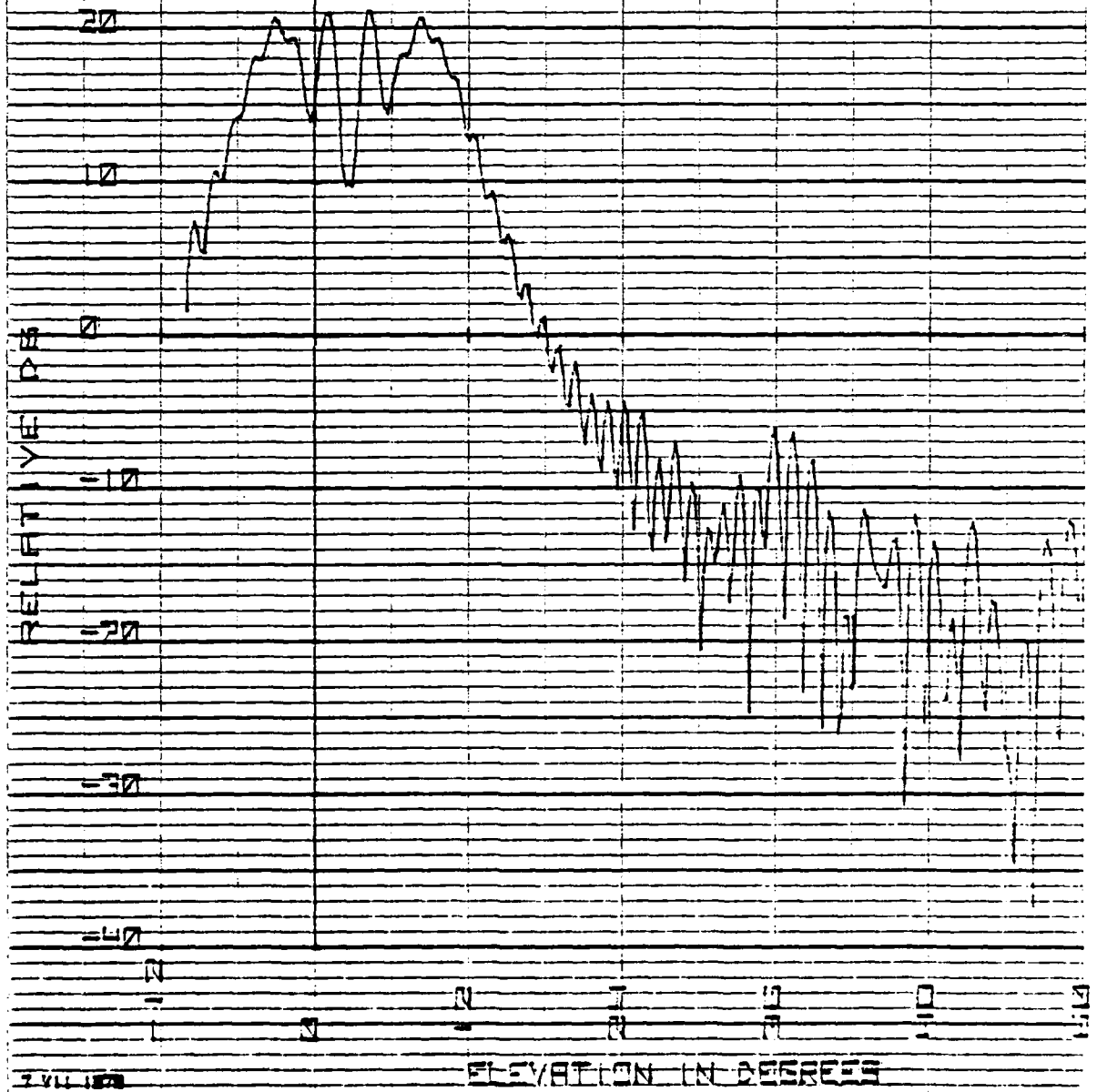
FIG. 3.31 10 DB SYSTEM ELEVATION PATTERN

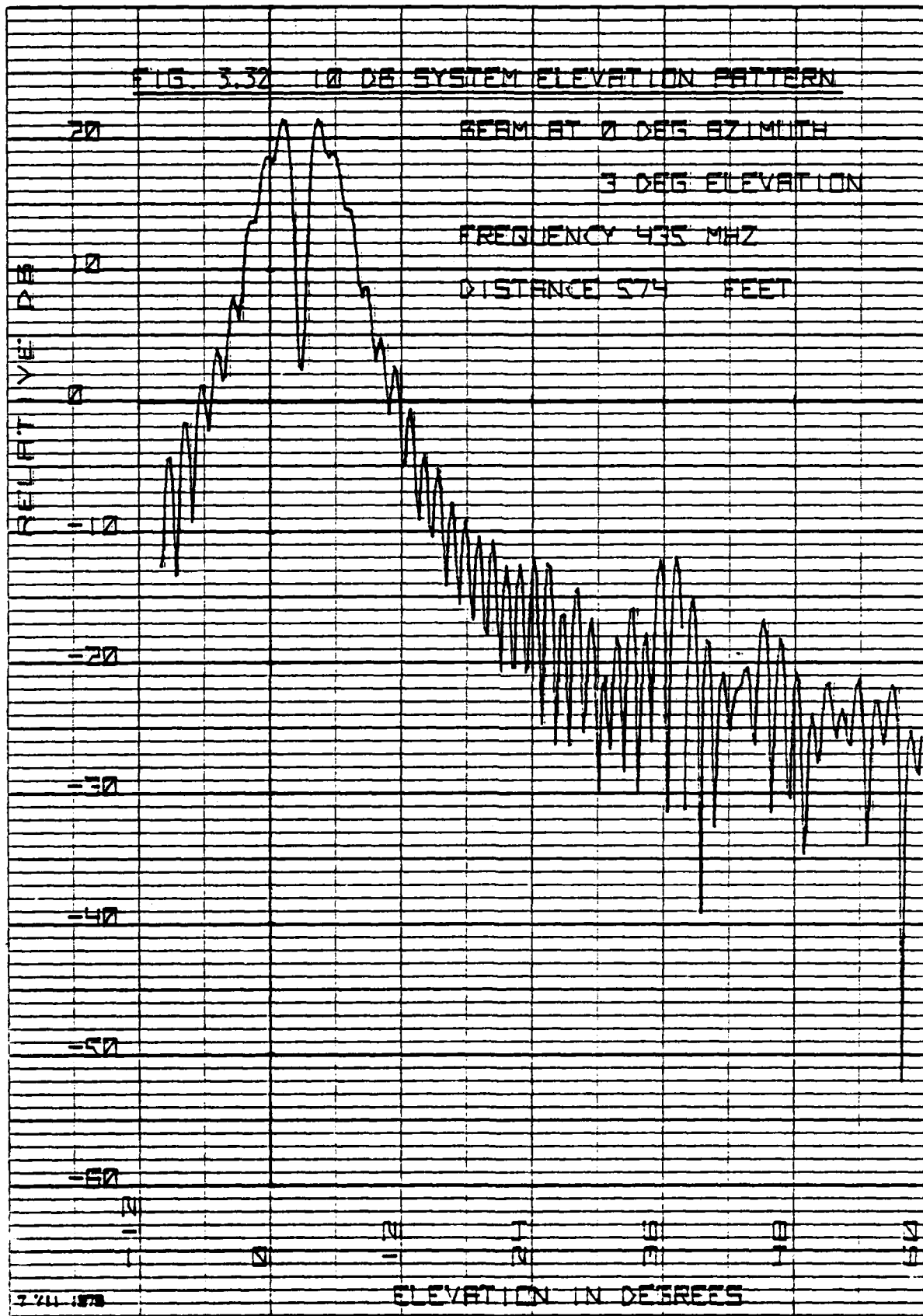
BEAM AT 0 DEG AZIMUTH

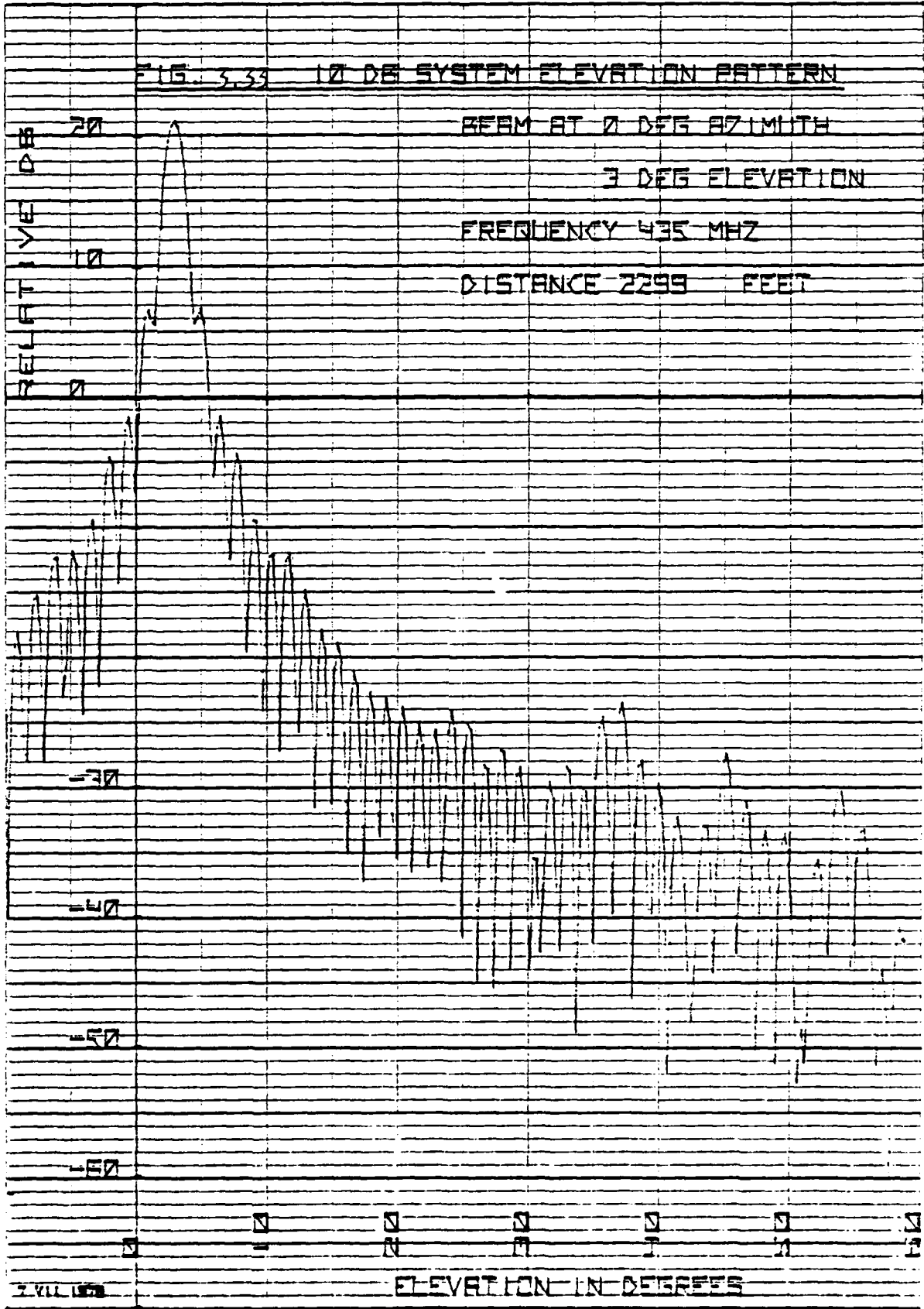
3 DEG ELEVATION

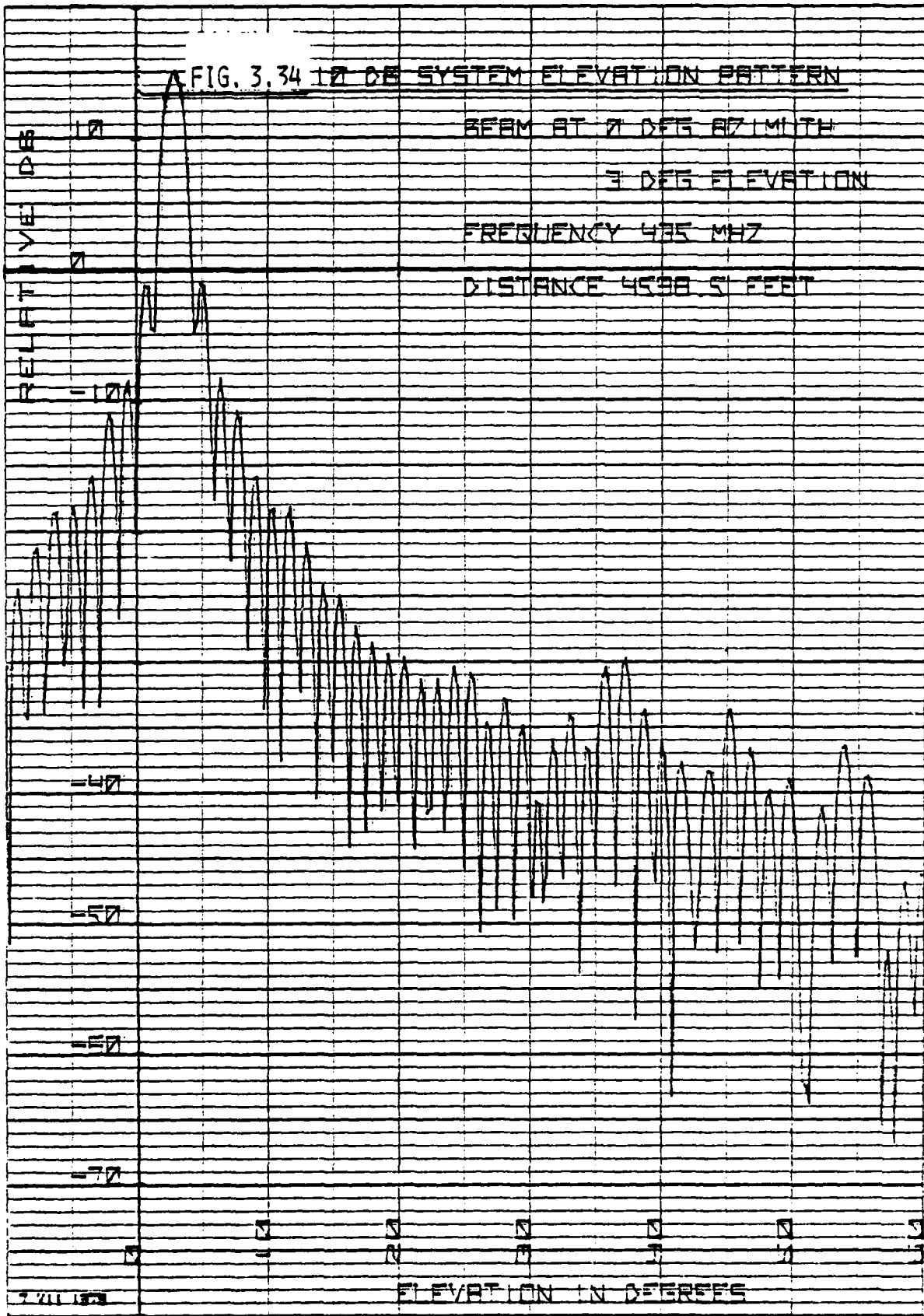
FREQUENCY 435 MHZ

DISTANCE 287.2 FEET









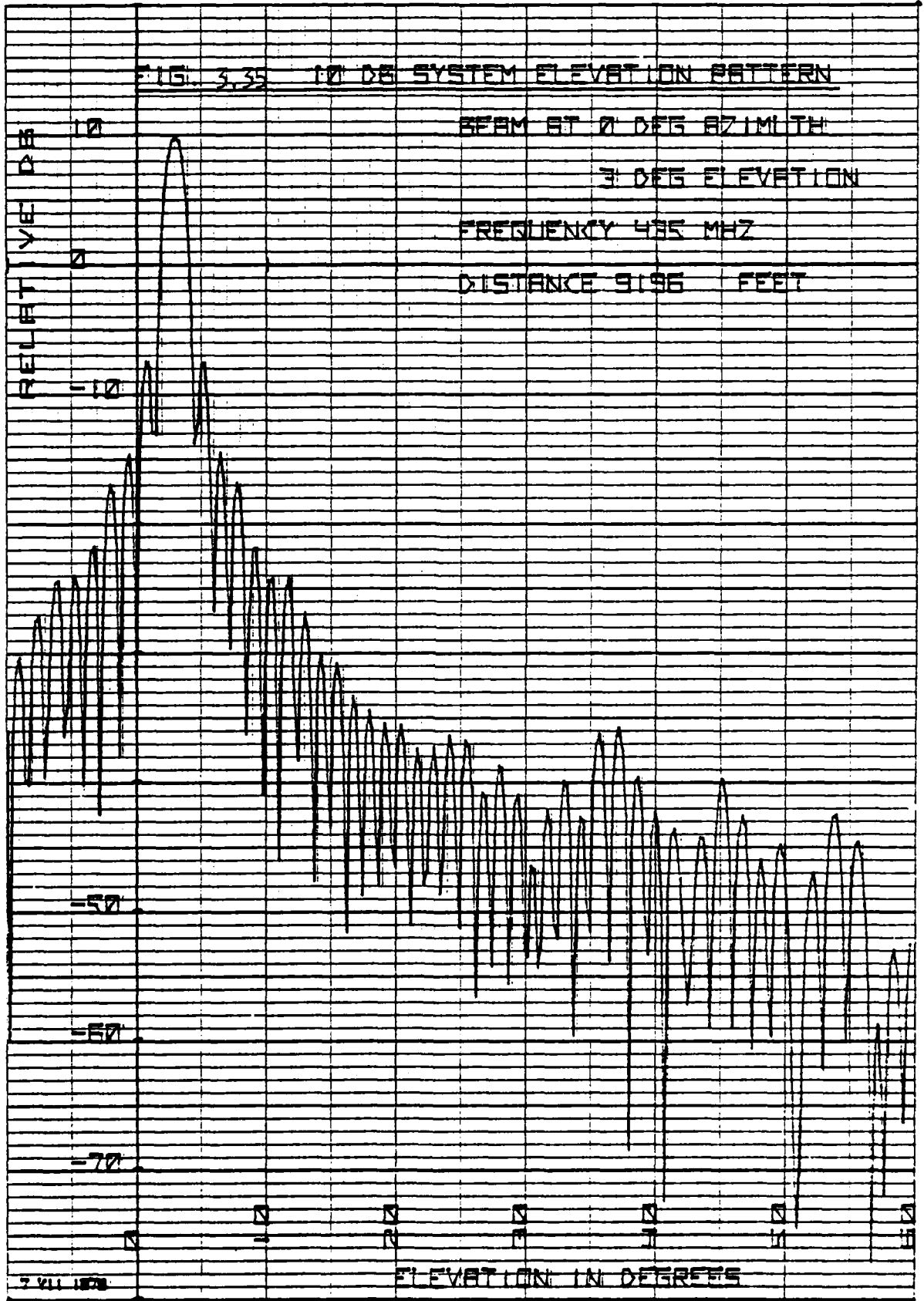


FIG. 3.36 BASELINE SYSTEM 10 DBM
ELEVATION LIMITS

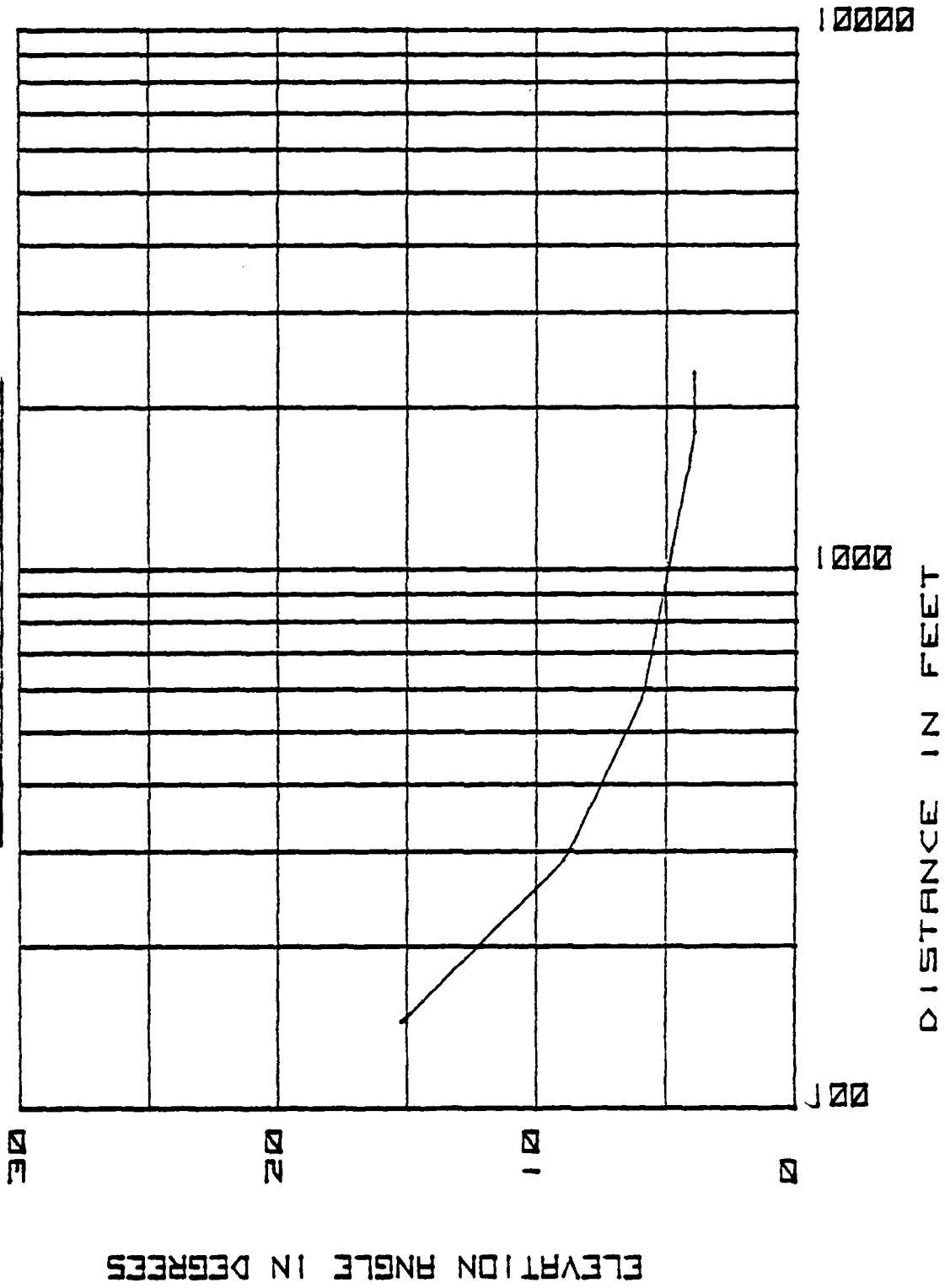


FIG. 3.37 SIX DB SYSTEM 10 DBM
ELEVATION LIMITS

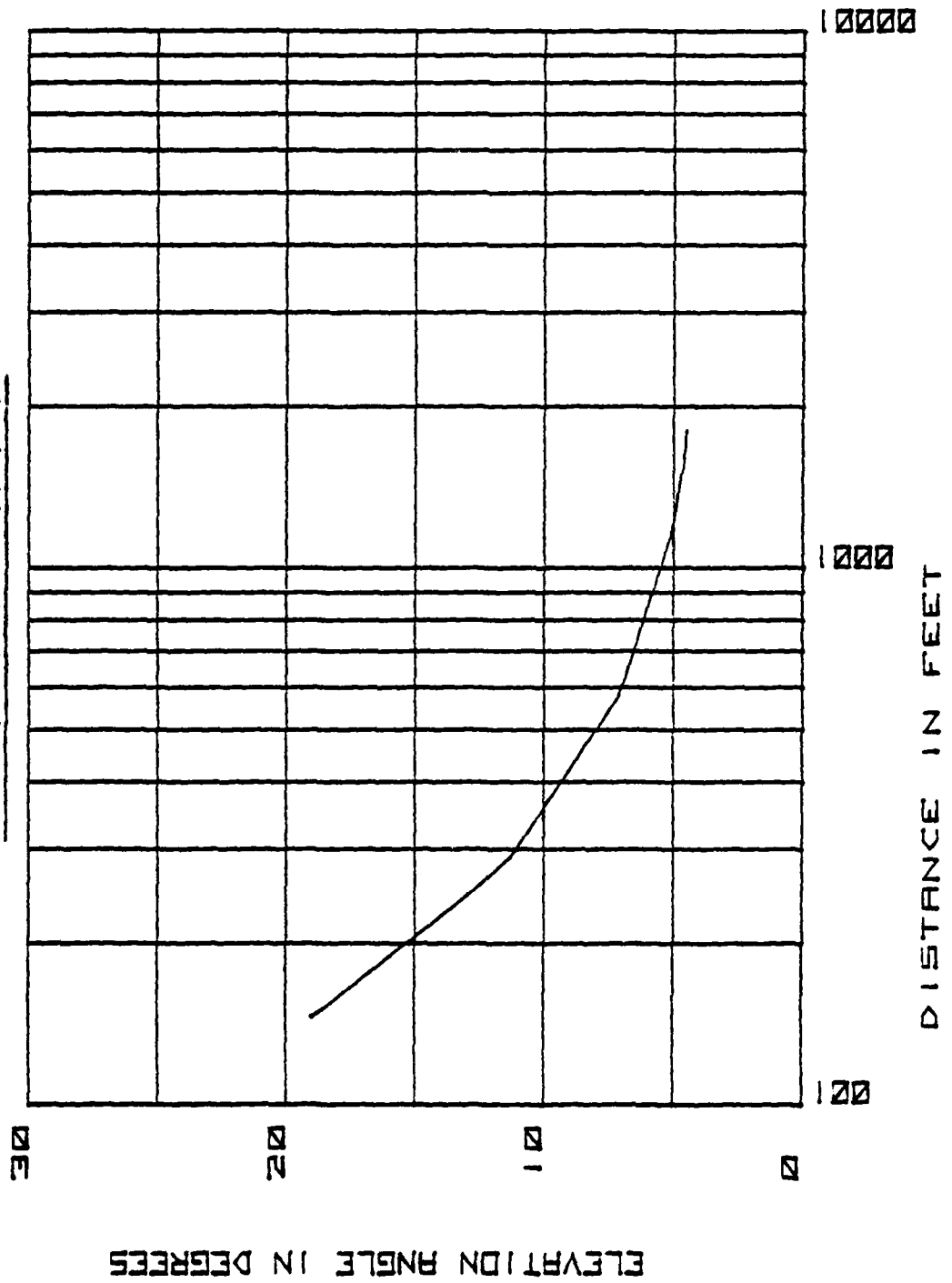
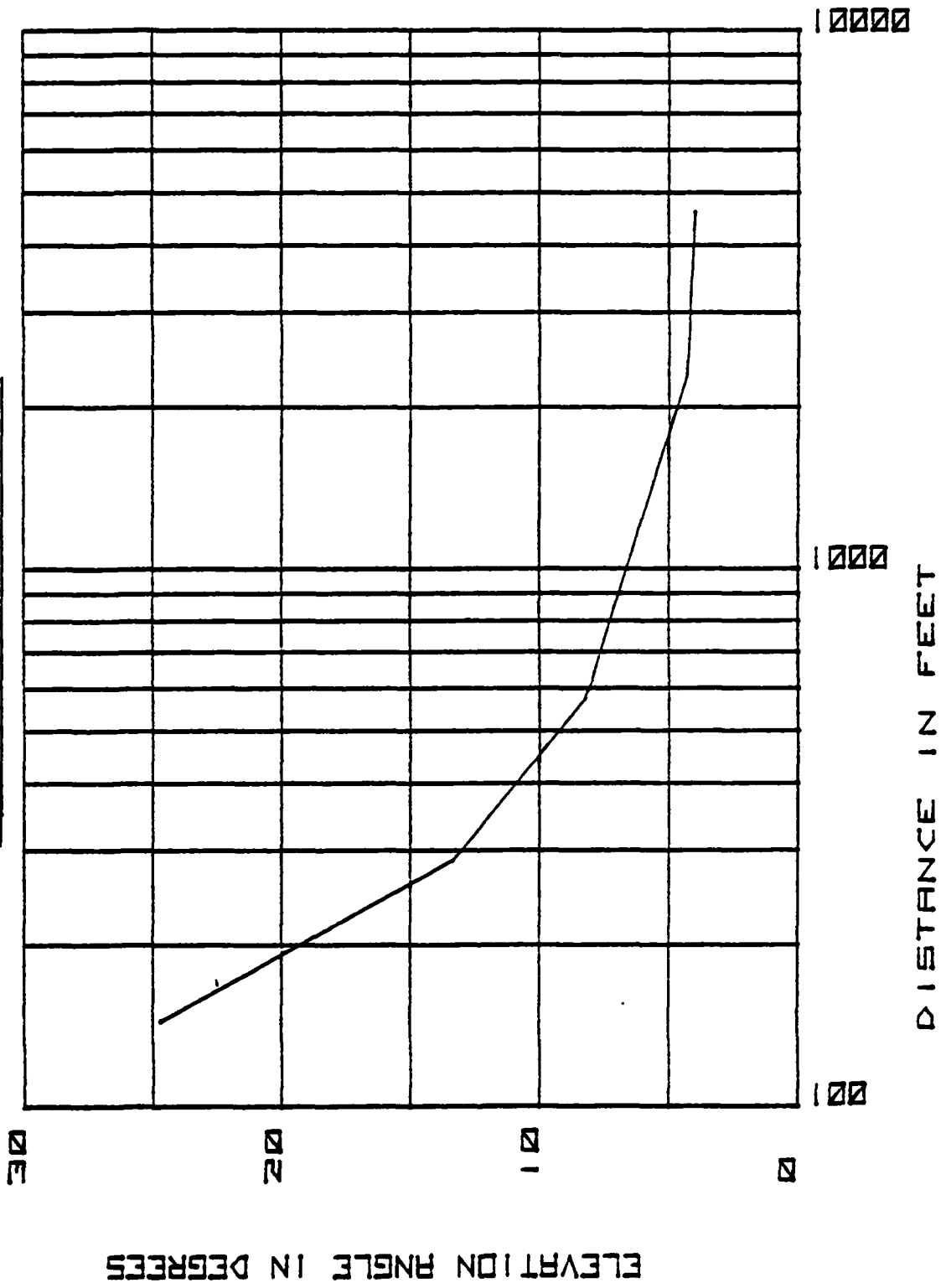


FIG. 3.38 10 DB SYSTEM 10 DBM
ELEVATION LIMITS



4.0 Ground Densities: To determine the possible radiation hazard levels to personnel on the ground, average power densities were calculated for the PAVE PAWS radar fence and for selected various ground points in the OTIS AFB vicinity when illuminated by a continuously moving search beam and a stepped search beam moving in accordance with the PAVE PAWS search algorithm. For the stepped beam case the RFR calculated values were compared with experimental data.

4.1 Hazard Fence: The radiation levels for the radar hazard fence were computed based on the geometry of figures 2.3 and 4.1. The fence was placed in the xy topocentric plane of Figure 2.3. Figure 4.1 shows the radar outline projection on the xy plane and the fence boundary starting from point D, proceeding through points L,E,F,I,M and ending at point N. The radiation levels were computed first for the field sample point Q on the linear portion of the fence (line segment LE) and then for the field sample point Q' on the circular portion of the fence illuminated by Face A. Because of the symmetry and the "windshield wiper" mode of the search operation, the levels calculated for the hazard fence portions illuminated by Face A were assumed to pertain also to the hazard fence portions illuminated by Face B when the radar Face B search fence is operating.

4.1.1 Linear Fence

The linear fence segment LQ is generated by equations (4.1)

$$\begin{aligned}x &= 69.82 + LQ \cos 30 \\y &= 19 + LQ \sin 30 \\z &= 0\end{aligned}\tag{4.1}$$

where the dimensions are in feet.

The increment LQ is a variable distance from the point L along the DE

line to the field sample point Q. The line DE is approximately 912 feet long. Since the power density at the hazard fence depends on the azimuth position of the search beam, the RFR program was used to determine the azimuth at which the power density at a fence point is maximum. The fence point chosen was at a 500 feet distance away from the radar (LQ = 500 feet). Figures 4.2 and 4.3 show the power density at this point versus beam azimuth position for the baseline and the SIX DB systems, respectively. The maximum power density at this point was 53.8 microwatts/centimeter squared with the beam at 56.25 degrees radar azimuth for the baseline system, and 136.5 microwatts/ centimeter squared at 57.25 degrees radar azimuth for the Six DB system. Figures 4.4 and 4.5 show the fence power density as the distance (EQ) from the array to the field point increases when the search beam is at its worst azimuth position. The density levels are fairly low. The maximum density levels are 0.183 milliwatts/ centimeter squared at a distance of 142 feet for the baseline system and 0.56 milliwatts/ centimeter squared at a distance of 40 feet for the Six DB system.

4.1.2 Fence Arc Segment: The fence arc is generated by equations (4.2)

$$x = 1070 \sin B$$

$$y = 1070 \cos B - 55 \quad (4.2)$$

$$z = 0$$

where the dimensions are in feet.

The fence central angle B is the angle (angle FCQ') measured from the y axis to the field sample point Q' and is taken positive in the clockwise direction. The extreme fence point E occurs at B = 58.14 degrees or at an azimuth of 60.7 degrees. The conversion of the fence angle B to the radar face of boresight azimuth angle (also taken positive in the clockwise direction) is given by equation (4.3)

$$A = \arctan (\sin B / (\cos B - 55/1070)) \quad (4.3)$$

Power densities were calculated for the fence arc segment extending over a central angle of -86 to 60 degrees. Since the points of maximum power density will occur at different fence points Q' for different azimuth positions, the power densities on the arc illuminated by Face A were computed for 4 representative beam positions of 0, 20, 40 and 60 degrees azimuth angles and at the 3 degree elevation. Figures 4.6 through 4.9 and figures 4.10 through 4.13 show the power density variation along the fence arc segment as a function of the fence angle for fixed beams at 3 degrees elevation and 0, 20, 40, 60 azimuth angles for the baseline and SIX DB systems, respectively. Shown in Table 4.1.1 are the maxima arc segment hazard fence power densities for both the baseline and SIX DB systems for the four fixed beam orientations. Even for the spotlight conditions, the levels are considerably under the OSHA standard.

Table 4.1.1 Hazard Fence Maxima Densities (Arc Segment)

Beam Azimuth Degrees	<u>Baseline System</u>		<u>SIX DB System</u>	
	Fence Angle Degrees	Density uw/cm ²	Fence Angle Degrees	Density uw/cm ²
0	+26.6	54.6	+26	152.1
20	-30.8	46.7	-11.1	133.5
40	- 6.2	69.1	3.1	91.9
60	40	42.5	16.2	69.5

4.2 OTIS AFB Vicinity: Power densities were calculated for seven off-base ground points selected as representative points in the OTIS AFB vicinity. Table 4.2.1 gives the physical location parameters for these

points.

Table 4.2.1 Point Locations

Point	Height	Azimuth	Radar	Distance
	Feet	Degrees	Azimuth Degrees	Feet
1. Proposed Highway 25	220	350	-57	2702
2. Mid Cape C	180	25	-22	3403
3. Mid Cape S	140	75	28	4404
4. Mid Cape N	150	350	-57	4803
5. Sagamore Town	100	10	-37	6004
6. Sagamore Bridge	217	350	-57	8601
7. Smoke Stack	400	49	2	10200

The C, S, and N designators for the Mid Cape Highway pertain to points on the center, southern and northern portions, respectively. The height values are with respect to Mean Sea Level; the azimuth is referenced to true north. The radar azimuth is referenced to the PAVE PAWS face boresight line. Figure 4.14 shows the map locations of these seven points. Figures 4.15 through 4.19 are the height profiles for these points. Some of the points are located in the PAVE PAWS radar shadow. This shadowing effect was disregarded in this study to arrive at conservative (higher) power density values. Figures 4.20 through 4.26 and Figures 4.27 through Figures 4.33 show the calculated power density levels existing at the points of Table 4.2.1 versus beam position with the beam fixed at various off-boresight azimuths and at 3 degrees elevation - the minimum elevation angle allowed for radiation for the the baseline and the SIX DB systems, respectively. The arrow on each figure points to the azimuth of a particular Table 4.2.1 point. The power density scales are shown in microwatts/centimeter squared and in

dBu, decibels above a microwatt/centimeter squared. Table 4.2.2 lists the average midband densities for the seven points for both the baseline and SIX DB systems.

Table 4.2.2 Average Point Densities for 435 MHZ

Point	<u>Baseline System</u>			<u>SIX DB System</u>		
	Azimuth Degrees	Maximum uw/cm ²	Sector Average uw/cm ²	Azimuth Degrees	Maximum uw/cm ²	Sector Average uw/cm ²
1. Proposed						
Highway 25	-54.25	10.57	1.52	-47.5	8.74	1.92
2. Mid Cape C	-15.75	3.55	0.62	-26.25	6.99	1.51
3. Mid Cape S	21.5	2.64	0.45	32.5	4.86	1.02
4. Mid Cape N	-54.25	3.74	0.48	-47.5	2.98	0.58
5. Sagamore						
Town	-32.5	1.48	0.23	-48	3.01	0.57
6. Sagamore						
Bridge	-56.5	4.66	0.91	-54.75	3.55	0.34
7. Smoke						
Stack	4.25	6.44	0.62	1.25	25.86	2.31

The maximum columns list the spotlight upper bound values. More realistic in practice are the sector average values obtained by considering uniform beam motion over a 40 degree azimuth sector. Since some of the PAVE PAWS radar energy resources must be allocated to the tracking function, the sector average power density values would be further reduced by multiplying these values by the search duty factor of about 11/25. The densities at the off-base points considered are very low -- well under 10 microwatts/centimeter squared and very comfortably under the OSHA standard of 10 milliwatts/centimeter squared.

4.3 Verification: Using the RADC RFR computer program, field intensities were calculated at four of the OTIS AFB site south face ground points for which field intensities were measured with the radar in the surveillance fence mode, i.e. the scanned mode. The calculations were performed on the basis of the PAVE PAWS CPCI-2 undithered beam schedule versus time and at the radar transmit frequencies varying from frequency No. 1 to frequency No. 24, inclusive. The doublet and triplet edge beam frequencies were offset from the center frequencies by the CPCI-2 specified frequency differences. The beam schedule template considered short range pulse schedules, long range pulse schedules, Aurora transmissions, calibration and free resource periods for the total 41.04 second search beam template period. Table 4.3.1 shows the locations of the ground points and their field intensities as measured by the field team, and as calculated by Raytheon and by RADC using the RFR computer program.

Table 4.3.1 Field Intensities

Point	Azimuth Degrees	Elevation Degrees	Range Feet	Average Field Intensities		
				Measured uw/cm ²	Raytheon uw/cm ²	Calculated RADC uw/cm ²
A	258	-2.03	1600	0.64	5	0.505
B	104	-2.68	1800	0.10	4.2	0.219
C	155	-0.75	3100	0.50	1.3	0.229
D	167	-0.01	3900	0.01	0.25	0.208

The field measured values are 10 second averages; the RADC RFR computer program calculated values are 41.04 second averages. The Raytheon values are higher than the measured values; by 8.9 dB for point A, 16.2

dB for point B, 3 dB for point C and 21 dB for point D. The RADC calculated values vary either side of the measured values and differ from them by -1.0 dB for point A, +3.4 dB for point B, -3.4 dB for point C and +13.2 dB for point D. Since the geometries for points C and D are comparable, one would expect comparable intensities. A decimal error is suspected in the stated point D measured intensity; the measured value is more likely 0.10 instead of 0.01.

Figures 4.34 through 4.45 show the search fence individual beam short term intensities i.e., intensities averaged over a radar resource period (54 milliseconds). The maximum short term averages are low and are 6.6 microwatts/centimeter squared at point A, 1.22 microwatts/centimeter squared at point B, 4.8 microwatts/centimeter squared at point C and 5.12 microwatts/centimeter squared at point D. The variations are due to a combination of the factors of distance, off-boresight losses and beam sidelobe structures due to the varying frequencies of transmission. Data similar to that in Figures 4.34 through 4.45 were also obtained for a surveillance fence but with a constant frequency of transmission (435 MHz) for the same search beam template period. The resulting maximum short term averages were 0.453 microwatts/centimeter at point A, 1.59 microwatts/centimeter squared at point B, 4.89 microwatts/centimeter squared at point C and 4.33 microwatts/centimeter squared at point D. The resulting 41.14 second search beam template averages are 0.453 microwatts/centimeter squared at point A, 0.239 microwatts/centimeter squared at point B, 0.245 microwatts/centimeter squared at point C and 0.231 microwatts/centimeter squared at point D. Relative to the varying frequency search beam template, the constant frequency beam template yields short term averages that are -1.6 dB at point A, +1.2 dB at point B, 0.08 dB at point C and -0.73 dB at point D; and long term (41.04

seconds) averages that are -0.47 dB at point A, -0.37 dB at point B, +0.29 dB at point C and +0.46 dB at point D. Relative to the varying search beam template the constant frequency beam template yields short term averages within roughly ± 1.5 dB and long term averages (41.04 seconds) within +0.5 dB. Therefore, if one is concerned over the long term averages, the data for these geometries suggest that the simpler constant frequency search beam template be used for the calculation of intensity. Table 4.3.2 compares the measured (by Raytheon) midband frequency vertical and horizontal beamwidth data with the far field values calculated by the RADC RFR computer program.

Table 4.3.2 Beamwidth Comparison

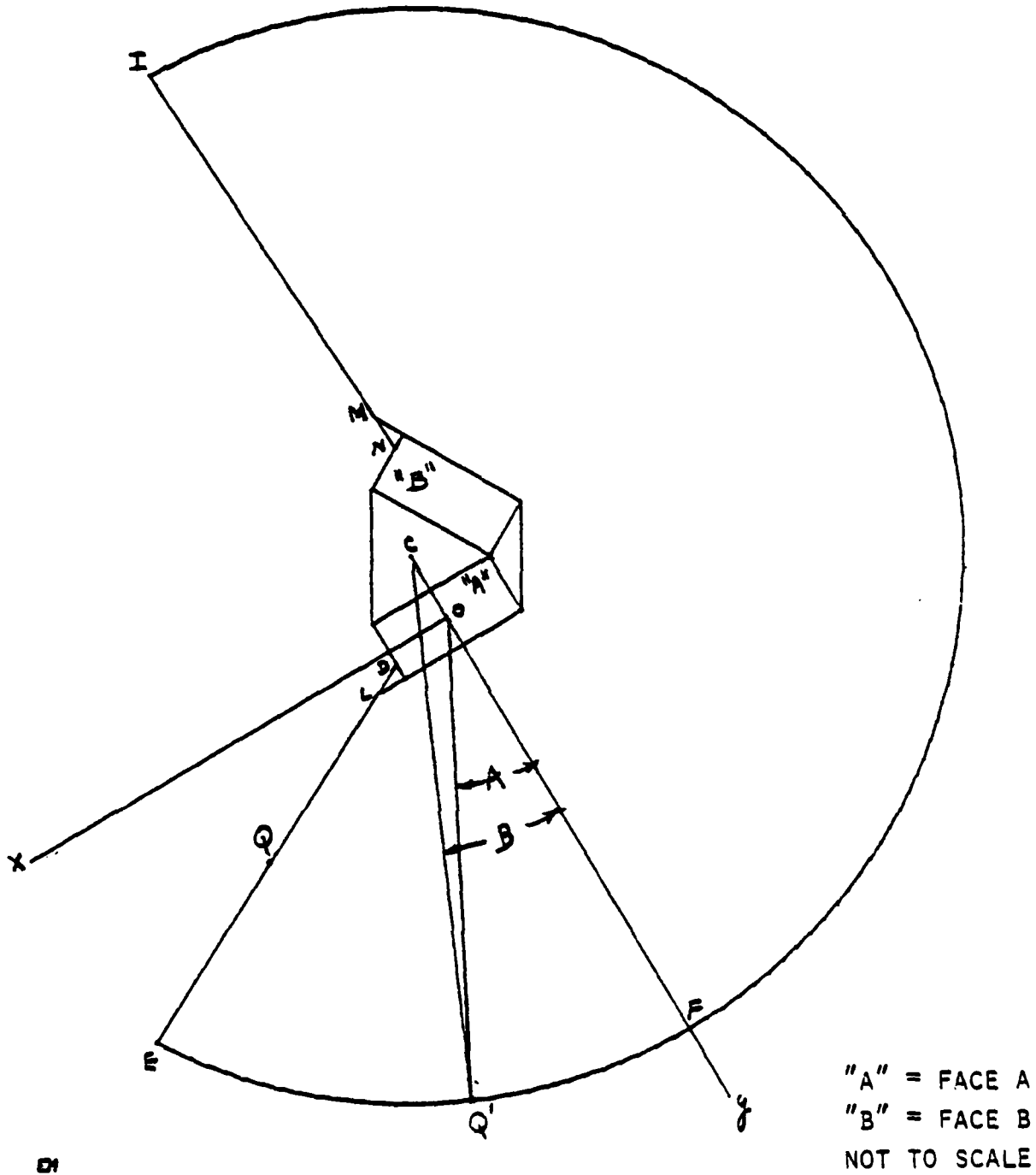
	Beamwidth	
	Vertical Degrees	Horizontal Degrees
Measured	2.149	2.236
Calculated	2.068	2.218
Percent of Measured	96.23	99.19

The agreement between the measured and calculated data for the ground point densities and for the beamwidth is good.

4.4 Ground Hazard: The radar hazard fence is well placed with the result that the radiation levels at its periphery are very low and safe levels -- below a milliwatt/centimeter squared. For the present baseline system, the highest power density levels are 0.183 milliwatts/centimeter squared on the linear portion of the fence and 0.069 milliwatts/centimeter squared on the arc segment of the fence. For the SIX DB system the highest power density levels are 0.56 milliwatts/centimeter squared on the linear portion of the fence and 0.15 milliwatts/centimeter squared on the arc segment of the fence. For

the ground points considered in the OTIS AFB vicinity, the calculations show that there is no hazard to personnel. For the worst case of a stationary beam, the densities are in the order of microwatts/centimeter squared. The power density values calculated by the RFR computer program agree with measured power density values within approximately 3.5 dB.

FIG. 4.1 HAZARD FENCE GEOMETRY



DI

HEWLETT-PACKARD 9270 1000

FIG 4.2 HAZARD FENCE POINT DENSITY
VS BEAM POSITION

BASELINE SYSTEM
BEAM ELEVATION 3 DEG

DB ABOVE MICROWATT/CM SQUARE

20
10
0
-10
-20
10 20 30 40 50

AZIMUTH OFF-BORESIGHT DEGREES

11 11 1988

FIG. 4.3 HAZARD FENCE POINT DENSITY

VS BEAM POSITION

SIX DB SYSTEM

BEAM ELEVATION 3 DEG

DB ABOVE A MICROMETRIC SQUARE

30

20

10

0

-10

-20

20

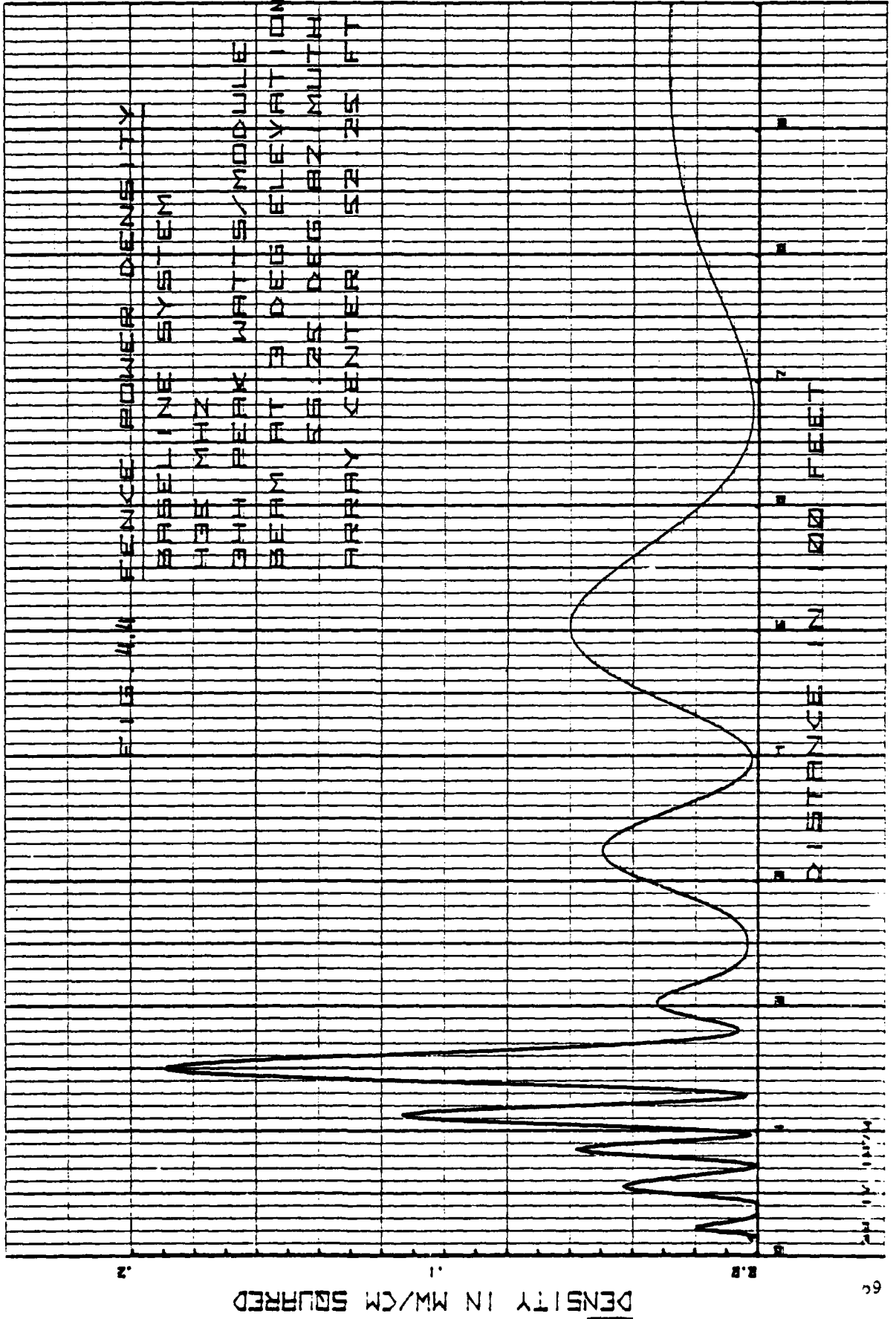
30

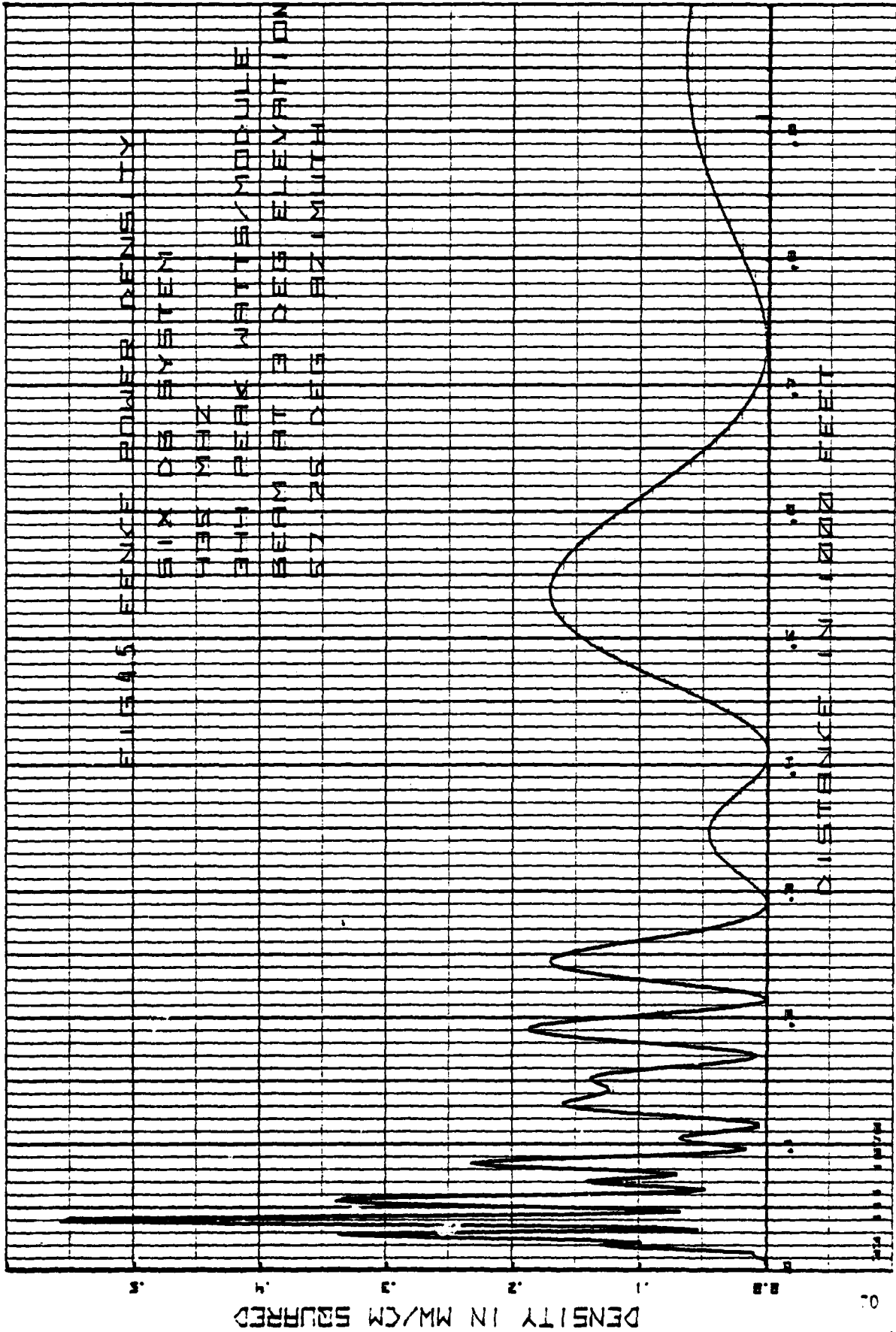
40

50

AZIMUTH OFF-BORESIGHT DEGREES

2 11 15

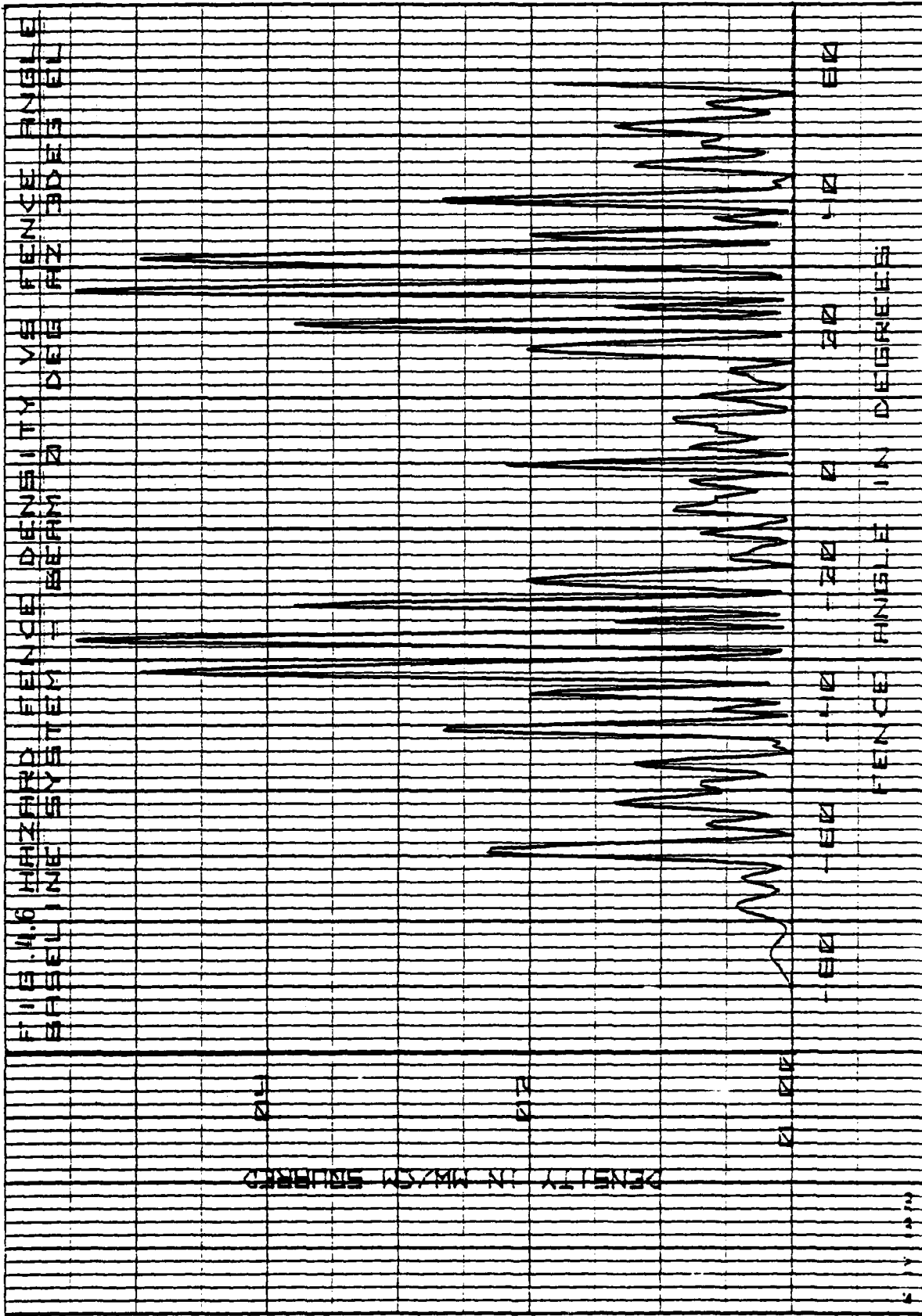




KITTINGER ENGINEERING CO. CHICAGO, ILL.

7-11-50

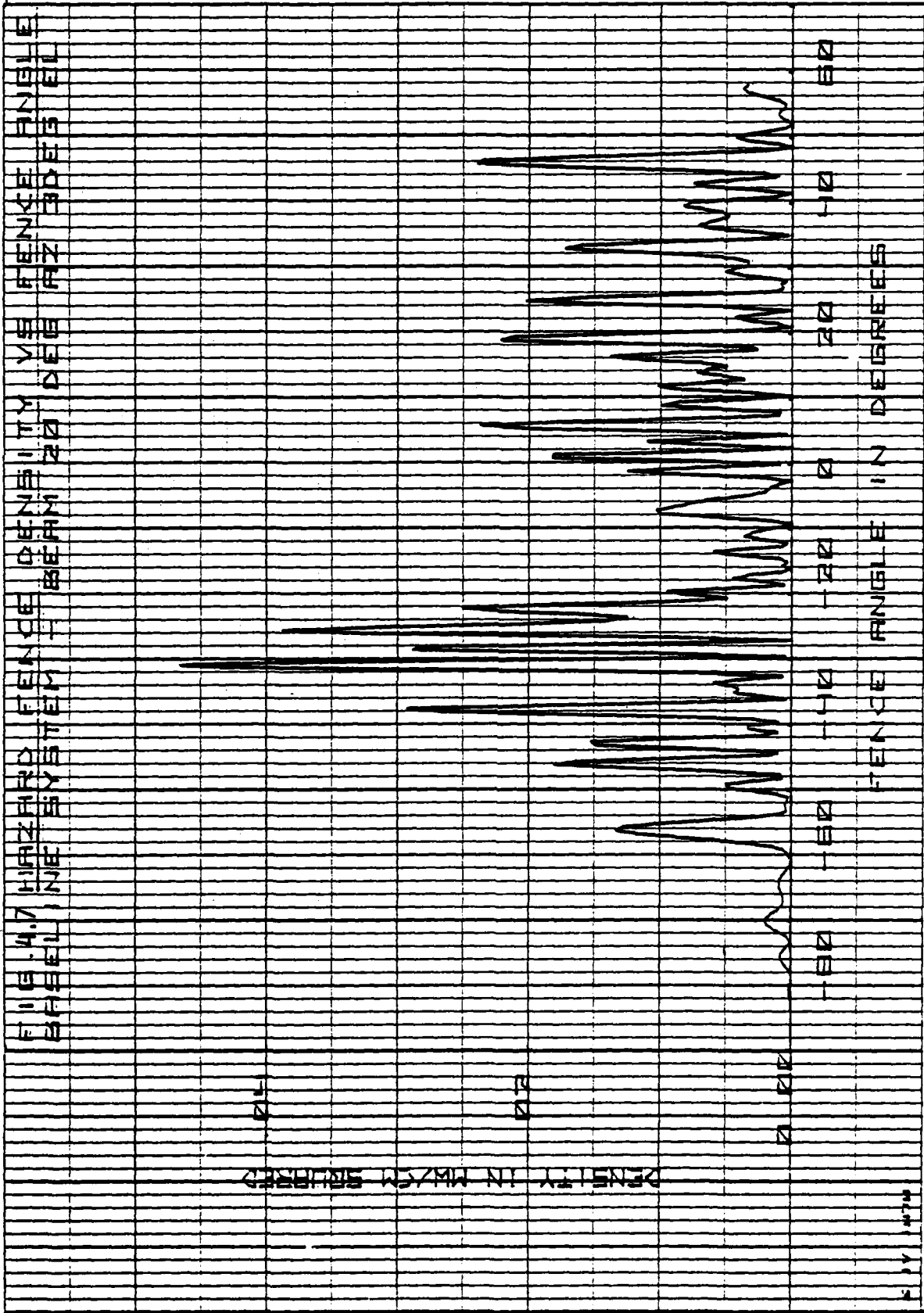
POSITION
0 1 2 3 4 5 6 7 8 9 10

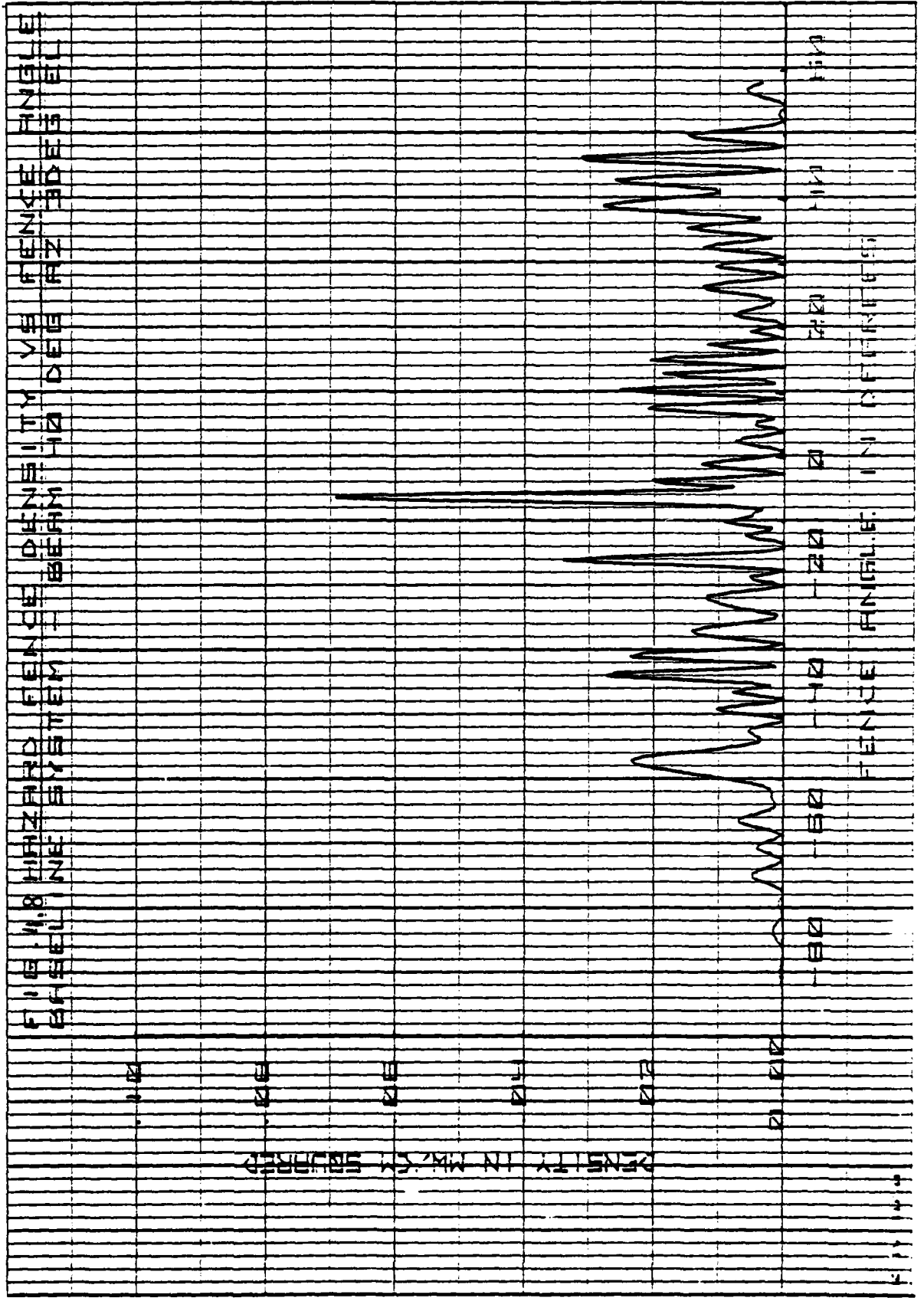


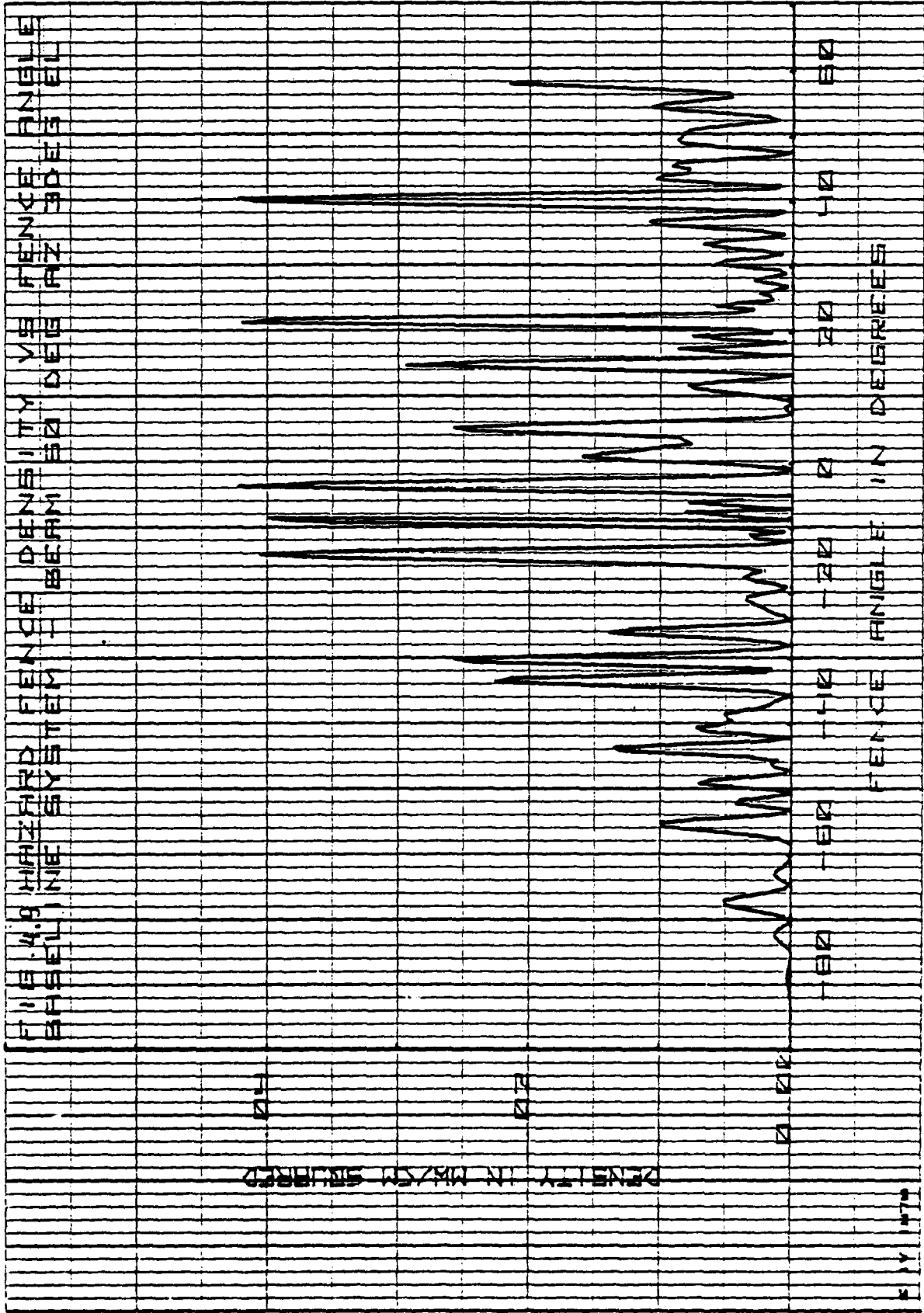
FILE 4.7 HIRAZARD FENCE DENSITY VE FENCE ANGLE
EPA 88-011 NIE SYSTEM - BRENNI 20 DEB HZ 30ES EIL

DENSITY IN M2/M2 SQUARED

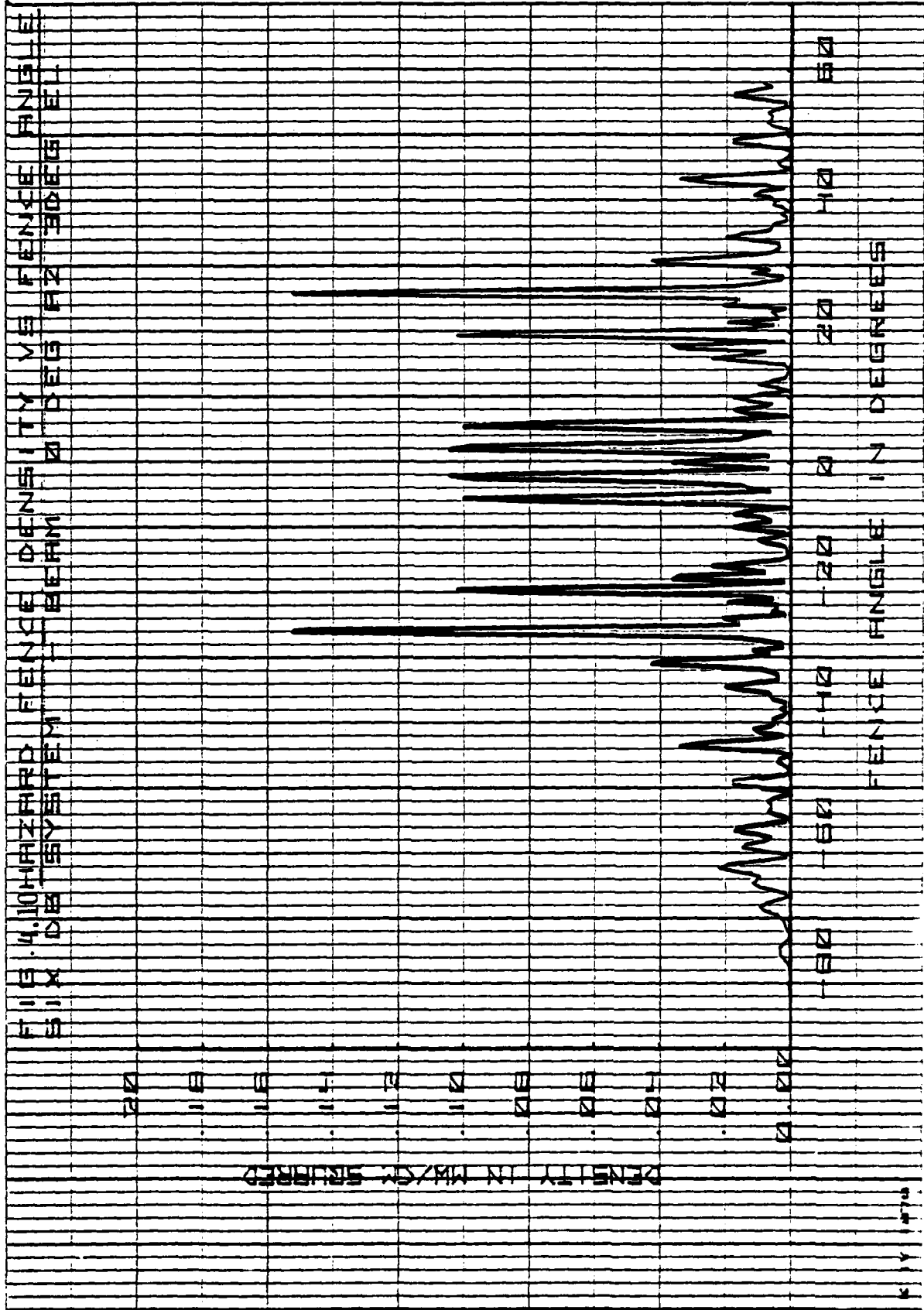
FENCE ANGLE IN DEGREES

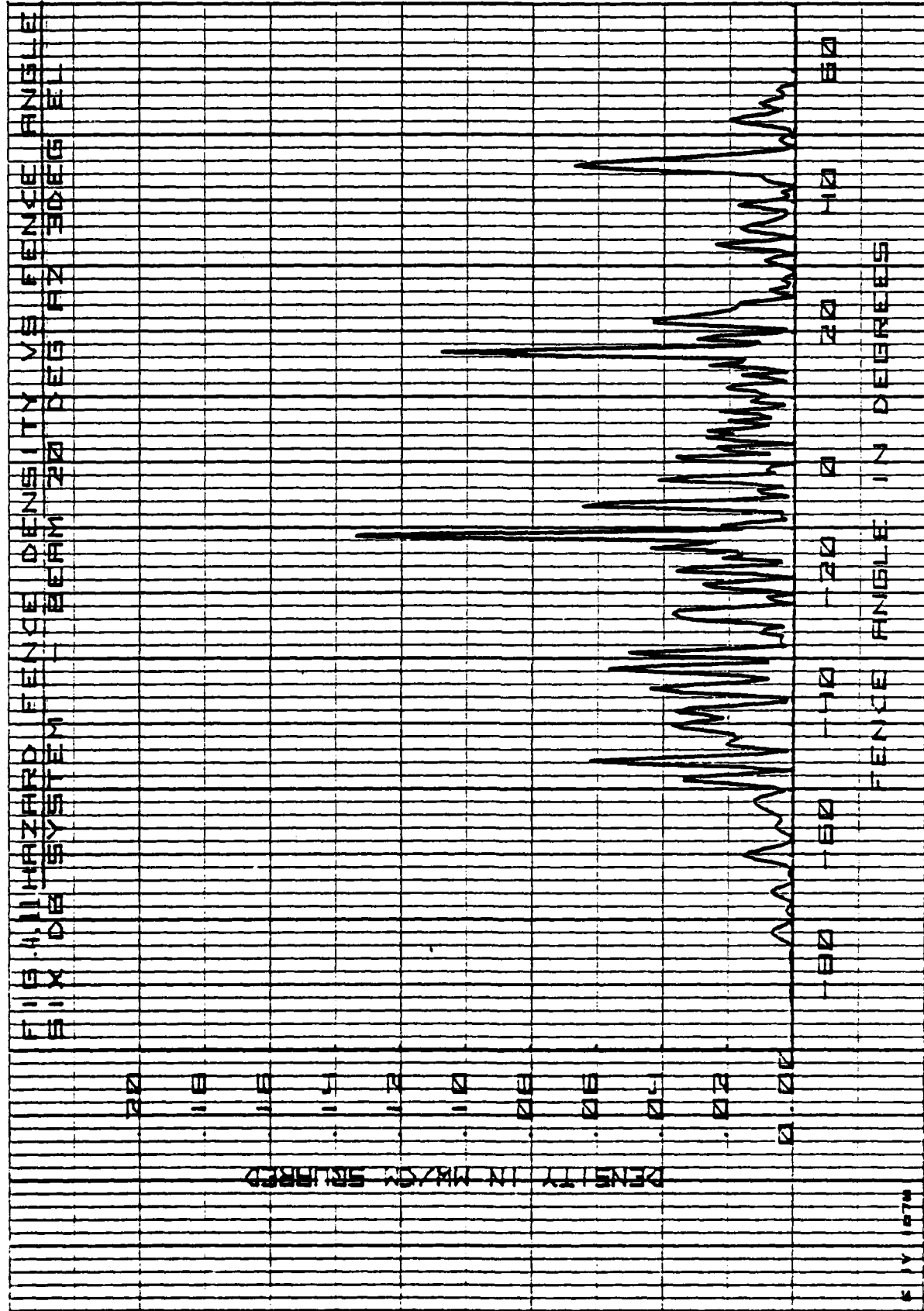


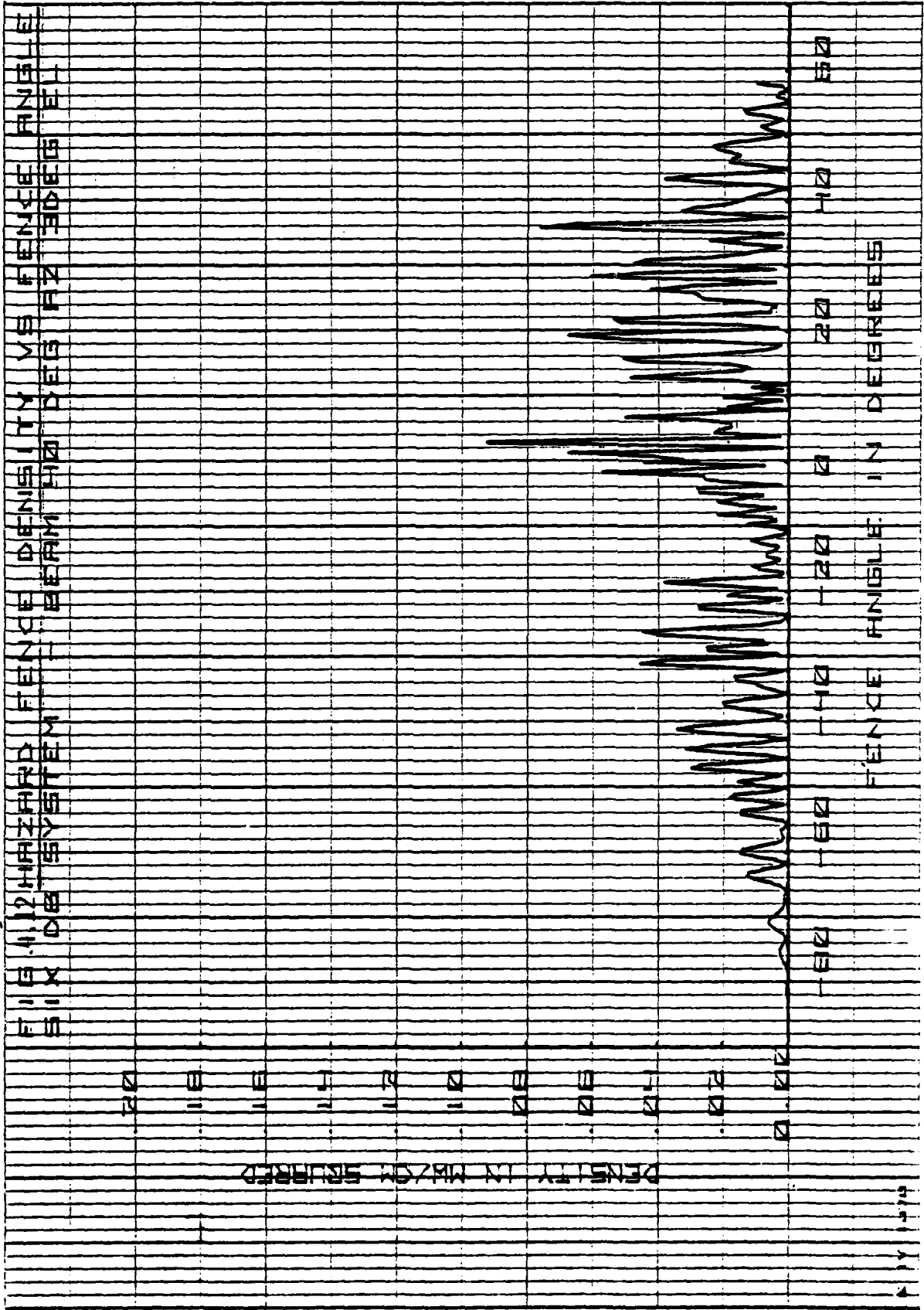


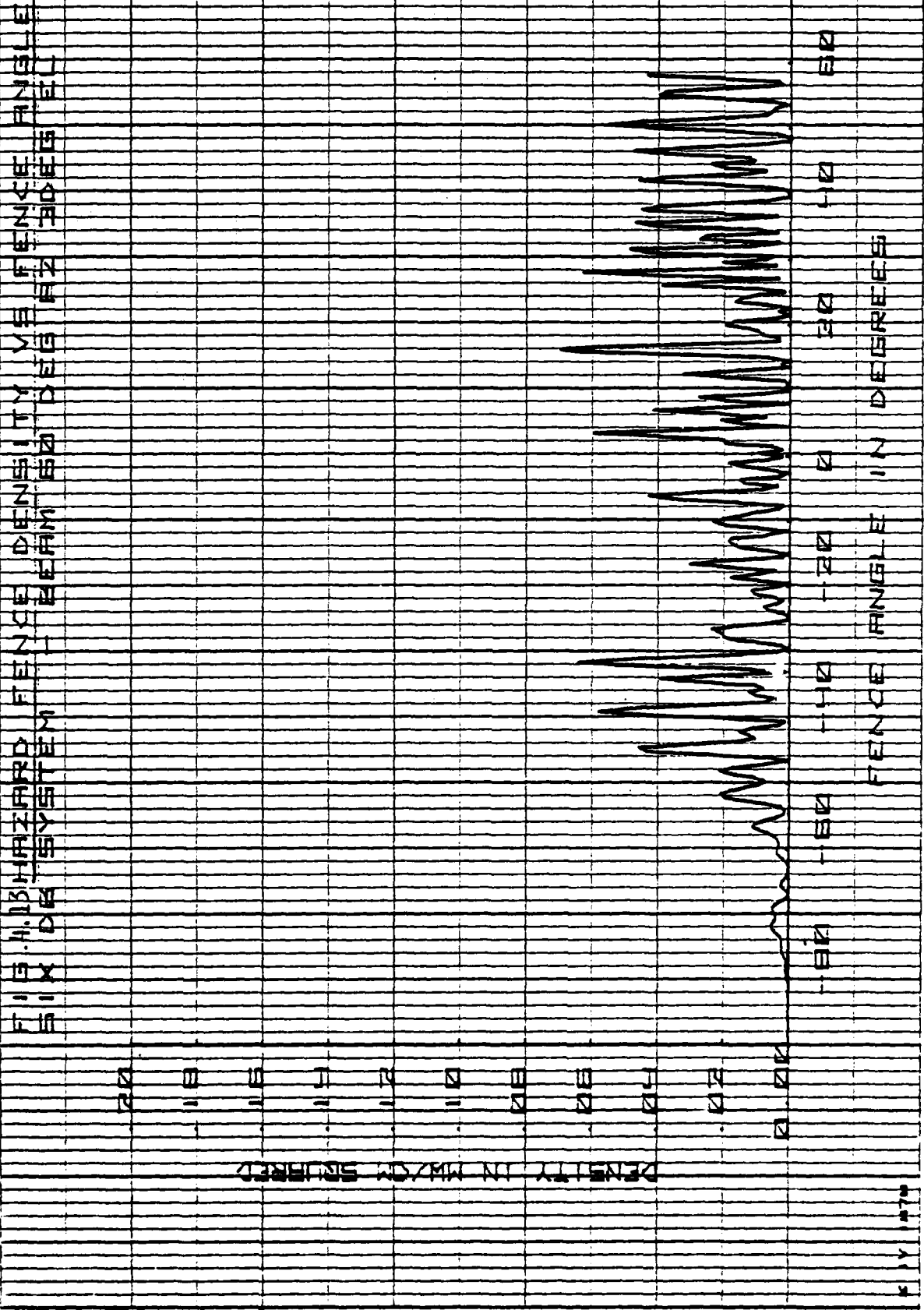


1170









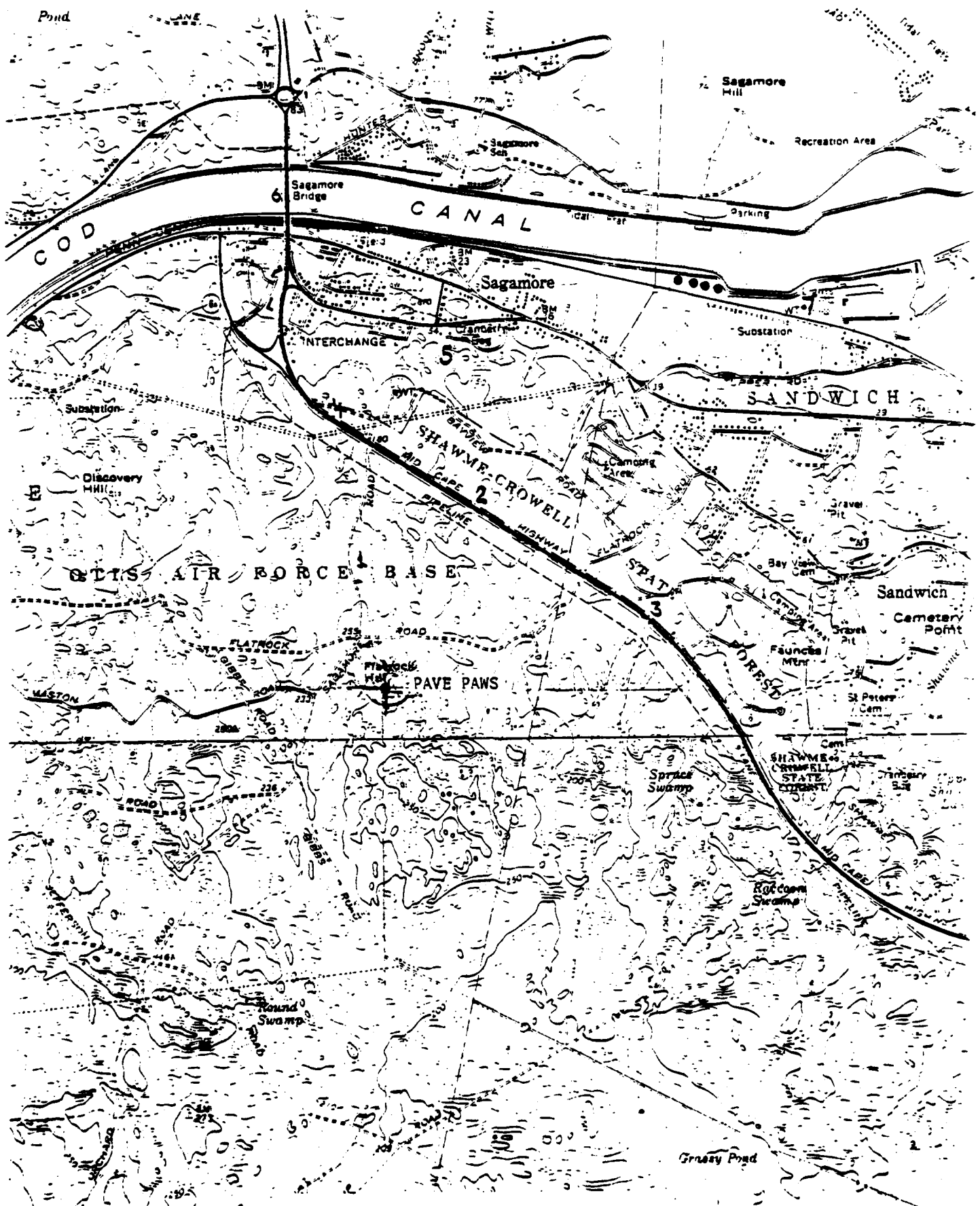
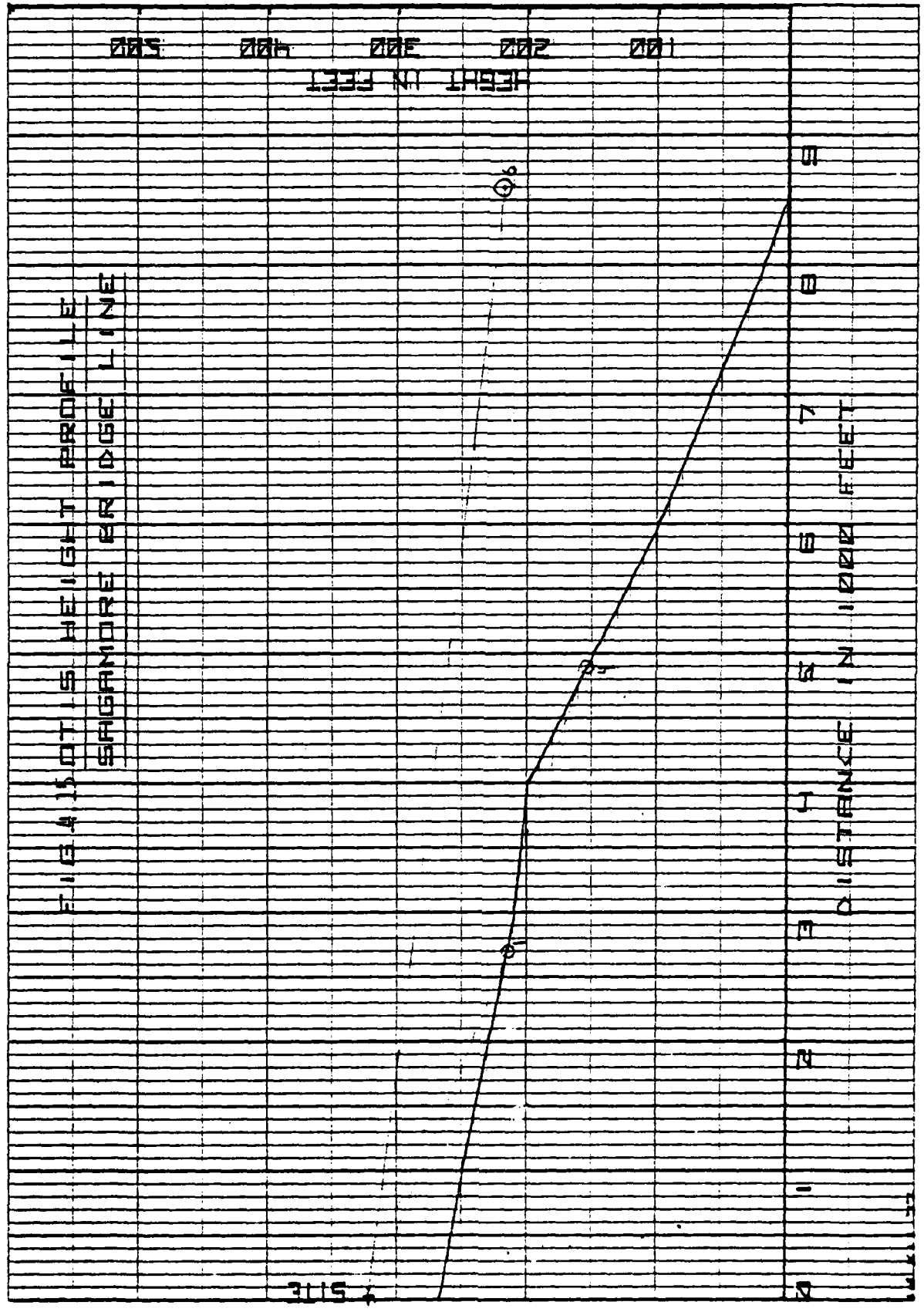


FIG. 4.14 SELECTED POINTS



3115

HEWLETT PACKARD 82701606

FIVE FOOT'S HEIGHT PROFILE
MID-CARE HIGHWAY C

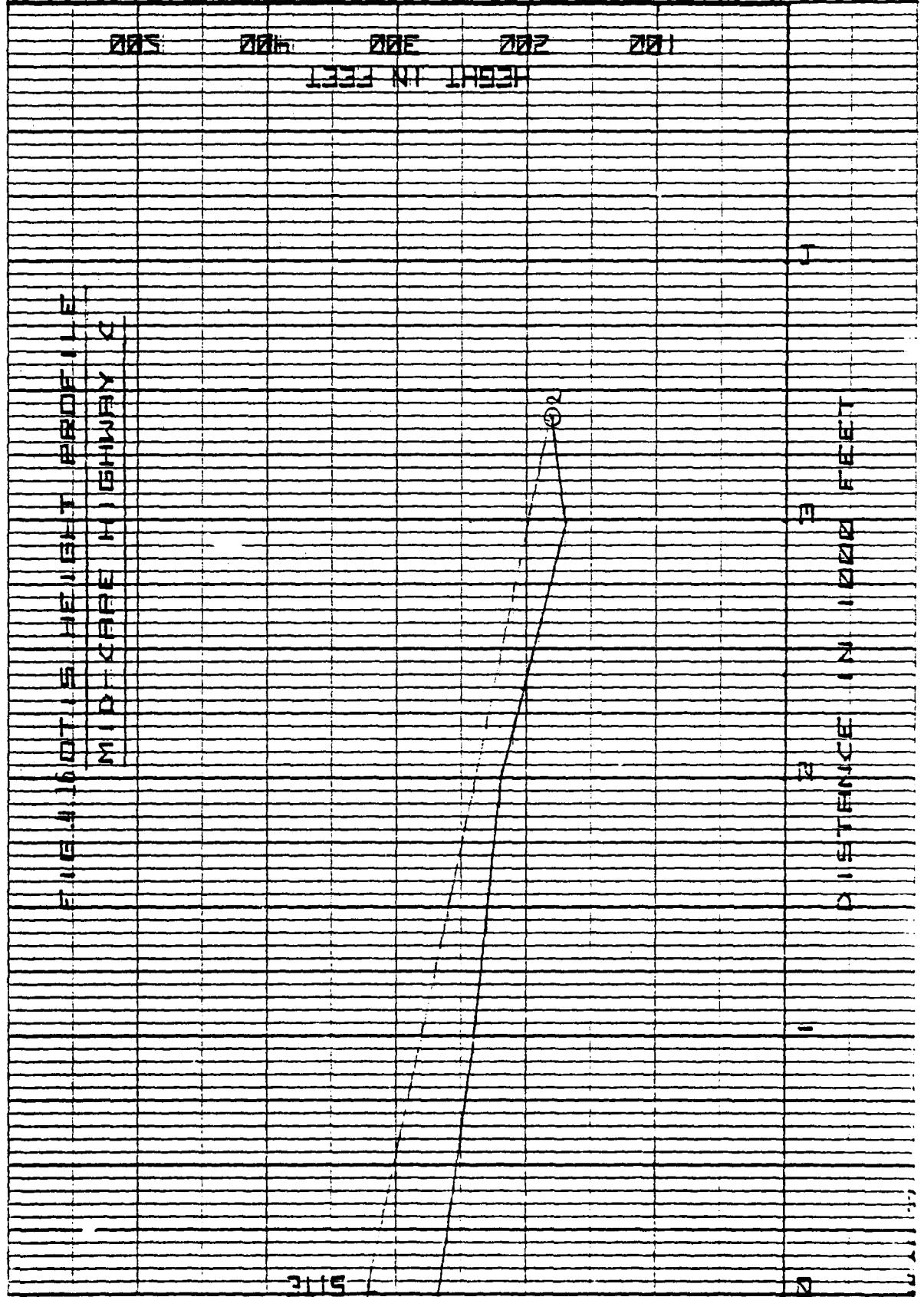
HEIGHT IN FEET

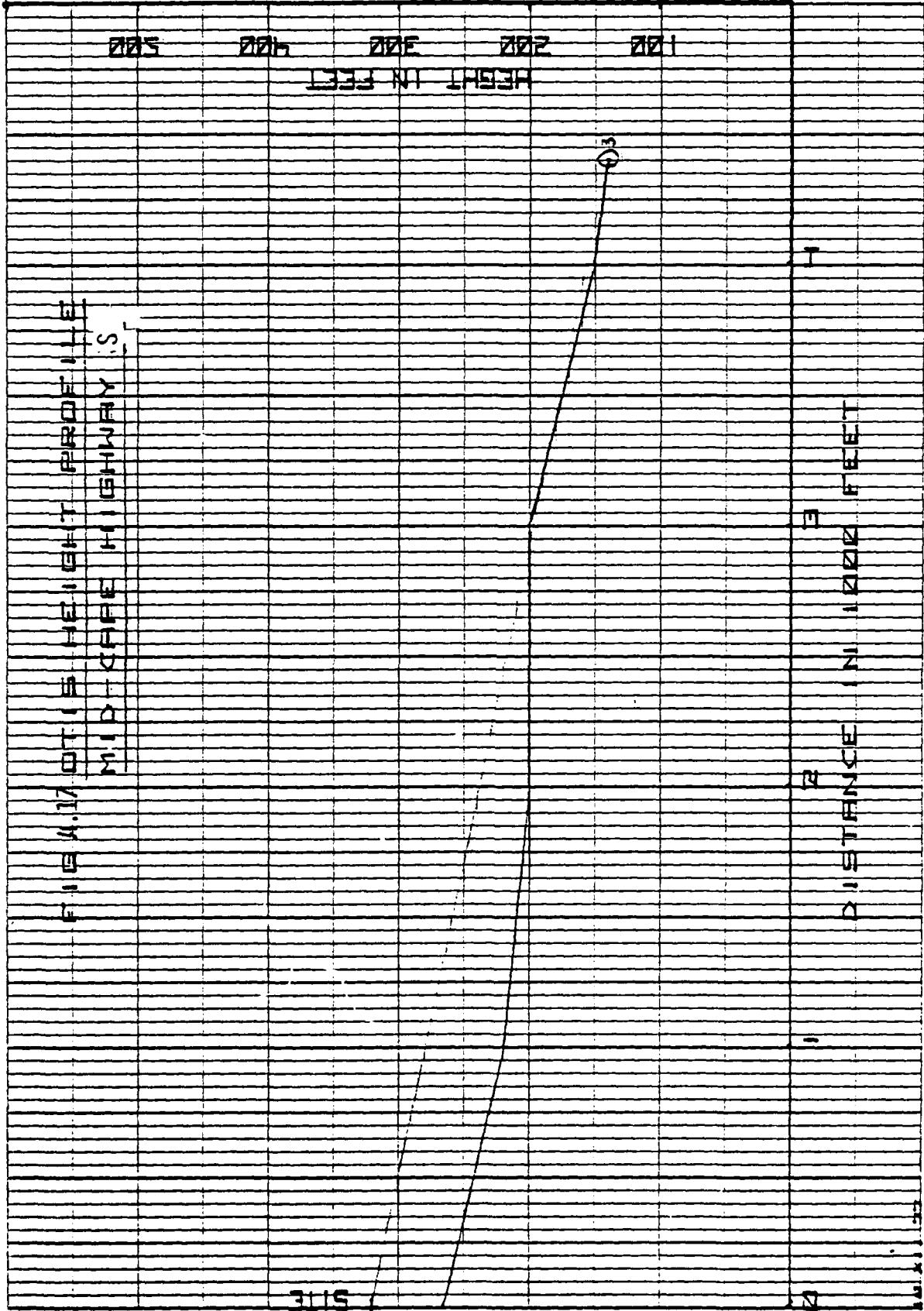
102 101 100 99 98

DISTANCE IN FEET

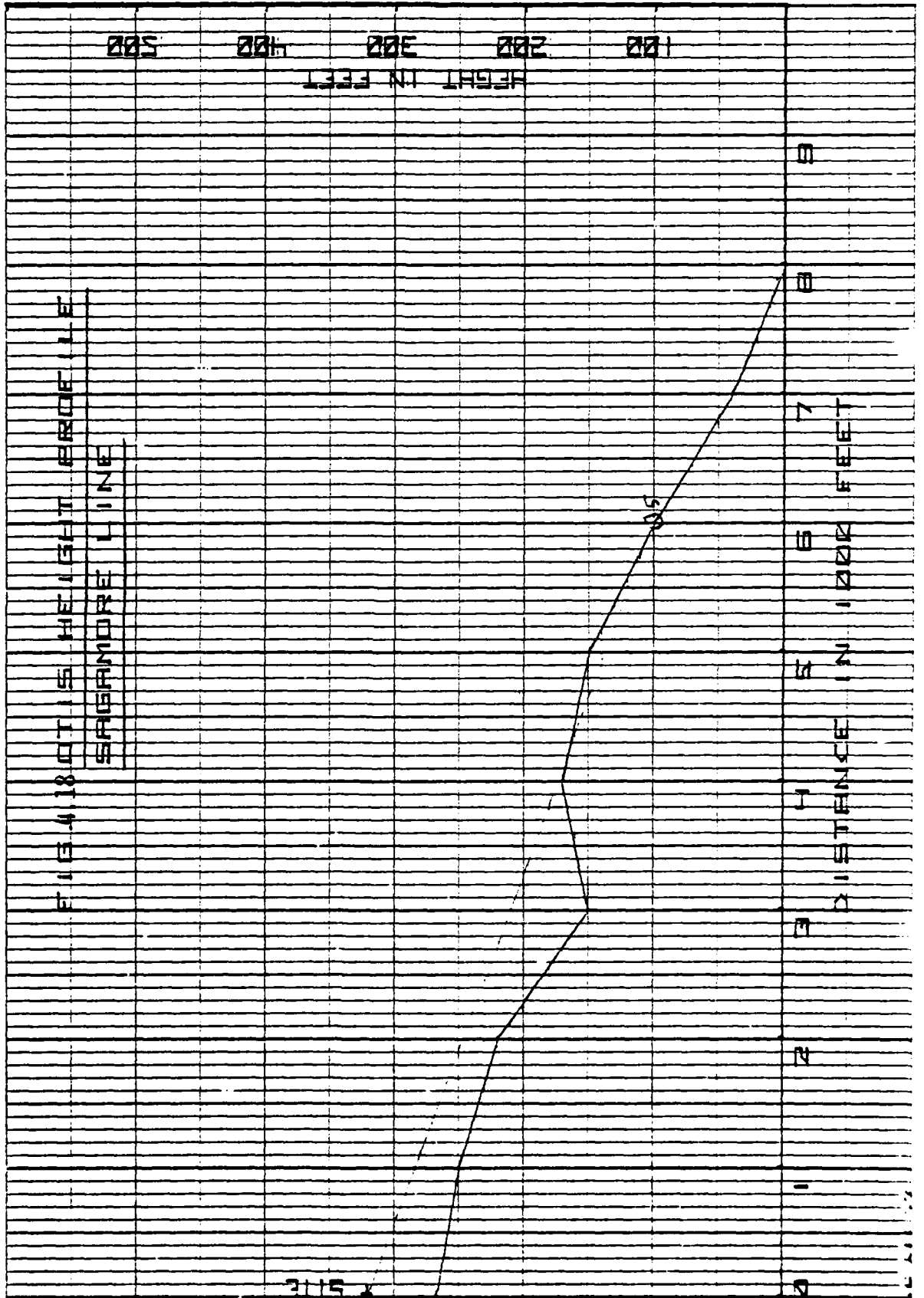
10 20 30 40 50 60 70 80 90 100

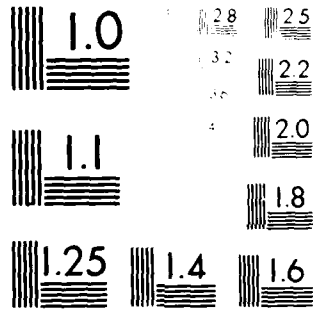
3115





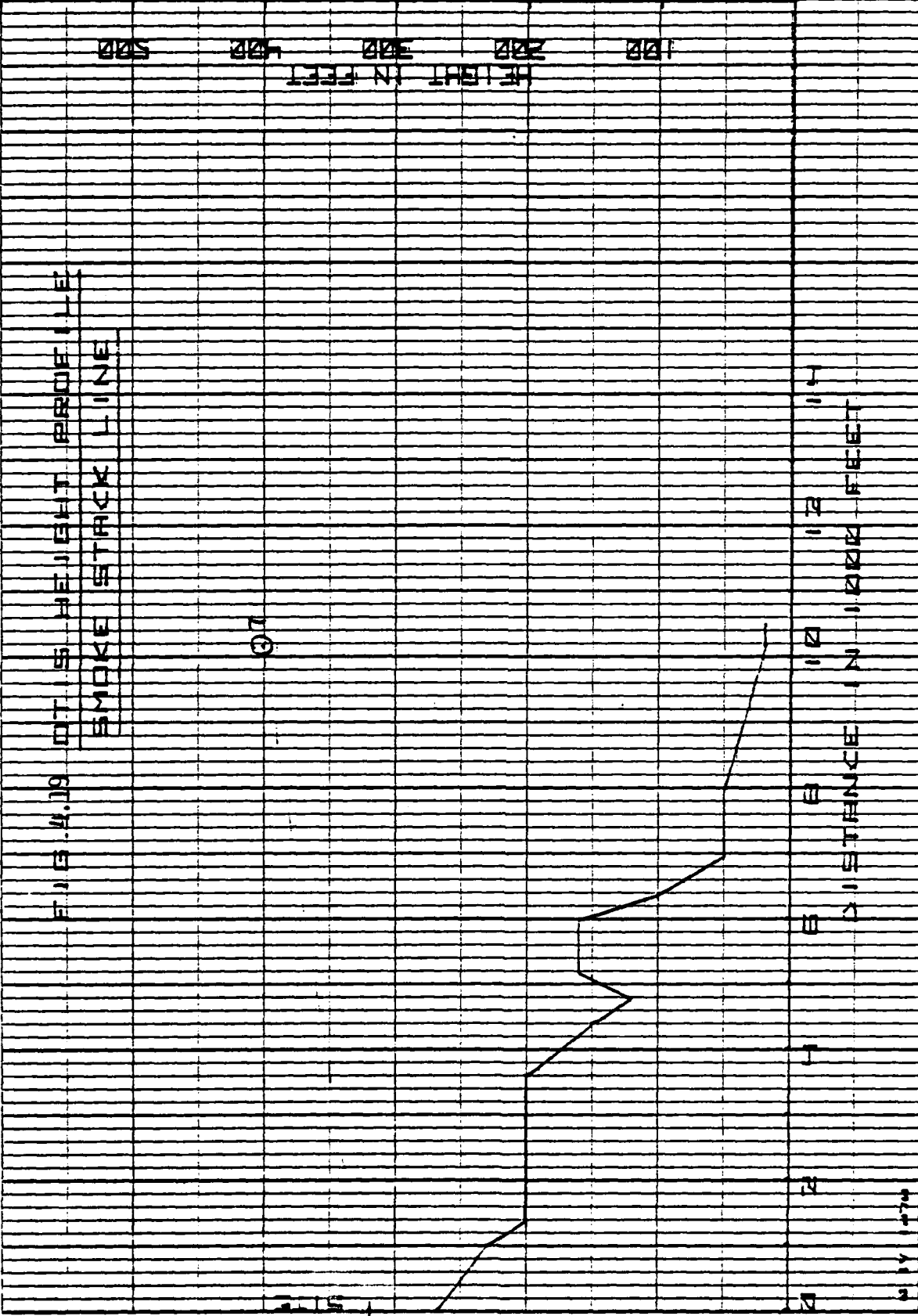
HEWLETT PACKARD 9270 1000





MICROCOPY RESOLUTION TEST CHART
NATIONAL BUREAU OF STANDARDS-1963-A

F113 4.19 DT 55 HEIGHT BRIDGE LINE
SMOKE STRICK LINE

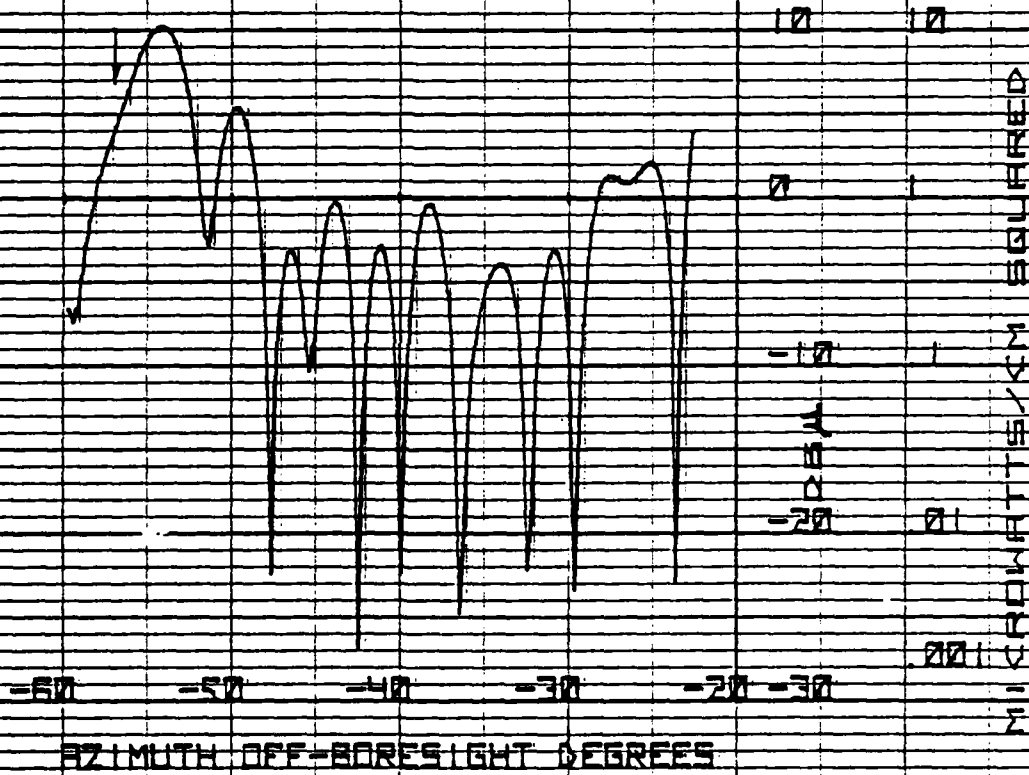


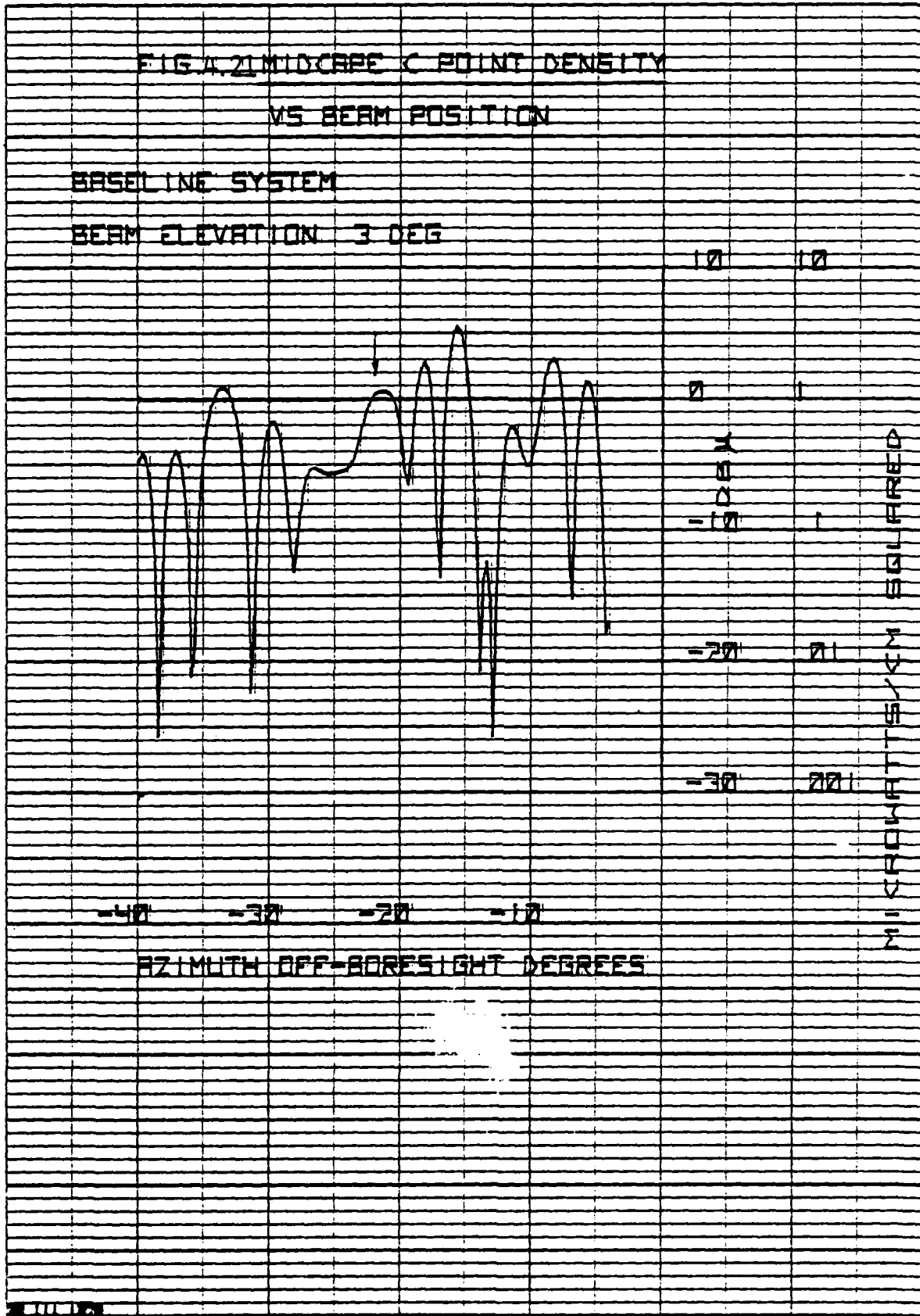
HEWLETT PACKARD 9270 1009

FIG 4.20 HIGHWAY 25 POINT DENSITY
VS BEAM POSITION

BASELINE SYSTEM

BEAM ELEVATION 3 DEG



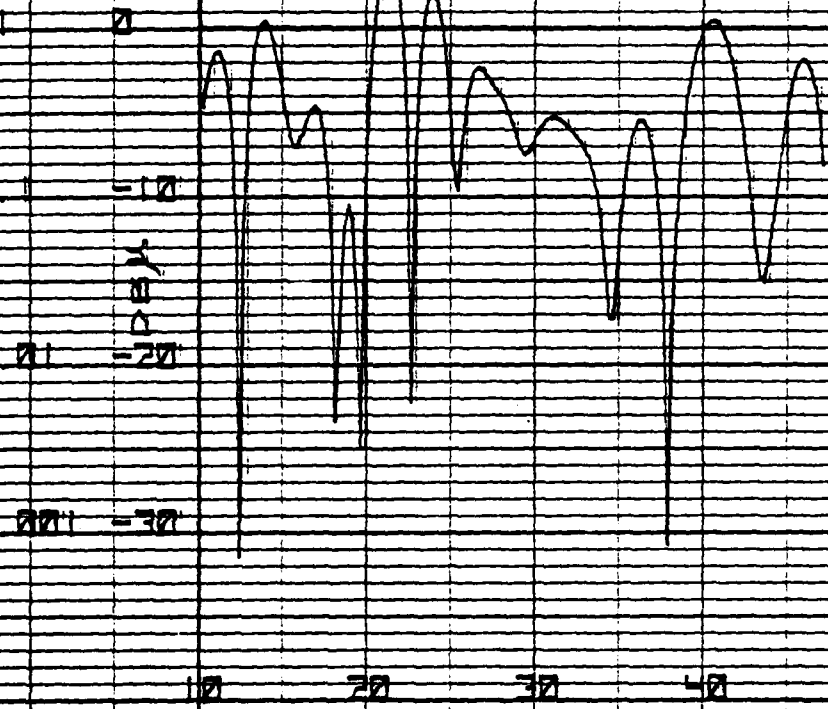


HEWLETT PACKARD 9270 1006

FIG. 4.22 MIDCBE 5 POINT DENSITY
VS BEAM POSITION

BASELINE SYSTEM
BEAM ELEVATION 3 DEG
10 10

MICROWATT/CM SQUARED

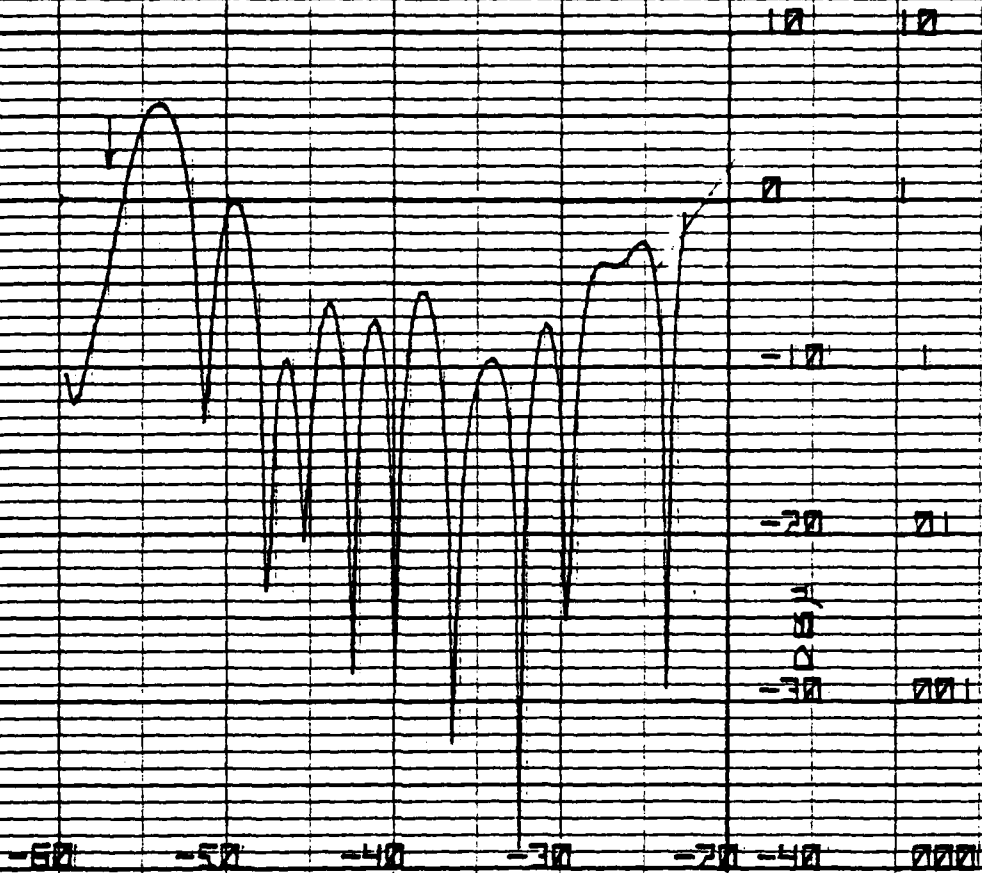


AZIMUTH OFF-BORESIGHT DEGREES

FIG 4.23 MIDCAPE N POINT DENSITY
VS BEAM POSITION

BASELINE SYSTEM

BEAM ELEVATION 3 DEG



AZIMUTH OFF-BORESIGHT DEGREES

POINT DENSITY

MIDCAPE N POINT DENSITY

HEWLETT-PACKARD 92701000

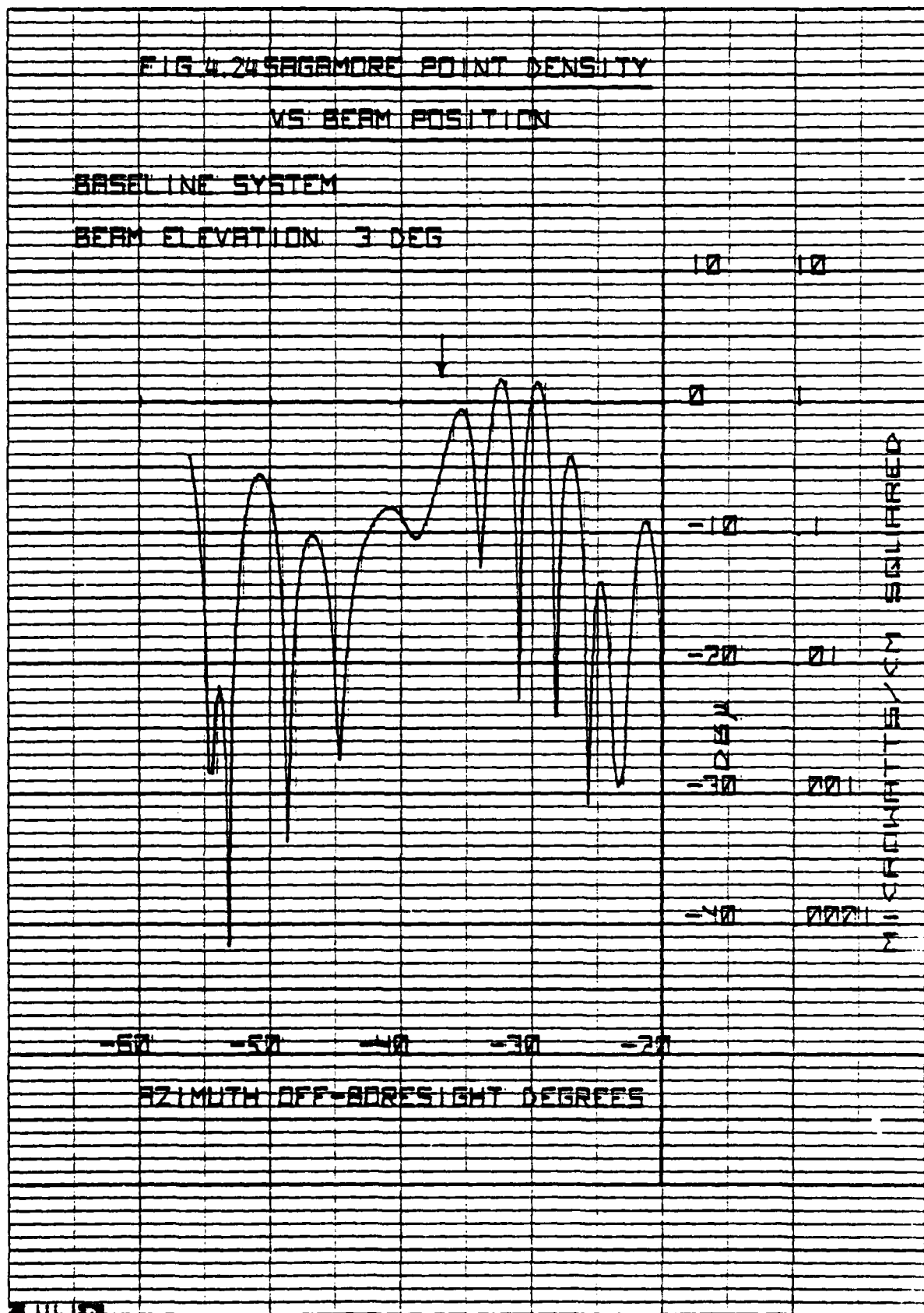
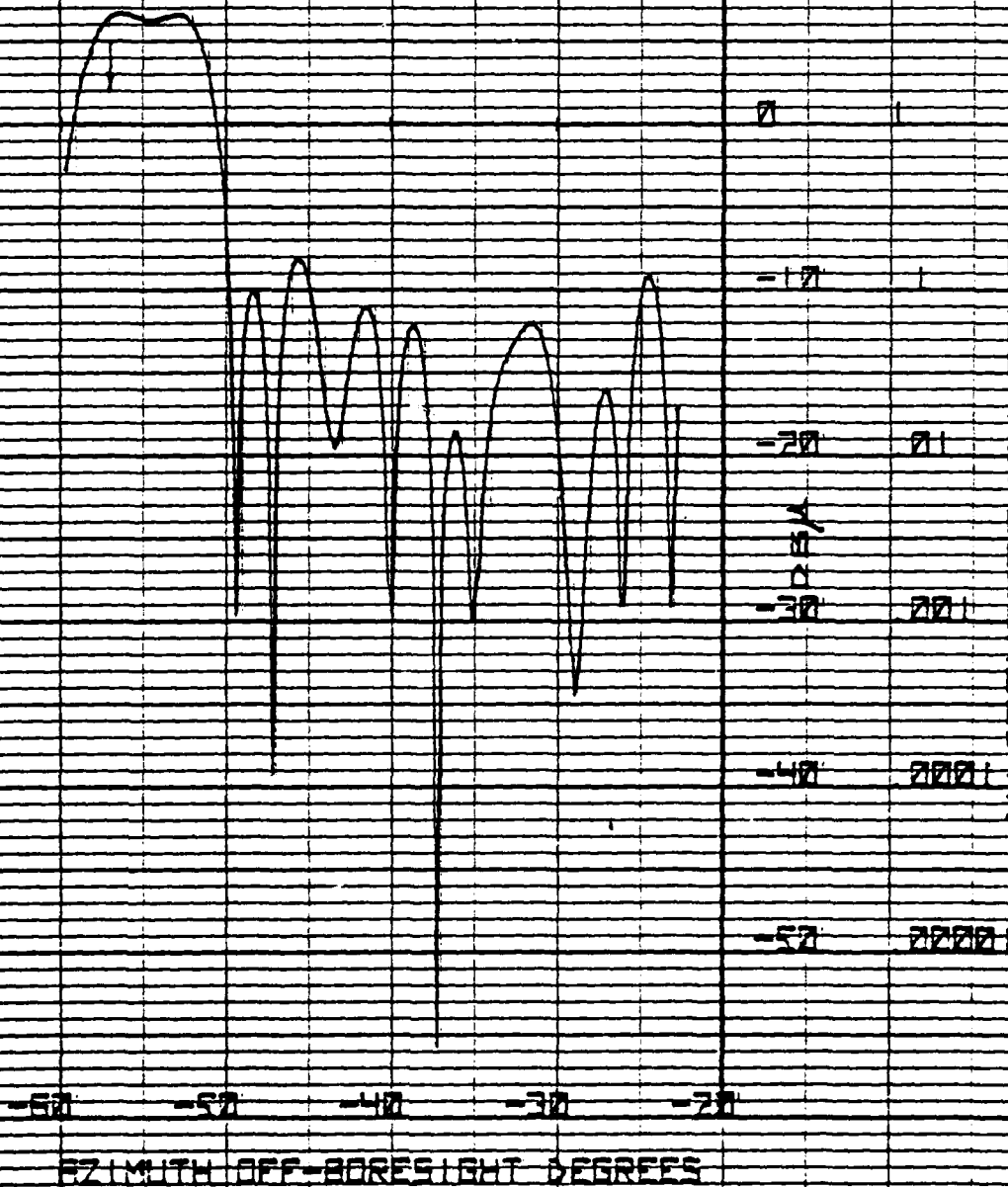


FIG 4.25 SAGAMORE BRIDGE POINT DENSITY

VS BEAM POSITION

BASELINE SYSTEM

BEAM ELEVATION 3 DEG



HEWLETT PACKARD 52701000

HEWLETT/PACKARD 9270 1006

FIG. 4.26 SMOKE STACK POINT DENSITY
VS BEAM POSITION

BASELINE SYSTEM

BEAM ELEVATION 3 DEG

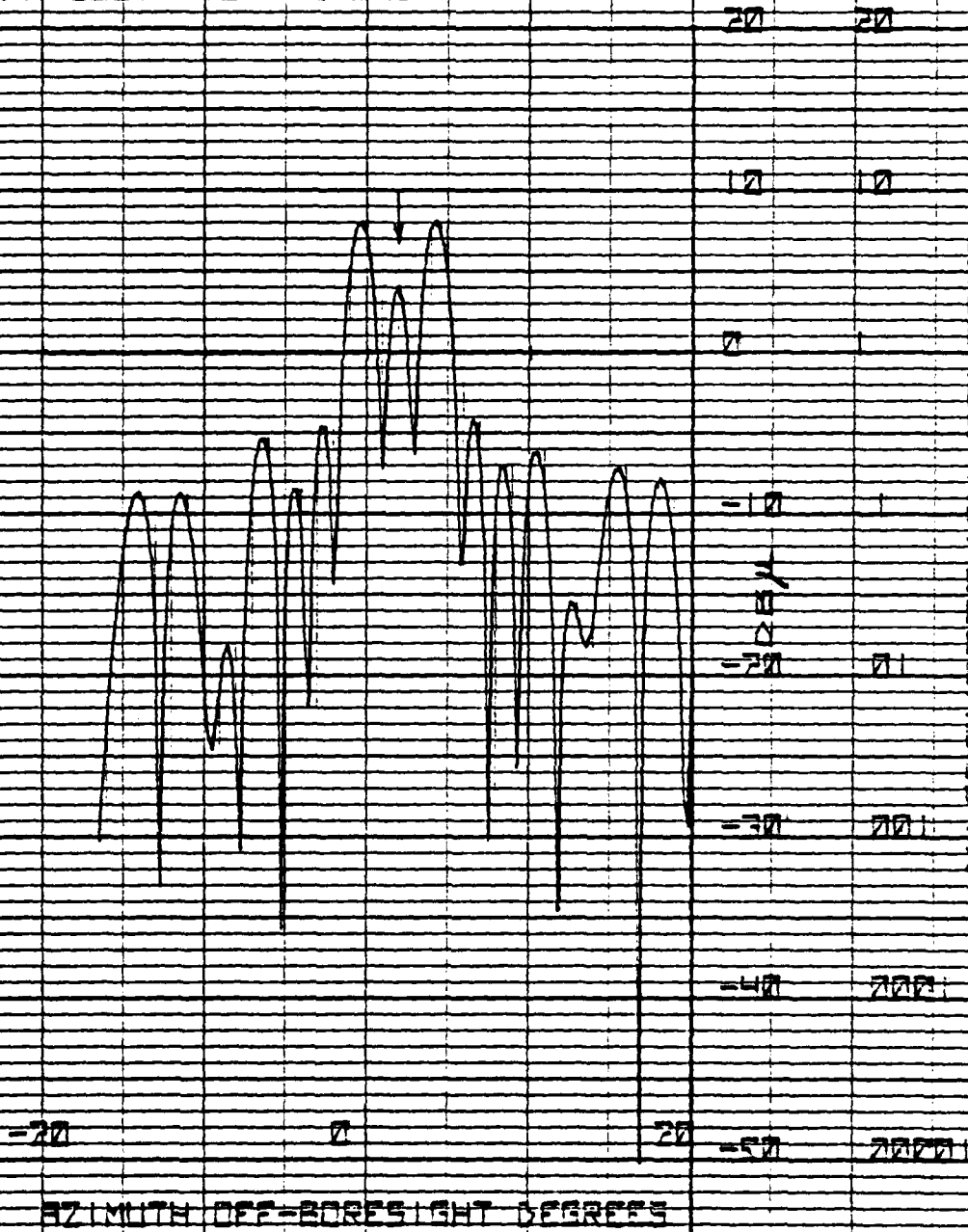
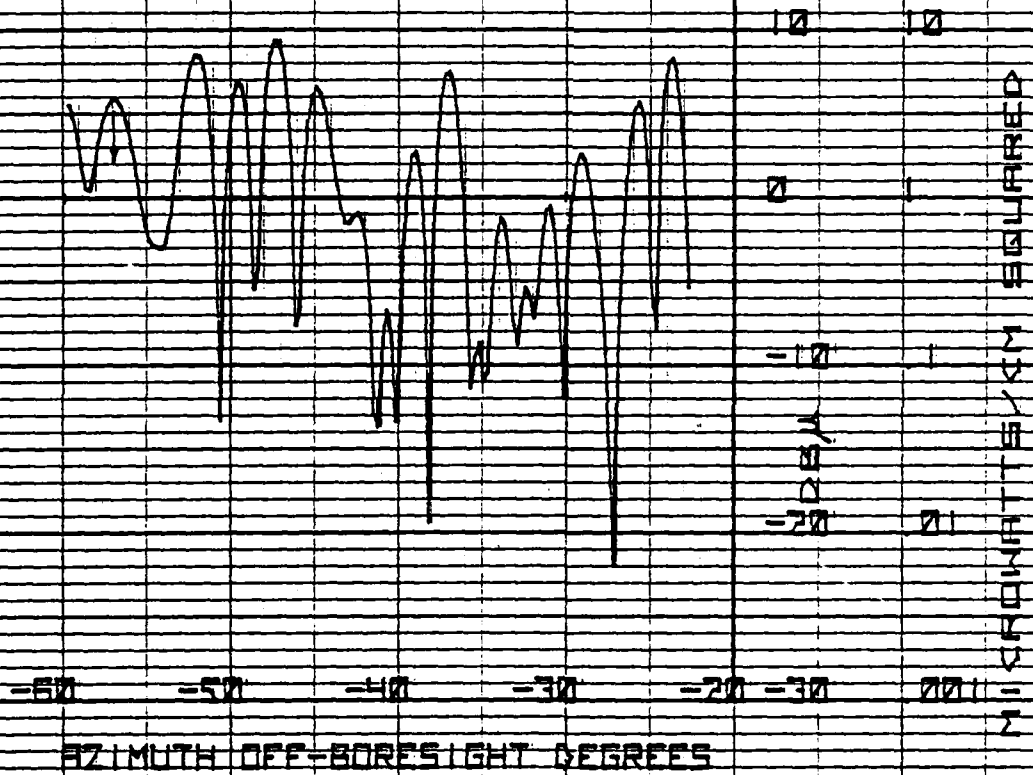


FIG. 4.27 HIGHWAY 25 POINT DENSITY
VS BEAM POSITION

SIX DB SYSTEM

BEAM ELEVATION 3 DEG



HEWLETT-PACKARD 5270 0000

HEWLETT-PACKARD 92701006

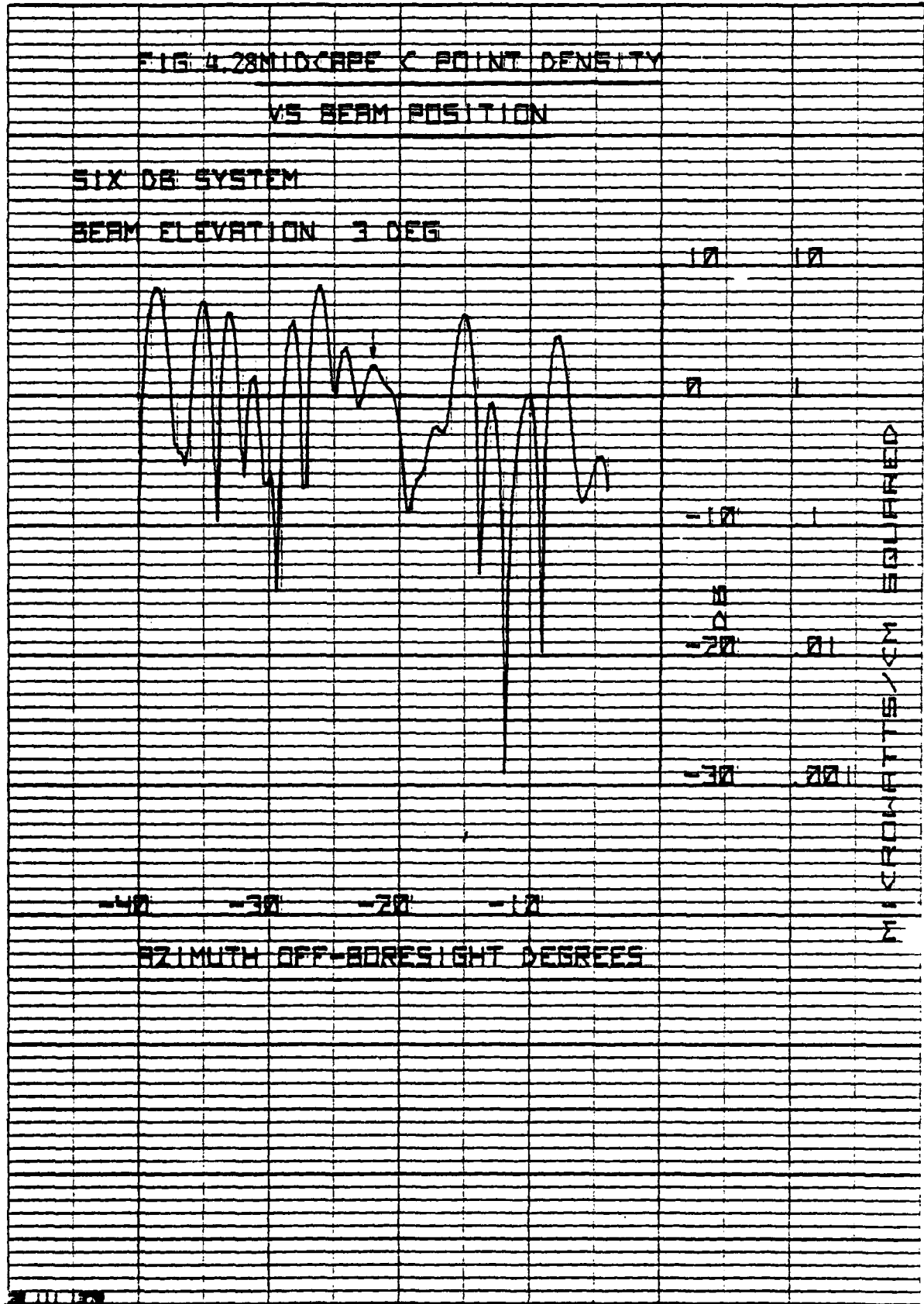
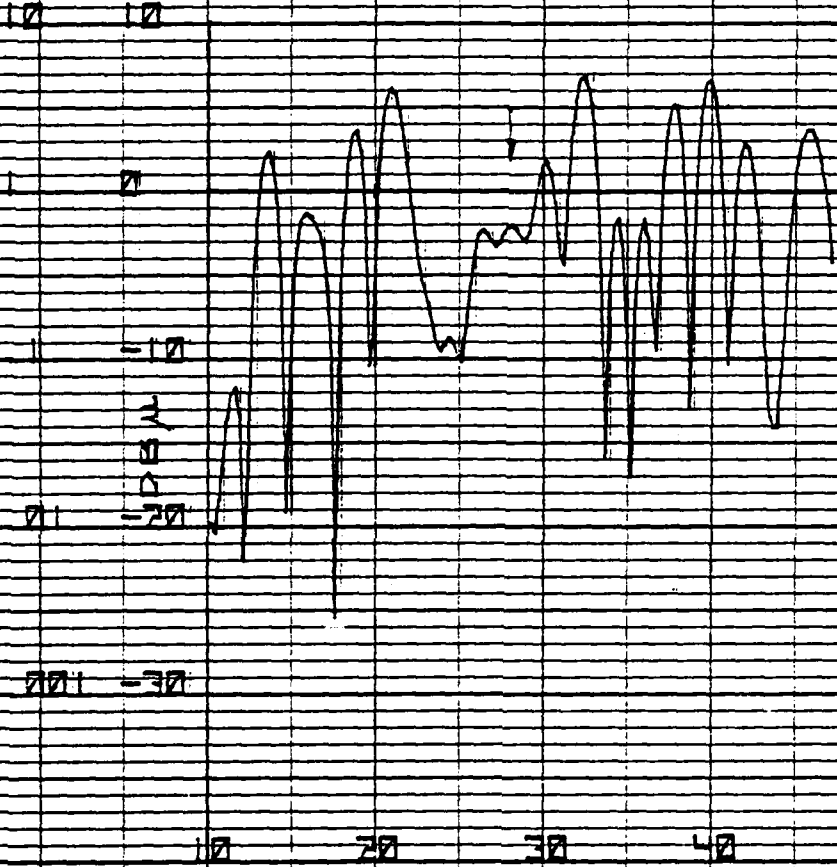


FIG. 4.29 MIDCBE 5 POINT DENSITY
VS BEAM POSITION

SIX DB SYSTEM

BEAM ELEVATION 3 DEG

MICROWATTES/KM SQUARED



AZIMUTH OFF-BORESIGHT DEGREES

HEWLETT PACKARD 9270 1000

20 JUL 1968

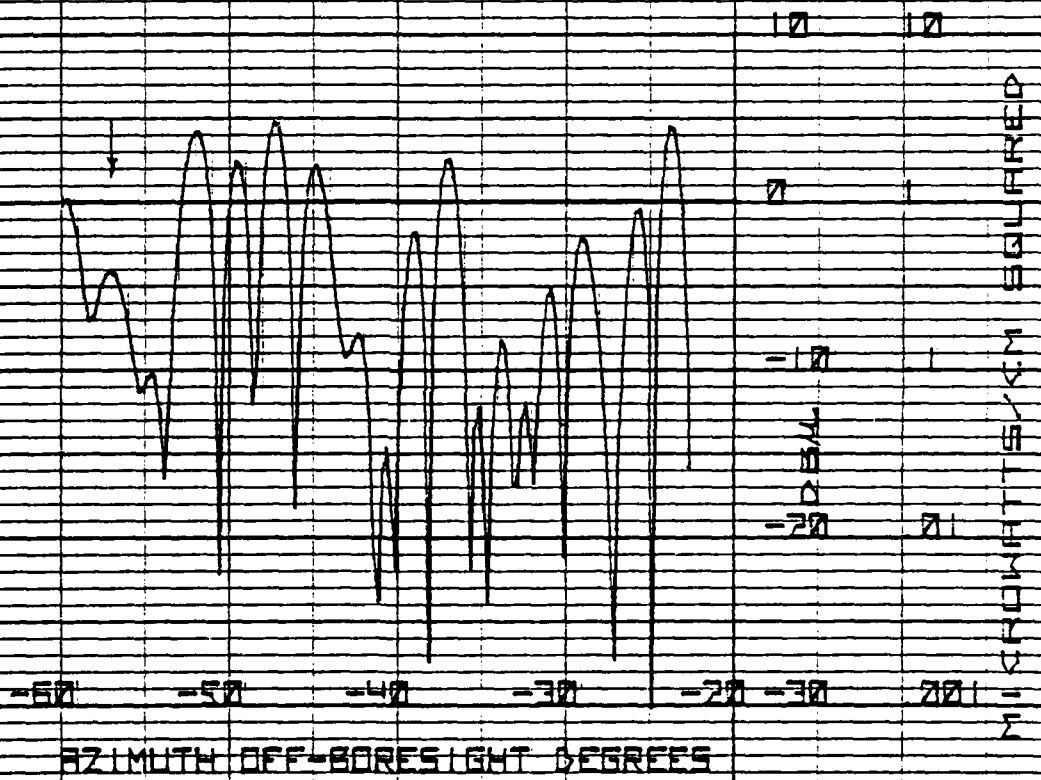
HEWLETT-PACKARD 92701000

FIG 4.30 MIDCAPE N POINT DENSITY

VS BEAM POSITION

SIX DB SYSTEM

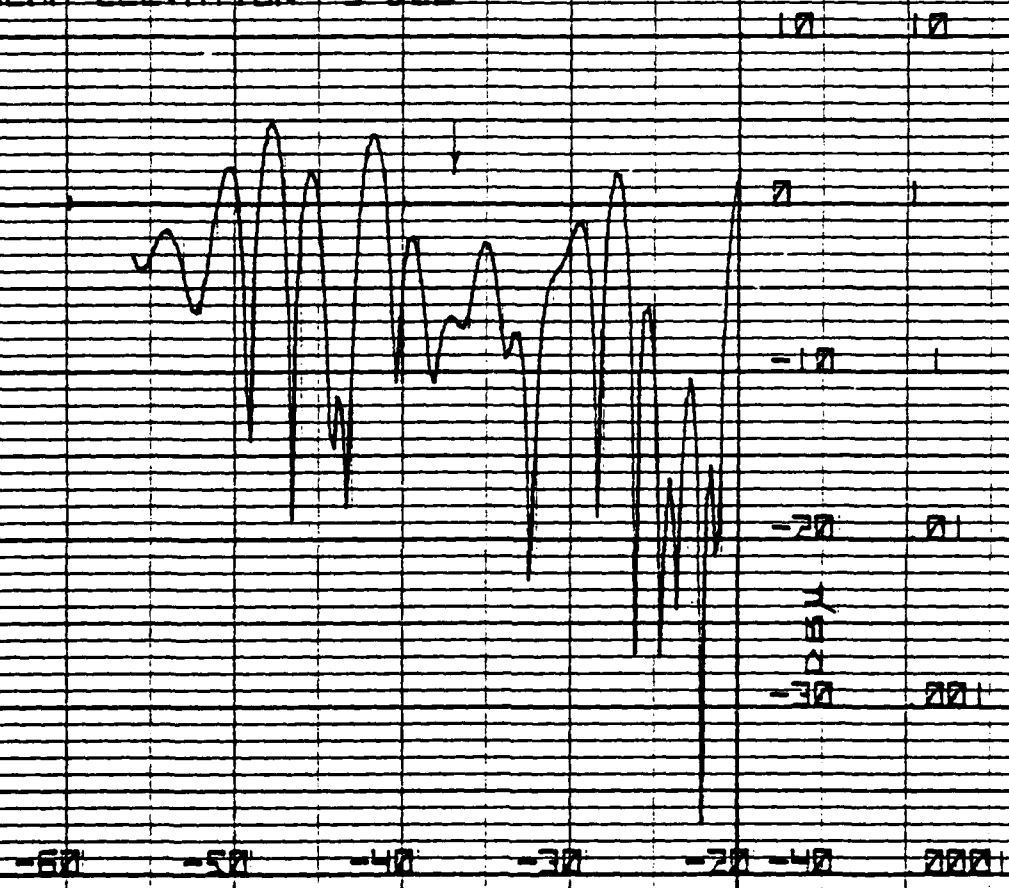
BEAM ELEVATION 3 DEG



111W1111PA RAH0 02/0 1000

FIG 4.31 SAGMORE POINT DENSITY
VS BEAM POSITION

SIX DB SYSTEM
BEAM ELEVATION 3 DEG



AZIMUTH OFF-BORESIGHT DEGREES

POINT DENSITY IN DB

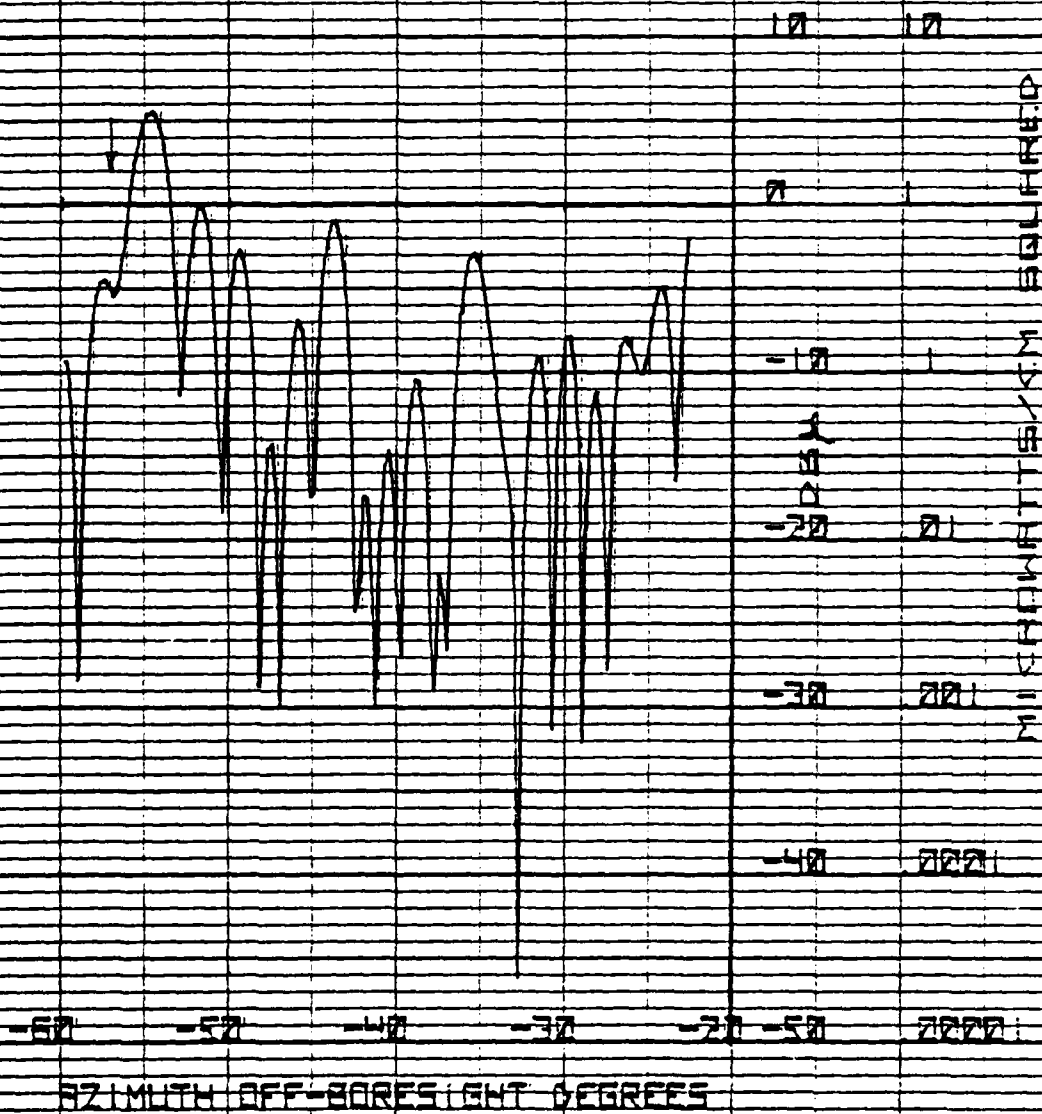
111W1111PA

HEWLETT PACKARD 52701006

FIG 4.32 SAGAMORE BRIDGE POINT DENSITY
VS BEAM POSITION

SIX DB SYSTEM

BEAM ELEVATION 3 DEG

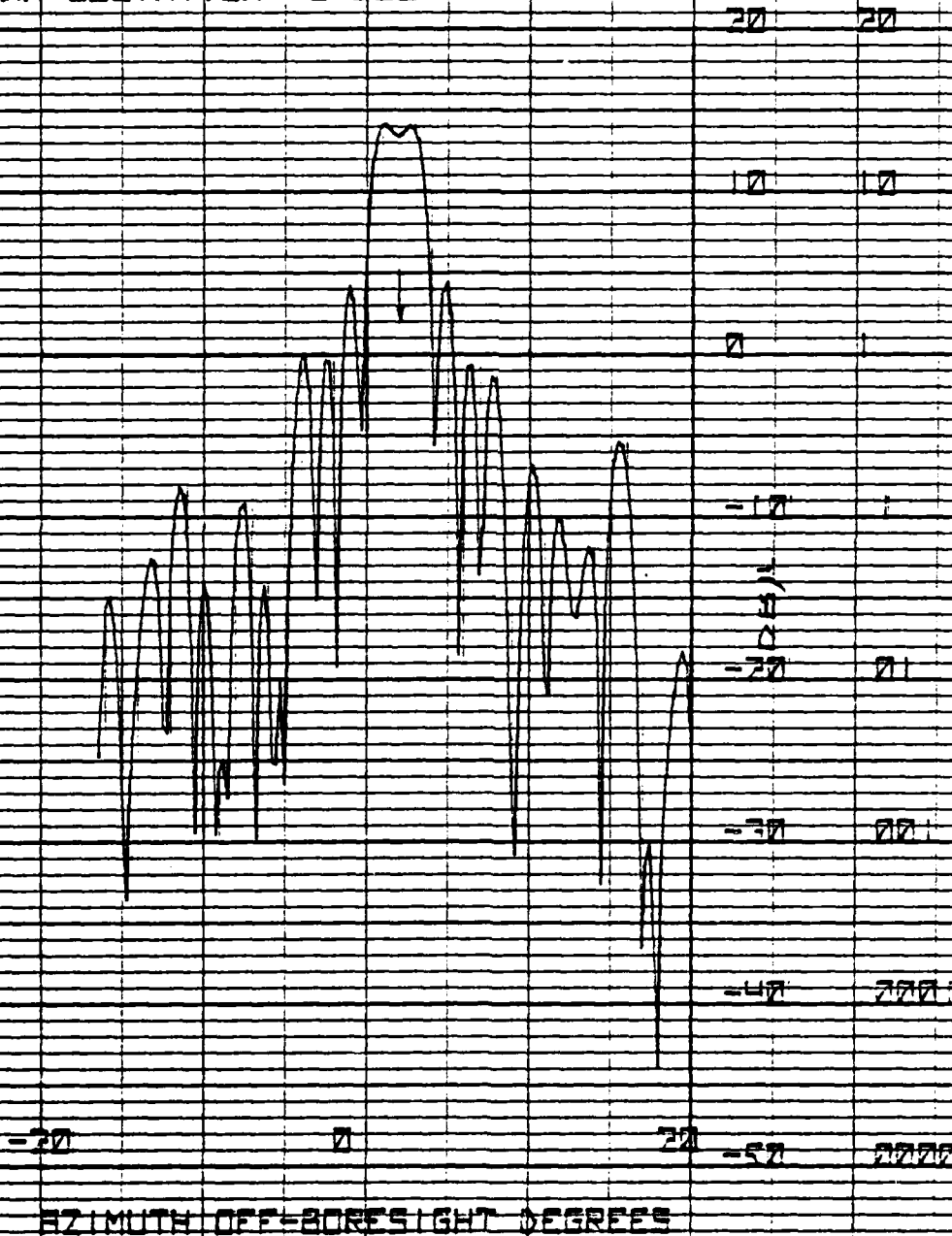


11 JUL 61 PALM BEACH 3270 1000H

FIG 4.33 SMOKE STACK POINT DENSITY VS BEAM POSITION

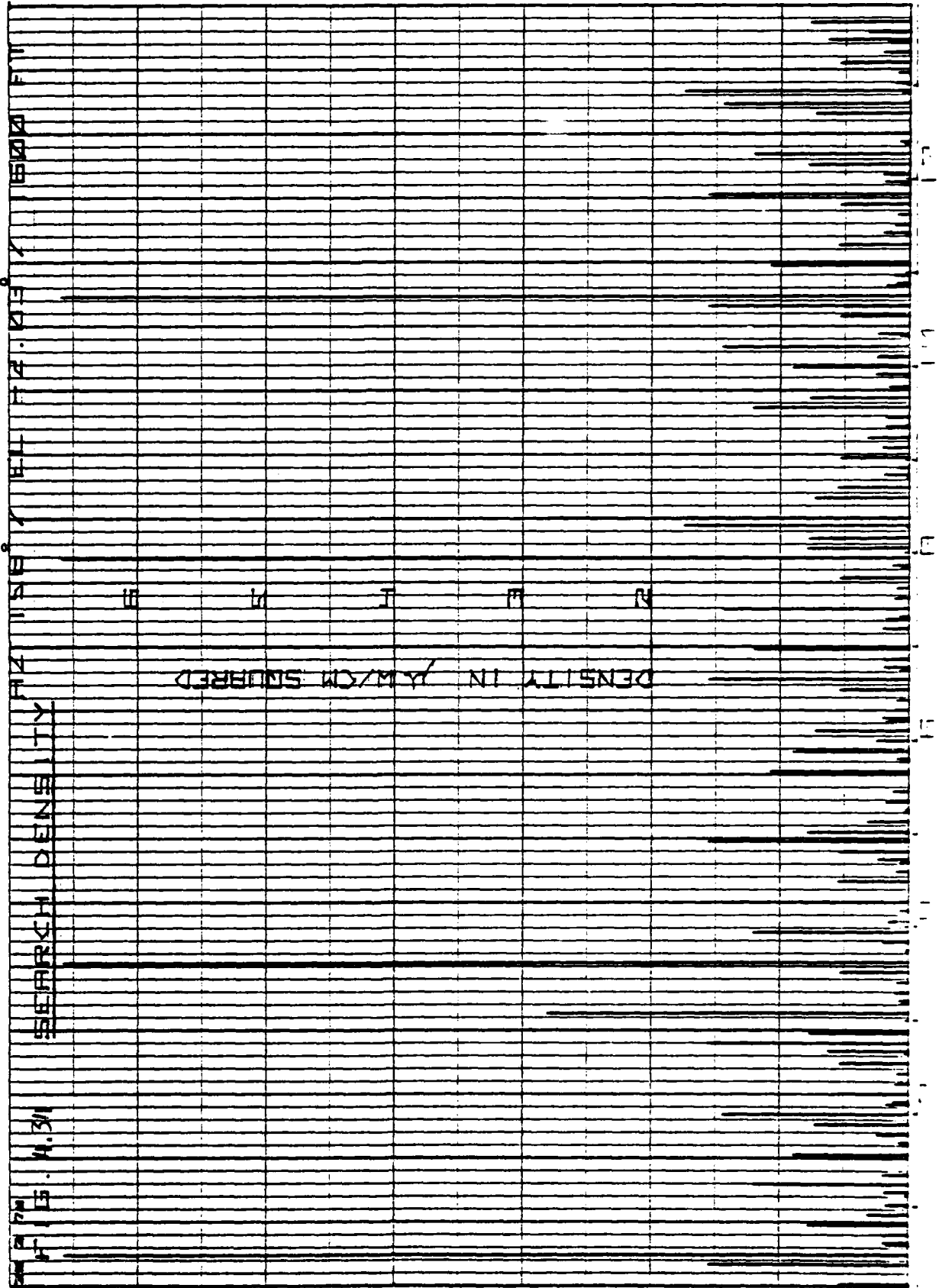
SIX DB SYSTEM

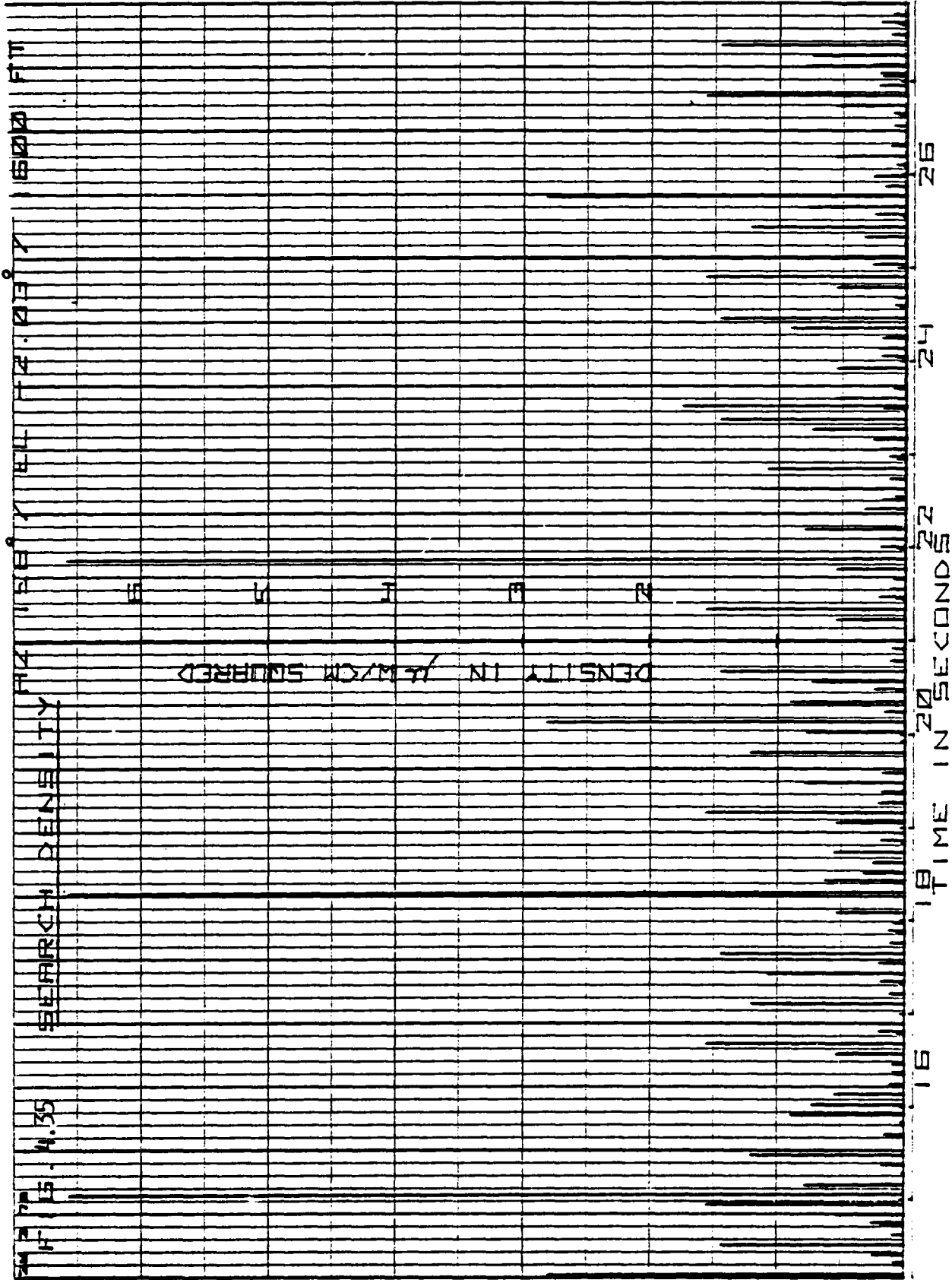
BEAM ELEVATION 3 DEG

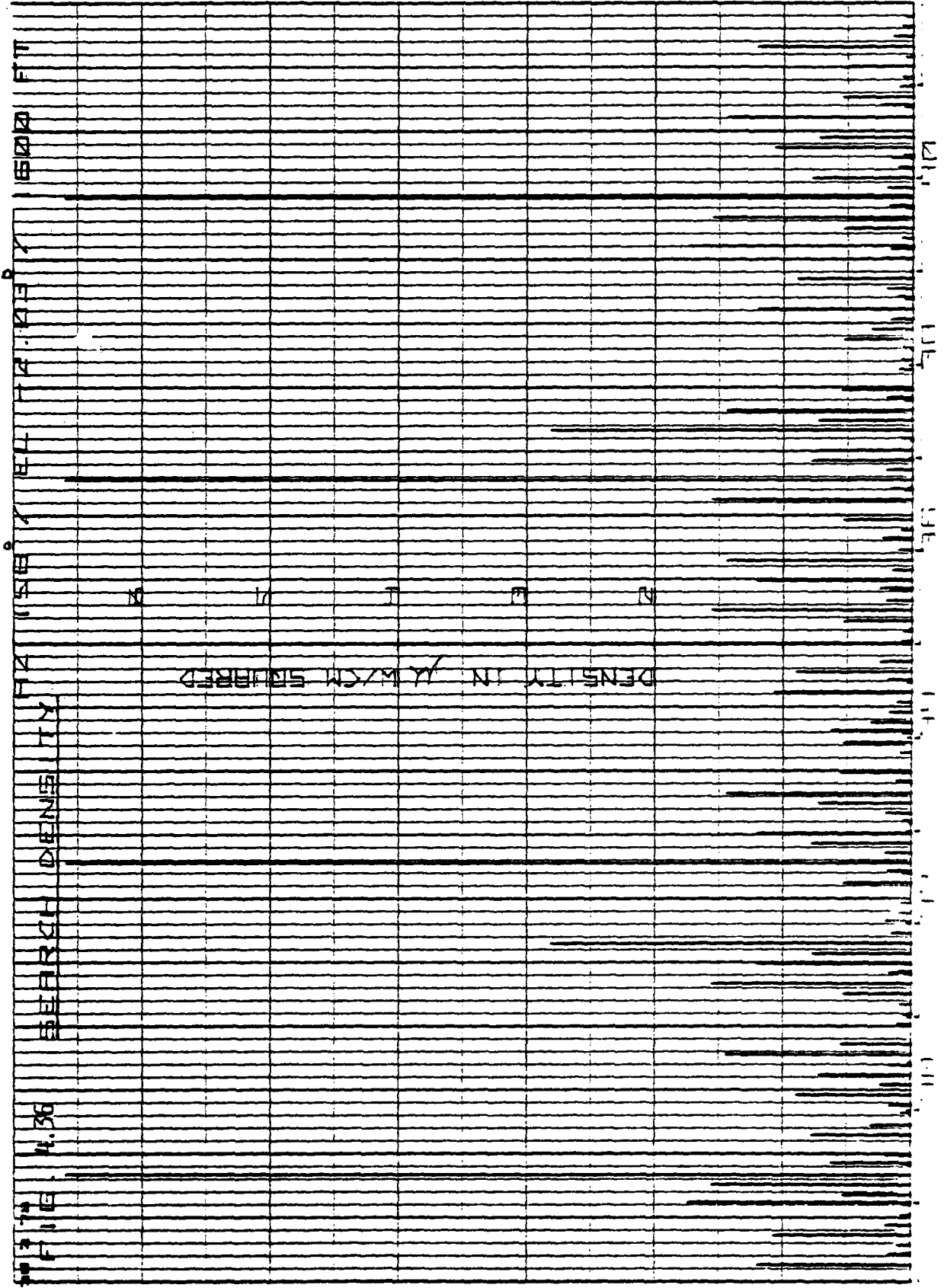


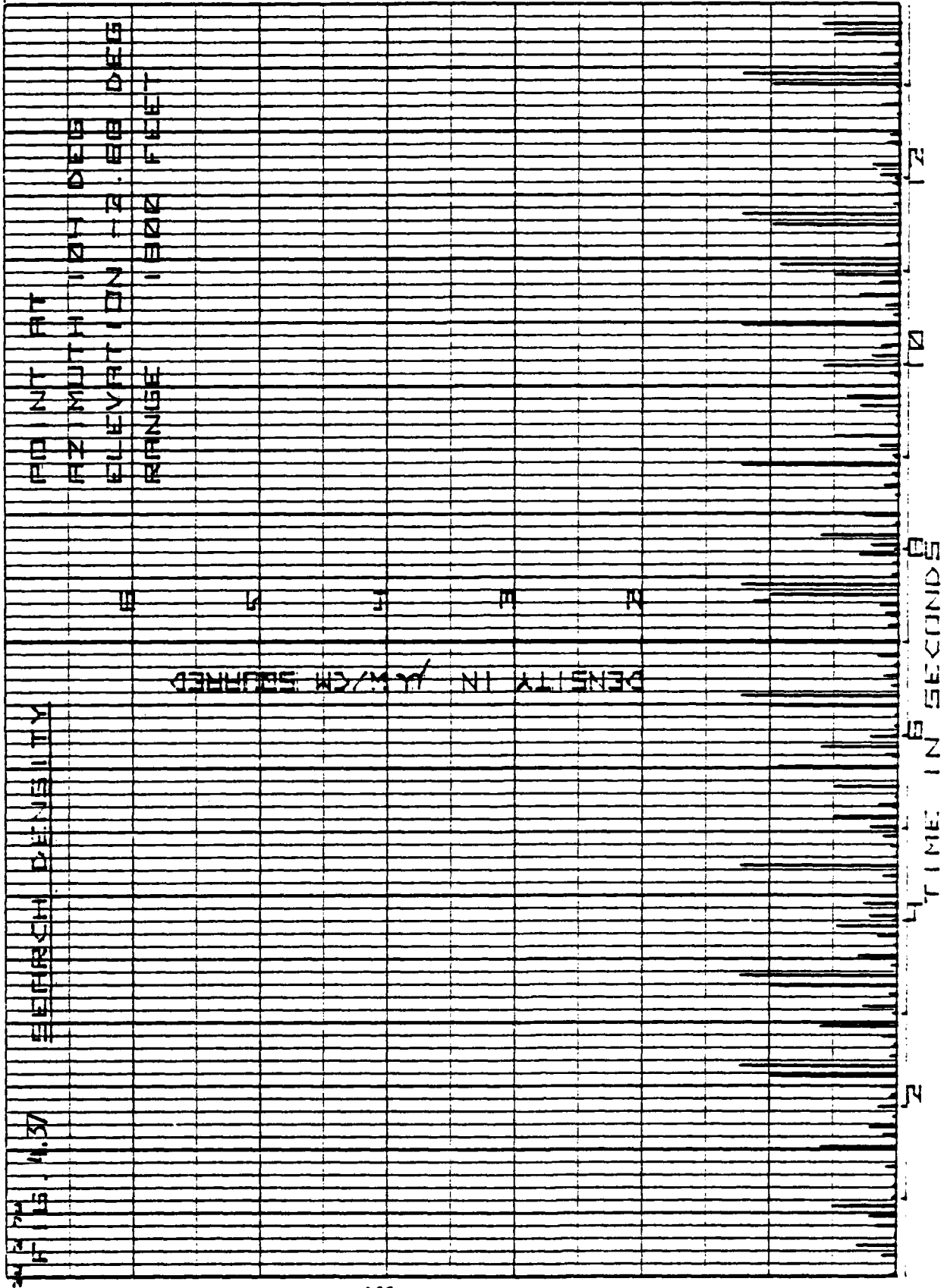
MICROGRAMS PER CUBIC METER

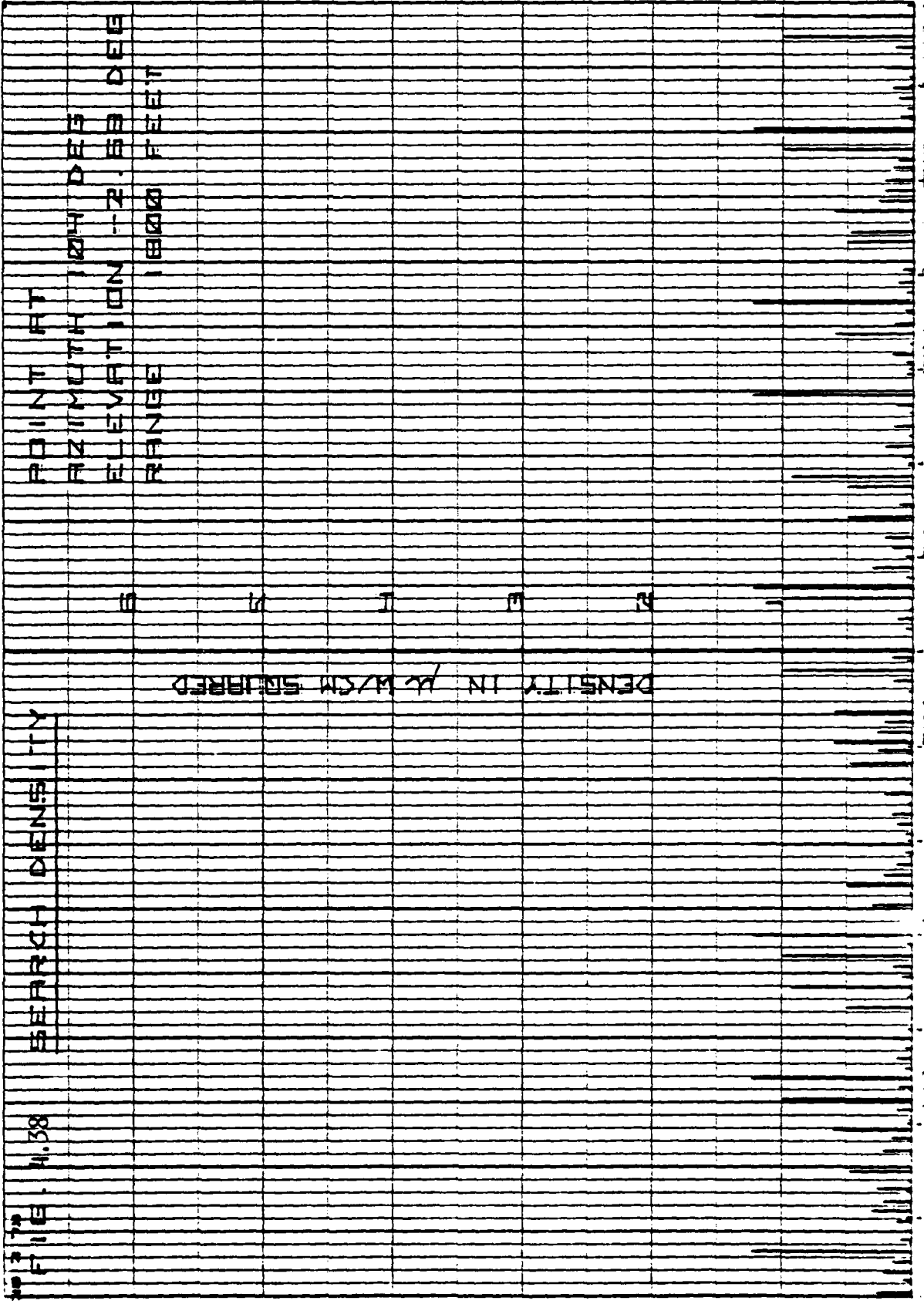
AZIMUTH OFF-BORESIGHT DEGREES

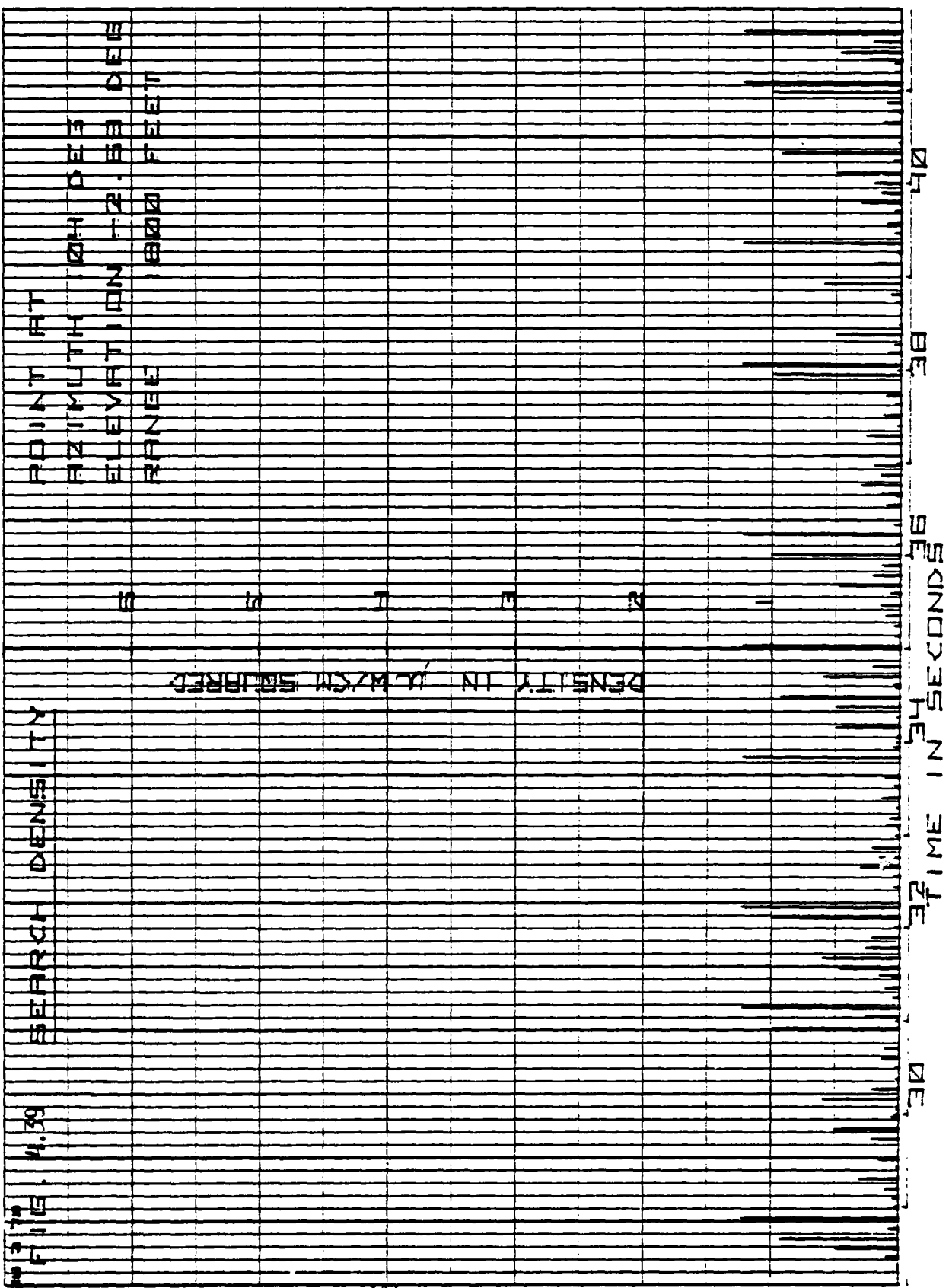












FILE 4.39

DEPTH DENSITY

POINT

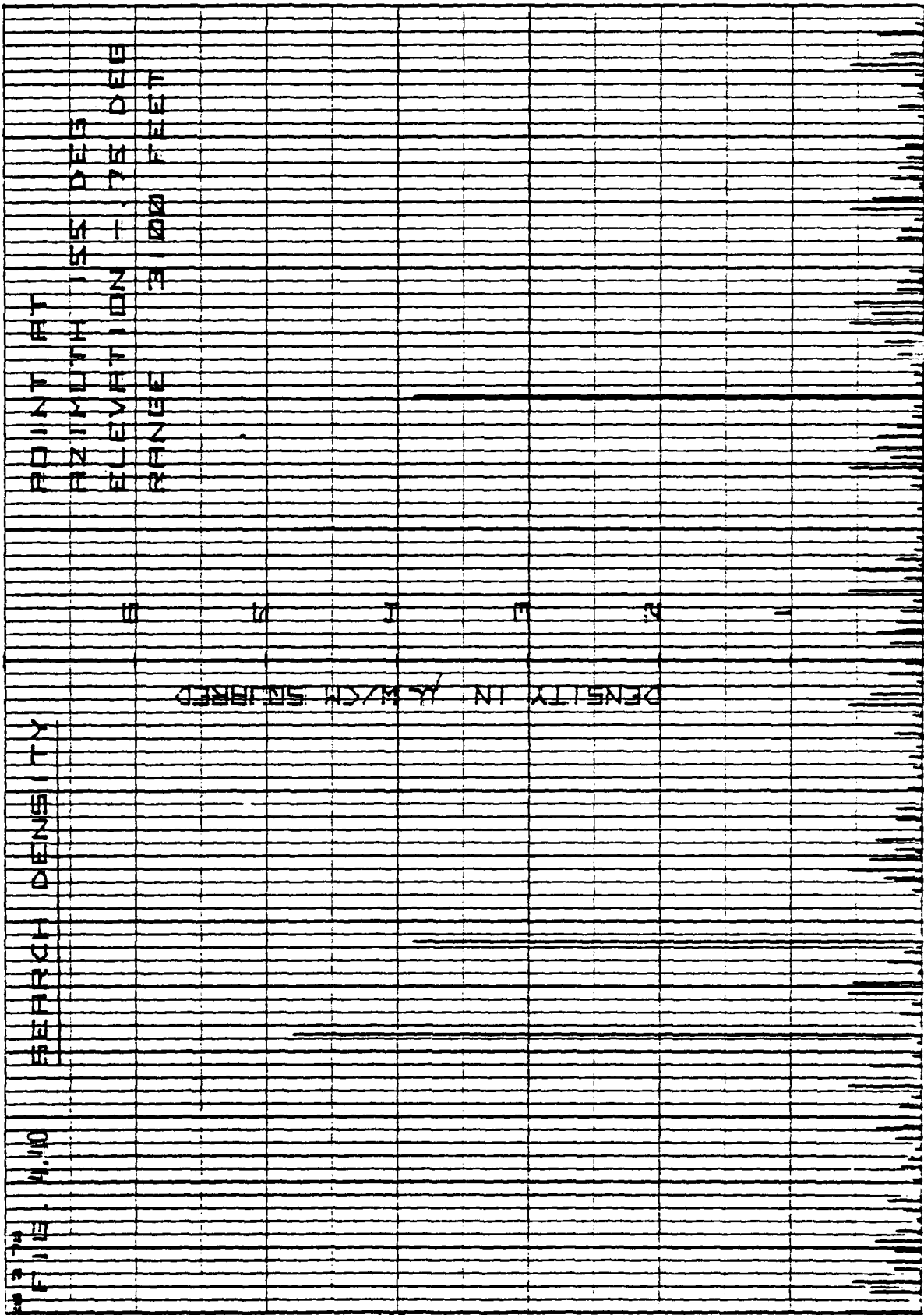
AZIMUTH

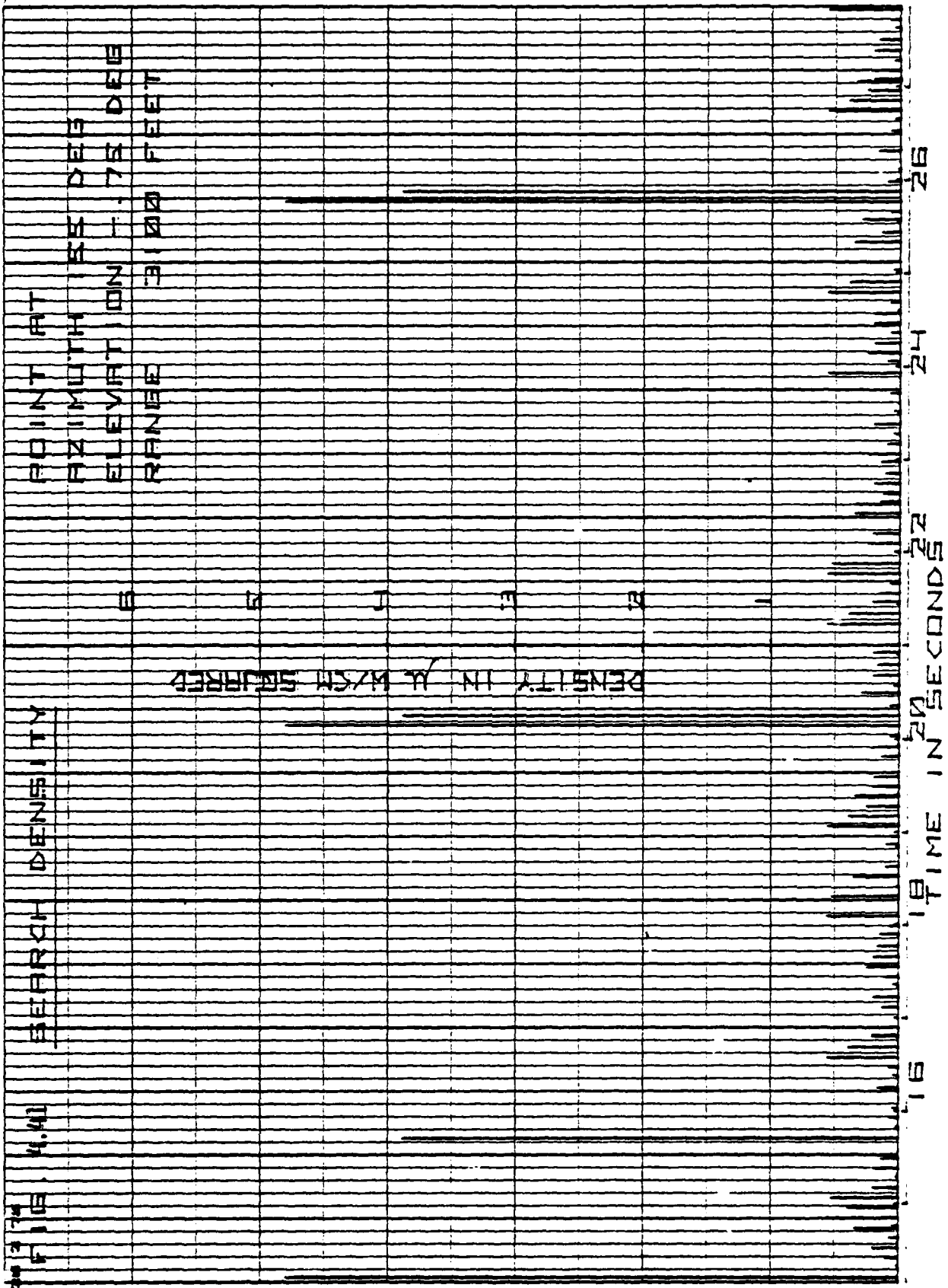
ELEVATION

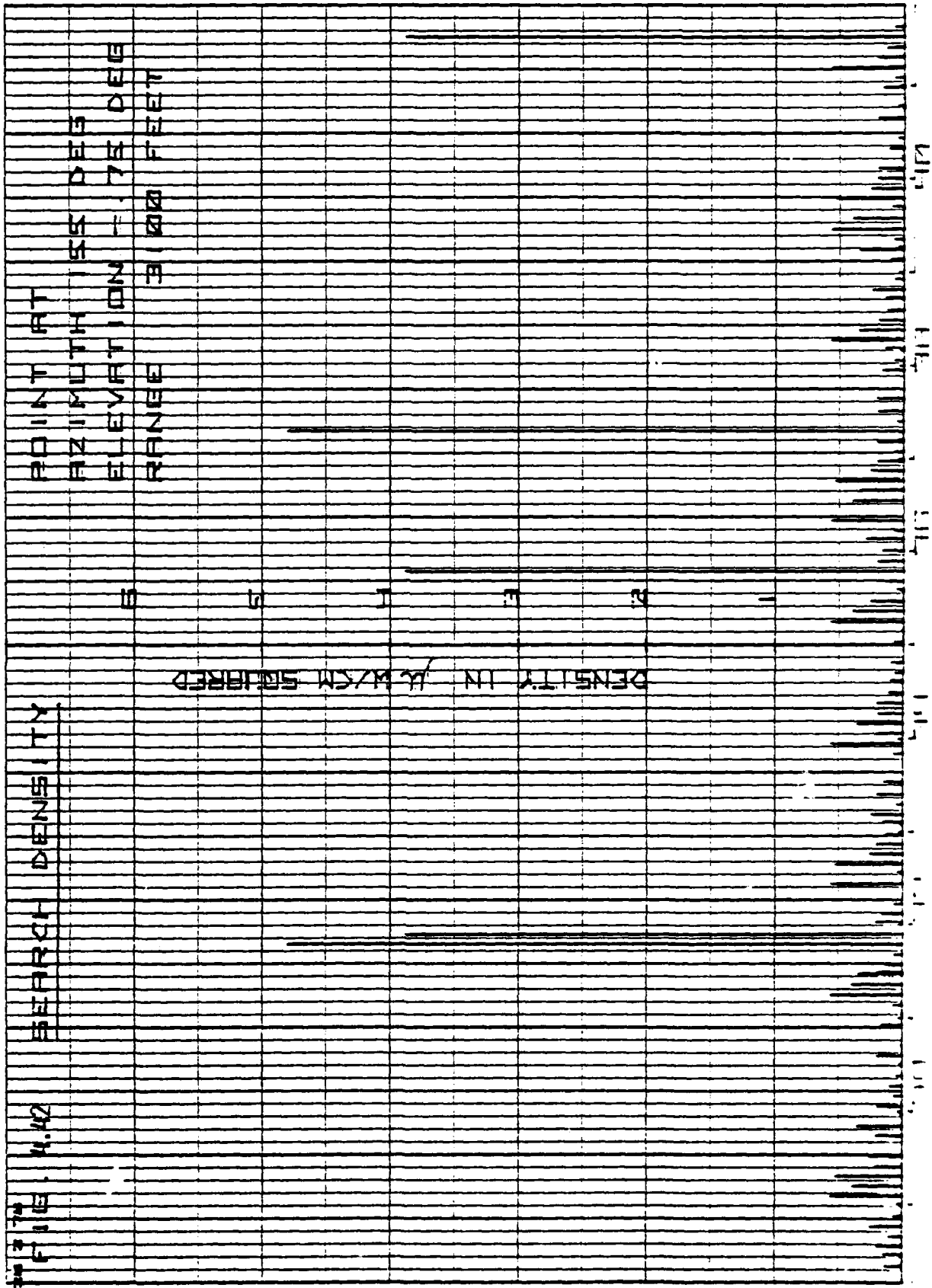
RANGE

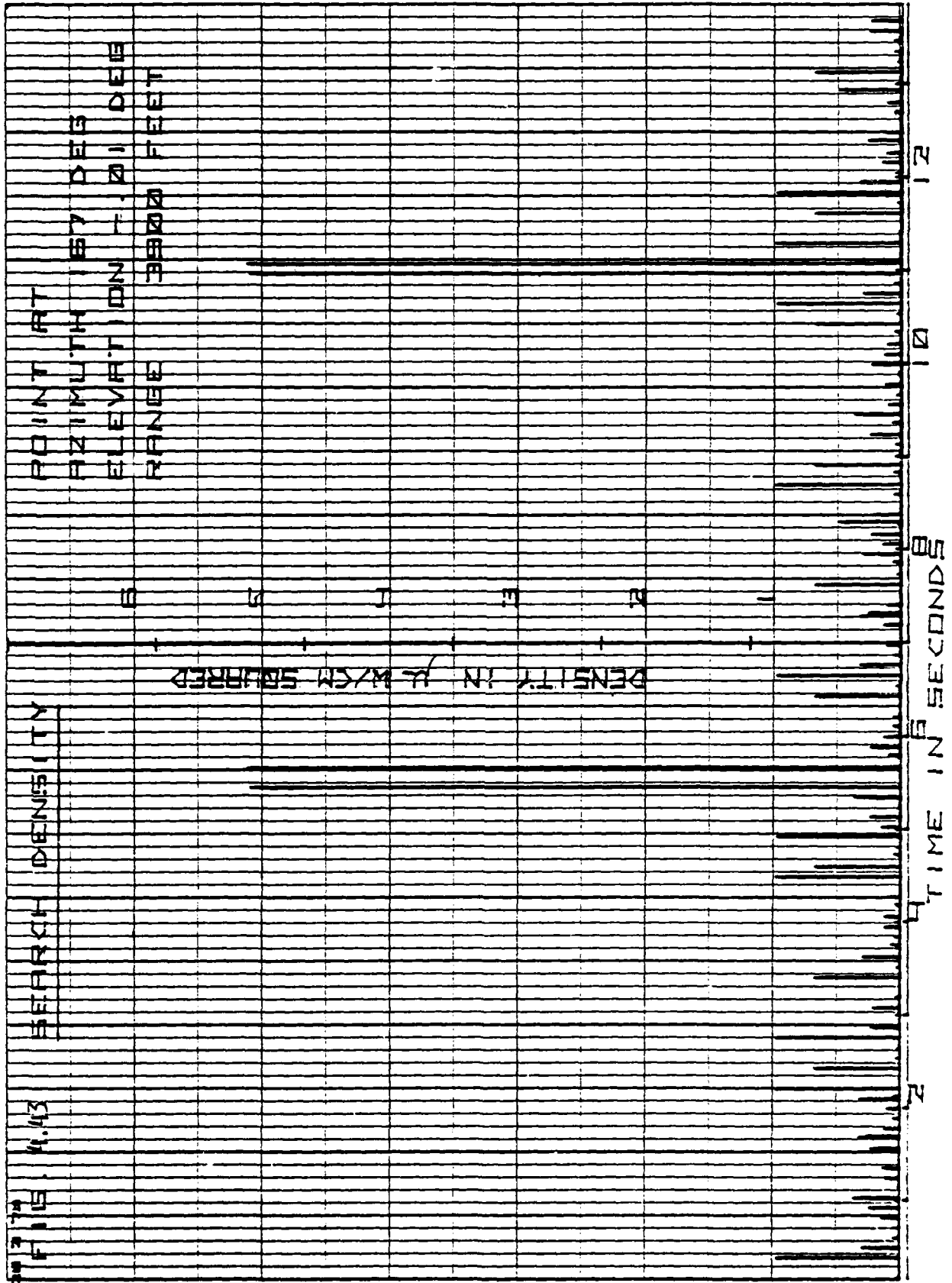
DENSITY IN g/cm³

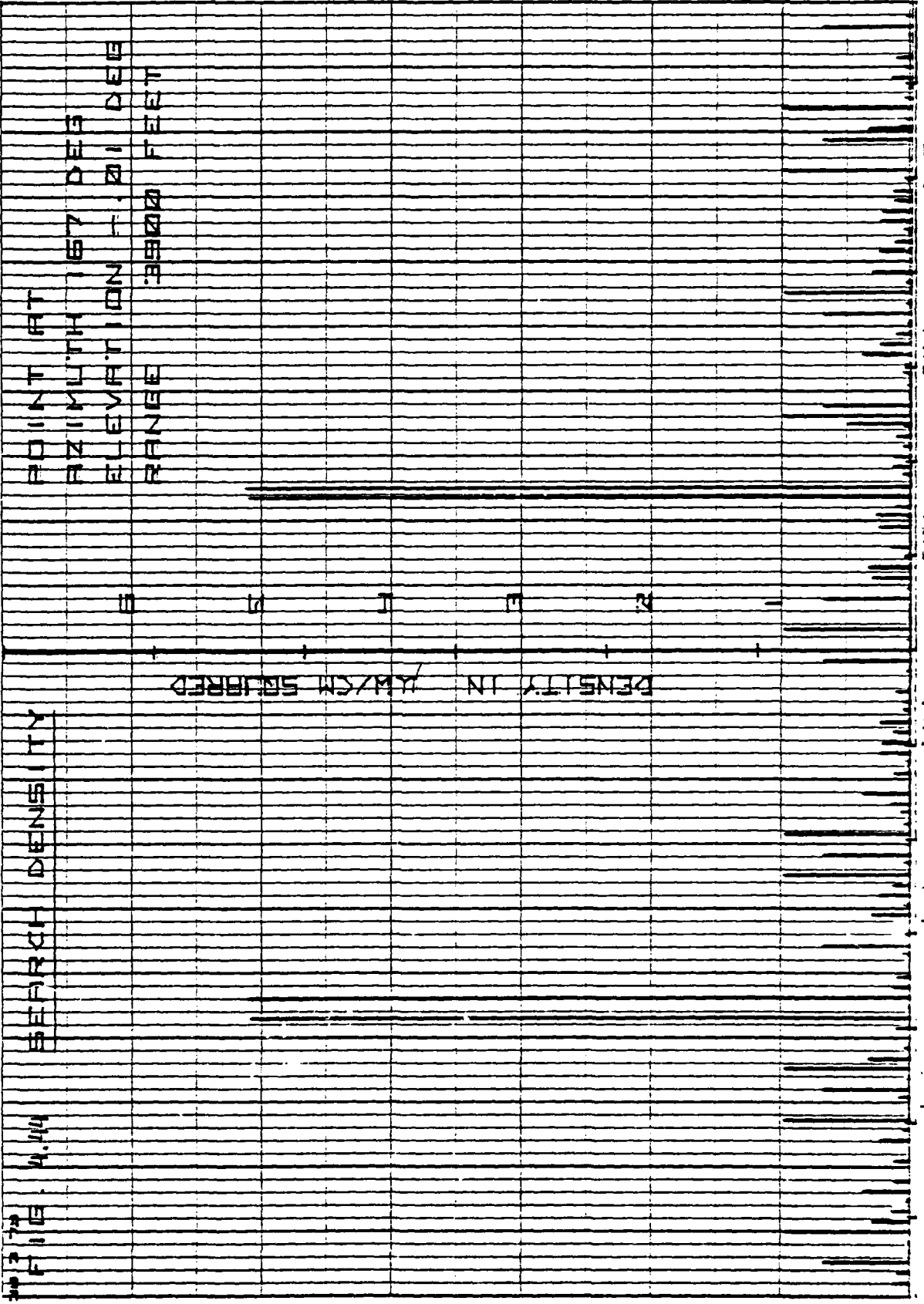
DEPTH IN METERS

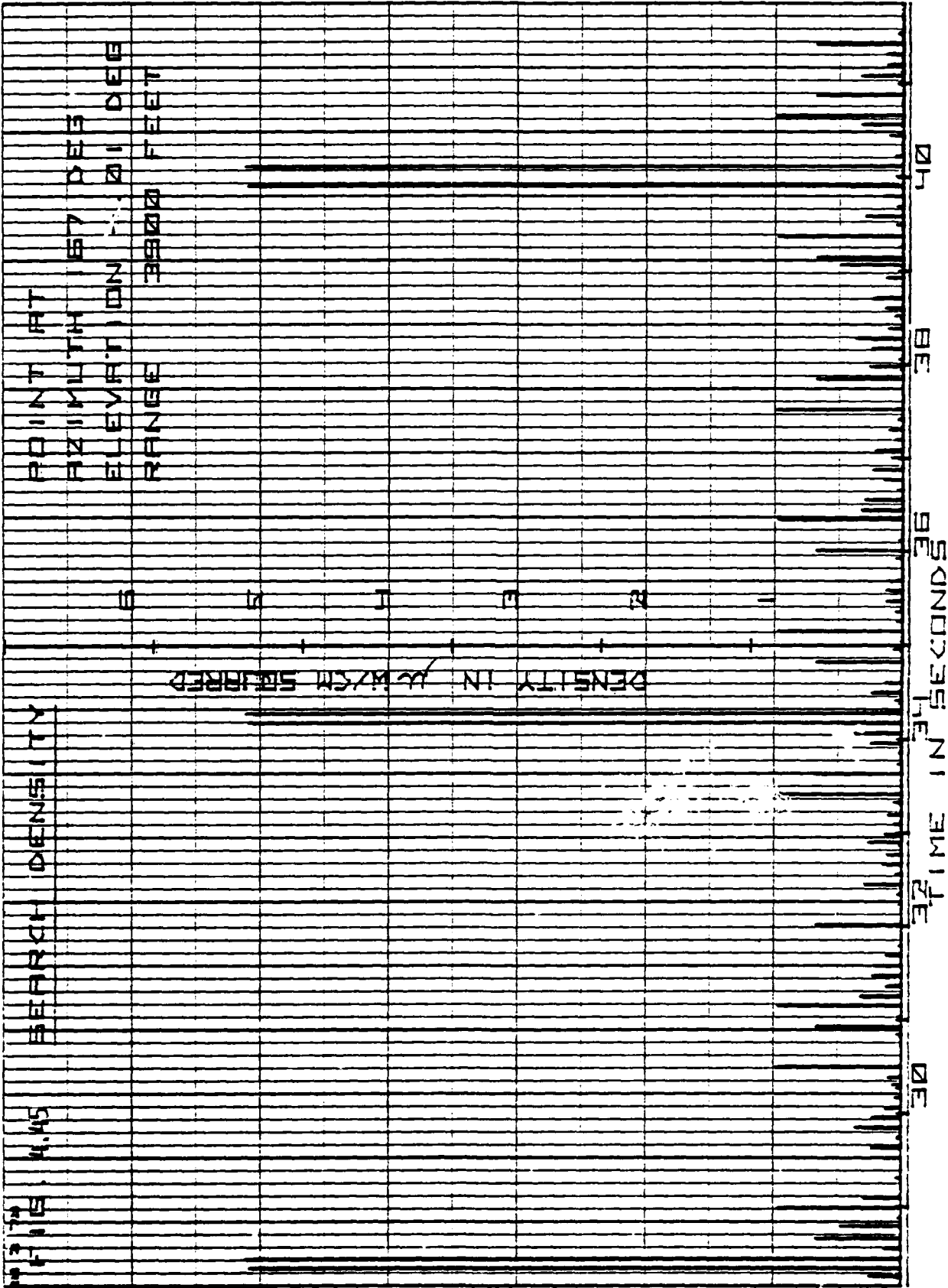












5.0 Subarray Failures: This section addresses the question of the effect of subarray outages on the far field elevation pattern power density of the PAVE PAWS baseline radar. Of major interest is the lower elevation region and this is where the emphasis is placed.

5.1 Method: Elevation patterns were generated at a 4646 foot distance from the radar for a transmit radar beam at zero degrees azimuth with respect to boresight and three degrees elevation for multiple subarray total failures. The number of failed subarrays was varied from zero (to provide a reference) to a maximum of 28 subarrays. There are 56 subarrays in the baseline system. Some of the number of failures considered are extreme. It is unlikely that the PAVE PAWS radar would operate with more than 6 failed subarrays (failed in the transmit mode only) because of e.g., the one dB degradation alert to the operators and maintenance personnel when 6 or more subarrays fail on transmit. A failed subarray was considered totally failed on transmit in that a failed subarray did not radiate at all but could continue to receive. The frequency was held constant at 445 MHz. The failed subarrays were chosen rather arbitrarily in the upper half of the array, maintaining the same vertical array dimension except for the 28 subarray failure case where the vertical dimension shrunk in half. The upper half was chosen because of its expected greater impact on the lower elevation angle region.

5.2 Results: The odd numbered Figures 5.1 through 5.19 show the particular subarrays failed. The failed subarray area is shown encircled in heavy outline. Figure 5.1 shows the normal baseline array for the limiting case of no subarray failures i.e., for all 56 subarrays functioning normally on transmit. The even numbered Figures 5.2 through 5.20 show the resulting elevation patterns. Figure 5.2 shows the

transmit elevation pattern for the array of Figure 5.1. Table 5.1 summarizes the main effects of the subarray failures on the transmit elevation pattern.

5.3 Analysis: The subarray failures degrade the transmit elevation pattern by decreasing the main beam peak level, increasing sidelobe levels, changing the beamwidth and increasing the power density level at a ground point considered here to be at zero degrees azimuth with respect to radar boresight, at zero degrees elevation and at a distance of 4646 feet. See even numbered Figures 5.2 through 5.20 and Table 5.1. The situation portrayed by Figures 5.1 through 5.10 and by Table 5.1 entries above the horizontal line could exist operationally when the system degradation does not exceed the one dB criterion.

5.3.1 Beam Peak: The boresight beam peak level varies with the square of the ratio of the number of active subarrays to the normal baseline array complement of 56 active subarrays. The agreement is within 0.1 dB except for the case where the entire upper half of the array is failed and is not transmitting. For this case the agreement is still good and is within 0.3 dB. The disagreement is attributed to the fact that, as the subarrays fail, the transmit array spatial (and equivalent amplitude) taper is changing. For the extreme case of the 28 failed subarrays, the normally evenly symmetrical array taper in the vertical dimension becomes asymmetrical.

5.3.2 Sidelobe Level: As the number of failed subarrays rises, the sidelobe level also rises. The sidelobe level increases faster than the main beam level decreases. As a result, the difference between the main beam level and the sidelobe level decreases rapidly. This difference which is 21.4 dB for the full array becomes 20, 18.6, 16.1, 10.6, 9.7, 7.8 dB as 1, 2, 4, 12, 16, 20 subarrays fail, respectively. It should

be noted that even with 6 subarrays failed (which is within the one dB system degradation criterion) the sidelobe level is only approximately 14 dB below the peak of the main beam. The lower elevation angle sidelobes plotted on Figures 5.12 through 5.20 are usually higher than the upper elevation sidelobes for the same number of subarray failures by a small amount -- under one dB.

5.3.3 Beamwidth: The beamwidth of the transmitted pattern changes with subarray failures. For the case of 6 subarray failures or less, the beamwidth decreases with the number of subarray failures. The decrease is slight -- less than 5 percent of the normal (no failed subarrays) beamwidth. For the case of 12 subarray failures and more, the 1.9 degree beamwidth for 12 subarray failures shows a decrease from the normal beamwidth of almost 10 percent, with the 1.9 degree beamwidth increasing as more than 12 subarrays fail to beamwidths wider than the normal beamwidth. For the extreme case of 28 subarray failures, the array vertical dimension shrinks in half and the resulting beamwidth is 3.9 degrees. This beamwidth is not quite double the normal beamwidth since the effective array dimension does not remain constant. It should be noted that the beamwidth numbers of Table 5.1 cannot be readily quantitatively extrapolated for different scenarios of subarray failures. This is due to the fact the elevation beamwidth depends on the effective array height and taper in the vertical dimension for the same frequency. The height and taper depend on the array positions of the failed subarrays.

5.3.4 Field Strength: Table 5.1 also shows the field strengths that exist at a point at a distance of 4646 feet, zero degrees azimuth and elevation for the various cases of subarray failures. Note that these field strength values are for the spotlight beam cases. The PAVE PAWS

radar system has built-in safeguards against beam spotlighting. In operation with the moving surveillance fence beams, the spotlight beam would be reduced by the beam motion factor. This factor depends on the relative geometry of the field point with respect to the radar. It should be noted that with proper maintenance it is unlikely that more than 2 subarrays would fail and stay failed for more than a short time due to the subarray test which occurs every 30 seconds, due to the element test which is routinely done every day and which can be commanded at any time, due to the low transmit transistor failure rates and finally due to the radar modular construction which permits rapid replacement of a defective module with interruption of the radar operation.

5.4 Failure Effects: Subarray transmit failures degrade the normal transmit elevation beam by decreasing the beam peak level, increasing the sidelobe levels, changing the transmitted beamwidth and increasing the power densities for the cases examined in this section. See Table 5.1. The increase in sidelobe levels with increasing numbers of failed subarrays is rapid and results in rapid deterioration and decrease of the sidelobe levels with respect to the peak of the failed beam. Prolonged subarray transmit failures of more than 2 are unlikely if proper maintenance procedures are followed. For the case of 2 subarray failures, the decrease in this main beam peak is small (0.32 dB), the upper sidelobe level with respect to the failed beam is 18.6 dB which is worse (higher) than the desired level of 20 dB, the beamwidth slightly decreases from 2.1 to 2.07 degrees and the field density increases by almost 2.5 times the normal case for the particular point considered to 24 microwatts/centimeter squared -- a value still considerably below the OSHA standard.

Table 5.1 Subarray Failure Effects

FAILED SUBARRAYS	BEAM PEAK		UPPER SIDELOBES		BEAMWIDTH		0° ELEVATION POINT		
	dbm	Level	Below Beam Peak	db	degrees	Level	Below Beam Peak	Field Strength	
Number							db	$\mu W/cm^2$	
0	6.03	15.4	21.4		2.10	-18.3	24.3	14.8	
1	5.87	14.17	20		2.09	-16.2	22.0	24.0	
2	5.71	12.85	18.6		2.07	-14.4	20.1	36.3	
4	5.38	10.72	16.1		2.03	-11.7	17.1	67.6	
6	5.04	9	14		2	-10	14	100	
12	3.94	6.64	10.6		1.90	-6.2	10.1	239.9	
16	3.11	6.6	9.7		1.91	-5.7	8.8	269.2	
20	2.19	5.56	7.8		1.95	-4.4	6.6	363.1	
24	1.17	*	*		2.24	-5	6.2	316.2	
28	0	*	*		3.9	-6.7	6.7	213.8	

* sidelobe not defined.

Note 1 The situations portrayed above the horizontal line could exist operationally within the 1 db system degradation bound criterion. Prolonged failures of more than 2 subarrays are unlikely due to the subarray tests.

(SEE LIST)
 O - GROUND
 Δ - ACTIVE
 □ - QUARRY

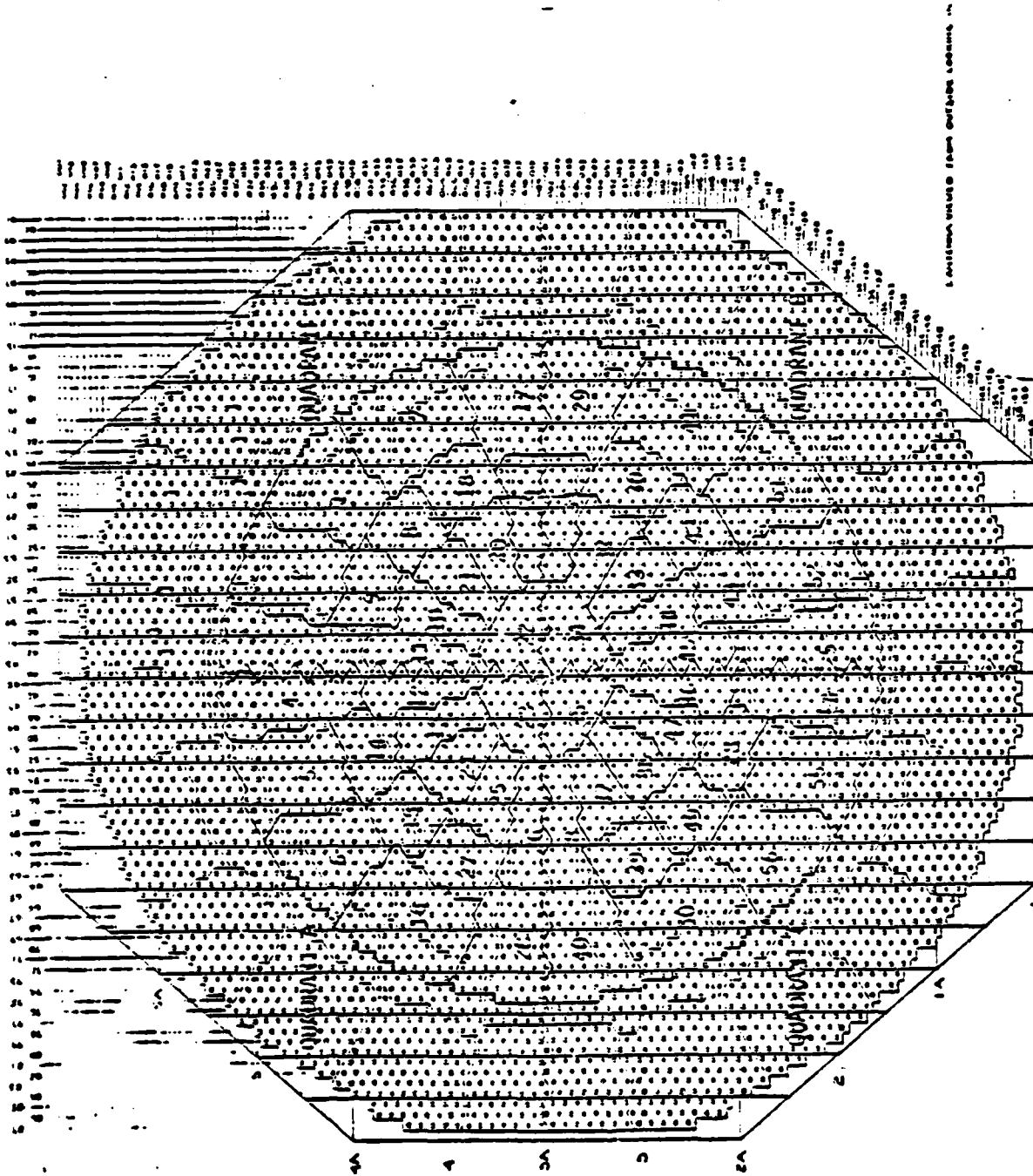
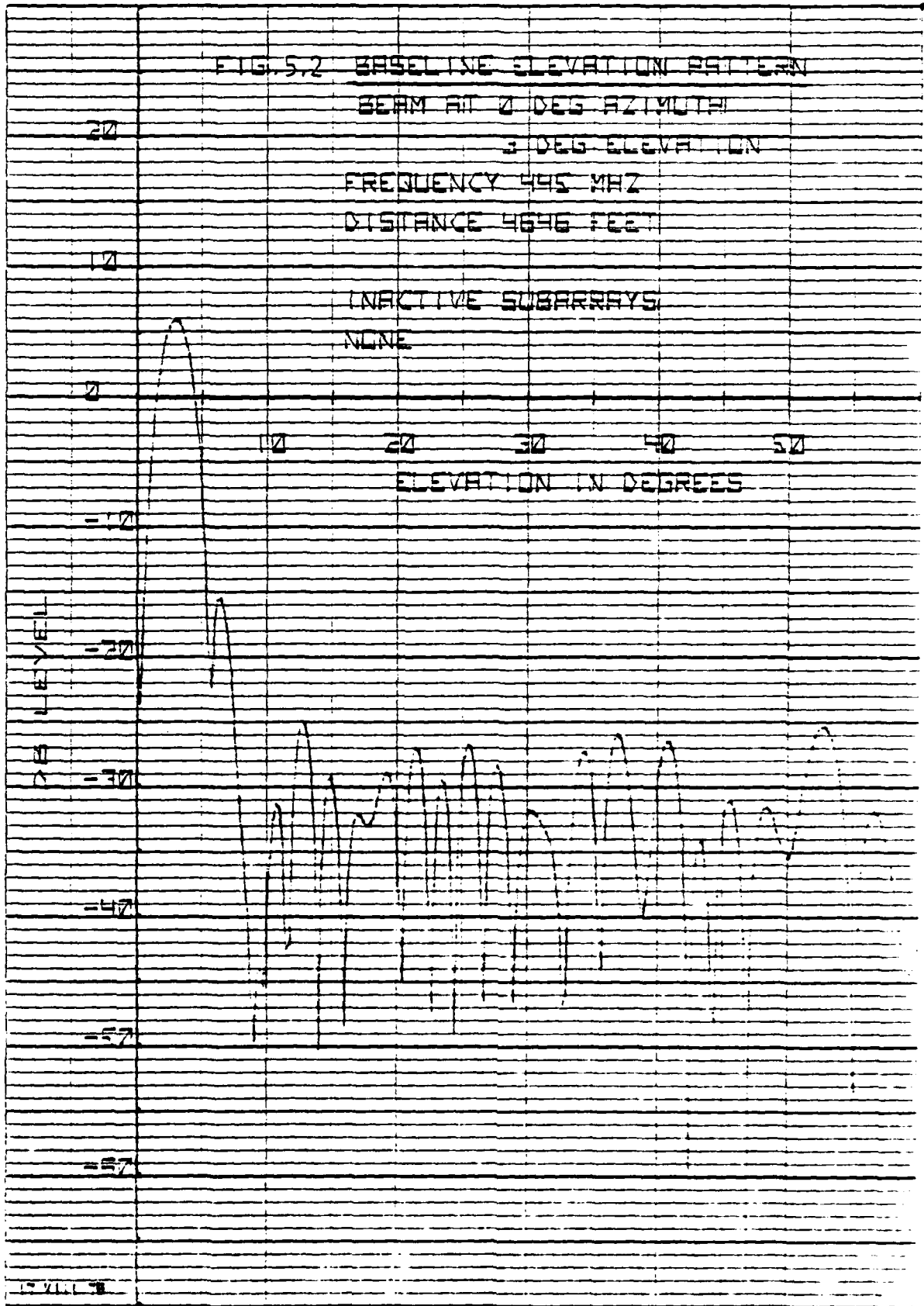
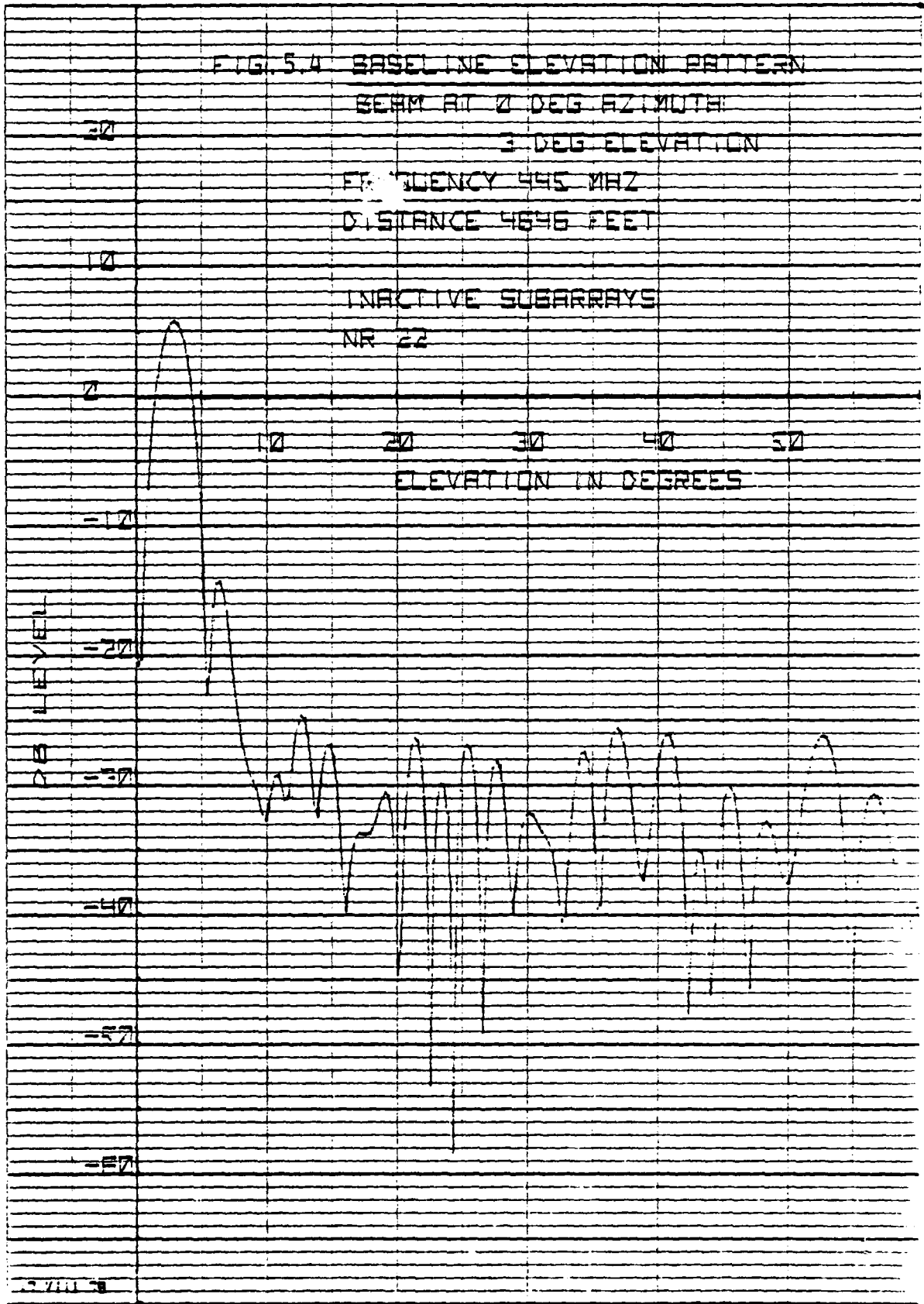


FIG. 1. ARRAY WITH 10 FAILED SUBARRAYS

90010776 00000000



HW 1111 PAI KARD 0270 1000



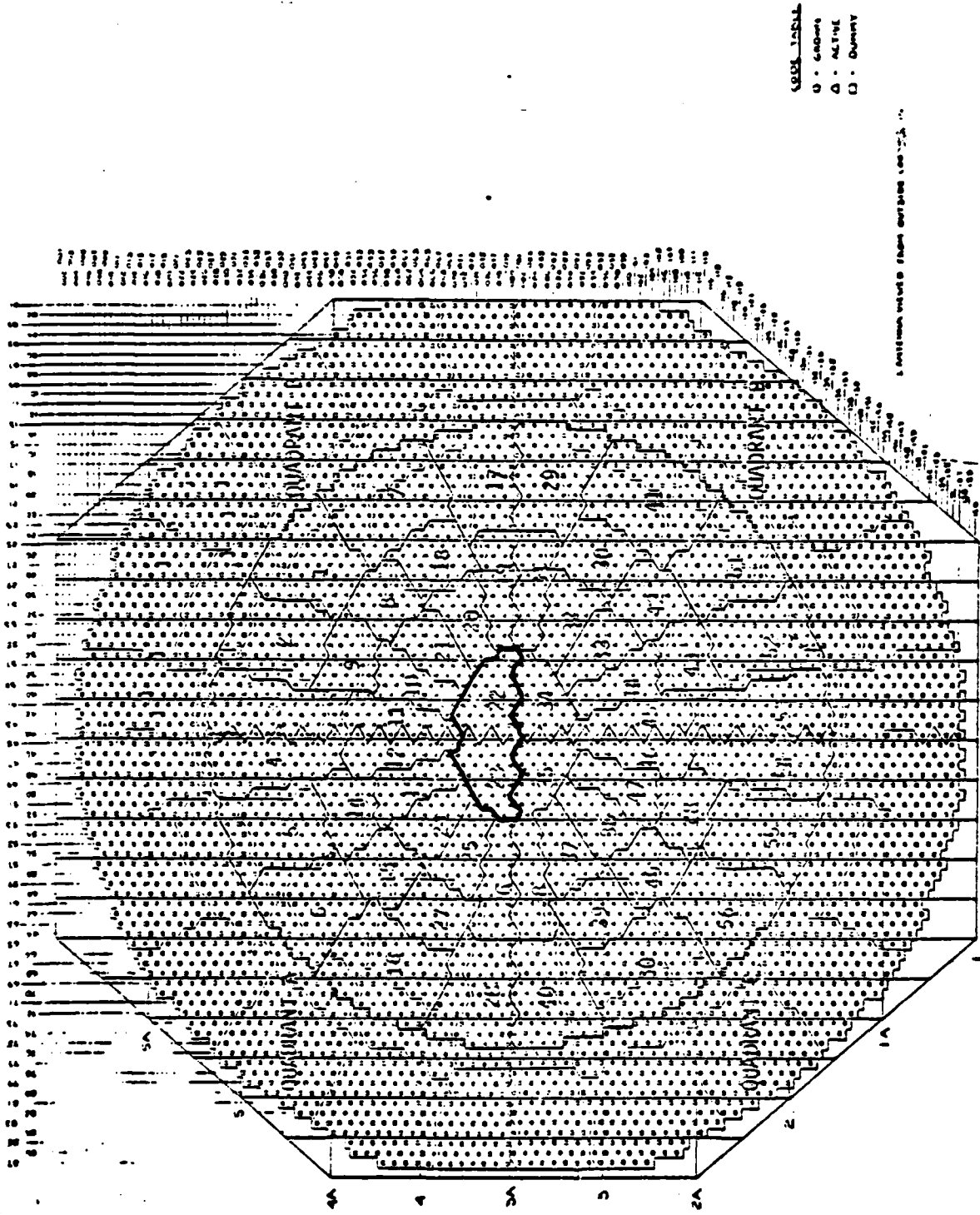
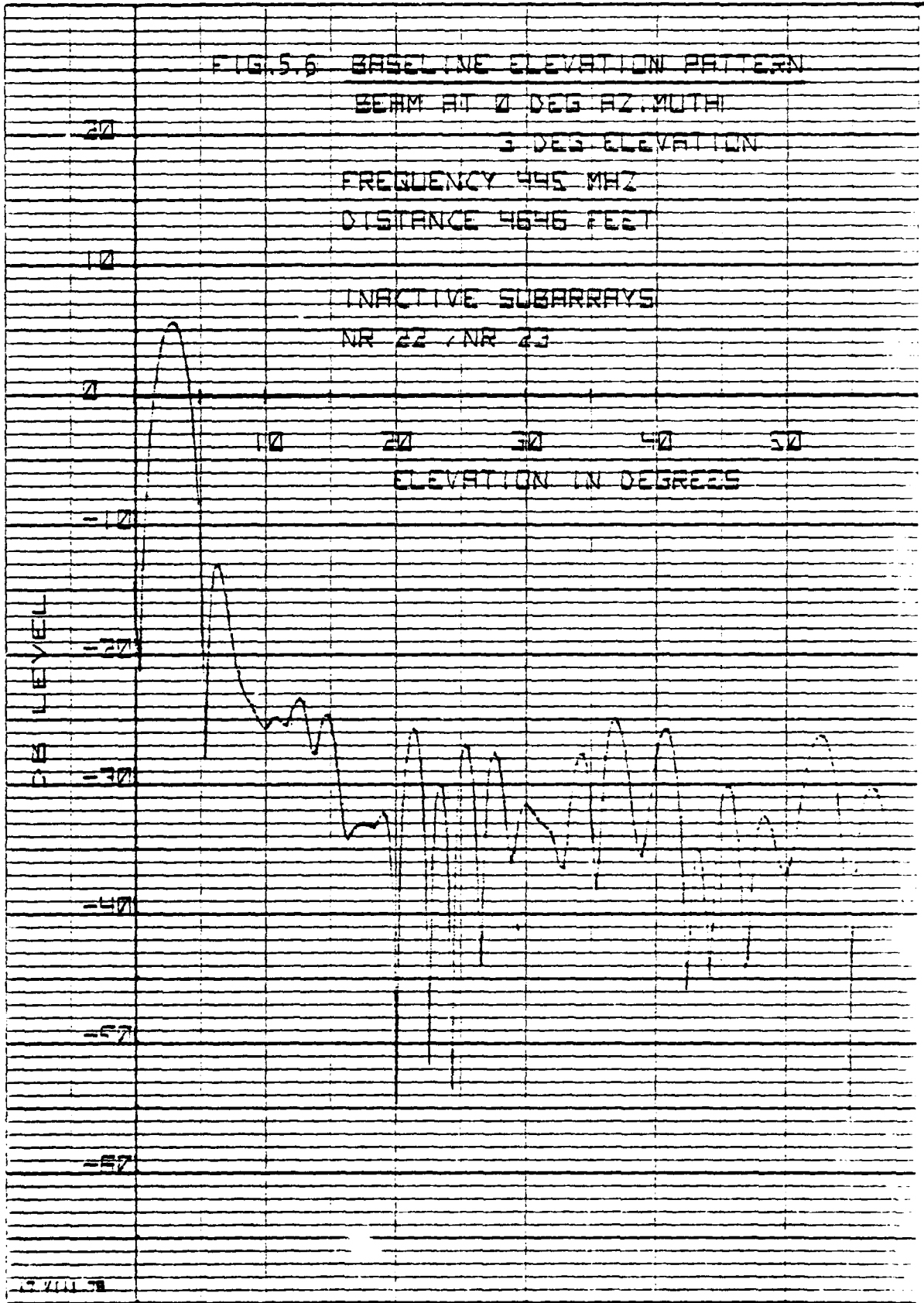


FIG. 5.5 ARRAY WITH 2 FAILED SUBARRAYS

DLW1111 PALMARD 02/01/0008



CODE TABLE
 O - GROUND
 Δ - ACTIVE
 □ - DUMMY

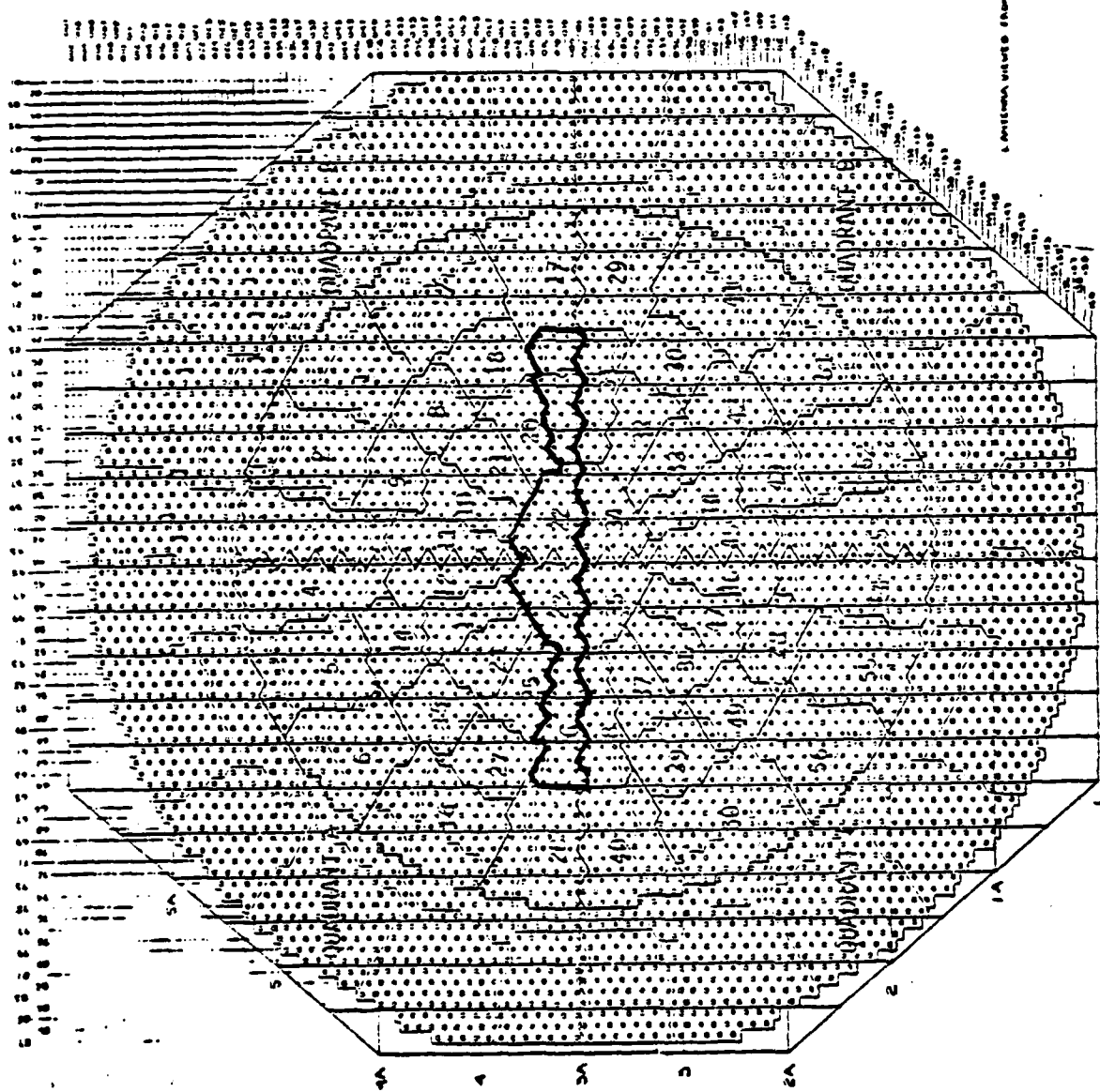
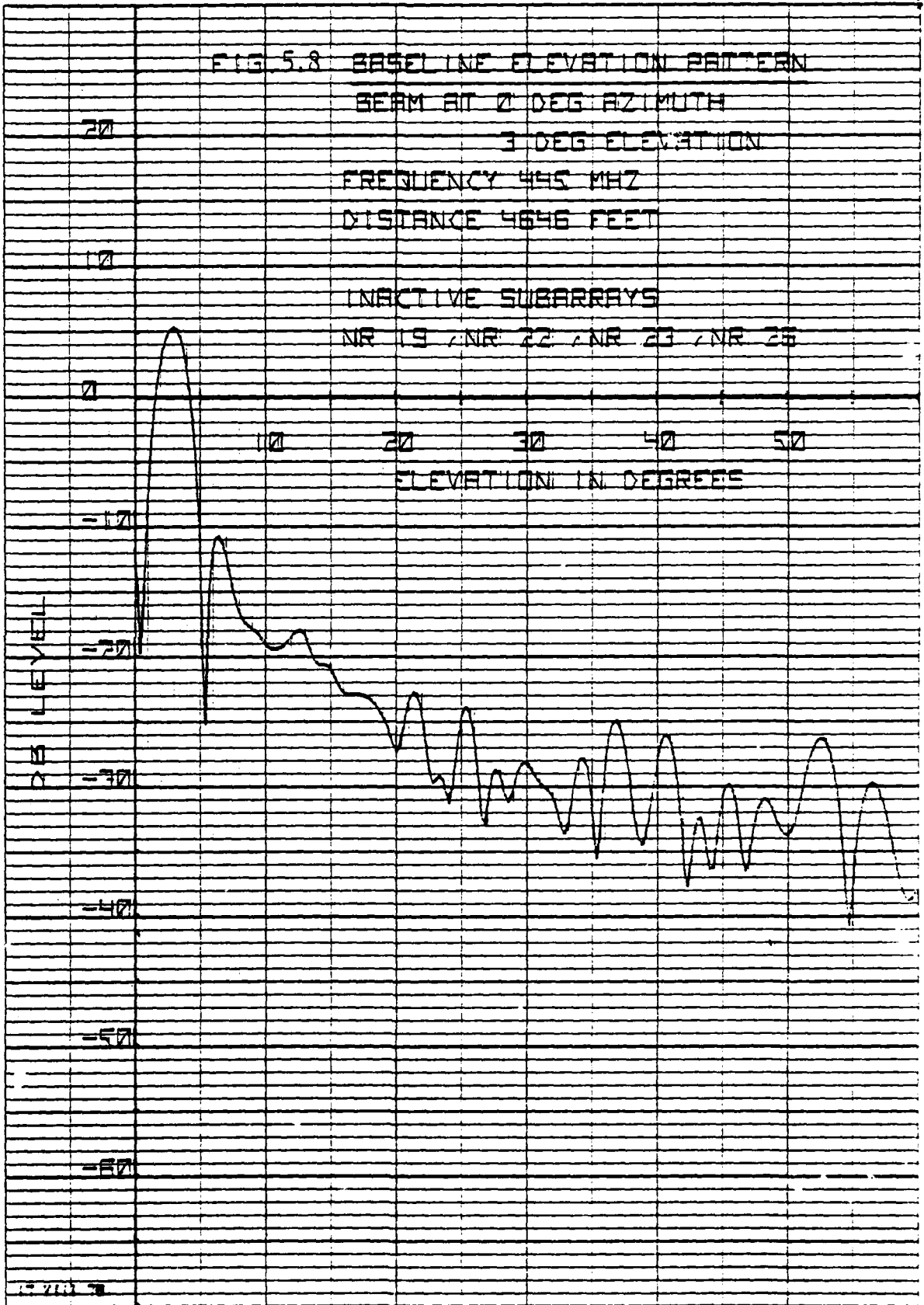


FIG. 5.7 ARRAY WITH 4 FAILED SUBARRAYS

HEWLETT-PACKARD 9270 1000



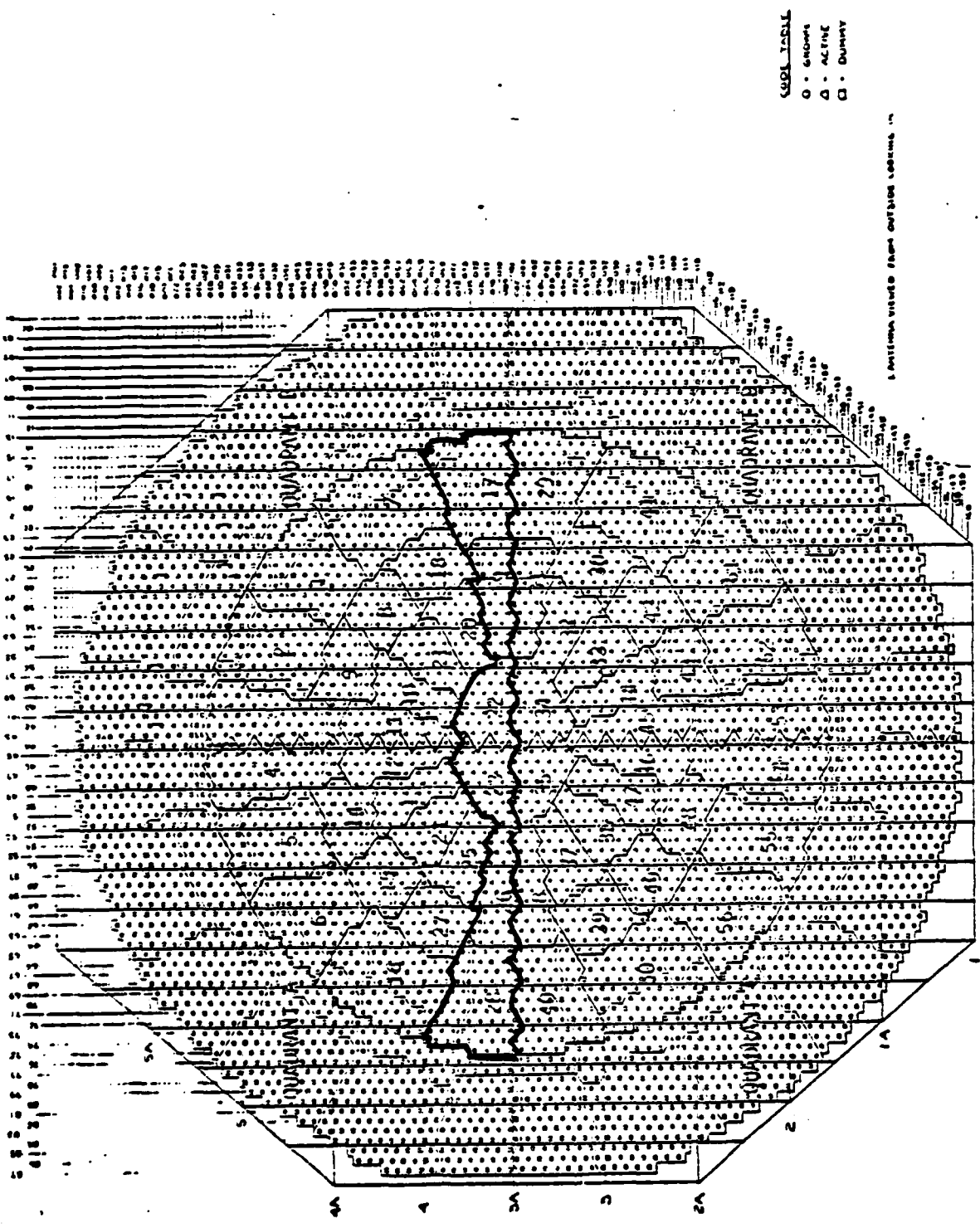
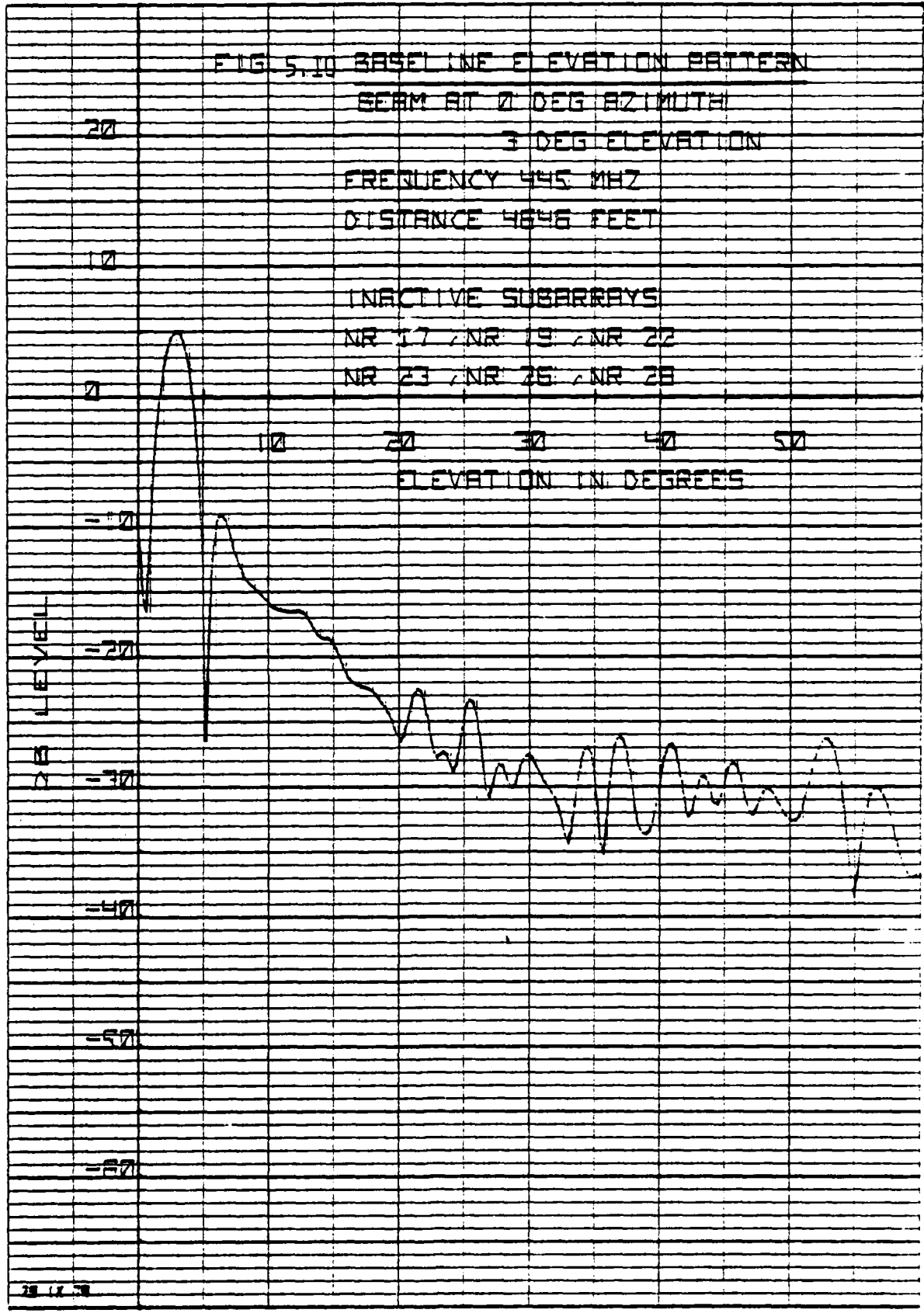


FIG. 5.9 ARRAY WITH 6 FAILED SUBARRAYS



CODE TABLE
 O - GROUND
 Δ - ACTIVE
 □ - DUMMY

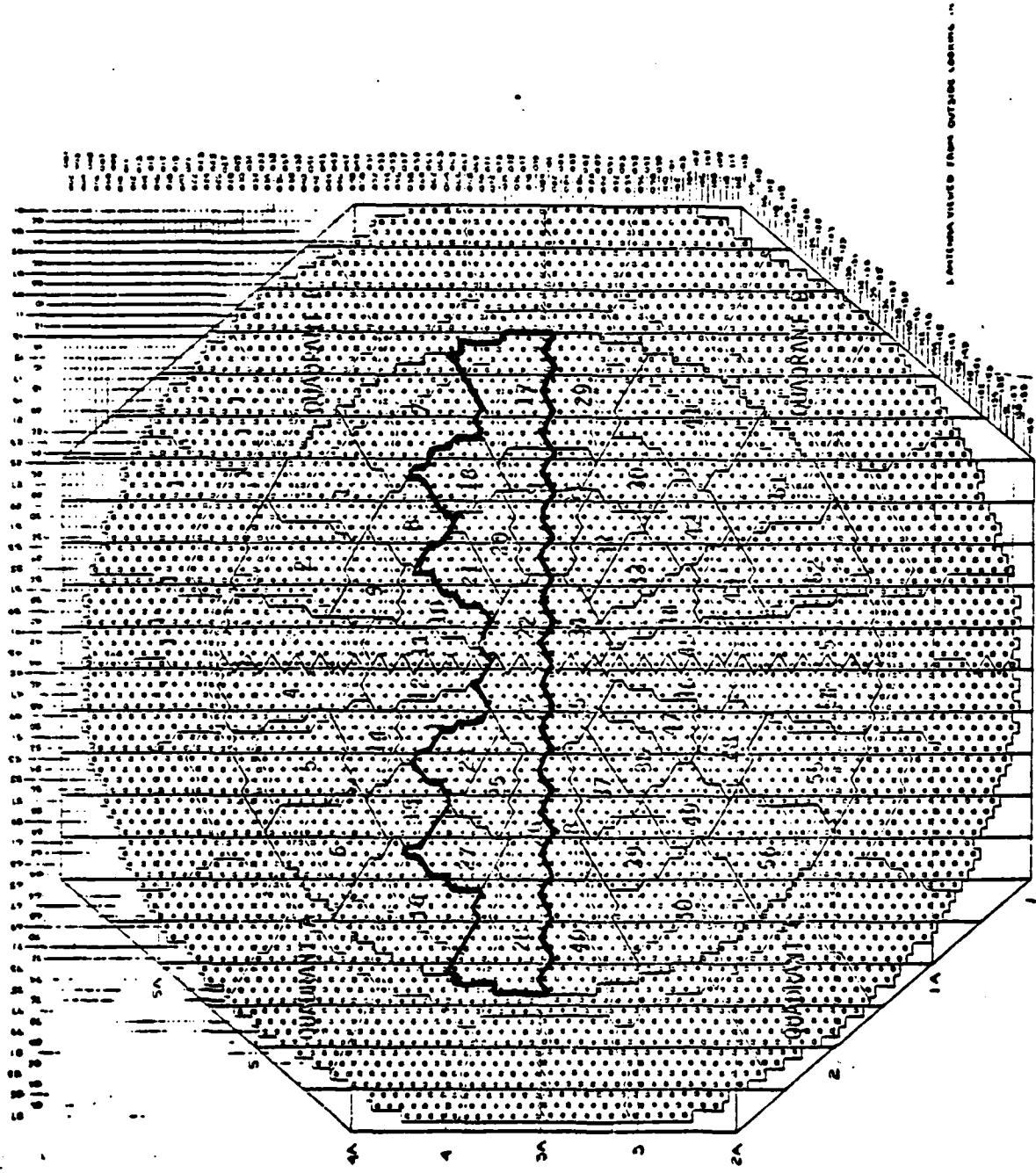
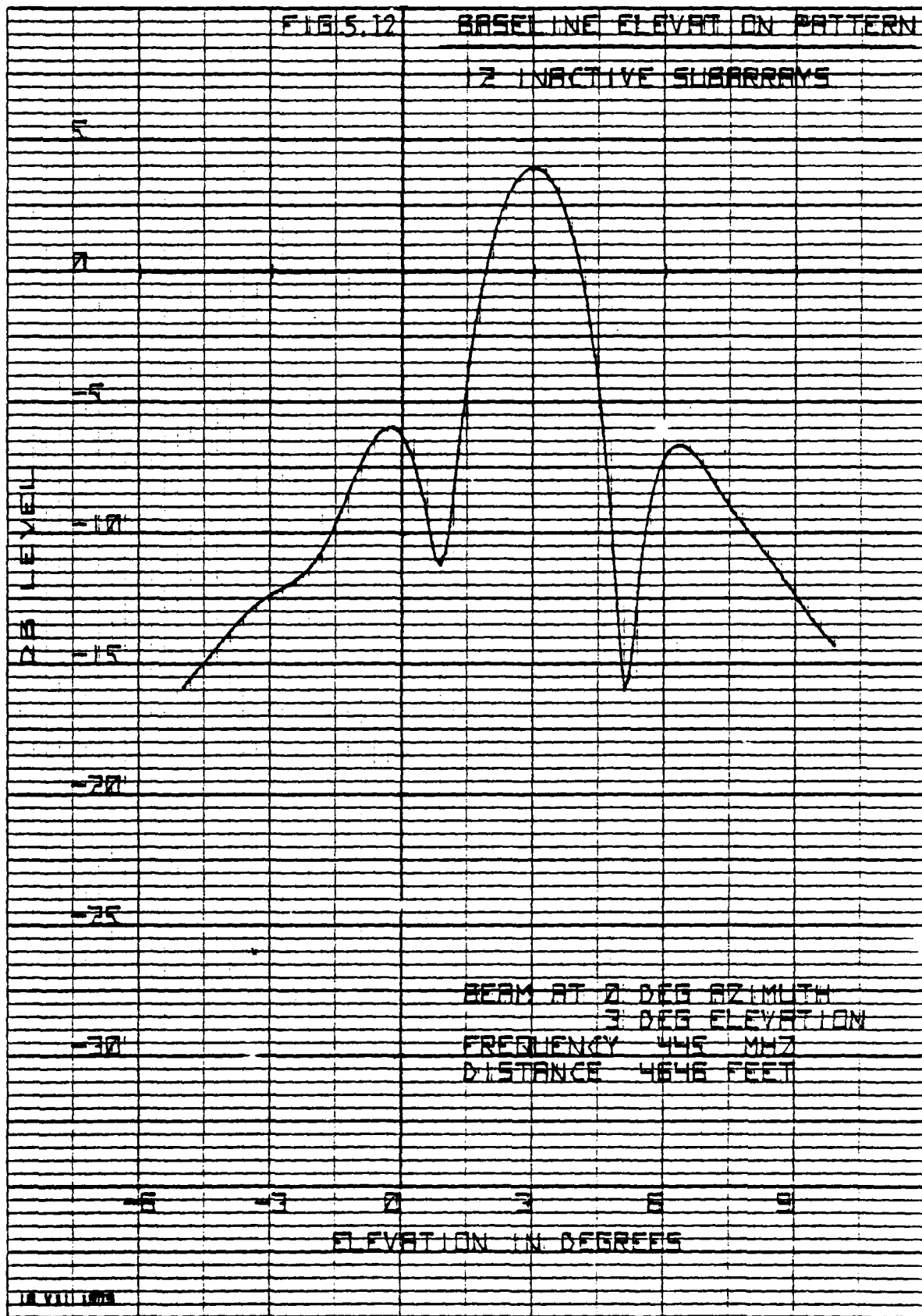


FIG. 5.11 ARRAY WITH 12 FAILED SUBARRAYS

NEWLETT PACKARD 9270-1008



CODE TABLE
 O - GROUND
 Δ - ACTIVE
 □ - DUMMY

1. ANTENNA VOLTAGE FROM OUTSIDE LEADING IN

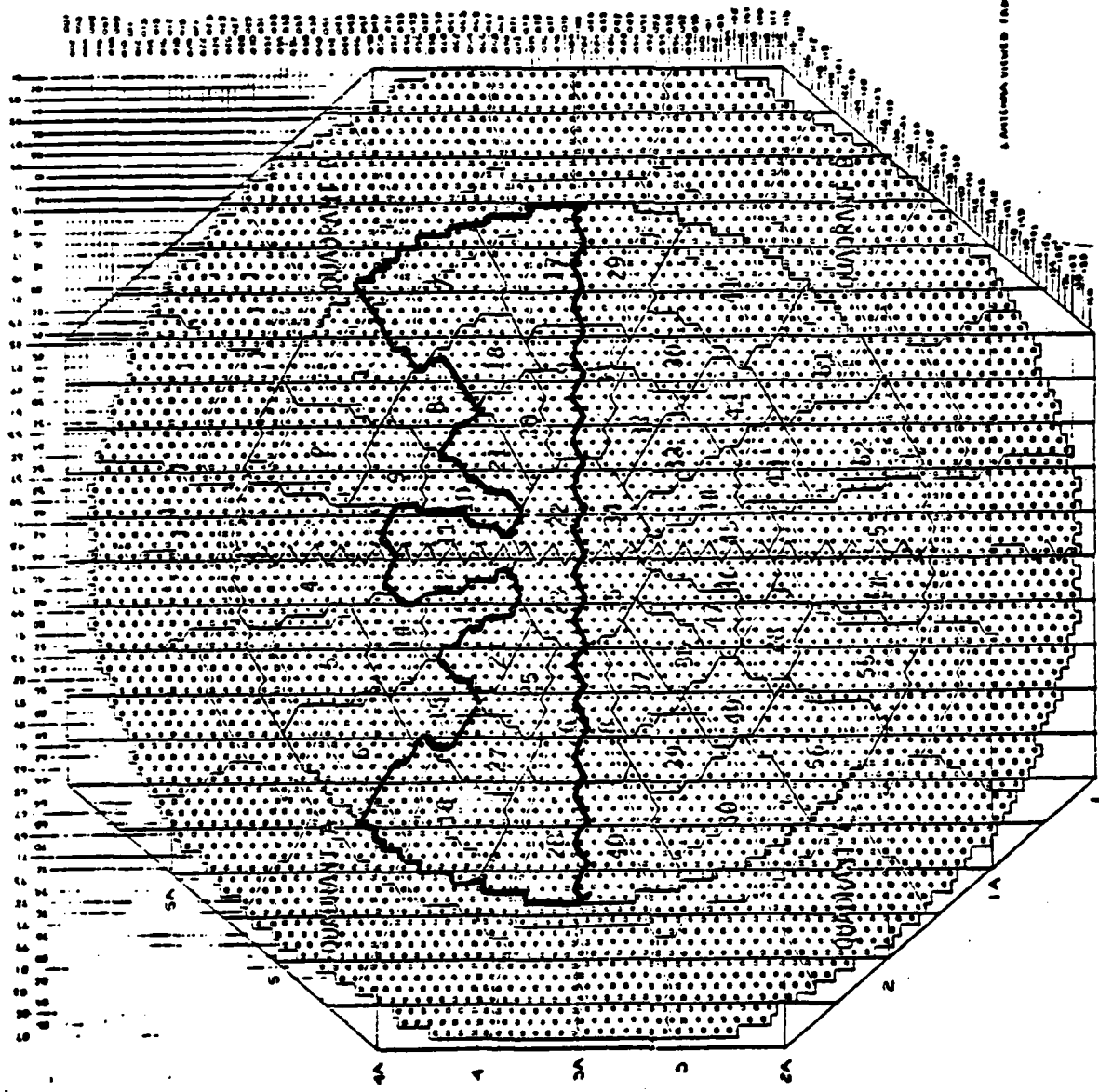
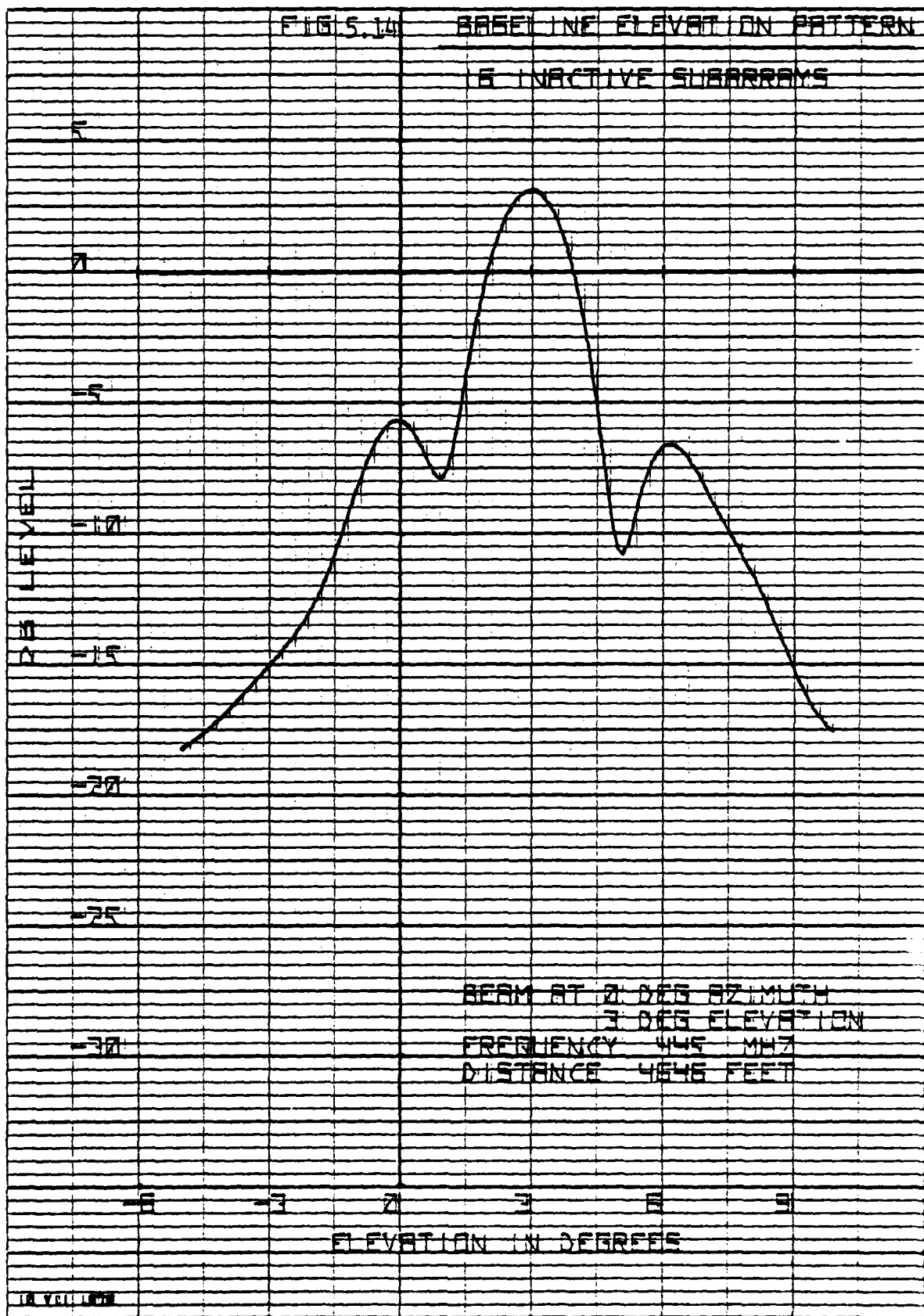


FIG. 5.13 ARRAY WITH 16 FAILED SUBARRAYS

HEWLETT-PACKARD 8270 1006



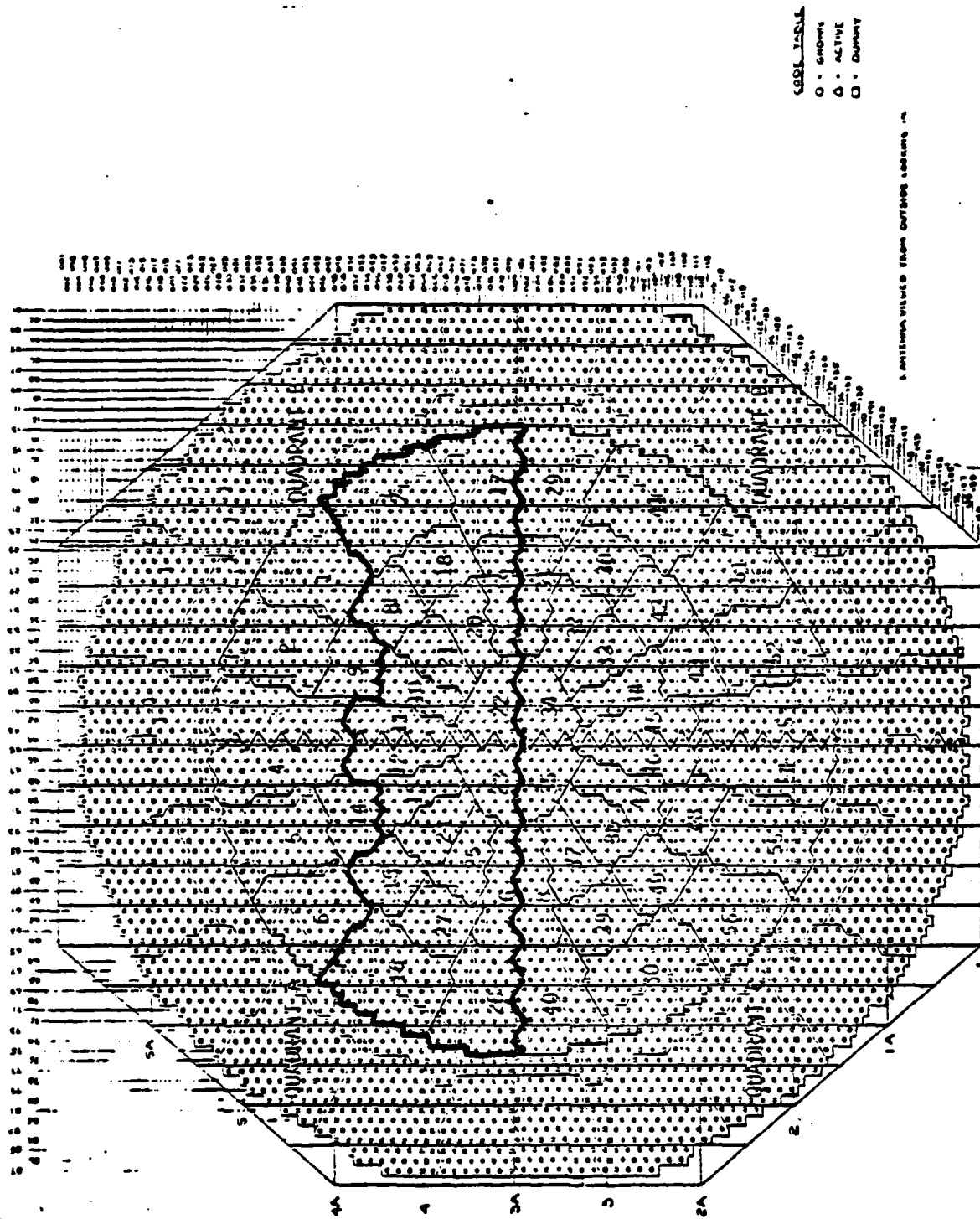
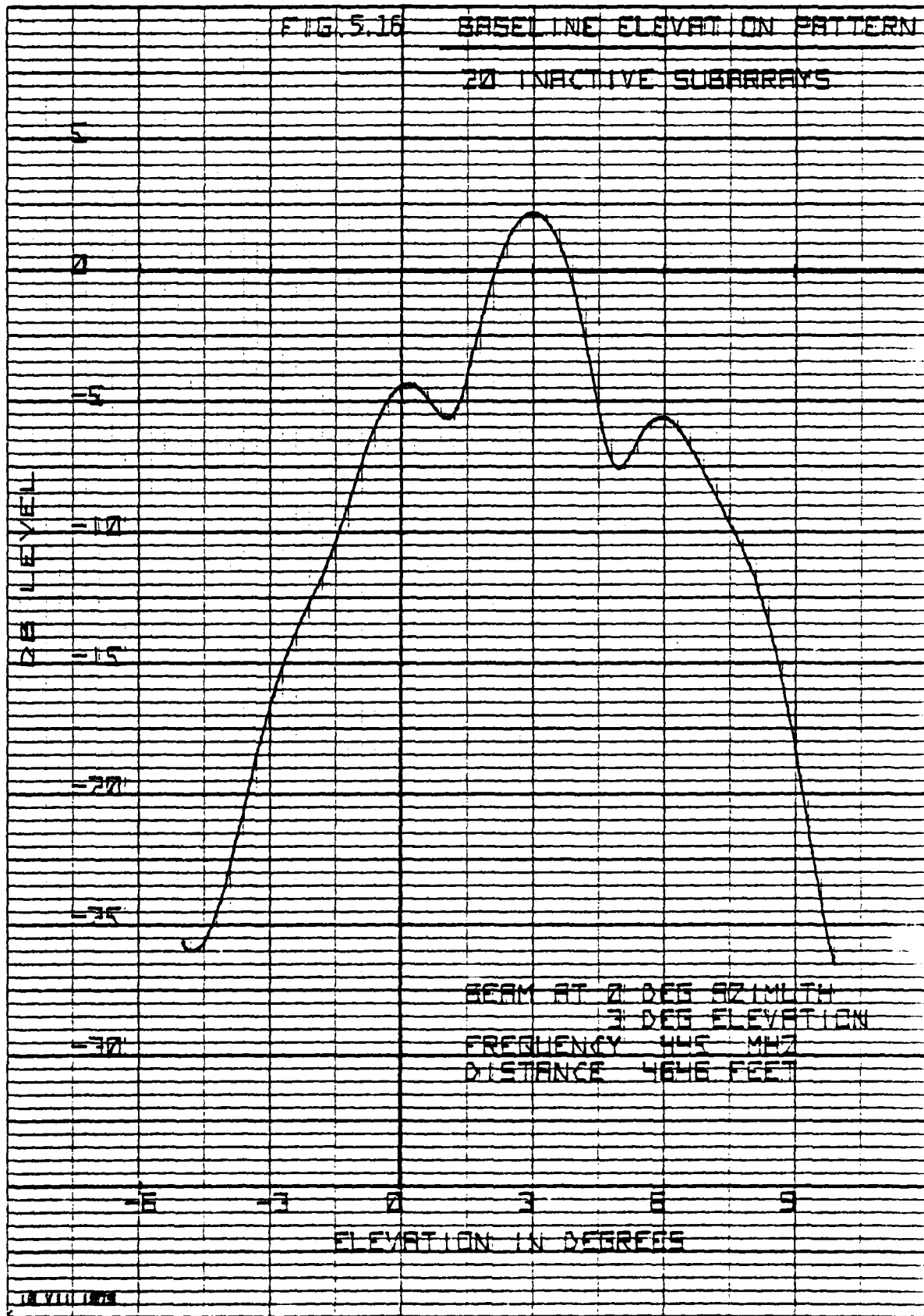


FIG. 5.15 ARRAY WITH 20 FAILED SUBARRAYS



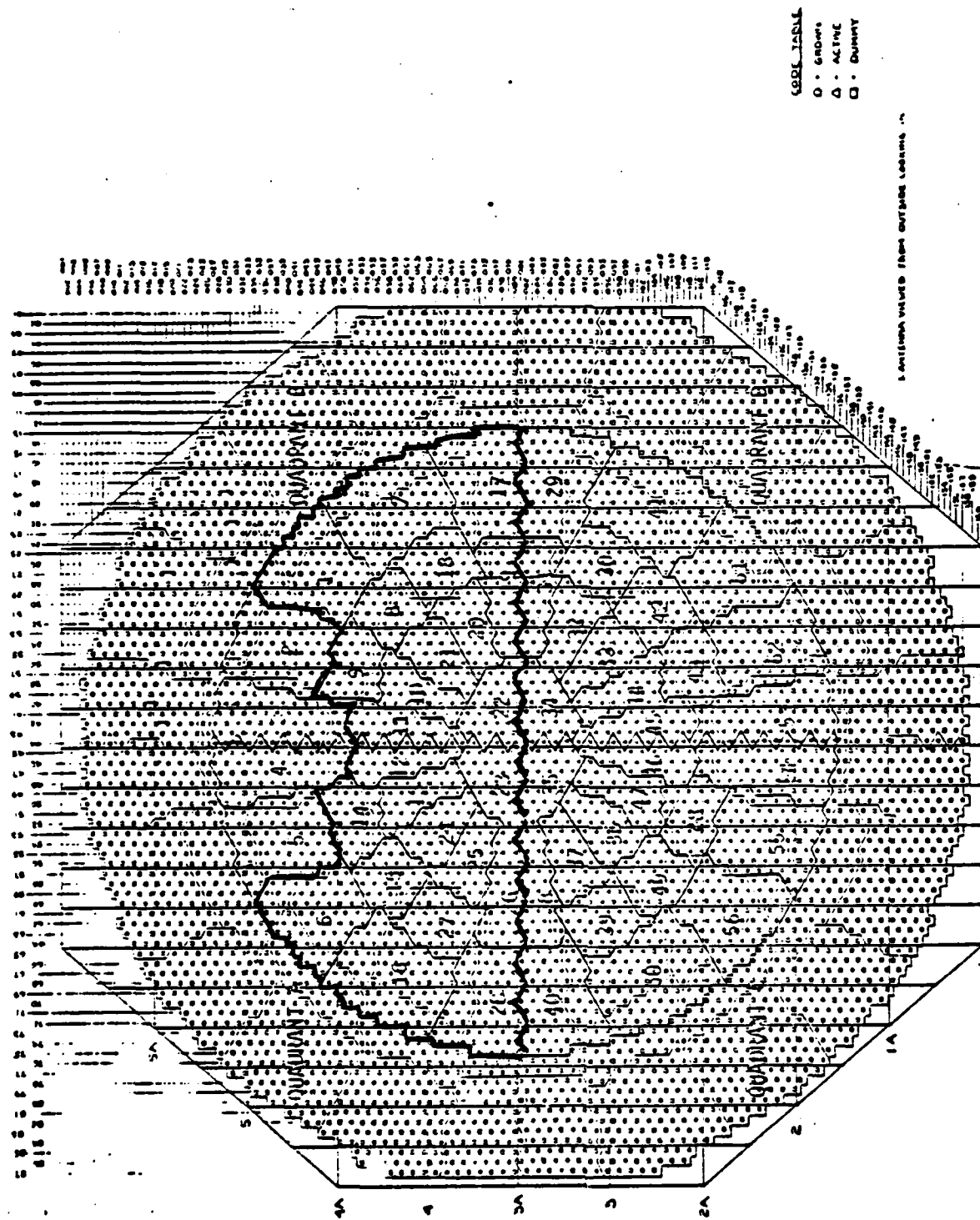
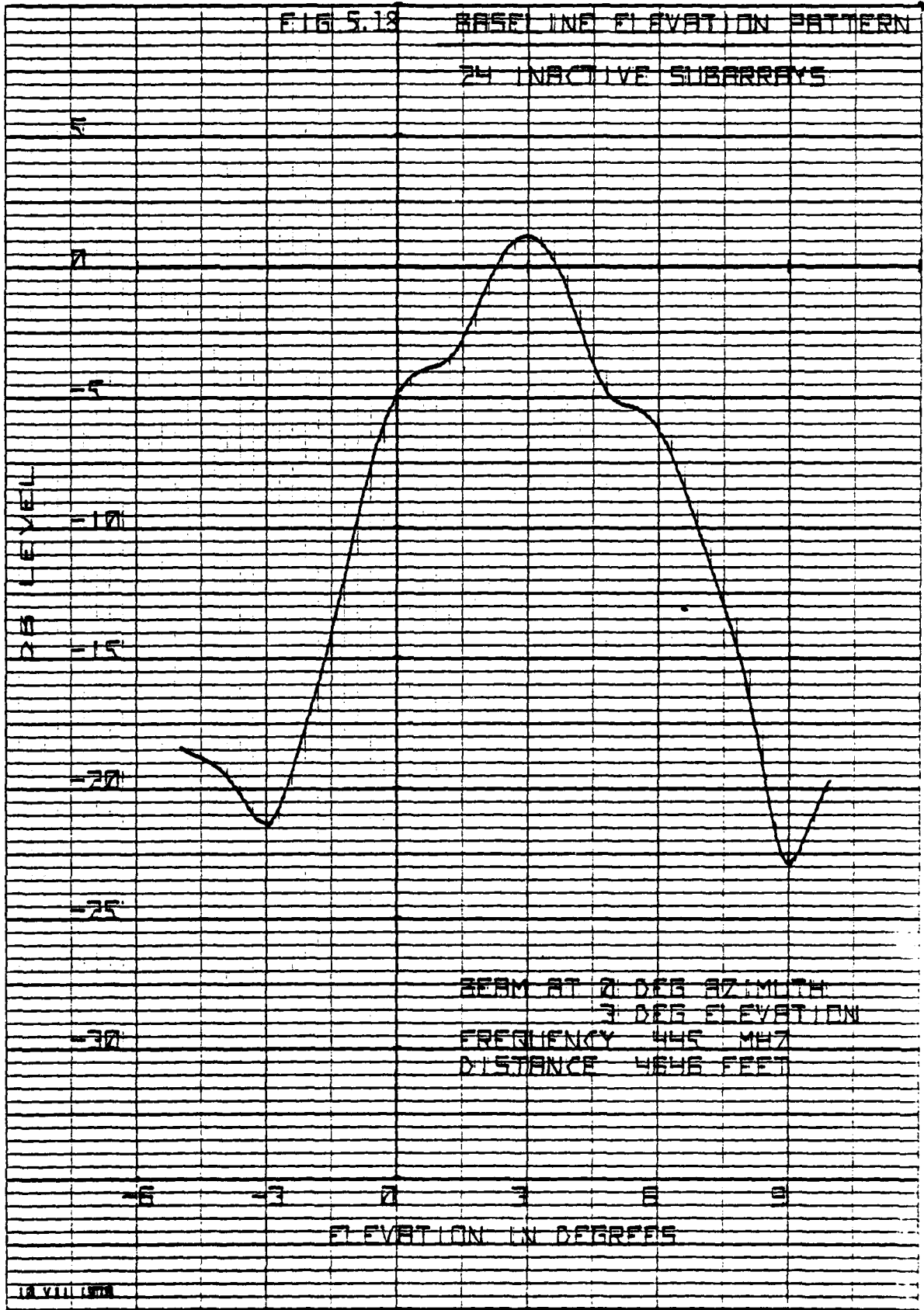


FIG. 5.17 ARRAY WITH 24 FAILED SUBARRAYS



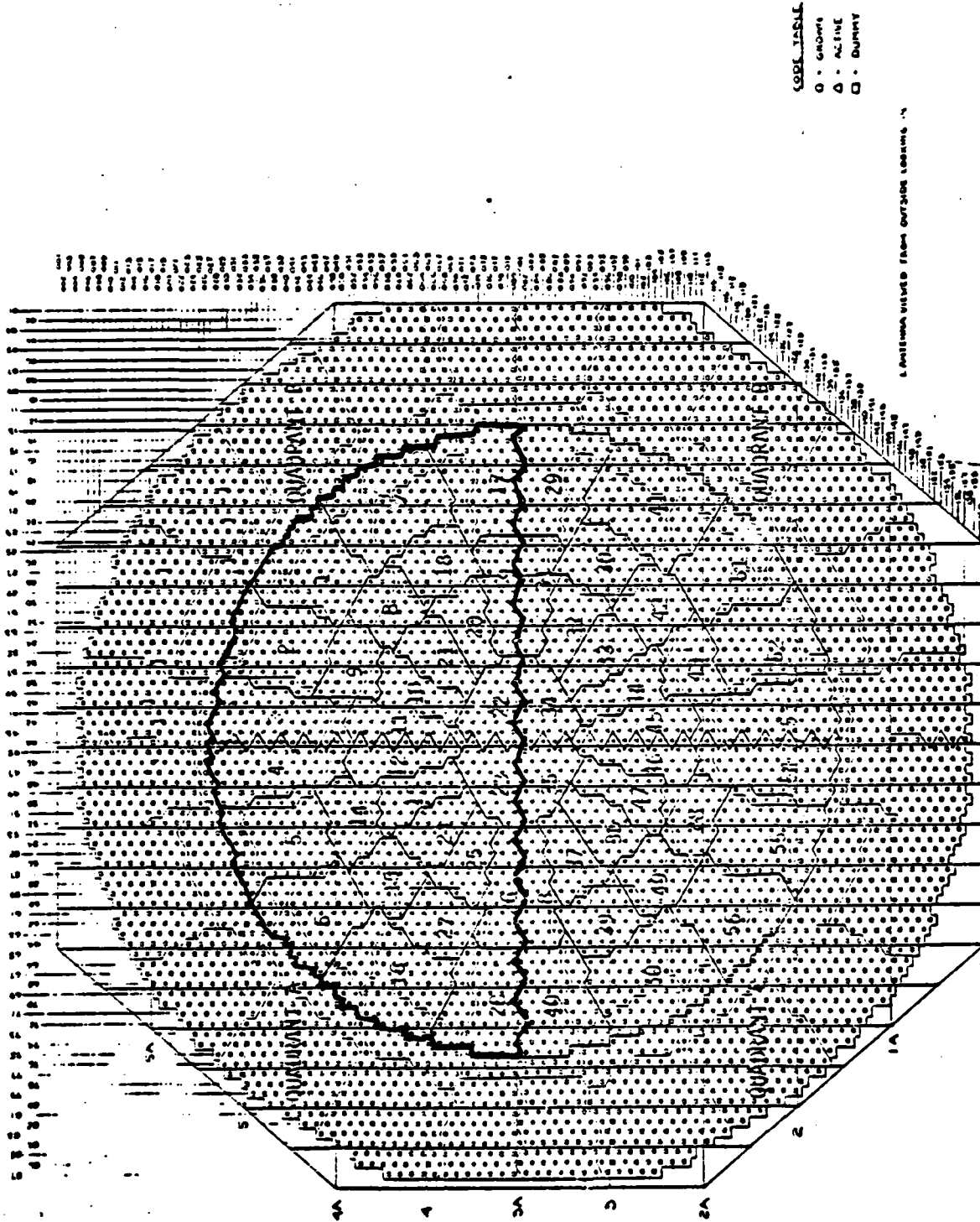
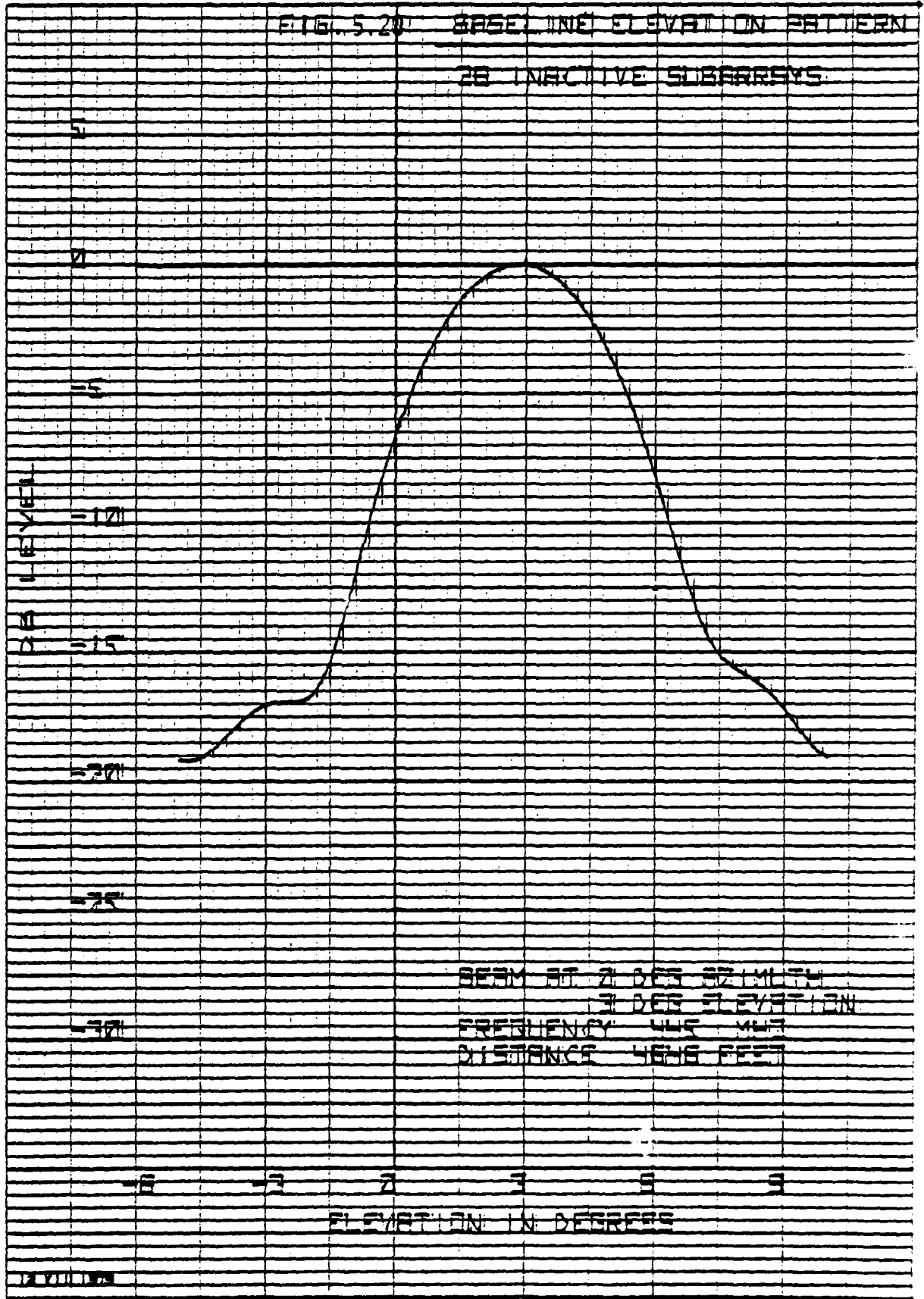


FIG. 5.19 ARRAY WITH 28 FAILED SUBARRAYS

HEWLETT PACKARD © 270-1006



6.0 Conclusions: It is concluded that the radar frequency radiation (RFR) by the PAVE PAWS radar system does not present a radiation hazard to personnel provided that there is no entry to the hazard zones. These zones are the air hazard zone (section 3) and the ground hazard zone within the hazard fence (section 4). The air hazard zone as conservatively defined in this report is a zone extending over an azimuth sector of 240 degrees (120 degrees per radar face) with a radius of approximately 3035 feet for the present baseline system, 6140 feet for the SIX DB system and 8710 feet for the 10DB system. Radiation levels calculated for various off-base ground points of interest are well below the OSHA standard of 10 milliwatts/centimeter squared and indicate no radiation hazard to personnel.

The RADC RFR computer program was verified by comparing the RFR computer program calculated values for four ground points with actual measured data obtained when the PAVE PAWS radar was operating in the surveillance fence mode. The agreement between the measured and calculated data is within plus or minus 3.5 dB. The disagreement may be due to multipath effects which were not considered in this report.

The RADC RFR computer program calculates the radiation levels in the near field, the transition region and the far field with no discontinuities between regions and offers a cost-effective method to determine radiation levels from a phased array radar especially in the near and transition regions. It is also useful in determining the effects of array anomalies such as partial array outages, steering phase errors and in determining the effect of changes in aperture taper.

References

1. AF Regulation 161-42, Radio Frequency Radiation Health Hazards Control, 7 November 1975.
2. Beltran, F., PAVE PAWS Coupling, Raytheon Memo, 11 May 1977.
3. Brodeur, P., The Zapping of America, W.W.Norton, New York, N.Y., 1977
4. Caswell, J.R., Minutes of Meeting: Antenna (Element) Critical Design Review for the PAVE PAWS, Raytheon Co. Memo A00B 16 December 1976
5. CI/Subsystem Test Report for Antenna-Receiver-Transmitter Group, No 975186, 1978
6. CPCI-2 Specification No 914214, 22 December 1976, as amended 1 September 1978
7. Desmond, R.J., Summary of PAVE PAWS RF Hazard Safety Feature, Raytheon Co., 30 Dec 1977.
8. Electromagnetic Radiation Hazards, Technical Manual, T.O. 31Z-10-4, AFCS, 1 August 1966 and Change 2, 1 June 1971
9. Environmental Impact Statement, Operation of the PAVE PAWS Radar System at OTIS AFB, MA, May 1979
10. Gwynne, P. et al, The Flap over the Zap, Newsweek, 17 July 1978
11. Hansen, R.C., Circular Aperture Axial Power Density, Microwave Journal, February 1976
11. Kraus, J.D., Antennas, McGraw Hill, New York N.Y., 1962
12. Malowicki, E., PAVE PAWS Predicted Power Levels, RADC Memo, 24 July 1978
13. Malowicki, E., Radar Frequency Radiation Reduction, RADC TR 79-363, January 1980
14. Malowicki, E., PAVE PAWS Interference, RADC Memo, 22 February 1979
15. NAS, Radiation Intensity of the PAVE PAWS Radar System, National Academy

of Sciences, Washington D.C., 1979

16. Raytheon Program Management Review, Raytheon Co., November 1978

17. Skolnik, M.I., Radar Handbook, McGraw-Hill, New York,
New York, 1970

18. Zfolkowski, F.P., Summary, PAVE PAWS Radiation Analysis, Raytheon Co.
Memo FPZ:150:76, 5 August 1976

Appendix A

Mutual Coupling

1.0 Introduction: The mutual coupling was determined on a partial array (320 elements) by exciting element (1,1) [see Figure A1] at the horizontal polarization H-port and measuring C_{HH} , the resulting coupling at the horizontal polarization H-port of an element (m,n), and measuring C_{VH} , the resulting coupling at the vertical polarization V-port of an element (m,n). This procedure was repeated for the vertical polarization port of the element (1,1).

2.0 Results: Figure A2 shows the magnitudes of C_{HH} and C_{HV} out to the element (1,29), i.e. the fourteenth neighbor element at 430 MHz. The C_{HH} coupling is approximately minus 27 dB at the nearest neighbor and, in general, decreases with increasing distance. The cross-polarized coupling C_{HV} is on the order of 13 dB lower than C_{HH} . Figure A3 shows the magnitudes of C_{VV} and C_{VH} out to element (1,29). The C_{VV} coupling is approximately minus 30 dB at the neighbor element and, in general, also decreases with distance. The cross-polarized coupling C_{VH} is on the order of 23 dB lower than C_{VV} . Table A1 shows the couplings from half of the first ring of elements closest to the center element, e., elements (1,3), (2,2), (-2,2) for 420 MHz the low end of the band and for 435 MHz the midband frequency. Table A2 shows the effect of frequency on the coupling from all the elements of the first ring of elements of the element (1,1) for the C_{VV} and C_{HH} couplings. As expected, the strongest degree of coupling exists at 420 MHz, the lowest frequency, and decreases monotonically with frequency. Table A3 shows the couplings from half of the second ring of elements, i.e., elements (1,5), (2,4), (3,3), (-3,3) and (3,1) at 420 MHz. Table A4 shows the second ring couplings at 435 MHz. Table A5 shows the resulting coupling

into the element (1,1) from the first ring of 6 elements, from the second ring of 12 elements, and from both of these two rings of elements for 420 and 435 MHz. The total coupling is low in the order of 12 dB for the C_{VV} and C_{HH} cases. The energy coupled into the antenna element will be partially absorbed by the element source impedance, partially reflected from the element source impedance and radiated depending on the element VSWR. The element highest VSWR over the total scan volume was measured as 2.1 at 450 MHz, the high edge of the band. This VSWR would reduce the coupled energy available for radiation by an element by about 14 dB.

3.0 Error: To bound the error in the field density calculation caused by neglecting the mutual coupling, let us assume that, since the actual antenna array is large (1792 elements), the edge elements partial coupling can be neglected and the coupling is the same for each element. Let us further assume that each element VSWR is 2.1. Then the antenna pattern

$$E = \sum^N (a_i e^{j\phi_i} + p a_e e^{j\phi_e}) \quad (A1)$$

where N is the total number of elements

a_i is the amplitude at each element

ϕ_i is the element phase

p is the element reflection coefficient magnitude of 0.35 for a VSWR of 2.1

a_e is the total coupling amplitude

ϕ_e is the total coupling phase

Since the second term in equation (A1) is assumed to be the same for each element

$$E = \sum_{i=1}^N a_i e^{j\theta_i} + N p a_c e^{j\theta_c} \quad (A2)$$

The error magnitude (er) in the field pattern calculation due to omitting mutual coupling coupling effect is

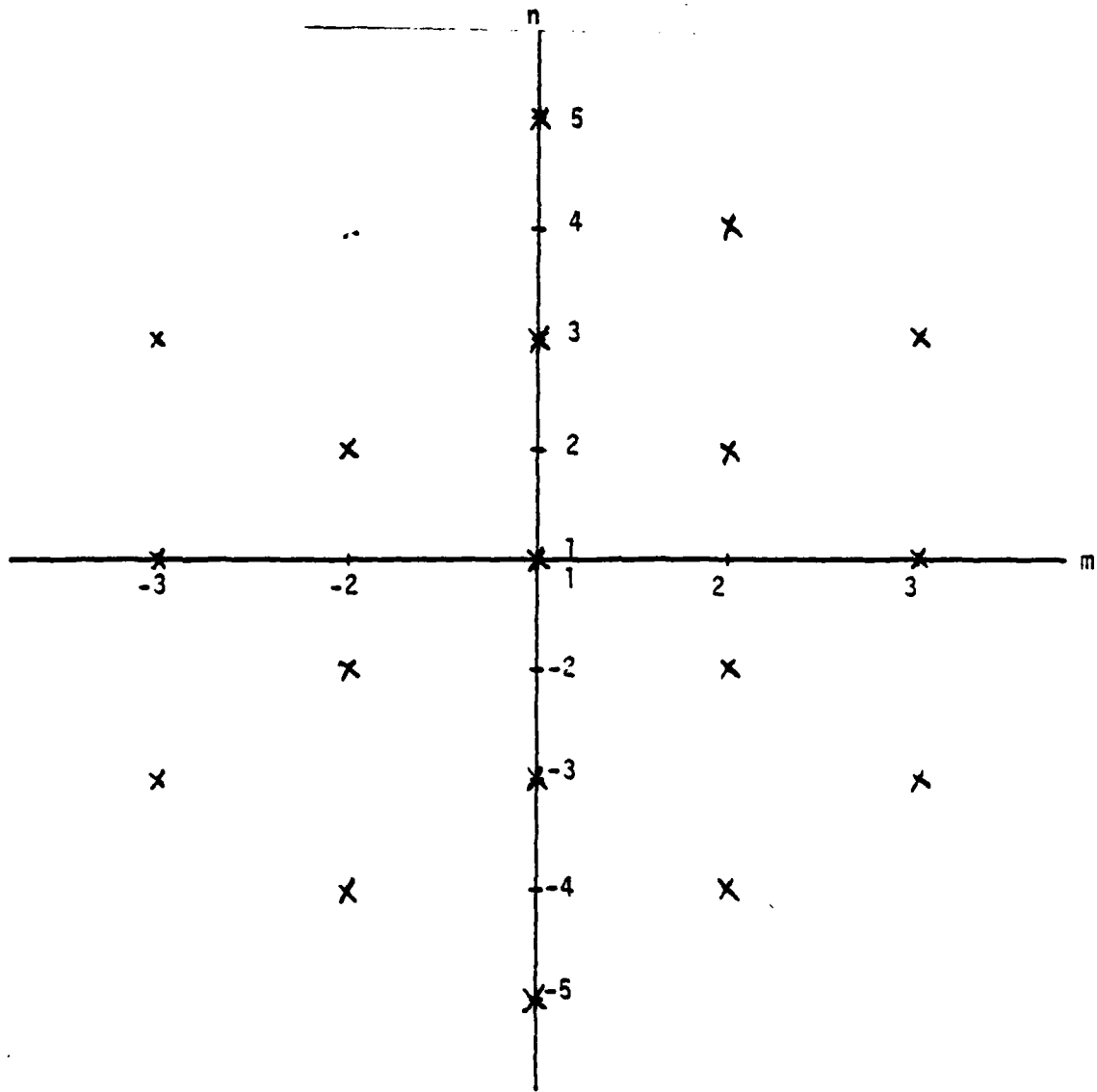
$$er = \frac{N p a_c}{p a e^{j\theta} + \sum_{i=1}^N a_i e^{j\theta_i}} \quad (A3)$$

For the boresight case and for unity excitations a_i

$$er = \frac{p a_c}{|p a e^{j\theta} + 1|} \quad (A4)$$

Taking the worst case (420 MHz) highest value of minus 12 dB at an angle of 15.7 degrees for the coupling, the error is 0.074. The error in the field density calculation due to omitting the mutual coupling effect is negligible -- less than minus 22 dB or less than 0.6 percent on a power basis.

FIG A1--ELEMENT GEOMETRY



HEWLETT-PACKARD 8270-1008

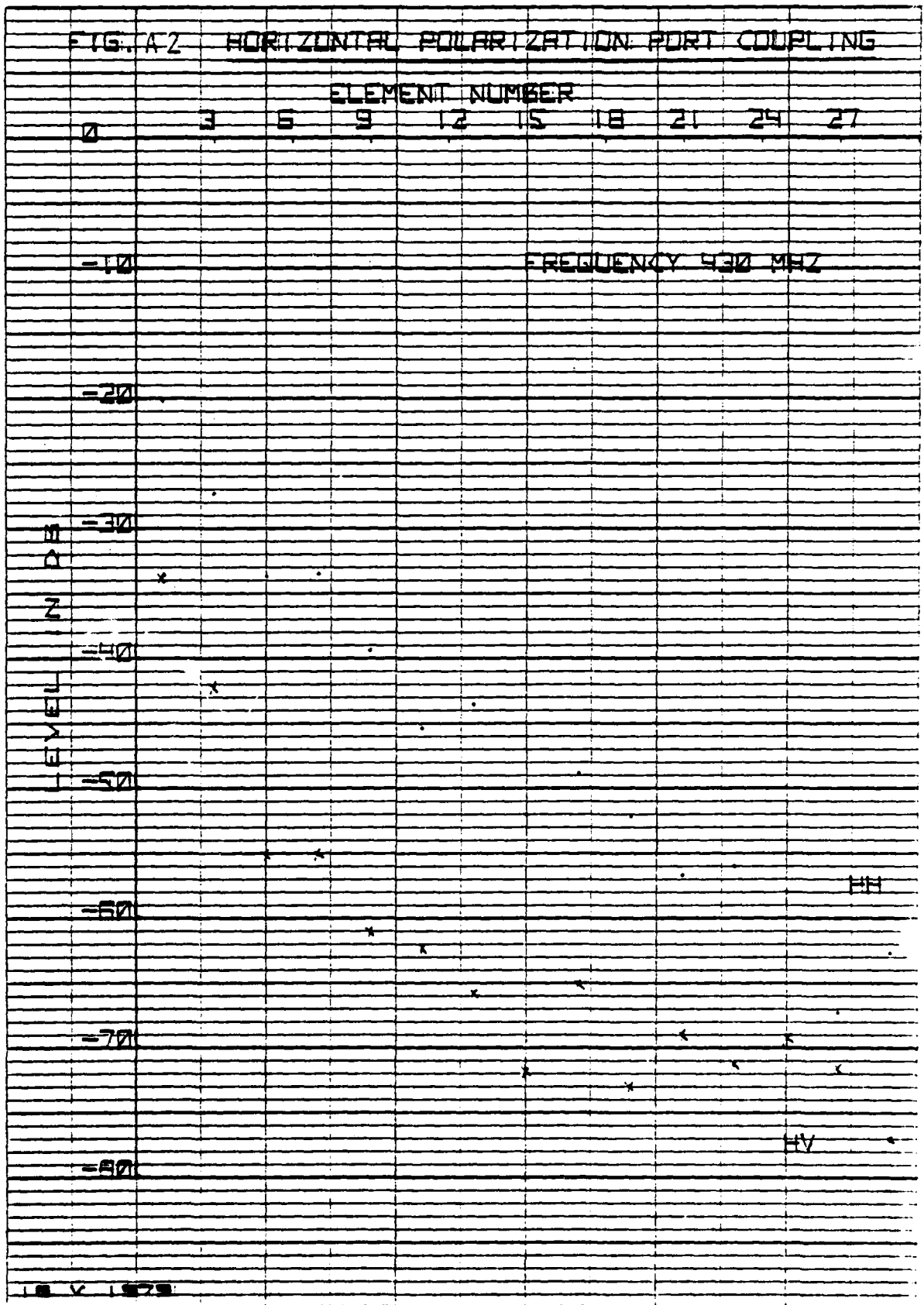


FIG. A-3 VERTICAL POLARIZATION PORT COUPLING

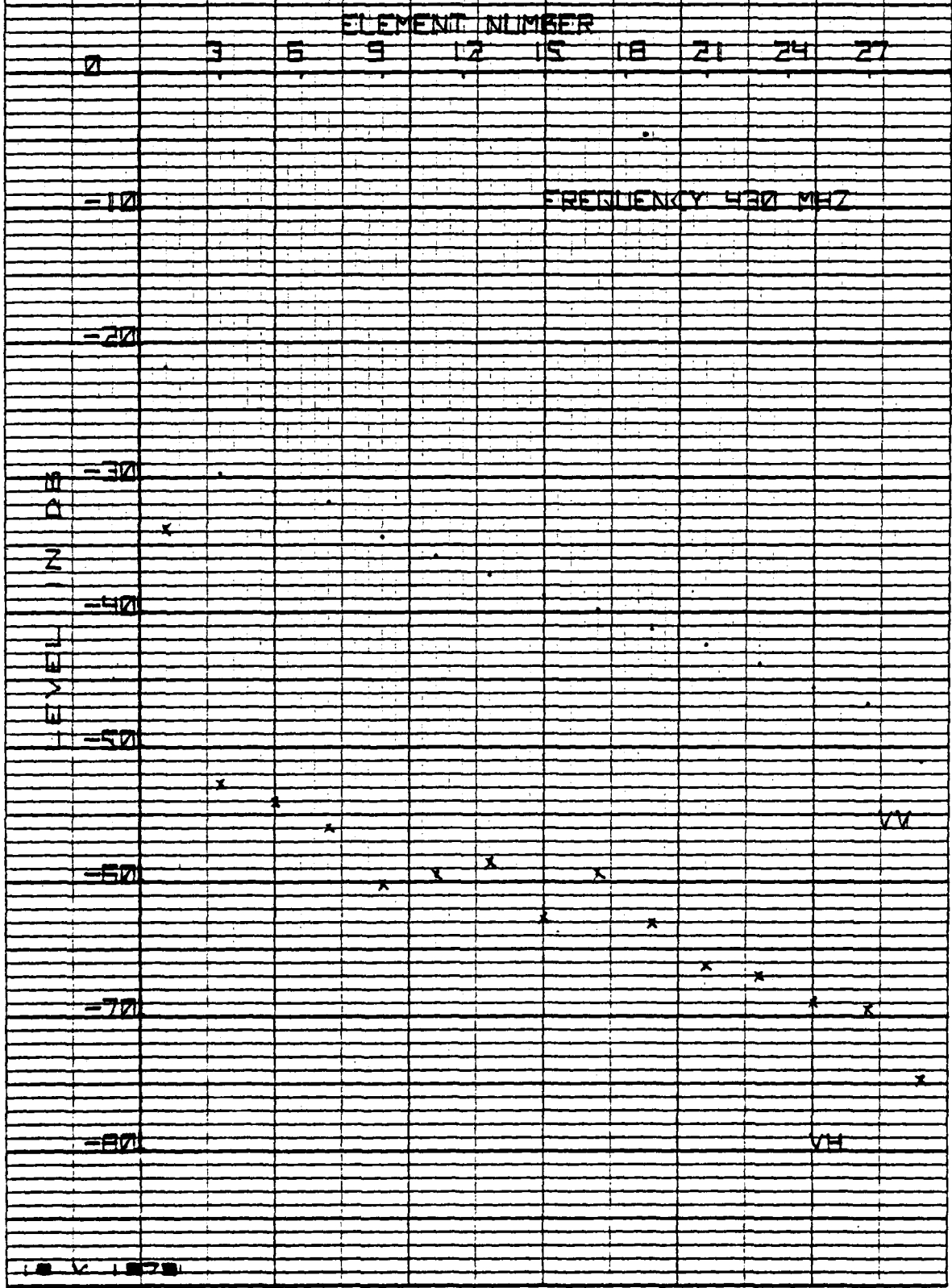


TABLE A1---FIRST RING COUPLING

FREQUENCY MHZ	ELEMENT	COUPLING	MAGNITUDE MINUS DB	PHASE DEG
420 ↓ ↓ ↓ ↓ ↓ ↓ ↓ ↓ ↓ ↓ ↓ ↓ ↓ ↓ ↓ ↓ 435	1,3 ↓	VV	25.5	35
		VH	54.8	21
		HV	42.4	118
		HV	16.7	-17
	2,2 ↓	VV	18.2	-12
		VH	26	155
		HV	26.8	155
		HH	22.4	9
	-2,2 ↓	VV	18	-16
		VH	26.1	-26
		HV	27.7	-17
		HH	22.4	4
	1,3 ↓	VV	31.3	12
		VH	53.1	-15
		HV	42.3	76
		HH	17.6	-59
2,2 ↓	VV	19.6	-55	
	VH	25.8	119	
	HV	26.4	119	
	HH	25.8	-34	
-2,2 ↓	VV	19.4	-58	
	VH	25.5	-62	
	HV	27.6	-54	
	HH	25.9	-35	

TABLE A2-EFFECT OF FREQUENCY ON THE FIRST RING COUPLING

<u>FREQUENCY</u> <u>MHz</u>	<u>C_{HH}</u> <u>MAGNITUDE</u> <u>MINUS DB</u>	<u>PHASE</u> <u>DEGREE</u>	<u>C_{VV}</u> <u>MAGNITUDE</u> <u>MINUS</u>	<u>PHASE</u> <u>DEGREE</u>
420	4.69	-5.04	4.84	-5.98
430	6.14	-35	6.3	-36.76
435	6.8	-48.34	7.03	-50
440	7.41	-60.69	7.64	-62.1
450	8.27	-82.89	8.17	-73.32

TABLE A3--SECOND RING COUPLING AT 420 MHz

<u>ELEMENT</u>	<u>COUPLING</u>	<u>MAGNITUDE MINUS DB</u>	<u>PHASE DEGREE</u>
1,5 ↓	VV	30.4	35
	VH	54.9	116
	HV	52.5	-121
	HH	30.2	100
2,4 ↓	VV	25.3	-176
	VH	32.8	9
	HV	32.8	10
	HH	22.3	-175
-2,4 ↓	VV	25.3	180
	HV	32.2	172
	HH	33.8	-160
	HH	22.5	180
3,1 ↓	VV	21.4	-177
	VH	47.7	-32
	HV	51.1	-140
	HH	27.6	179
3,3 ↓	VV	31.1	89
	VH	38.3	-9
	HV	38	-4
	HH	32.1	57
-3,3 ↓	VV	31.5	84
	VH	36.2	167
	HV	36.4	180
	HH	32.2	51

TABLE A4---SECOND RING COUPLING AT 435 MHz

<u>ELEMENT</u>	<u>COUPLING</u>	<u>MAGNITUDE MINUS DB</u>	<u>PHASE DEGREE</u>
1,5	VV	31.5	-38
	VH	54.4	57
	HV	55.9	-172
	HH	33.7	93
2,4	VV	28.8	114
	VH	34.8	-38
	HV	34.4	-38
	HH	25.3	125
-2,4	VV	28.9	110
	VH	33.1	143
	HV	35.7	157
	HH	25.7	120
3,3	VV	37.3	74
	VH	35	-50
	HV	34.9	-47
	HH	36.6	-18
-3,3	VV	38.9	74
	VH	33.8	123
	HV	34.4	132
	HH	36.6	-30
3,1	VV	24.2	126
	VH	47.3	-88
	HV	49.5	172
	HH	31.2	101

TABLE A5--TOTAL COUPLING

<u>FREQUENCY</u> <u>MHz</u>	<u>COUPLING</u>	<u>FIRST RING</u>		<u>SECOND RING</u>		<u>TOTAL</u>	
		<u>MAGNITUDE</u> <u>MINUS DB</u>	<u>PHASE</u> <u>DEGREE</u>	<u>MAGNITUDE</u> <u>MINUS DB</u>	<u>PHASE</u> <u>DEGREE</u>	<u>MAGNITUDE</u> <u>MINUS DB</u>	<u>PHASE</u> <u>DEGREE</u>
420 ↓	VV	4.84	-5.98	9.01	159	12.11	15.7
	VH	55.76	8.05	35.63	138.35	35.68	98.7
	HV	30.43	111.77	35.79	251.64	21.40	-76.69
	HH	4.69	-5.04	8.81	159.2	11.9	72.21
435 ↓	VV	7.03	-50	11.74	105.89	12.57	-23.31
	VH	20.2	52.06	43.26	122.32	19.98	55.75
	HV	29.95	78.55	31.3	216.66	32.59	101.39
	HH	6.8	-48.34	11.68	106.29	12.1	-21.57

Appendix B

PAVE PAWS Face C Element Failure

1.0 Introduction: This section concerns itself with the effect of Face C element failures on the signal strength seen by Face C when illuminated by the Face C NFE (Near Field Element). Here, the term Face C element denotes the combination of the Face C antenna element and its corresponding SSM (Solid State Module). Failures considered included total element failures where the failed element provided no signal output at all and element single bit failures where the beam steering phase of 180, 90, 45, or 22.5 degrees was not provided when required.

2.0 Geometry: Figure B1 shows the Face C/NFE geometry used in this analysis. The NFE beam center is taken to point to the Face C array center. The dimensions are given in feet.

3.0 Method: The RADC RFR computer program was used to calculate the signal levels. The Face C array was amplitude tapered in accordance with Table B1.

Table B1 Face C Amplitude Taper

Element Numbers	Amplitude in dB
1,21	12.5
2,20	11.5
3,19	9.5
4,18	7.5
5,17	5.5
6,16	3
7,15	2
8,14	1
9,13	0.5
10,11,12	0

4.0 Results

4.1 Total Failures: Figures B2 through B6 show the effect of single element total outages in Face C on the signal level at the Face C output in this failed mode when illuminated by only a test signal from the Face C NFE. The failed element is identified by a number from 1 to 21 corresponding to the failed element position in the Face C array. Note that the failed 0 coordinate indicates no failed element and is used to provide a reference. In Figure B2 this reference is with respect to the signal level existing at the Face C output for no element failures and no beam steering in azimuth. In Figures B3, B4, B5 and B6 this reference is with respect to the signal existing at the Face C output for no element failures and with the beam steered in azimuth to 7, 17, 37, and 57 degrees, respectively. For the case where the beam position is on the Face C boresight (zero degrees relative azimuth), the Face C signal level change is fairly insensitive to single total element failures and could not be used to identify the failed element on a maintenance oscilloscope or spectrum analyzer (assuming a one dB granularity). As the beam is steered off boresight, the signal level changes are more pronounced when an element fails. For the case where the beam is steered to 7 degrees (Figure B3) relative azimuth, the Face C signal level changes are greater than the boresight beam case and are within plus one dB and minus 2 dB, respectively. These amplitude changes can be measured and used to detect a failed element condition for some elements. Unfortunately, the failed element variable is not a single valued function of the signal level change throughout most of the range of the element variable. This together with the small changes in the signal level from neighboring element failures does not allow a unique identification of the failed element. For the case where the

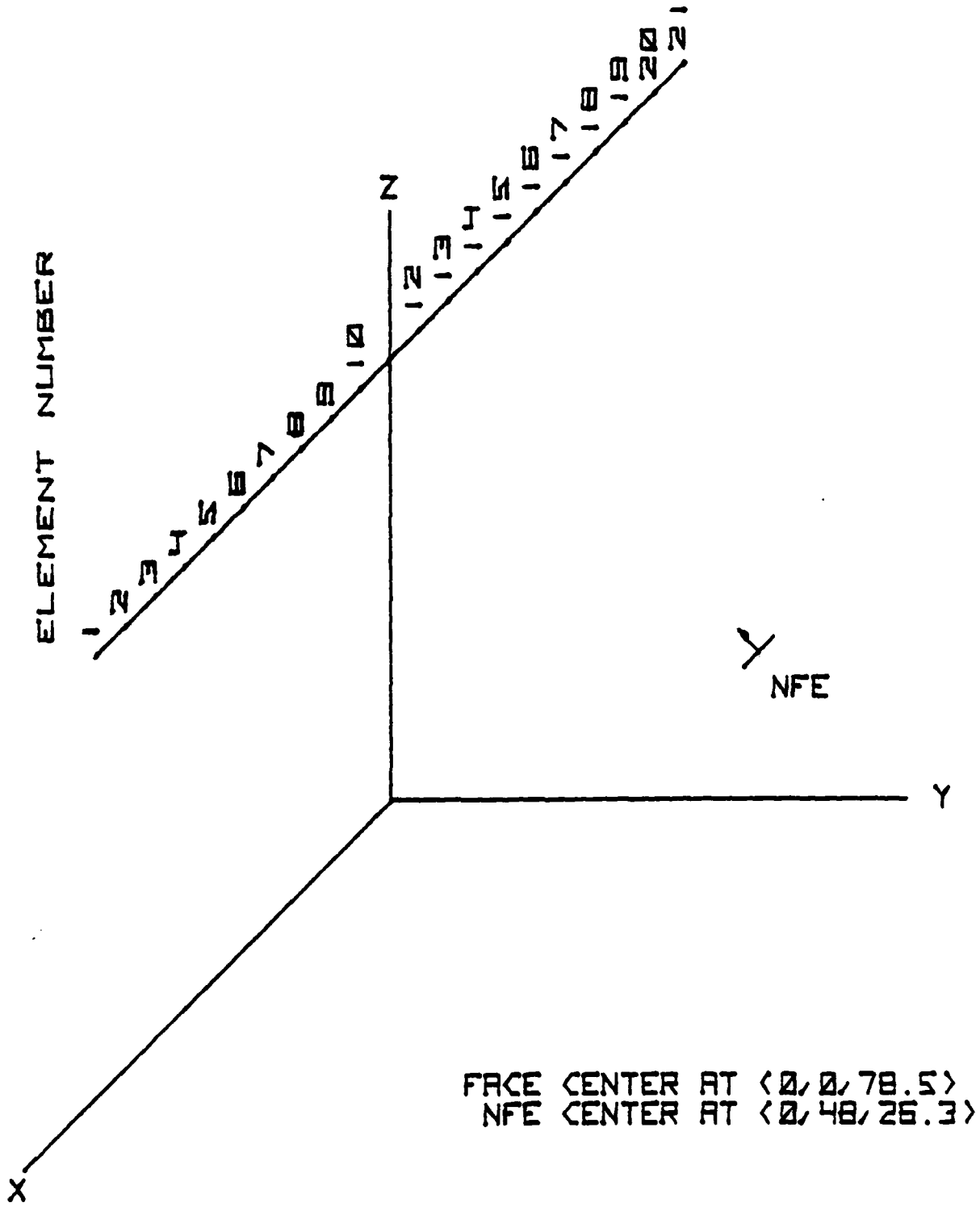
beam is steered to 17 degrees (Figure B4) relative azimuth, the signal amplitude changes are large and are easily measured. But, again the failed element variable is not a single valued function for most of the failed elements. Again, a unique determination of the failed element is not possible for most of the elements. Where the function is single valued i.e. for failed element Number 12, the identification of this failed element is possible. Similar conclusions can be drawn for the cases where the beam is steered to 37 degrees relative azimuth (Figure B5) and 57 degrees relative azimuth (Figure B6). Figure B5 shows that for the failed elements 1 and 11 the failed element variable is a single valued function and would identify either of these failed elements. For the case where the beam is steered to 57 degrees relative azimuth (Figure B6) the failed element variable is single valued when element Number 11 fails. But, since the signal level change between failed element Number 11 and failed element Number 9 is 0.1 dB, it would be better to identify this failed element Number 11 by steering the beam to 37 degrees (Figure B5) where the relative signal level change between failed element Number 11 and failed element Number 8 is 0.86 dB.

4.2 Steering Bit Failures: Figures B7 through B10 show the effect on the signal strength at Face C when a steering bit failure occurs for various elements of the Face C array and for various bit failures. The steering bit failures considered here are those bit failures, occurring one at a time, that fail to provide the phase steering bit when it is required by a commanded azimuth. The signal level is referred to that existing for no bit failures at a particular beam. As evident from Figures B7 through B10, there are element bit failures which can be identified by measuring the Face C signal levels for various commanded beam azimuth positions.

4.3 Far Field: The Face C signal levels change sometimes rather drastically when element errors occur. Largely, this is due to the fact that these signal levels are a result of Face C illumination by the Face C NFE which is at more than minus 47 degrees below the Face C and is in the near field of Face C. The Face C NFE is at about $0.3 D^2 / \lambda$ distance from the Face C array. Figures B11 and B12 depicting the near field azimuth pattern through the NFE for no failed element and element Number 1 totally failed clearly show the sidelobe region effect and the drastic change in Face C signal level as a result of sidelobe mobility due to element Number 1 failure even though this particular element has a severe 12.5 dB amplitude taper. Figures B13, B14, B15 and B16 compare the far field patterns for zero and 57 degrees azimuth and for no failures vs element totally failed. The changes in signal amplitude due to element Number 1 failures are slight for far field illumination, as expected.

5.0 Conclusions: It is concluded that injecting a known interference signal into Face C NFE test antenna provides some limited capability to identify totally Face C elements and Face C steering bit failures when a maintenance oscilloscope or spectrum analyzer is used and when there is no external interference. This capability will be degraded when other external interference is present. This external interference usually varies in intensity and frequency.

FIG. B.1 FACE C/NFE GEOMETRY



FACE CENTER AT $\langle 0, 0, 78.5 \rangle$
NFE CENTER AT $\langle 0, 48, 26.3 \rangle$

NOT TO SCALE

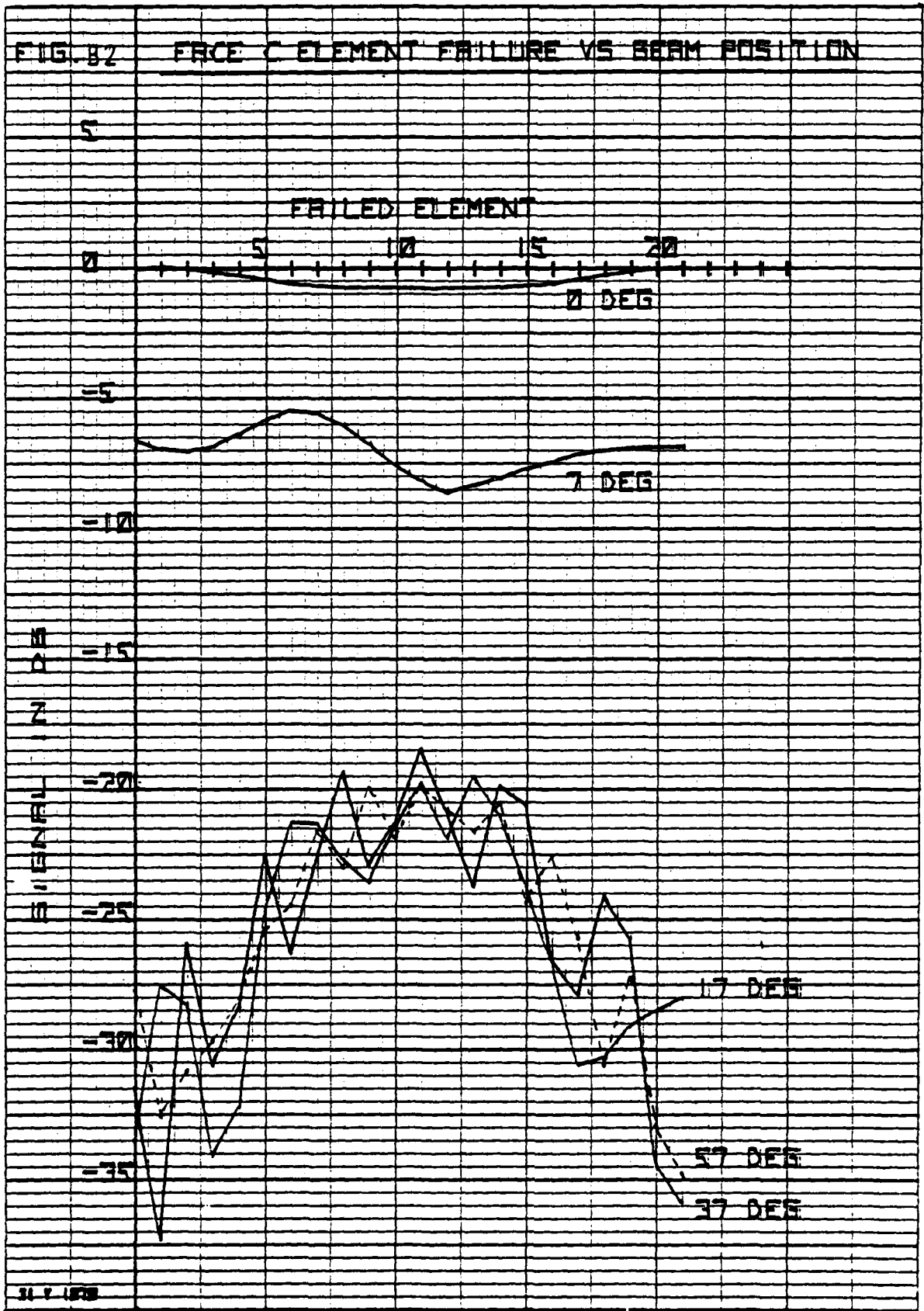
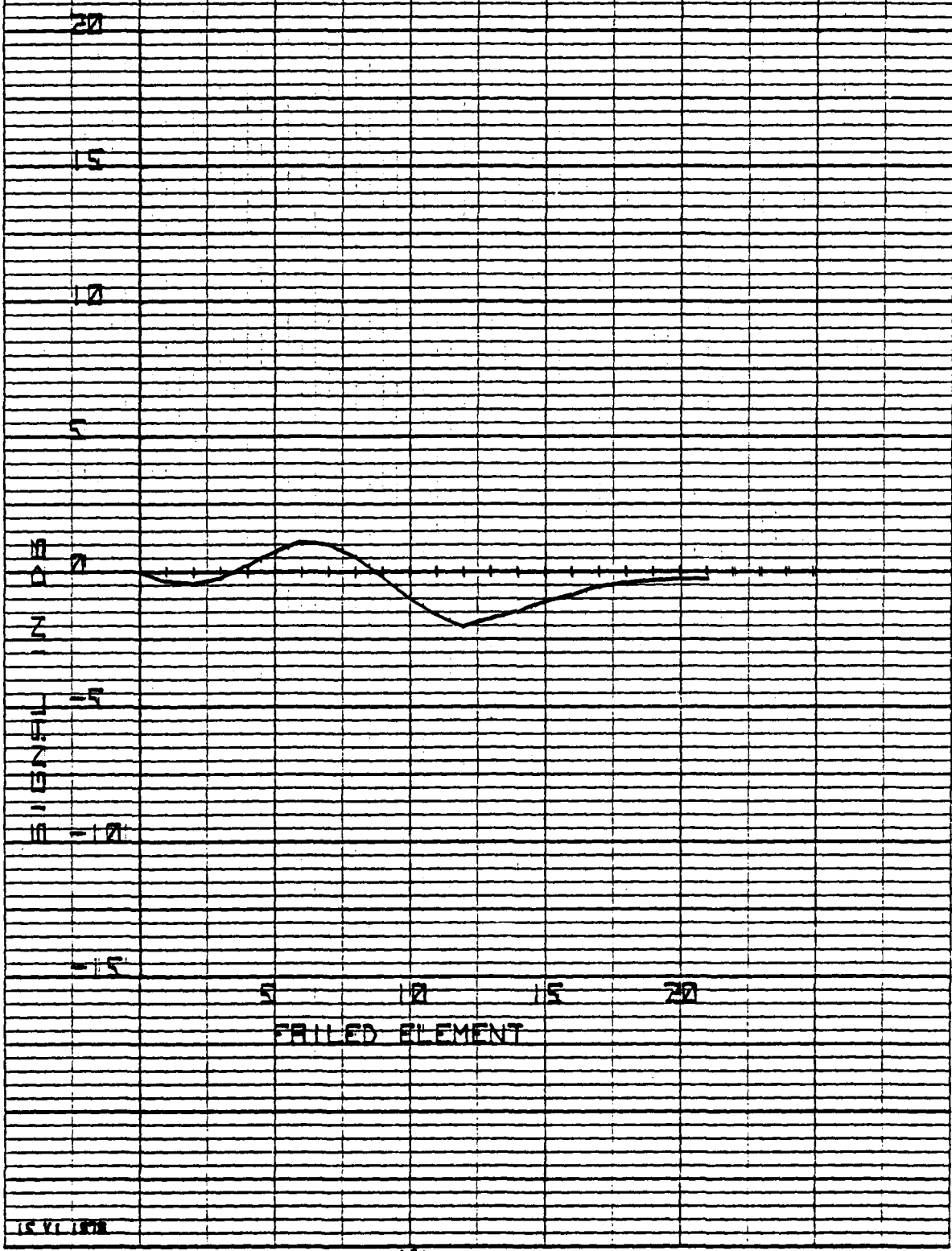
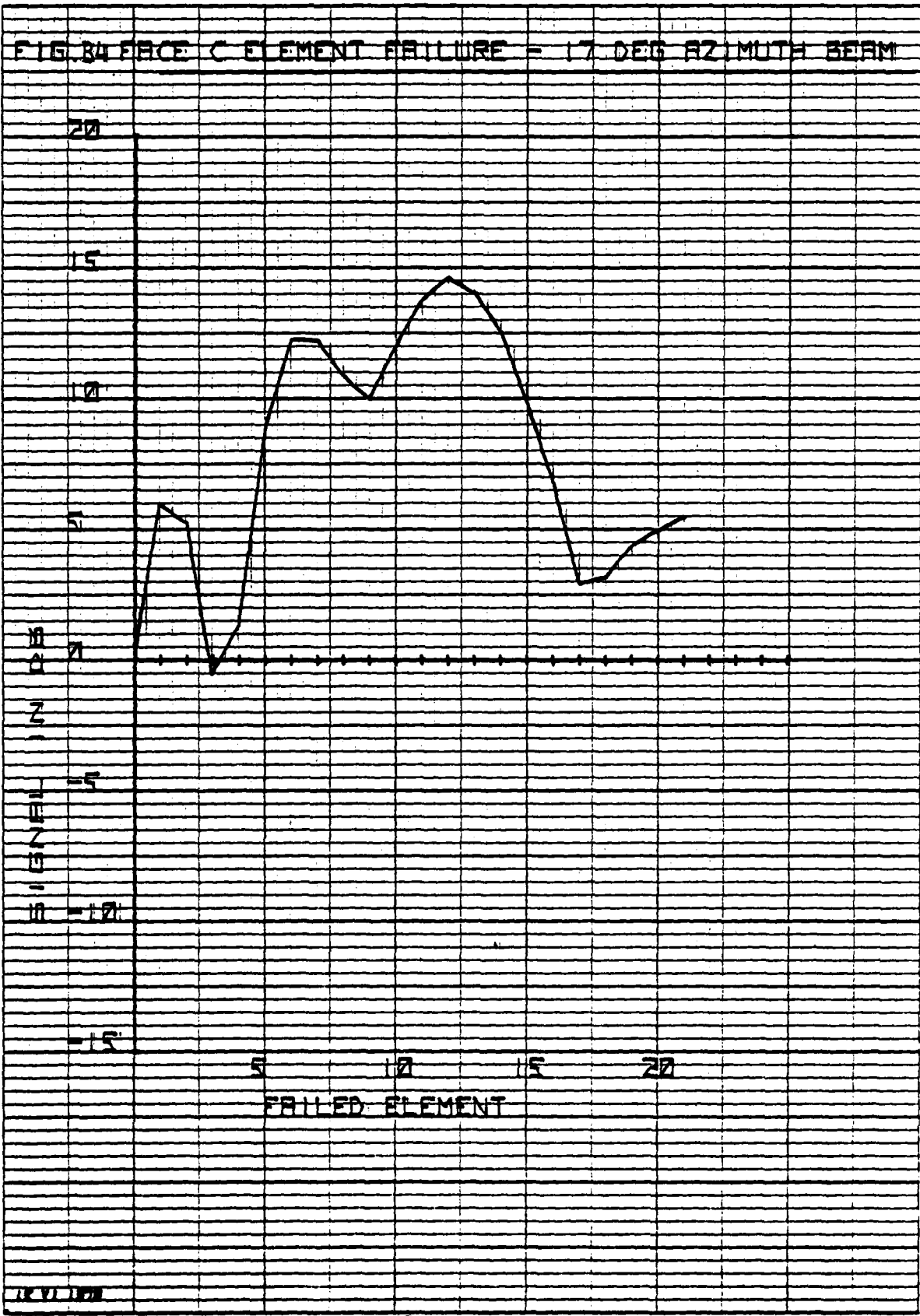


FIG. 83 FACE C ELEMENT FAILURE - 7 DEG AZIMUTH BEAM



15 VI 1978

HEWLETT-PACKARD 9270-1006



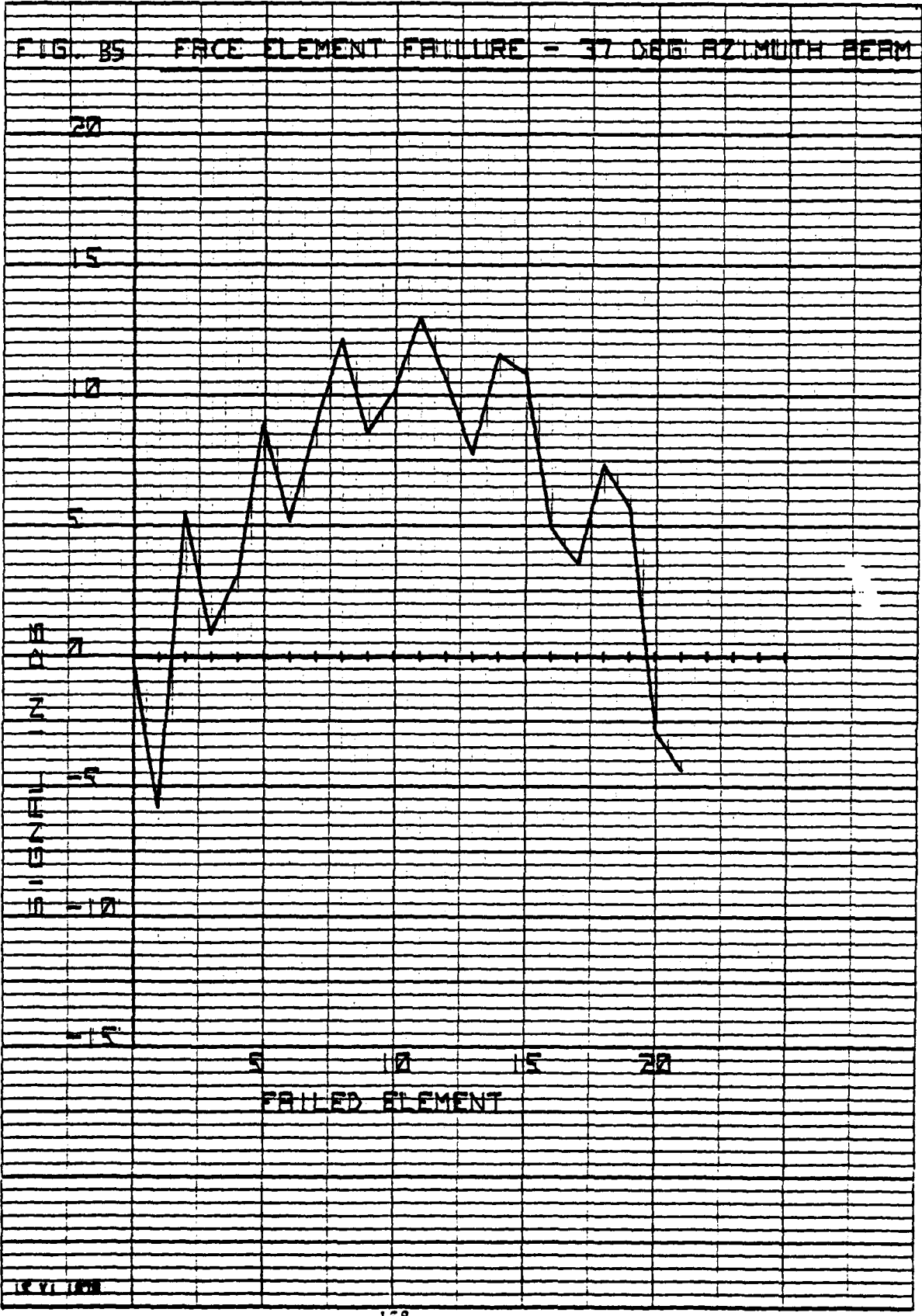
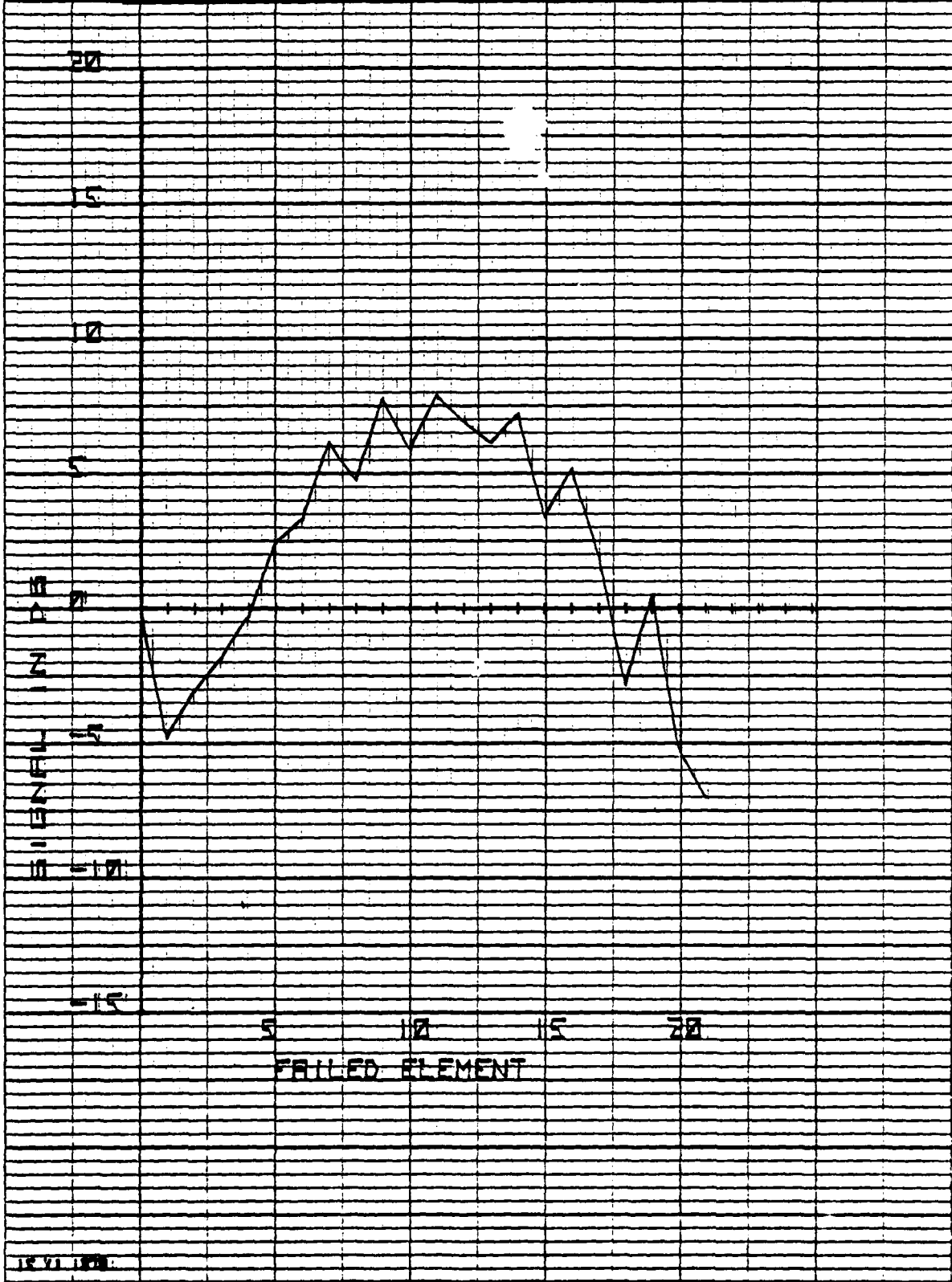


FIG. 86 FORCE C ELEMENT FAILURE - 57 DEG AZIMUTH BEAM



12 VI 1961

FIG. 87 FACE C STEERING BIT FAILURES

7 DEG BEAM AZIMUTH

30

25

20

15

10
8

Z

J 5

U

Z

10
11

5

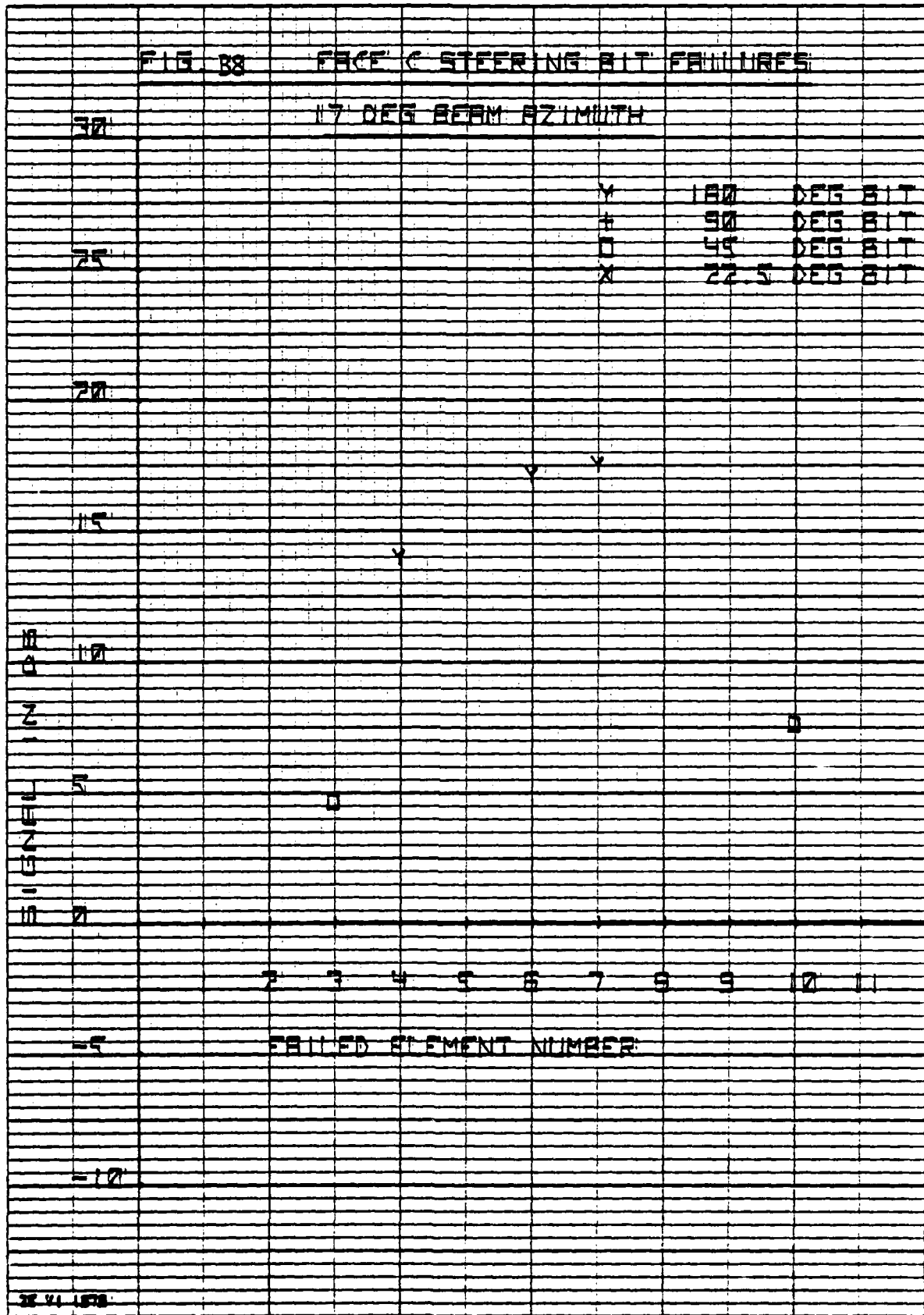
12

Y 180 DEG BIT
90 DEG BIT
0 45 DEG BIT
X 22.5 DEG BIT

FAILED ELEMENT NUMBER

2 3 4 5 6 7 8 9 10 11

22 VI 1978



ILWALEI PALKARD 9270 1000

FIG. 89 FACE C STEERING BIT FAILURES

37 DEG BEAM AZIMUTH

30

25

20

15

10

5

0

-5

-10

-5

-10

Y	100	DEG	BIT
+	90	DEG	BIT
0	45	DEG	BIT
X	22.5	DEG	BIT

*

Y

Y

Y

Y

Y

+

Y

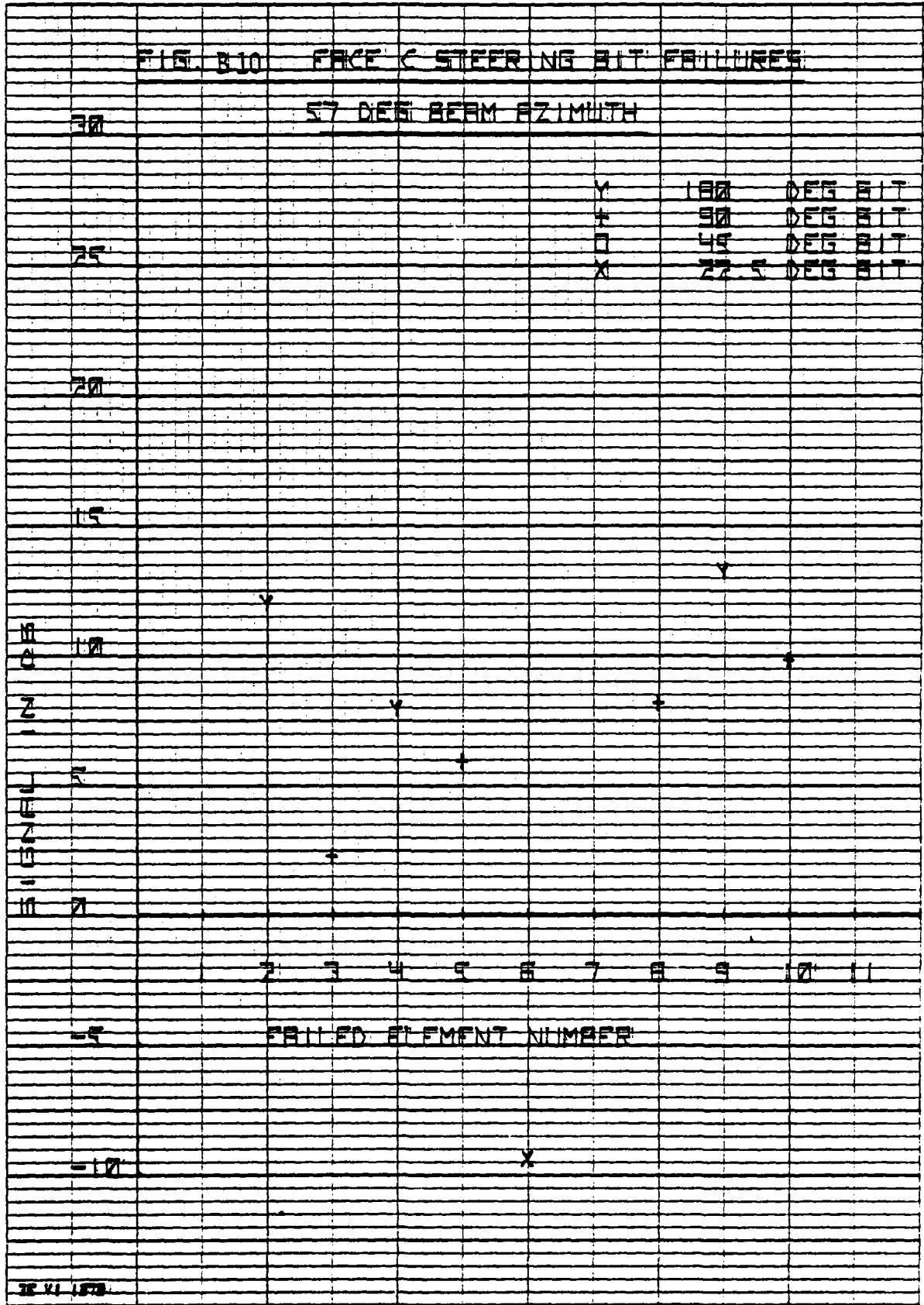
+

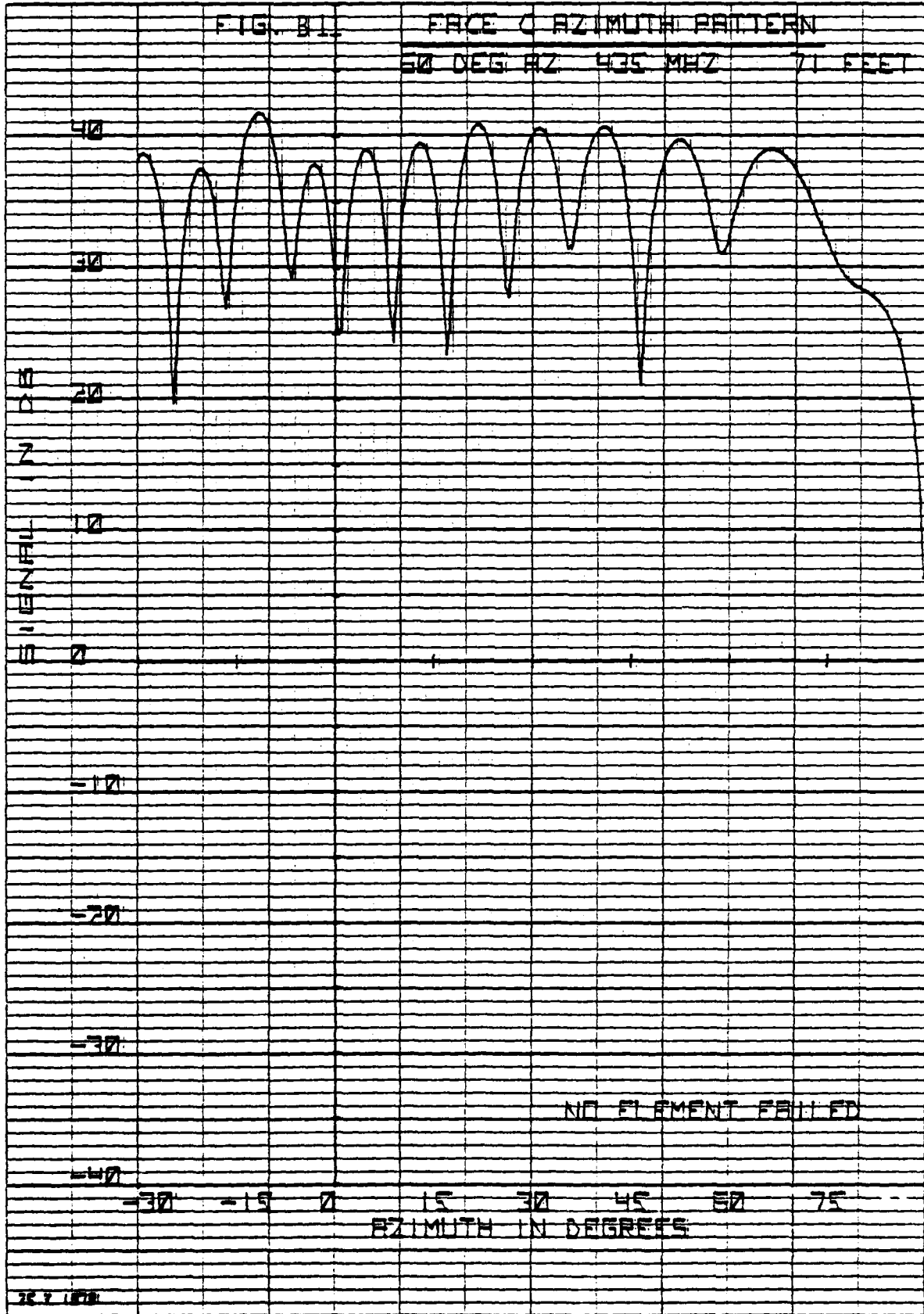
2 3 4 5 6 7 8 9 10 11

FAILED ELEMENT NUMBER

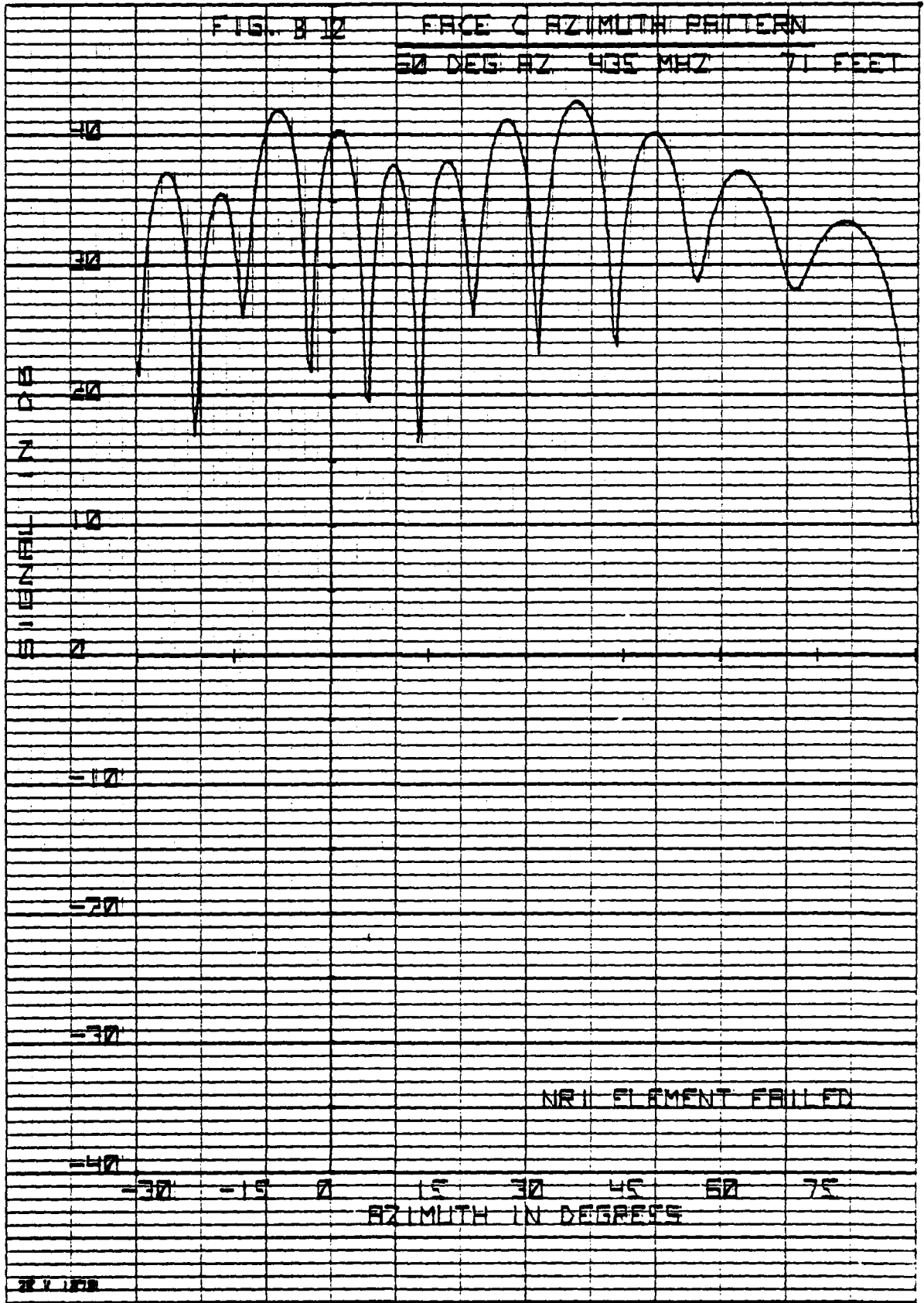
0

28 VI 1978

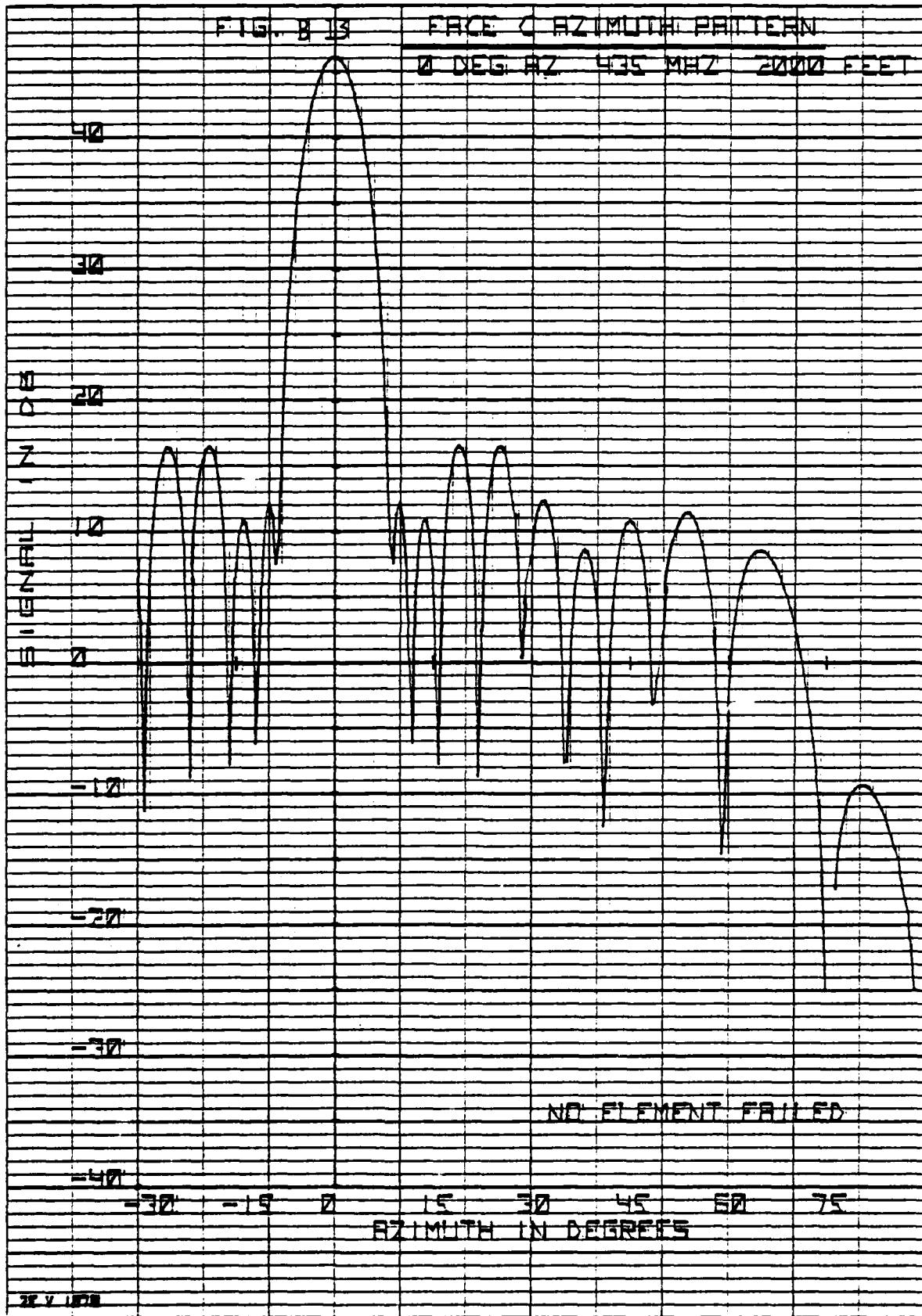




HEWLETT-PACKARD 9270-1008



HELWELI PACKARD 34701000



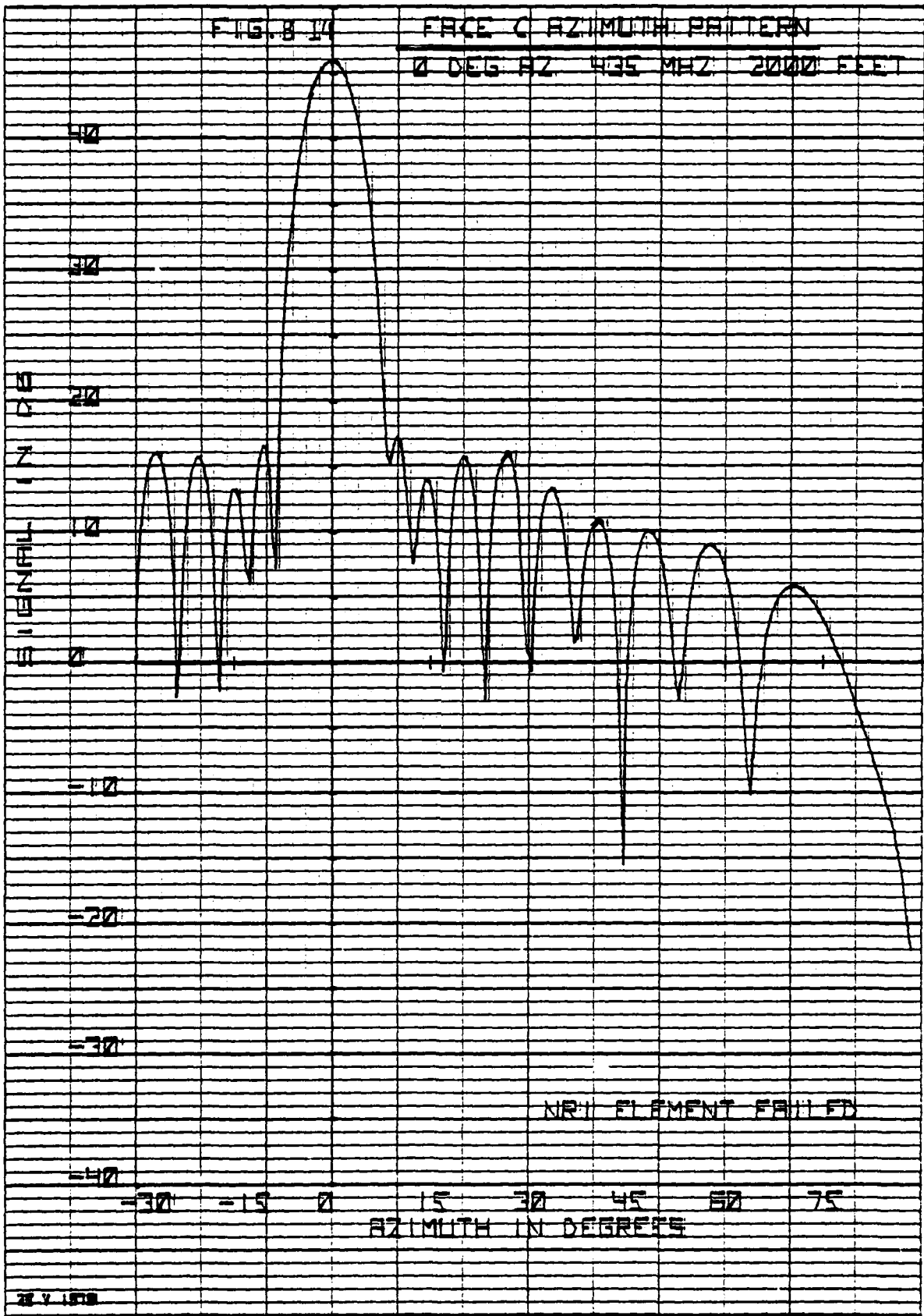
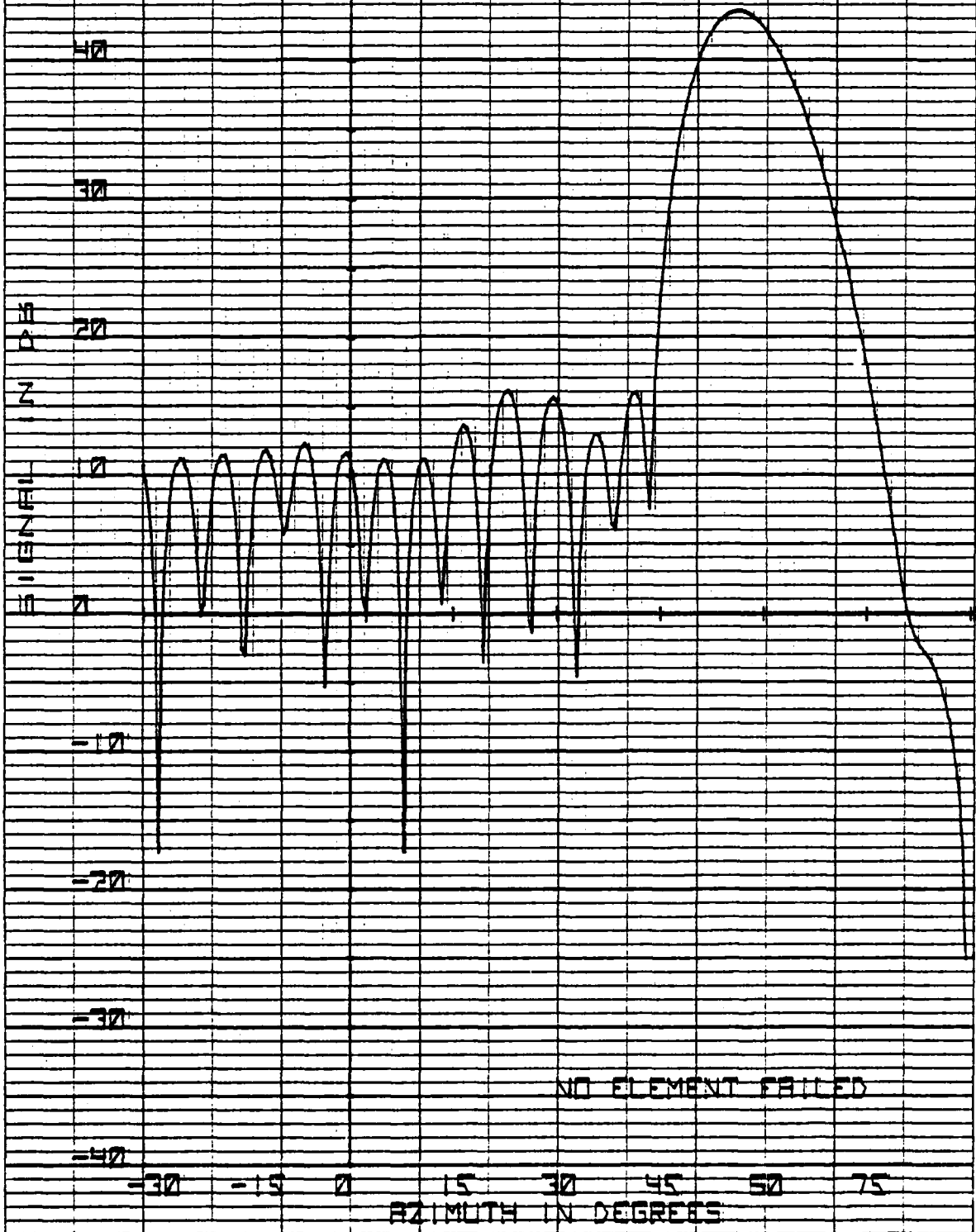


FIG. 8 15

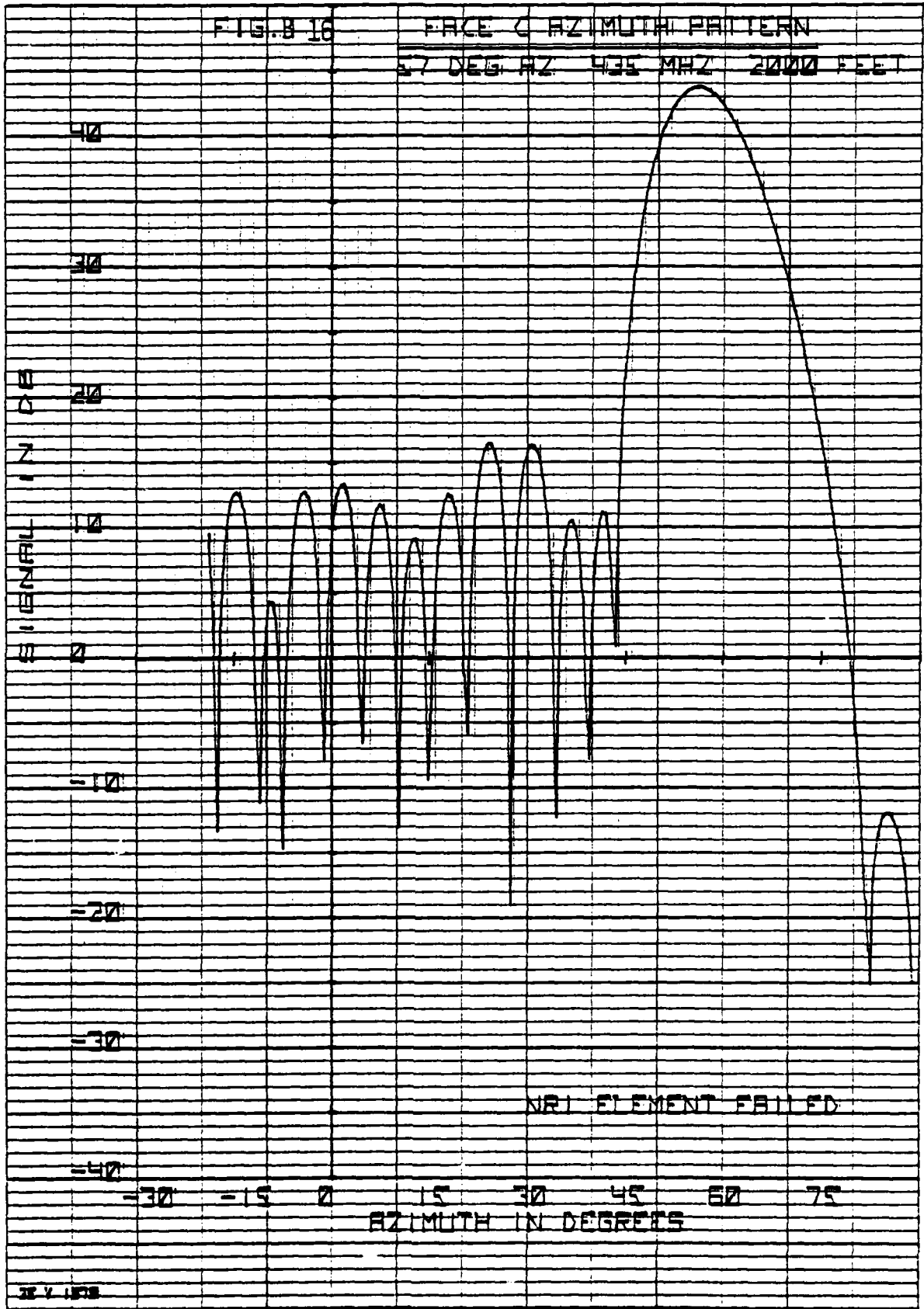
FACE C AZIMUTH PATTERN

57 DEG AZ 435 MHZ 2000 FEET



NO ELEMENT FAILED

28 V 1973





FILMED
4-8